Alteration mineralogy and whole-rock geochemistry of the Tauhara Geothermal Field

A thesis

submitted in partial fulfilment

of the requirements for the degree

of

Master of Science in Earth Sciences

at

The University of Waikato

by

Kate Mauriohooho

THE UNIVERSITY OF
WAIKATO
Te Whare Wānanga o Waikato

2015

"Ko te manu e kai ana i te miro, nōna te ngahere.
Ko te manu e kai ana i te mātauranga, nōna te ao."

The bird that partakes of the miro berry reigns in the forest.
The bird that partakes of the power of knowledge has access to the world.

-- Whakataukī, Māori proverb --

For my sister Penny, the bravest person I know

Abstract

The Tauhara Geothermal Field lies over a central zone of rhyolitic volcanism and caldera formation in the TVZ where extension allows magma to penetrate the crust and NE-SW oriented faults permit hot fluids to ascend and convect as individual hydrothermal systems. The Jurassic greywacke basement hosts the heat source critical to geothermal systems, the Waiora Formation is the permeable reservoir hosting fluids and the Huka Falls Formation is the cap rock to the system. 304 drill cutting samples and six drill core samples were collected from three wells across the Tauhara field (TH9, TH10 and TH12) at 20 m intervals, and a variety of petrographic, mineralogical and geochemical techniques were applied to the samples. New information on fluid flow pathways (feed zones), alteration types, alteration zones, hydrothermal conditions and mineral inferred temperatures were identified and interpreted from the data collected.

Using both alteration mineralogy data (from powder x-ray diffraction, short wave infrared or SWIR, and petrography) and geochemical data (from x-ray fluorescence and portable x-ray fluorescence), three main zones of alteration were identified across all wells: A shallow zone of argillic to intermediate argillic alteration followed by a transition zone with increasing depth as propylitic alteration begins to dominate and an intense propylitic alteration zone at the deepest levels.

Mineral inferred temperatures are generally cooler than measured well temperatures in all wells except in TH10. Here, mineral inferred temperatures agree with hotter measured well temperatures (> 280 °C) and strong potassic alteration indicates that TH10 is closest to the major upflow zone, making south Tauhara a prospective area for geothermal production. In TH12, mineral inferred temperatures are inconsistent with measured well temperatures implying a recent increase of fluid temperature. However petrographic evidence of an illite-calcite overprint suggests a cooler fluid at the bottom of well TH12 which is supported by petrography in this study showing pervasive illite alteration. TH12 is perhaps more marginal to the upflow zone and the change in temperature regime may be related to blind faults at depth bringing the cooler fluid in. An alteration halo based on geochemical data was identified in the

vicinity of the dike in TH9 at ~1400 mRF by high alteration index values determined by pXRF data, which is useful because illite and chlorite detected by SWIR did not show any appreciable mineralogical alteration halo.

The pXRF technique on cuttings correlated well with lab XRF on powdered cutting samples crushed using a ring mill, showing excellent correlation (rs >0.8) for elements As, Ba, Ca, K, Nb, Rb, Sr, Y, and Zr but poorer correlation (rs <0.7) for others. Samples analysed by XRF were classified as rhyolite/dacite or andesite/andesite-basaltic. One sample was reclassified as andesite/andesite-basaltic rather than ignimbrite and this finding was corroborated by downhole pXRF geochemical data which show it belongs in the andesitic lithic crystal breccia unit. These results mean that downhole pXRF geochemical trends of immobile elements (Zr, Y, Nb) can be used to refine lithological boundaries, which cannot be identified from visual logging alone. In addition, downhole immobile element trends are able to separate lithology packets and distinguish subunits or internal stratigraphic variations. Conversely, variations in mobile element concentrations (Ba, K, Ca, As, Rb and Pb) indicated feed zones or permeable zones of fluid movement by depletions or elevations in element concentrations. The ($AlOH$ / H_2O) ratio derived from SWIR data was plotted against depth downhole and changes in the ratio appear to coincide with some of the locations of feed zones (fluid pathways) in TH9 and TH12.

This study is the first to apply pXRF to geothermal drill cuttings and has proven that the data collected can be used to aid visual logging, and quantify alteration intensity. Application of rapid geochemistry on existing and future wells will generate detailed geology models and enable correlation between wells and across fields. This newly developed approach can be applied worldwide to any geothermal fields, provided that appropriate quality assurance techniques are used to ensure consistency of data.

Acknowledgements

This thesis would not have been possible without the encouragement, inspiration and mentoring from some important people as well as the support from certain iwi and organisations. I am thrilled that I can express my utmost thanks and appreciation here. A huge thank you to my supervisors Dr Shaun Barker, Dr Adrian Pittari from the University of Waikato and Dr Andrew Rae, GNS Science, Wairakei for their support, help in reviewing chapters, advice in writing this thesis and conference papers and their willingness to help when I was stuck. Choosing a topic that was especially challenging for me in terms of the chemistry aspects and fluid-rock interactions is probably the hardest thing I've had to grasp my head around but it has taught me a lot about myself. Special thanks to Mark Simpson for showing me how to operate the laboratory equipment at GNS and for being so welcoming and reassuring and Fiona Simpson for rescuing me from the core shed when my car went flat!. I would also like to thank Dr Vicki Moon for her humour, support and belief in me, without it I am not sure I would have the confidence in myself to pursue my dream. Also thanks to Dr Alison Campbell and Kevin Eastwood for being there when it got rough. Thank you to the Earth and Ocean technical staff from the School of Science at the University of Waikato: Annette Rodgers, Renat Radosinsky, Ganqing Xu and Janine Ryburn for guidance in the laboratory work.

This research would not have been possible without the financial support of several iwi trusts and key organisations of which I am greatly appreciative: Ngā mihi nui ki a Tauhara North No 2 Trust, Aotearoa Trust, Tuaropaki Trust, The Sir Hugh Kawharu Foundation, The Todd Foundation and The Australasian Institute of Mining and Metallurgy. Thank you for your tautoko, my achievements are not mine alone. In addition thank you to Contact Energy Ltd, specifically Sophie Milloy for providing access to their core shed at Wairakei and allowing me to collect samples.

To the team that helped me survive the thesis madness: my whānau, thank you for being patient, understanding and for dropping off food and laughs. To Mum and Dad, I have learnt so much. Thanks Dad for helping me collect samples and being a trooper, next project we'll do some mad field work! Mum, thank you for the dinners and chats on the phone Penny my rival and best friend thank you for being with me every step of the way, Jilly, thanks for the care package. My fellow colleagues, namely Amy Christophers and Neeltje de Groot, you guys pulled me through 2013 and beyond, I will never be able to thank you enough. To Gabz and Ariaan, thanks for reminding me that there's a life outside of university. A massive thank you goes to my partner Ihaia Greensill who has been invaluable throughout my studying years. Cooking dinner, giving me a hug when I am stressed, I honestly don't know how I can ever repay you. And finally, the reason why I came to study geology – tōku kuia, who had those awesome fossils, rocks and dinosaur toys that piqued my curiosity as a kid.

To everyone I've mentioned you guys ROCK. Pun fully intended ☺.

← The fossil that started it all…

Kingdom: Animalia
Phylum: Mollusca
Class: Bivalvia
Subclass: Pteriomorpha
Order: Arcoida
Family: Glycymerididae
Genus: Glycymeris
(glykys – sweet, meris – part)

Miocene, 10 million years old
Tongaporutuan Stage
Wanganui River

Table of Contents

List of Figures

Chapter 1

Chapter 2

Chapter 3

Chapter 4

Chapter 5

List of Tables

Chapter 3

Chapter 4

Chapter 5

Chapter 1
Introduction

1.1 INTRODUCTION

Hydrothermal systems within the top few kilometres of the earth's crust circulate hot fluids from which the thermal output can be harnessed into geothermal energy. The energy is extracted by drilling deep boreholes or wells into specific locations in a geothermal field. The thermal energy carried by the steam or water is converted to electricity through turbines. Fluid collection and disposal consists of wells and sequential casings drilled ~2-3 km deep into the crust. The steam, fluid or steam-fluid mixture may go through several stages from the well to the power plant. For a steam-fluid mixture it travels in pipes from the wells to separators in order to separate the phases. The steam goes to turbines or heat-exchangers and the fluid goes straight to reinjection wells unless the fluid can be utilised further through heat exchangers where it is heated and vaporised to drive the turbine. It is then cooled, condensed and reinjected (Dickson & Fanelli, 2004). This process of electricity generation varies at certain stages depending on the characteristics of the geothermal resource which dictates the type of geothermal power plant used e.g. dry steam, flash steam and binary cycle.

Geothermal fields are characterised by areas of high heat flow due to present or recent magmatic activity; or less commonly orogenic activity or radioactive decay of Th (thorium), U (uranium) and K (potassium) isotopes (Allaby, 2008). A geothermal field is the surface extent of a subsurface geothermal system and is typically delineated using resistivity surveys (Hunt et al., 2009). As geothermal fields are areas of high heat flow, the high thermal gradient in the geothermal field raises the temperature of deep permeating water. The geothermal gradient is the increase of temperature with depth in the Earth's crust. The global average geothermal gradient with depth is ~25-35 °C per kilometre penetrated into the crust, at two kilometres it is ~65-70 °C, at three kilometres ~ 90-105 °C (Kühn, 2004). However in tectonically active areas like around plate margins or in active

geothermal areas, the gradient can be ten times the average (Kühn, 2004). Terrestrial geothermal systems may have waters that circulate at depths of ~ 5 km or greater.

When reviewing literature the distinction between hydrothermal system and geothermal system is unclear. In other publications the terms may be used interchangeably or differently. For clarity, according to Jackson (1997) a geothermal system is defined as any system that transfers heat from within the Earth to the surface, for example hot rocks alone (with no water influence), are considered geothermal. In Greek, "geo" means earth and "therme" denotes heat. Hydrothermal on the other hand, is the transfer of heat by water in a liquid or vapour state, hence the use of the term "hydro" (meaning water) (Heasler et al., 2009). Common hydrothermal features include geysers and hot springs. Milicich et al. (2014) use the term hydrothermal system as being a convecting cell that is discreet, isolated spatially over time and associated with a heat source. This thesis will use the terms hydrothermal and geothermal as stipulated by Jackson (1997) and Milicich et al. (2014).

1.1.2 Geothermal development

After the oil crisis of the 1970's, alternative forms of energy were contemplated and it was thought the market for renewable energy would increase. Nevertheless renewable energies such as geothermal, solar, wind were perceived as riskier financially because of their high initial capital costs. However the advantages of renewable energy such as less air pollution from conventional energy systems and less long term health and safety issues began to make renewables attractive. Geothermal energy in particularly is advantageous in that it is not impeded by the weather like solar and wind. It is considered renewable and sustainable but only if the rate of extraction is less than the rate of recharge, allowing the system to maintain its 'renewable' status in a sustainable manner.

Among the first to develop geothermal energy in a significant amount to constitute part of their countries energy requirements were Italy, Iceland, Japan, New Zealand and the western United States, all areas of active tectonism and volcanism. Many countries are actively involved in contemporary geothermal development, with most

using steam or water dominated high enthalpy systems of at least 180-200 °C for large scale electricity generation. According to Lund et al., (2010) 78 countries now directly utilise geothermal energy, either as direct use or electricity generation (Fig. 1.1). Besides electricity generation, it is only recently that the benefits of using low enthalpy geothermal resources have been considered for direct use such as space heating in homes, industrial process heating, horticulture ventures, greenhouse and covered ground heating, agricultural crop drying, aquaculture pond heating, melting snow on pavements (as in Iceland) and space cooling (Lund et al., 2010).

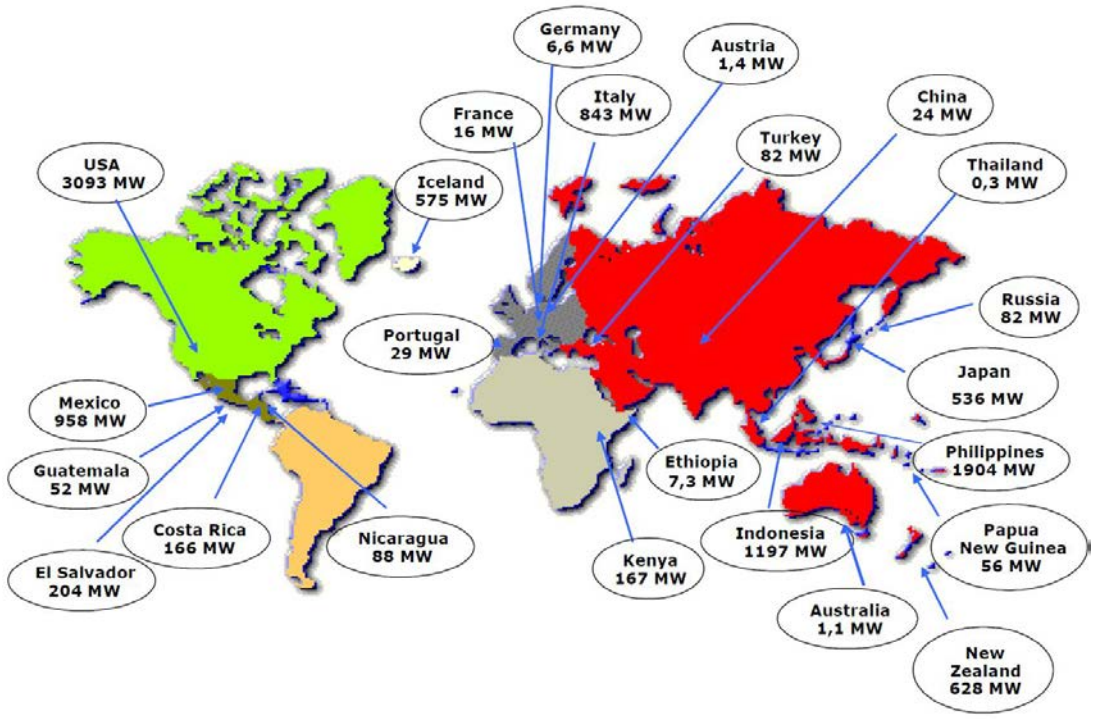

Fig. 1.1 Installed geothermal capacity across countries worldwide as of 2010 (10.7 gigawatt). MW = megawatt. Updated values expected at the World Geothermal Congress in April 2015. (Bertani, 2010).

Harnessing geothermal energy was first attempted at Lardarello, Italy in 1897 where natural steam was used to heat a boiler that produced steam to drive an engine. The first turbine generator installed at Lardarello in 1912 was driven by purified steam obtained from evaporators since the natural steam gas rich and would affect the vacuum in the condenser. Post-WWII the reconstructed plants had a capacity of 400 MW (Ellis & Mahon, 1977) which has more than doubled since. In 2008, the installed capacity was 810.5 MW which was increased to 842.5 MW in 2009 by the addition of two more units. As of 2010, all of the geothermal power operations in

Italy were located in the Lardarello-Travale and Mount Amiata areas of Tuscany (Cappetti et al., 2010).

In 1932, following the developments at Lardarello, Bruce & Shortland recommended recording data on the hot spring areas of New Zealand and conducting small-scale experiments similar to the Lardarello geothermal scheme. This recommendation was delayed until an electric power shortage and national energy crisis re-ignited interest in geothermal power, initiating scientific research in the Taupo Volcanic Zone (Ellis & Mahon, 1977). In the early 1950s prospective drilling began at Wairakei, leading to the country's first geothermal power station built in 1958 and subsequent large scale steam and hot water production. As a result Wairakei was the second developed geothermal field in the world after Lardarello.

Since then two geothermal resources, Wairakei and Kawerau have sustained energy extraction for 56 years and geothermal operations have occurred in four main development phases: 1958 (Wairakei, Kawerau), 1989 (Ohaaki), 1996-1999 (Poihipi, Rotokawa, Ngawha, Mokai) and 2013-2014 (Ngatamariki, Te Mihi) (Bromley et al., 2010). From 2007-2010 additional changes also arose at Mokai, Kawerau, Ngawha, Tauhara and Rotokawa. According to Bromley et al. (2010), geothermal power generation has increased greatly in New Zealand since 2007, when it supplied 8% of total electricity. Currently geothermal production contributes approximately 15 % of New Zealand's total electricity (Ministry of Business, Innovation & Employment, 2014).

1.1.3 Māori and geothermal

The link between humans and geothermal resources goes back to primeval times where geothermal water from hot springs and pools was used for cooking, bathing and warmth by many cultures such as the Romans, Turks, Japanese, Russian, Icelandic, French and Māori, the indigenous people of Aotearoa (New Zealand). Māori customary use of geothermal resources consists of ritual, bathing, heating/warmth, cooking, healing and therapeutic uses with each customary use allocated separate areas. A detailed description of customary uses is given by Stokes (2000) and is summarised in the following section. Certain geothermal areas were

considered *wāhi tapu* (sacred) as they were burial places or used by *tohunga* to perform purification rites. Bathing areas or hot springs (*waiariki*) were temperature regulated by digging a small canal to funnel cool water in. The hot water was considered therapeutic for muscular aches, arthritis and the communal baths a place of social interaction. Separate pools were also used for washing garments. Boiling springs served as cooking places to immerse food. *Kai* (food) was wrapped in leaves and/or matting and placed over hot steam emanating from fissures or placed in holes dug into hot ground. The sprouting of kumara tubers was aided by hot ground in preparation for spring planting and tawa berries were laid out on slabs of sinter to dry over fumaroles at Rotomahana. Sulphur deposits were used medicinally for skin issues: applying sulphurous muds to skin infections, bathing in sulphurous hot springs and burning sulphur to ease respiratory problems. Altered clays e.g. iron oxides were used to create red ochre. Mixed with shark oil it produces a red ceremonial pigment called *kokowai*. In the Tokaanu and Rotomahana areas hydrothermally altered clays were also eaten on occasion and used as soap. Processed flax was dyed with black mud (*paruparu*) and woven cloaks or mats were softened by soaking in pools.

Māori have maintained our relationship with geothermal surface manifestations as some of these customary uses are still practiced today (Stokes, 2000). The connection between surface and subsurface activity or *ahi komau* (earth heat) is recognised in the journey of Ngatoroirangi and his sisters which explains the formation of the TVZ according to Maori oratory. Increasingly the relationship with geothermal activity has changed as some tribes partner with power companies (Mighty River Power, Contact Energy) to harness geothermal energy or develop their own geothermal resources. Any venture for a tribe is guided by cultural values and with tribal members in mind. *Tikanga* (protocols) revolving around the natural environment (*mana whenua, mana moana, ngahere, kararehe* – tribal lands, tribal waters, forest, animals) is influenced by the overarching concept of *kaitiakitanga*. Kaitiakitanga is the practice of conservation customs and traditions (e.g. *rāhui* – enforced ban) and is loosely translated as ‘guardianship’. The act of kaitiakitanga serves to enhance the *mauri* (lifeforce or the physical and metaphysical attributes) of an entity (Hikuroa et al., 2010). Hence, any development that affects the mauri of

the entity (in this case geothermal activity) by adversely affecting its environment must be avoided. Kaitiakitanga carries an obligation to your *tūpuna* (ancestors) to ensure the natural environment and ecosystems are maintained for the benefit of future generations (White et al., 1995; Hikuroa et al., 2010).

One such issue of kaitiakitanga highlighted by Morgan (2006) is water recycling. The mauri in recycled water influences how it is reused. In geothermal energy, a form of water recycling occurs when fluid is re-injected back into the ground. This is appealing to Māori as the fluid returns to the area of extraction, albeit with a lower enthalpy, thus restoring mauri. The recycling of wastewater for other uses is rated favourably and more sustainable instead of discharging into other water bodies (Morgan, 2006). A good example of water recycling is the tourist venture Wairakei Terraces, where silica rich waste water from the Wairakei geothermal plant is artificially channelled to a space allowing the natural process of precipitation to form sinter terraces and hot pools for therapeutic use.

Geothermal energy is attractive to indigenous peoples because of its sustainable and renewable attributes provided it is managed correctly. The delay in geothermal development in New Zealand is partly attributed to whether a resource can sustain its output but also the complex legislation that surrounds who has the right to develop the resource because of various Acts of Parliament and court case outcomes (White et al., 1995). Confusion arises as to who owns the infrastructure from which geothermal energy is able to be harnessed (the power company) and the land where the system is situated (the hapū/iwi) (White et al., 1995).

Most of the undeveloped high enthalpy resources in New Zealand have either been set aside for tourism purposes (Waimangu, Waiotapu) or lie within tribal land with multiple landowners (Hikuroa et al., 2010). Progress may be facilitated easier by incorporating indigenous values into geothermal development. A suggested way to achieve this is the Kaitiaki Geothermal Development Model (KGDM) developed by Hikuroa and others (2010) (Figs. 1.2a, 1.2b). The model is based on the Mauri model (Morgan, 2006) and is guided by kaitiakitanga principles combined with consent requirements, geothermal science, engineering, governance and management

ensuring all stakeholders are given a voice whilst adequately assessing geothermal development opportunities.

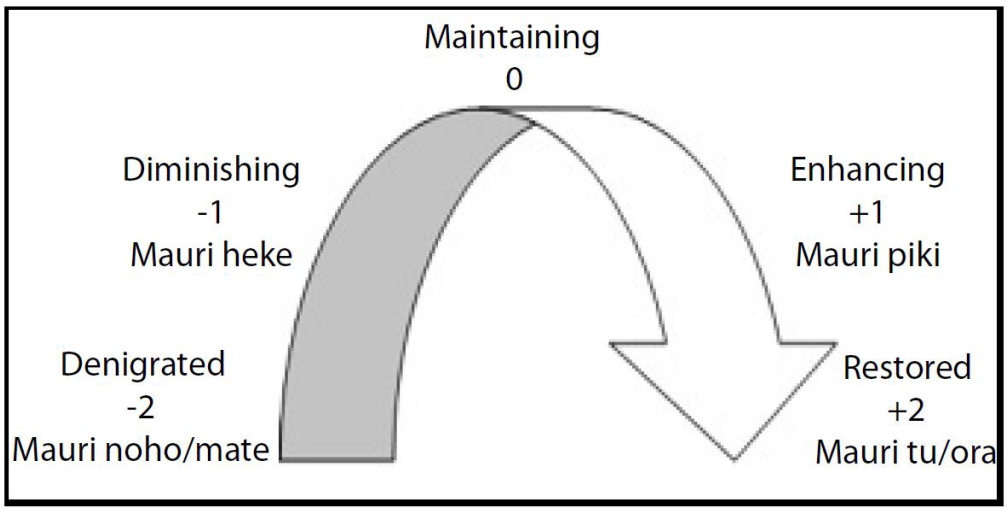

Fig. 1.2a. The Mauriometer used for sustainability assessment. Indicators are assigned a value from the Mauriometer (Hikuroa et al., 2010).

	Indicator	Status Quo	Group 1	Group 2
Environmental	Surface Features	0	0	-1
	Waste Water	0	0	0
	Subsidence	0	-1	-1
Economic	Cost/Benefit	0	+1	+1
	Cash Flow	0	+1	+1
	Employment	0	+1	+1
Cultural	Ancestral Connection	+1	+1	+1
	Kaitiakitanga	+1	+1	+1
	Returning Home	-1	+1	+1
Social	Sustainability	0	+1	+1
	Community Resilience	-1	+1	+1
	Aesthetic Environment	0	-1	-1
	Results:	0.00	0.5	0.42

Fig. 1.2b. Mauri model based Kaitiaki Geothermal Development Model assessment. Scores are totalled and divided by the number of indicators to give a final result (Hikuroa et al., 2010).

The economic gains made for a tribe from geothermal energy is primarily reinvested into members of that tribe in the form of: education (grants for *rangatahi* (youth), *ngā tauira* (students), healthcare assistance particularly for seniors and special grants to recognise kaumatua and kuia contribution on marae (e.g. speaking on *paepae*). There is also the added benefit of further flow on ventures that align with renewable energy. An example of this is the Gourmet Mokai glasshouse co-owned and established by Tuaropaki Trust that is heated using steam directly from the Mokai geothermal field.

1.2 THERMAL EVOLUTION

Hydrothermal systems from which thermal energy is extracted from the liquid or steam, cause alteration of the original host rock lithology due to fluid-rock interactions. These changes in mineralogy and geochemistry convey the changing conditions occurring in the hydrothermal system. In industry, hydrothermally altered minerals are used to assess the physical and chemical conditions at the time the altered minerals were formed such as temperature, permeability, fluid acidity/pH and initial rock composition (Yang et al., 2001). This information is used to locate appropriate positions to drill a borehole or determine whether a retrieved drill core is in the centre or periphery of a geothermal field by alteration mineral zonation. Hydrothermal minerals and mineral assemblages can also indicate a host of useful aspects such as what thermal history a hydrothermal system has undergone, if it is currently active and if so what its current temperature regime is. Whole rock geochemistry is used to identify lithology and alteration types as well as quantify metasomatism and alteration.

Hydrothermal systems are also temporary systems in geologic terms as evidenced by ore deposits (the remnant deposits of extinct hydrothermal systems), hence the overall purpose of investigating the Tauhara geothermal field is to determine the past and present behaviours of the system i.e. has it decreased in temperature and is perhaps past maturity or increased, therefore is it still in infancy stages with a certain amount of longevity left. Studying the mineral assemblages down core provides information on past temperatures and fluid pathways that can be compared to present

day measured temperatures and activity to help uncover the evolution of the Tauhara geothermal field.

1.3 RESEARCH AIMS AND OBJECTIVES

The principal aim of this thesis research is to complete a detailed analysis of the hydrothermal alteration mineralogy of the Tauhara geothermal field. This research has been undertaken in collaboration with GNS Science, Wairakei and provides information on the location of fluid flow pathways and hydrothermal alteration occurring in the Tauhara Geothermal Field, using new and traditional analysis techniques. This information will add to the existing knowledge of the geothermal field and may be applied to other geothermal fields. The research objectives are:

- To collect hydrothermal alteration data in the drill cores TH9, TH10, TH12 in order to determine transition mineral alteration zones down the cores.
- To determine mineral species and chemical composition using a variety of analytical methods. This data will yield information on the hydrothermal conditions, define fluid pathways and enable mineral inferred temperatures to be compared to present day measured temperatures.

These objectives are achieved by analysing and interpreting data collected via x-ray diffraction (XRD), short wave infrared (SWIR), portable x-ray fluorescence (pXRF), x-ray fluorescence (XRF) and petrography data collected from drill cuttings and available core from three wells (TH9, TH10 and TH12, TH = Tauhara). Specific questions that are addressed in this thesis are:

- What does the petrography, XRD, SWIR, XRF and pXRF reveal about hydrothermal conditions and fluid pathways?
- What does the stable isotope chemistry, for example the epidote, chlorite and clays convey with regards to the geothermal hydrology across geothermal reservoir?
- TH9 has an interpreted rhyolite dike (1425-1450 mRF). Is there an alteration halo surrounding the dike?

1.4 THESIS OUTLINE

The remaining chapters of this thesis are organised by geological background, hydrothermal alteration, alteration mineralogy (including remnant primary mineralogy) and geochemistry, followed by an overall summary and concluding remarks.

- Chapter 2 outlines the tectonic setting and geological background of the Tauhara Geothermal Field.

- Chapter 3 details the formation of hydrothermal systems and resulting useful hydrothermal alteration mineral associations in geothermal exploration and evolution.

- Chapter 4 describes the primary and secondary (alteration) mineralogy resulting from SWIR, XRD and petrographic analyses. This chapter also discusses the mineral inferred and measured well temperatures and illustrates the geothermal hydrology across the geothermal field.

- Chapter 5 quantifies major and trace element abundances from pXRF and XRF analyses. Rock compositions, alteration types, metasomatism and fluid flow pathways are interpreted and discussed from geochemistry.

- Chapter 6 provides a summary of the research and concluding remarks.

Chapter 2
Geological Setting

2.1 INTRODUCTION

The Tauhara Geothermal Field lies within a segmented rift axis system called the Taupo Volcanic Zone. The magma rises from depressions in the crustal axis rift zone and hydrothermal fluid flow is focused through NE-SW fault lineaments. This chapter will detail the tectonic setting of the subduction zone that is responsible for the volcanic arc and back arc setting that forms the TVZ. It will then outline the geological background of the Tauhara Geothermal Field, describing in detail the geological formations present that host the hydrothermal fluid flow.

2.2 GEOLOGICAL SETTING

2.2.1 Tectonic Setting

During the mid-Eocene a convergent margin was established as the tectonic behaviour of the Australian and Pacific plates was reconfigured. Subduction propagated southwards along the margins of the two plates and from 23 Ma to 11 Ma the subduction trench began to rotate clockwise. The rotation pushed the southern portion of Zealandia on the Pacific plate clockwise until it collided with the northern portion on the Australian plate. This rotation (at 1.27°/m.y., Cole et al., 1995) and oblique movement still continues today with emergent mainland New Zealand the result of the convergent plate boundary.

The Hikurangi Trough and subduction zone lie to the east of New Zealand (Fig. 2.1). The oblique convergence and resulting contraction has resulted in the formation of a subduction (accretionary) wedge 200 km wide in the central Hikurangi forearc domain. Part of the forearc of the Hikurangi subduction zone is the eastern margin of the North Island.

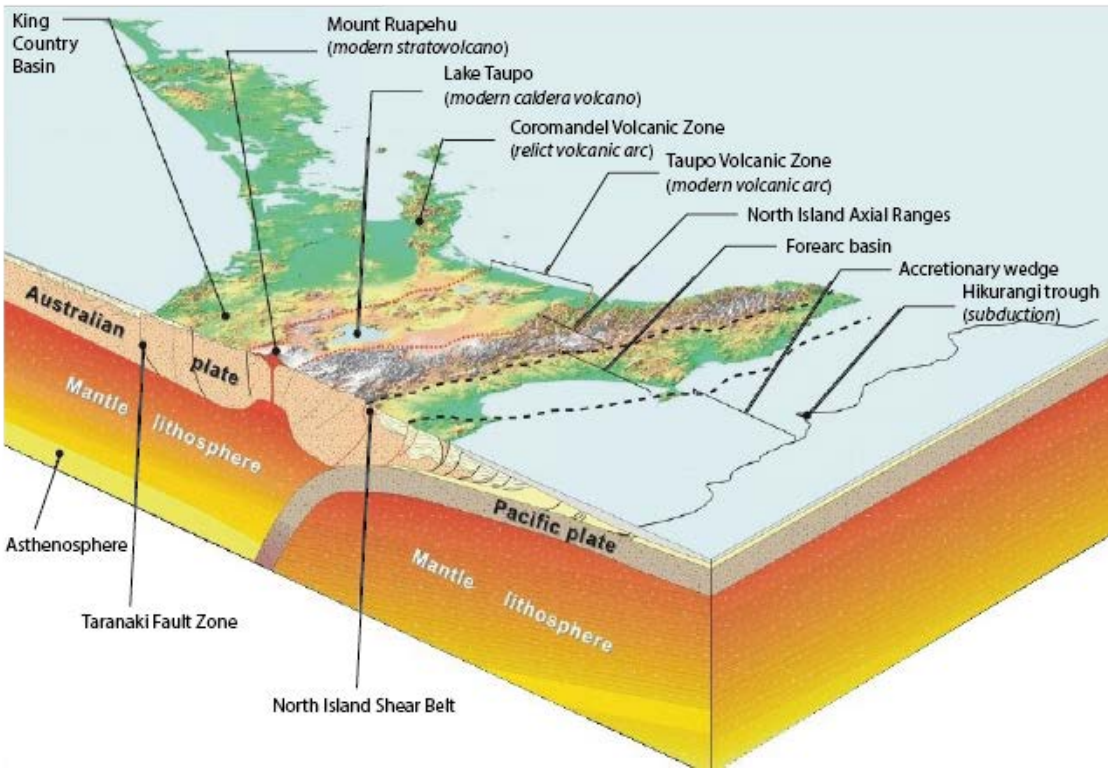

Fig. 2.1. Slice of North Island geological life. 3D schematic shows the main tectonic products in the upper north Island resulting from the convergent plate boundary. (modified from Bland et al., 2008).

The Hikurangi Trough and subduction zone are collectively known as the Hikurangi Margin. It is here that the Pacific plate subducts obliquely west beneath the Australian Plate (Fig. 2.1., Nicol et al., 2007; Bailleul et al., 2013) at a rate of ~50 mm/yr (Cole et al., 2000). The Hikurangi Margin to the north transforms into the Kermadec Trench and to the southwest it becomes the Alpine Fault. The Alpine Fault is a large dextral (right lateral) transform fault that connects the subduction zone dipping westwards in the northeast of the North Island (Hikurangi Margin), to the subduction zone at the southern reaches of the South Island (Puysegur Margin) (Furlong & Kamp, 2009).

The plane of the subducted plate has a N45°E strike and dips northwest. The subducted slab has been defined by seismic studies which have shown that for 250 km along the Hikurangi Trench east of North Island it dips at a shallow angle of 12-15°. It then steepens, increasing its dip to 50° at a depth of 80 km. The line where its dip increases corresponds with the surface trend of the TVZ and forms a Wadati-

Benioff zone beneath the rift axis of the TVZ (Fig. 2.1) (Kamp, 1984). Kamp & Furlong (2006) show that the subduction zone is migrating eastwards.

2.2.2 Subduction related volcanism

The TVZ corresponds to a change in the orientation of the plate boundary as the Havre Trough began opening 4 Ma ago (Cole et al., 1995). The 2800 km Tonga-Kermadec-Taupo volcanic arc system and the Lau Basin-Havre Trough-Ngatoro Basin is the northern representation of a back-arc zone of crustal thinning, rifting and subsidence while the TVZ is the southern manifestation (Fig. 2.2., Cole et al., 2000). Hence, the TVZ is described in literature as a volcanic arc and back-arc basin of the Taupo-Hikurangi arc trench system (Cole, 1990, Cole et al., 2000). This zone stretches from White Island in the north to Mount Ruapehu in the south covering an area 200 km long and 60 km wide. The TVZ is estimated to be ~ 2 Ma (Quaternary) in age (Wilson et al., 1995) and results from the westward subduction of the Pacific plate.

The TVZ is the youngest onshore volcanic expression of around 22 Ma Cenozoic arc evolution. In its current configuration (<340 ka) it is a structurally and magmatically segmented rifting volcanic arc system (Rowland et al., 2012). The modern location and geometry result from subduction migration, slab roll-back and tectonic evolution. Interpretations from authors on the structure and evolution of volcanism have generally agreed that the degree of extension is somewhat related to eruption volume and style (Wilson et al., 1995; Houghton et al., 1995, Rowland et al., 2012). Andesitic composite volcanoes in the southern end of the TVZ is associated with more dextral transtension while the highly active rhyolitic Taupo and Okataina calderas have the most extension (Spinks et al., 2005). It appears that magma is erupted along the rift axis zone and volcanism arises through caldera structures adjacent to the axial zone (Spinks et al., 2005).

Wilson et al. (1995) divides the history of the TVZ into ‘old TVZ’ which represents activity from 2.0 to 0.34 Ma up to when the Whakamaru group eruptions began and ‘young TVZ’ from 0.34 Ma to the present day. The magnetic signature of volcanic deposits supports this subdivision as the volcanic deposits in the western section are

older at 0.73-2 Ma compared to the eastern part with an age of <0.73 Ma, (Soengkono et al., 1992). This finding indicates that volcanic activity has shifted with older volcanoes in the west and presently active volcanoes in the east (Fig. 2.3).

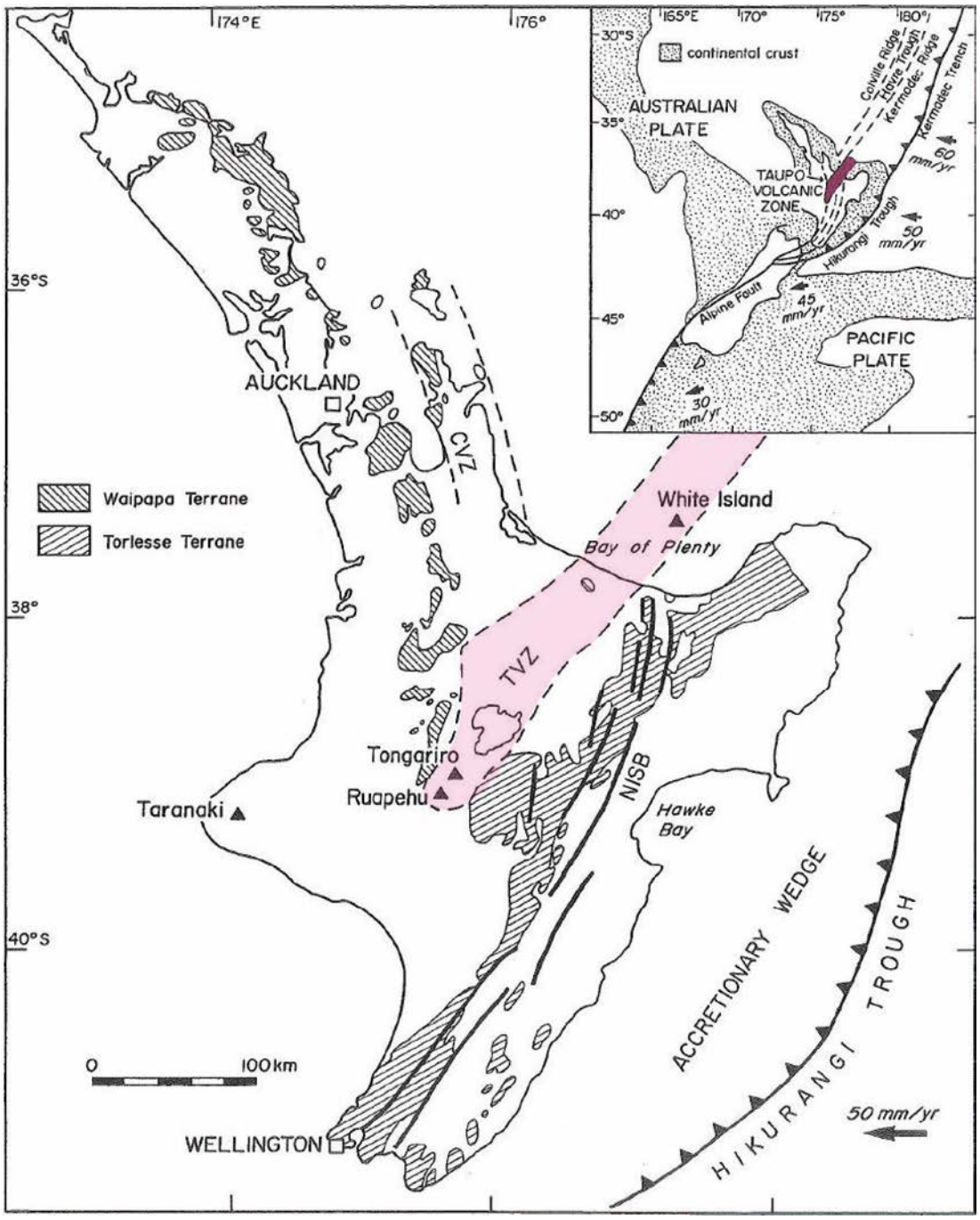

Fig. 1.2. Map of the North Island of New Zealand showing the location of tectonic and geological features and their relation to the Taupo Volcanic Zone (shaded purple). CVZ = Coromandel Volcanic Zone. NISB = North Island Shear Belt. Arrows show rate and direction of the Pacific plate subducting underneath the Australian Plate. Inset illustrates mainland New Zealand overlying the plate boundary. (Hobden, 1997).

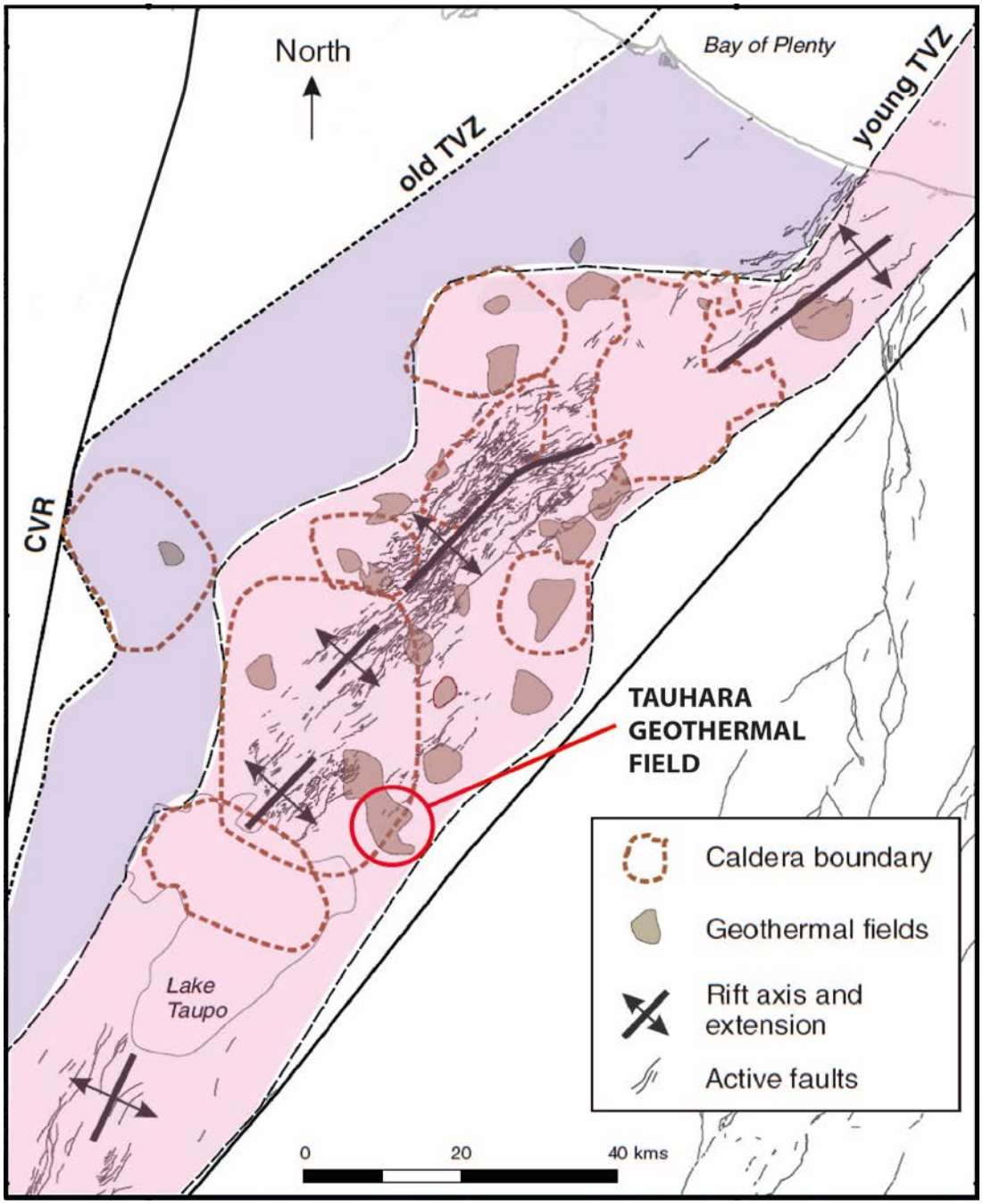

Fig. 2.2. Schematic map of the Taupo Volcanic Zone. The locations of geothermal fields, calderas, active faults and the rift axis and extension occurring are defined (modified from Chambefort et al., 2014). The old TVZ is shaded in purple, the new TVZ is coloured in pink.

2.2.3 Taupo Volcanic Zone (TVZ)

Development of the TVZ and subsequent volcanic activity occurred over the last 2 My. Houghton et al. (1995) stated that voluminous rhyolitic activity and calc-alkaline andesite lava began erupting around 1.6 Ma ago. Over 6000 km^3 of silicic magma has been discharged from twenty five eruptions, most caldera forming. Consequently, the TVZ is one of the most productive Quaternary silicic volcanic systems on earth in terms of volume, only equalled by Yellowstone in the US (Wilson et al., 1995; 2009).

Extension and strike-slip faults in the arc and back-arc basin are thought to be responsible for the formation of multiple calderas (eight major silicic caldera volcanoes, Cole, 1990) and associated geothermal systems. Extension rates in the TVZ are ~7mm/yr in the north and 18 mm/yr in the south. Subsidence is about 1-2 mm/yr and rates of shear strain between $0.18\text{-}0.5x10^{-6}$ per year (Cole et al., 1995). Vent positions are also subject to change and trend towards a NNE-SSW linear arrangement. The coincidence of volcanic vents and fault lineaments is obvious (Browne & Lloyd, 1987) and many hydrothermal systems are located above these faults as they provide permeable pathways for ascending hot fluids.

The TVZ is subdivided into three segments: the northern, central and southern areas (Wilson et al., 1995). The northern and southern areas have large andesitic to dacitic composite volcanoes (Tongariro, Ruapehu, White Island) with vent hosted hydrothermal systems. From Kawerau in the northeast to the southern margins of Lake Taupo is the central TVZ which is characterised by rhyolitic volcanism and heavily faulted continental crust. The basement terrane is downfaulted or downwarped resembling a graben like structure (Adams et al., 2009). It is buried over 3-3.5 km deep beneath the TVZ but does outcrop to the west and east.

Magma concentrated within the central TVZ supplies heat, volatiles and chemicals through to the 23 large high temperature (>250 °C, Fig. 2.4) hydrothermal systems lying above that have a combined thermal output of ~4.2 GW (Bibby et al., 1995; Rowland & Simmons, 2012; Chambefort et al., 2014). One of these hydrothermal systems is Tauhara. The thermal outputs of each geothermal system are on the order

of <50 to 600 MW (Bibby et al., 1995). Geothermal systems are typically spaced 10-15 km apart. Rheologic arguments and the significance of the spacing (which is double the seismogenic depth) imply that the full depth of the seismogenic zone hosts fluid circulation (Rowland & Simmons, 2012).

2.3 GEOLOGICAL BACKGROUND

Understanding the Tauhara geothermal system began with foundation studies on the Wairakei system that was soon found to be connected hydrologically to Tauhara, and thus referred to as Wairakei-Tauhara. Pioneering studies by a number of authors Grange (1937), Grindley (1965, 1974), Healy (1974), Steiner (1977), Browne (1970, 1978) established our knowledge of the stratigraphic sequence, architecture and lithology. More recent work on the Wairakei-Tauhara system has been completed by a number of authors (Rosenberg et al., 2009; Bignall et al., 2010, Bromley et al., 2010). Extensive drilling at Wairakei and Tauhara from 2006 to 2013 resulted in additional geological information, prompting stratigraphy and geology reviews such as those by Rosenberg et al., (2009) and Bignall et al., (2010). As a result the distribution, thickness and hydrological role of host rocks were updated, new formations were described and older wells revised.

2.3.1 Reservoir and wells

Since 2002, 25 wells have been drilled by Contact Energy for exploration, production and to assess subsidence. Evidence of multiple upflows is found at Tauhara where deep wells have discovered higher temperatures (279 °C) compared to Wairakei. Temperatures in excess of 250 C within an area twice that of Wairakei suggests the potential for geothermal energy is large (Rosenberg et al., 2010). Apart from the domestic use of shallow lying aquifers in residential Taupo, the Tauhara Geothermal Field is utilised in two ways: power generation and supplying heat for industry. Three production wells reaching a depth of 1.1 km and three reinjection wells 0.4-1.2 km deep were erected in 2010. Recent numerical simulation of the reservoir has shown that the generating capacity, assessed at > 250 MWe (megawatts electrical i.e. electric power) is sustainable. The Tauhara geothermal resource is

three times the size of the resource at Wairakei and Rotokawa fields (Wairakei has an installed capacity of 220 MWe) (Rosenberg et al., 2010).

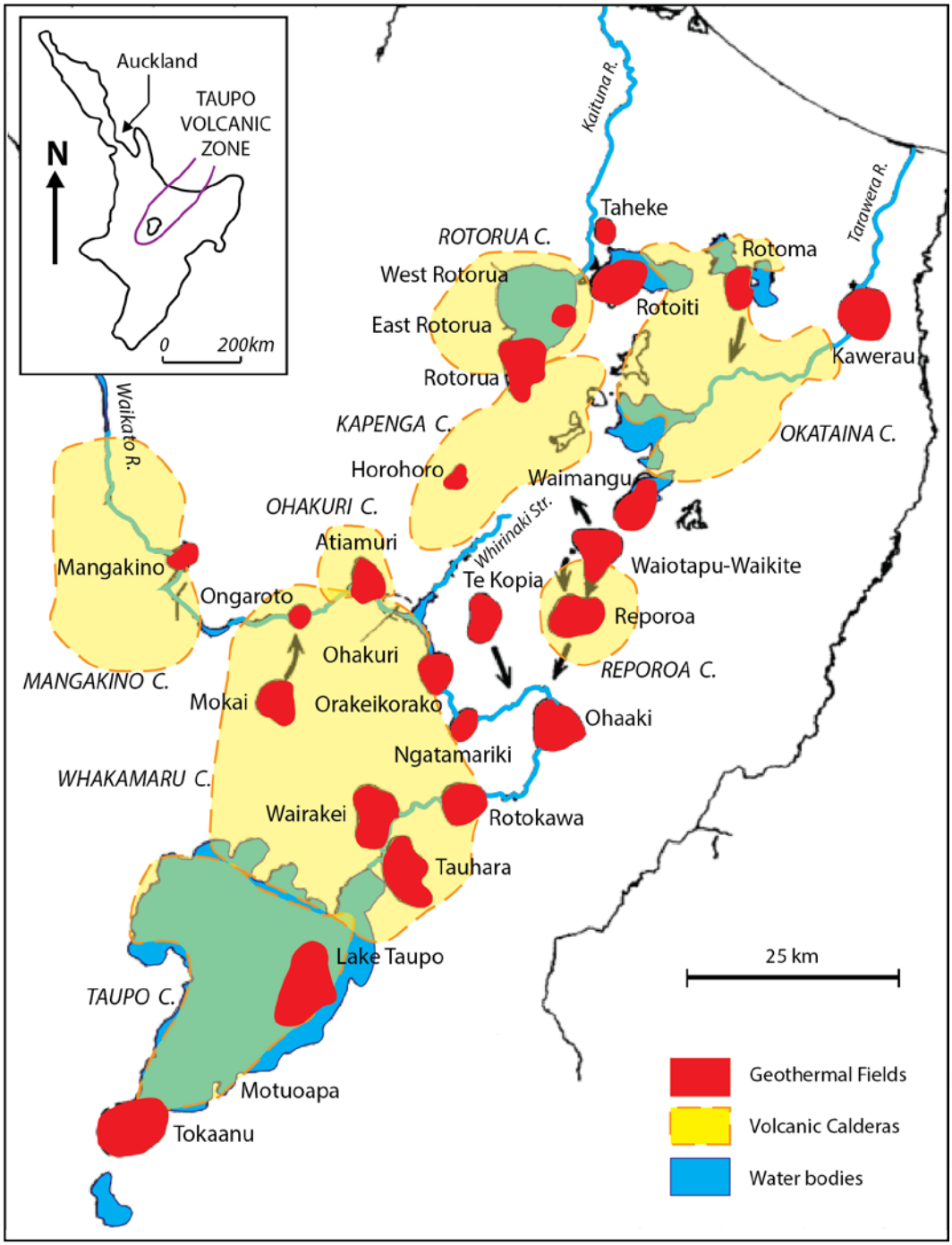

Fig. 2.3. Location map of Tauhara Geothermal Field and other geothermal fields of the Taupo Volcanic Zone (redrawn from Bibby et al., 1995; Kissling & Weir, 2005). Capitalised labels refer to indicated calderas. Most of the geothermal systems occupy the space between the two active silicic calderas Okataina and Taupo.

2.3.2 Field site

The Tauhara Geothermal Field has a total surface area of 50 km² (Rosenberg et al., 2010) and is located within the Taupo Volcanic Zone in the central North Island, New Zealand, 3 km northeast of Lake Taupo (Fig. 1). The Waikato River borders the western side of the Tauhara field and Mt Tauhara, an extinct dacite volcano, is on the southeast (Steiner, 1977) (Fig. 2.5). It is classed as a high enthalpy resource, with a natural energy output at 110 MW (megawatts) (Bibby et al., 1995). To the south-east of Wairakei is the Tauhara geothermal resource. Although both fields have separate upflow zones previous studies have documented a hydrological connection between the two fields, with pressure drawdown at Tauhara linked to long-term production at Wairakei (Hunt & Graham, 2009; Milloy & Wei Lim, 2012). The boundary between the two systems is placed at the Waikato River.

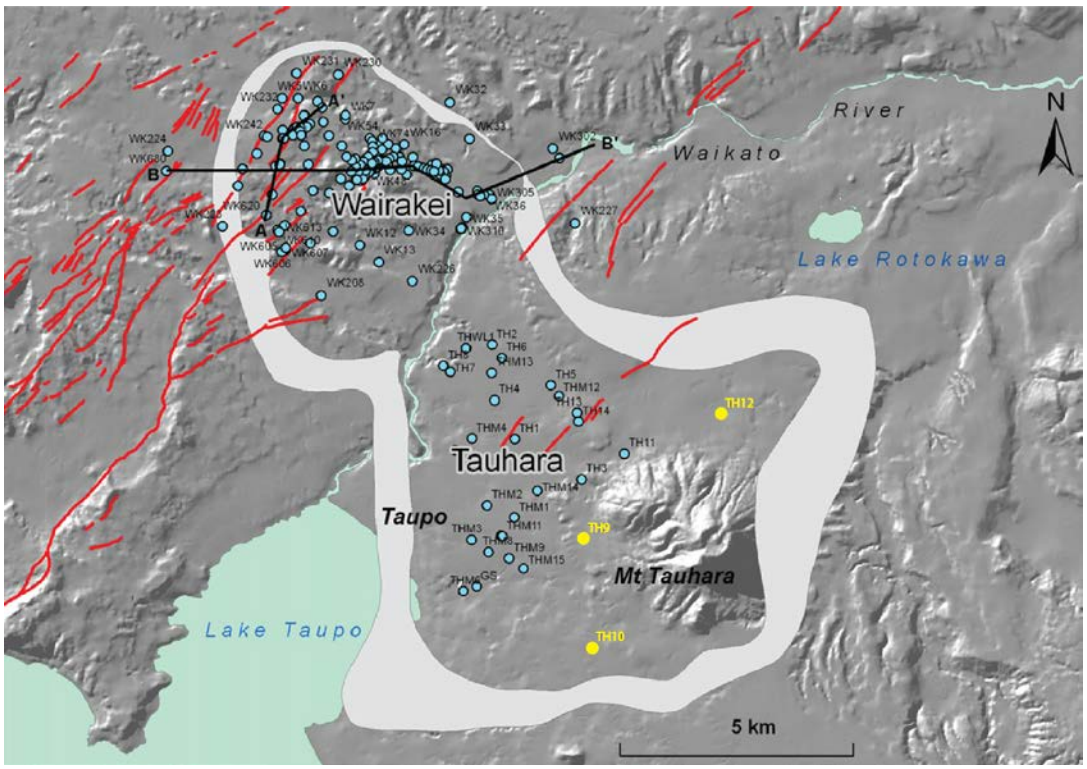

Fig. 2.5. Map of the Tauhara Geothermal Field (southeast) as part of the Wairakei-Tauhara geothermal system (after Rosenberg et al., 2009). TH9, TH10 and TH12 geothermal wells shown by yellow circles. Resistivity boundary (to a depth of 500 m) is delineated by the light grey shaded area. Red lines are active faults.

2.3.3 Geophysics

Stagpoole and Bibby (1999) conducted gravity and magnetic studies at a regional scale in 1999. The results indicated that a deep broad depression in the greywacke basement, extending over tens of kilometres, is infilled by sediments and low density pyroclastics (Bignall et al., 2010). Bibby et al. (1995) suggests the volcaniclastic cover over the greywacke TVZ basement is generally 2.5 km thick, but this varies due to the depth at which the greywacke basement is intercepted (or not) by geothermal drilling. The broad basinal like structure in the greywacke basement lies beneath the Wairakei-Tauhara Geothermal Field. The gravity structure has been verified from geothermal exploration drills and geological mapping but the variations in lithology, thickness and spatial extent (both vertical and lateral) of strata have made 3D interpretation difficult (Hunt et al., 2009). However Cattell et al. (2015) has illustrated one such 3D interpretation (Fig. 2.6).

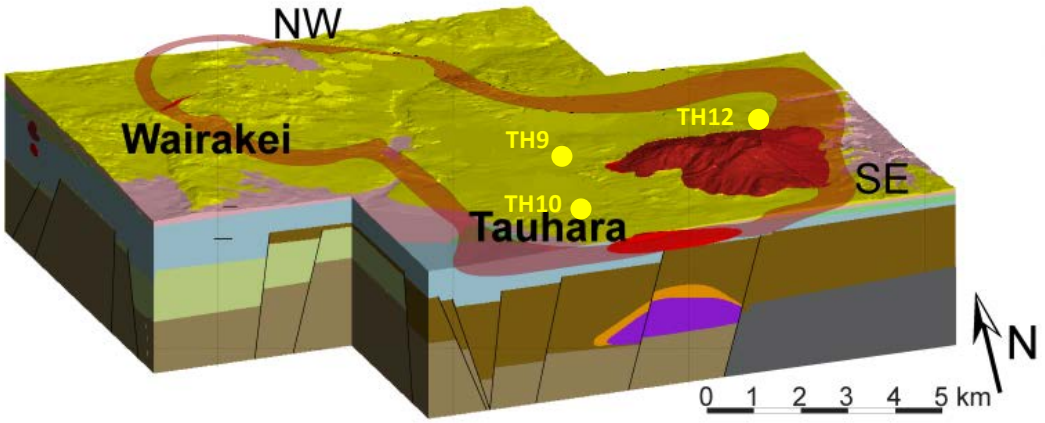

Fig. 2.6. Conceptual geological 3D interpretation of the Wairakei-Tauhara system, (Cattell et al., 2015). Yellow dots are well locations in this study.

In the southwest between Wairakei and Lake Taupo is another depression. Picked up through early gravity surveys as a positive anomaly it extends from Lake Taupo to Wairakei and was thought to be an elevated greywacke basement block or dense mafic intrusions in the crust (Beck & Robertson, 1955). An alternative suggestion by Healy (1984) is that it is related to a huge slab of Wairakei Ignimbrite tilting towards the east. Because drilling had not yet reached evidence for a basement horst, Stern (1982) proposed that lateral variations in the density of the volcaniclastic rock cover was the reason behind the gravity high, rather than a structural feature. It was suggested to be a collapsed volcanic structure by Rogan (1982) and the resulting depression subsequently filled with welded pyroclastics and rhyolite lavas. Rogans

hypothesis is consistent with stratigraphy intercepted by drilling at Tauhara (Rosenberg at al., 2009; 2010) and more detailed 3D gravity modelling by Soengkono (2011), which showed a good match between depressions in the basement, and the volcanic centres of Okataina, Rotorua, Kapenga, Maroa, Reporoa and Mangakino.

3D gravity modelling by Soengkono (2011) also inferred that low density masses exist beneath the basement. These low density areas potentially represent magnetic crustal masses according to airborne magnetic data. Sub-volcanic plutons formed by successive rhyolitic intrusions (to account for their low density) are interpreted to be the magnetic crustal masses (Soengkono, 2011).

Aeromagnetic surveys conducted by helicopter were flown over Wairakei in 1990 and Tauhara in 2008 for Contact Energy that offered more detail (Hunt et al., 2009). Buried volcanic magnetised bodies such as rhyolite domes and lava flows were discovered at shallow levels, improving the information on the stratigraphy but more importantly allowed aquifers to be targeted for shallow injection and the installation of monitoring wells (Hunt et al., 2009).

2.3.4 Structure

Updated basement regional structure data from Rowland and Sibson (2001) and basement surface contours from drillhole data (Rae et al., 2007) indicates that beneath Wairakei-Tauhara the likely basement structure is a northeast striking graben that deepens towards the west (Rosenberg et al., 2009). Drillhole data is from the Rotokawa and Ohaaki fields 10 and 25 km east to northeast of the Wairakei-Tauhara fields.

An upfaulted block of Wairakei Ignimbrite in the Wairakei field has fault controlled basins on either side (Bignall et al., 2010). This block is a part of a horst and graben like structure which makes up the core structure of the Wairakei-Tauhara system. Continuing towards the Tauhara field in the east, a broad fault set related to the upthrusted Wairakei block affords a geometric control on the Wairakei Ignimbrite.

Lying to the southeast of the Wairakei upfaulted block are planar and stratified acid volcanics associated with the Tauhara Geothermal Field.

This sequence of flat-lying volcanics form a shallow basin that thins to the north, west and south of the Tauhara field and is at its thickest near TH1 (west of Mt Tauhara). The shallow basin extends eastwards beneath Mt Tauhara which conceals the basins eastern margin. This broad basinal structure is also demonstrated by Bouguer gravity anomalies and low magnetic values and is on the southern margins of the Taupo-Reporoa depression (Grindley, 1974).

2.3.5 Local and regional faulting

Closely spaced high angle normal faults striking NE to SW, cross the Wairakei-Tauhara fields (Figs. 2.3. 2.5). Some scarps have remained from the 1922 and 1983 Taupo earthquakes that caused ground rupture on the Kaiapo Fault. Recently deposited volcanic products have since obscured most surface traces of faults or they have been eroded. However, fault zones are probably responsible for influencing the upflow of reservoir fluids at Wairakei-Tauhara, especially those that were active in the late Quaternary (Rosenberg et al., 2009; Bignall et al., 2010).

From geodesy studies, approximately 2-8 mm of crustal extension in a NW to SE direction occurs in the TVZ per year. Oblique extension from NE to SW may accommodate some of the stress between rifting portions (Rowland & Sibson, 2001; 2004). Fault activation and deformation connected to the rifting sustains fluid pathways in the host rock (greywacke, lava, welded ignimbrite). Geothermal fluids are then spread through more permeable pyroclastic strata.

The suggestion that feed zones may correlate with fault zones made by Grindley, (1965) was supported by breccia and slickenside textures found in several Wairakei wells but permeability associated with faults in the volcano-sedimentary succession although possible, is still not conclusively proven. Recent drilling at Wairakei-Tauhara has shown that in well cuttings from permeable zones do not show any distinctive fabrics and mapped surface faults are not soley responsible for the formation of permeable zones. Completion tests (where wells are left to heat up to

their pre-drilling temperature) show areas and points (feed zones) of high permeability. These areas are associated with intraformational contacts such as those between flow units in the Waiora Ignimbrite (Wa1) or inter formational contacts such the breccia, rhyolite and andesite lava bodies within the Waiora Formation or the underlying contact of the Tahorakuri Formation.

Compared to the Wairakei field in the northwest, the Tauhara Geothermal field is not as strongly faulted. Young pumice alluvium and ash flows < 20,000 years old, are cut by minor fault traces. However a larger fissured zone linked to faulting was intersected in TH1 (at ~700 m). In the north-west of the Tauhara field this fault is downthrown and is likely related to basin subsidence. One of the main discharge points on the border of the Tauhara field is the Spa Sights thermal area on the Waikato River. At this location a pattern of small fracture lineaments is observed (Grindley, 1974).

2.3.6 Hydrology and groundwater

The prevailing opinion for how the geothermal fluids in the Taupo Volcanic Zone convect and create the modern active hydrothermal systems (Fig. 2.7) has evolved since the 1950s when geothermal exploration and research began in earnest. According to Rosenberg et al. (2009) Wairakei and Tauhara Fields are sustained by separate upflows as indicated by geochemical differences in the fluids. In the top most 500-700 m the boundary between the two fields merges, the shallower fluids are dispersed to connect the two fields. The northeast to southwest resistivity boundary trend is interpreted to be the top of an upflow that runs parallel with the strike of the TVZ structure. Hydrothermally altered rock lying above the fluid upflow reflects the shape of the field boundary while its specific location is likely the result of a magmatic intrusion or heat source in the crust.

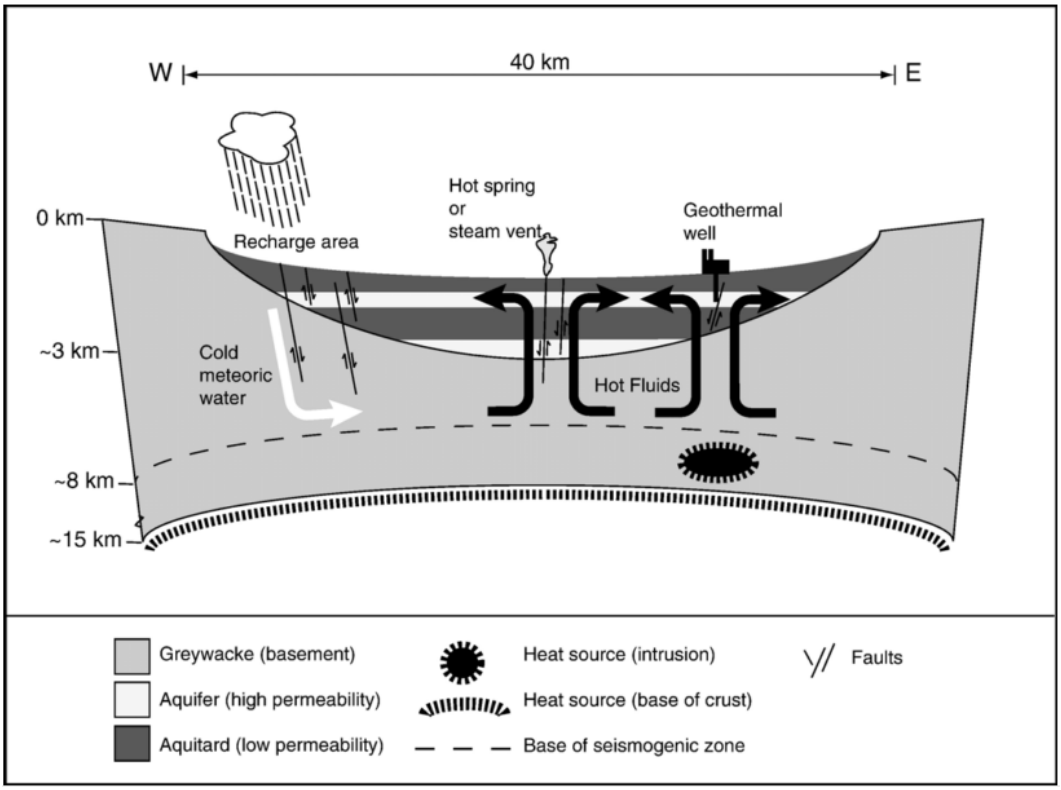

Fig. 2.7. Schematic diagram of the accepted model showing the basic structure and hydrology of the TVZ. The heat source is at the base of the crust with additional intrusions giving off heat. The basement greywacke stretching across the TVZ rift is shaded light grey, overlying the basement are formations that function as aquifers and aquitards (Hole et al., 2007).

Certain formations in the Tauhara geothermal field play key roles in the hydrology of the hydrothermal system at Tauhara. The Oruanui Formation and Taupo pumice (Recent Alluvium and Tephra) host groundwaters and hot water enabling residents of Taupo to tap into the shallow strata via shallow bores. The Huka Falls Formation acts as a leaky cap rock to the system with the thick mudstones of the Upper and Lower HFF acting as a mudstone aquiclude. Tuff and breccia in between these layers (Middle HFF) is another aquifer that hosts fluids of mixed origin which supplies the thermal activity seen around Taupo. The Waiora Formation hosts the main geothermal reservoir of chloride-rich fluid. This formation also contains impermeable mudstone layers and rhyolite breccias that may be aquifers (Bromley et al., 2009). The greywacke basement (ancient marine meta-sediments) will likely have fluid flow through fractures due to the rifting (Grindley, 1974).

Since development began at Wairakei-Tauhara, water levels, temperatures and chemistry changes in the groundwater aquifers lying above the geothermal producing

aquifers have been detected. Two sectors of the Wairakei-Tauhara system have seen the most notable changes. The Eastern Borefield and Alum Lakes at Wairakei experienced a decline in water levels due to pressure decline as fluid was extracted from steam zones lying underneath those areas (Bromley et al., 2009). Water levels could be maintained if a lateral groundwater inflow supply was able to negate the loss from downflow through existing fractures or when the stable steam zone pressures sustained water levels. At Tauhara in the Crown Road-Taupo Golf Course area, the water level of the steam heated Tauhara upper aquifer hosted in the Oruanui and Taupo formations declined, resulting in the demise of the Kathleen Spring and AC Spring but an increase in flowrate in nearby Otumuheke Springs. Continuous internal downflows from the upper to lower aquifers through boreholes is thought to have contributed to shallow aquifer drainage (Bromley et al., 2009).

In contrast, no significant change in the southern Tauhara sector of shallow aquifers (with a groundwater-deep chloride fluid mix) has been recorded even after 50 years of development. An explanation for this is that the southern area is supplied by an independent upflow that remains impervious to pressure drawdown, or a two phase upflow supplies continuous chloride water recharge beneath Mt Tauhara, or a southern groundwater aquifer with a mass of chloride water is unaffected by hot fluid recharge.

2.3.7 Regional and surface geology

The regional geology was illustrated by Grange (1955). Grindley (1965) further outlined the geology of the Wairakei geothermal field (Fig. 2.8). The Wairakei-Tauhara area mostly consists of pyroclastic fall and flow units outcropping on the surface and sediments that derive from them. The most obvious feature that outcrops on the surface in the Tauhara Geothermal Field is Mt Tauhara, a composite volcano aged at least 190 ka built from dacite domes, breccia and pyroclastic deposits. It is described later in this chapter under Tauhara Dacite. Local hills that outcrop are composed of small rhyolite domes such as Maunganamu Hill (south of Mt Tauhara) and Ngangiho in the north of Wairakei (Rosenberg et al., 2010).

The 26,500 year old Oruanui ignimbrite of the Oruanui Formation surrounds Mt Tauhara. This plateau is covered by fall and flow pyroclastic deposits from the TVZ with interbedded paleosols and recent stream and lake alluvium. Fall and flow deposits (ignimbrite) from the 1.8 ka Taupo eruption stretch across the region. In the lower right corner of the map is the Rangitaiki Ignimbrites (Fig. 2.8). Following the Oruanui and Taupo eruptions, pumiceous sediment derived from the eruption products and subsequent break out floods were deposited, building terraces in the valley (Manville, 2002).

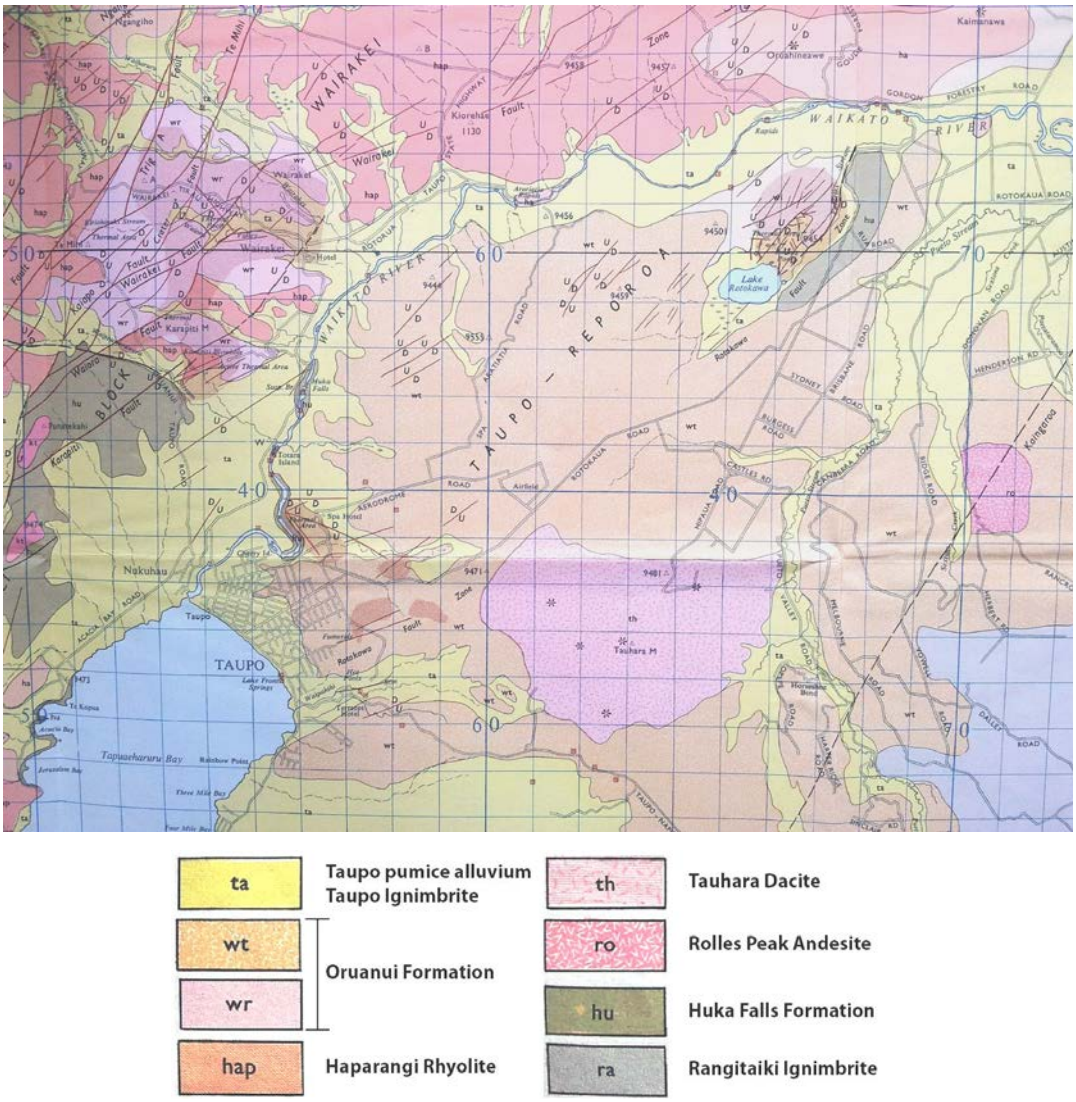

Fig. 2.8. Section of surface geology surrounding the Tauhara Geothermal Field (west of the Waikato River) taken from Grindley (1965). An updated map is unavailable. East of the Waikato River is the Wairakei Geothermal Field.

2.3.8 Stratigraphy

The stratigraphy of Tauhara (Fig. 2.9) starting from the surface with depth starts with superficial deposits and tephra which is underlain by the Oruanui Formation. Beneath the Oruanui Formation is the Huka Falls Formation subdivided into the Upper, Middle and Lower Huka Falls Formation members. Underlying the Oruanui Formation is the Waiora Formation in which Grindley (1965) has distinguished five members: the basal unit is Wa1, the Waiora Ignimbrite. The Crowbar and Racetrack Rhyolite bodies are found interbedded in this formation. Following the Waiora Formation is the Wairakei Ignimbrite, andesite lava and breccias further underlain by the Tahorakuri Formation.

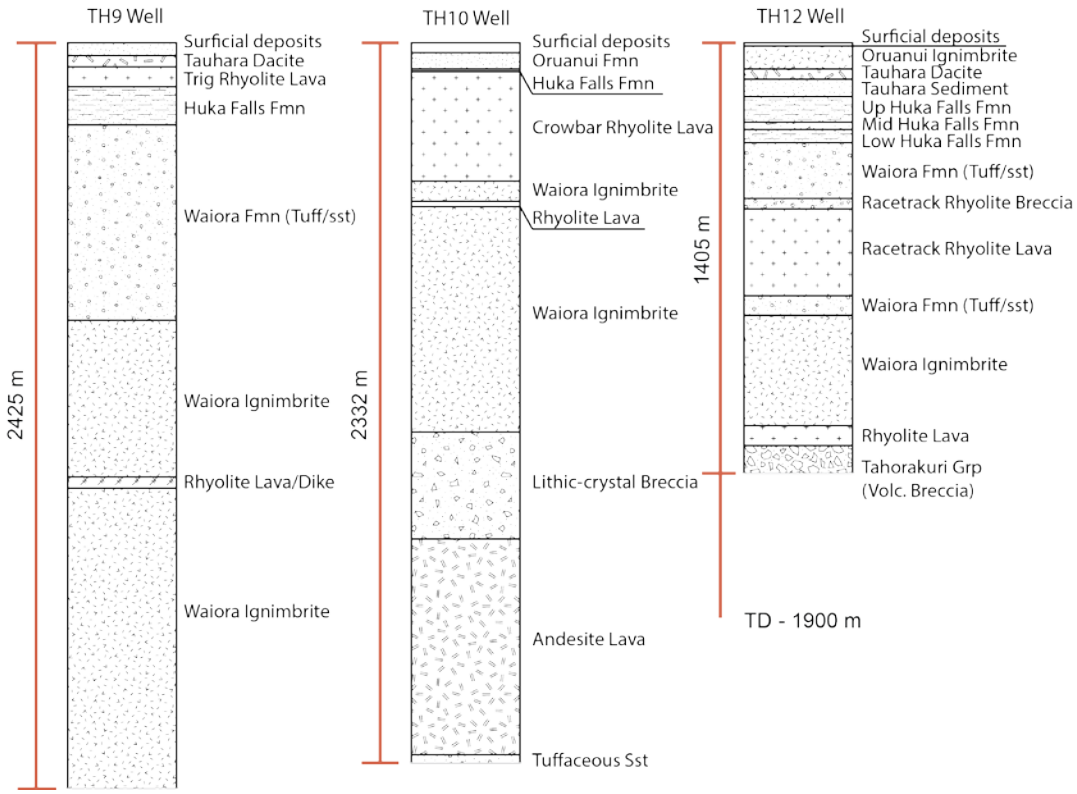

Fig. 2.9. Stratigraphic logs from wells TH9, TH10 and TH12. TD=total drill depth.

Superficial deposits and Tephra

Superficial deposits comprise material from either the 1.8 ka Taupo eruption (Wilson, 1993) or material before that eruption but post-date the Oruanui Formation. Material derived from the eruption consists of pyroclastic fall, non-welded ignimbrite with minor lacustrine and fluvial pumiceous sand. Breccia deposits from hydrothermal

eruptions are distributed locally (Browne & Lawless, 2001). Compared to the younger Taupo layers, the older post Oruanui sequence is very diverse in origin because of 20,000 years of landscape evolution (Rosenberg et al., 2009). Volcanic ash and pumice fall from small to moderate silicic eruptions mantle the surface (Wilson, 1993) interspersed with paleosols, andesitic cryptotephra and basaltic tephra sourced from Ruapehu, Taranaki and Tongariro volcanoes with some sedimentary and aeolian deposits. Permeable beds within the surficial deposits (Taupo and Oruanui tuffs) host shallow groundwater aquifers containing cold and thermal waters. The residents of Taupo Township have hot water bores supplied by these perched reservoirs (Bignall et al., 2010).

Tauhara Dacite

Mt Tauhara and the Tauhara volcanic complex lie partly in the Taupo Volcanic Centre and on the rim of the Maroa Volcanic Centre. Mt Tauhara is constructed from at least seven dacite domes, lava flows, breccia and locally distributed pyroclastic flows making it a composite volcano (Graham & Worthington, 1988). The main complex is not yet radiometrically dated, but lava from one of the domes, the Hipaua dome is dated at 190 ka (Wilson et al., 1995). The Hipaua and Trig M domes are both older than Breached dome while other domes are physiographically younger (Graham & Worthington, 1988). On the western side of Mt Tauhara (well TH3) sediments in the HFF have evidence of remains of a previously erupted dacite. This finding contrasts with wells drilled towards the north, northwest and south of Mt Tauhara where layers of dacitic lava, pyroclastic and weathered debris post-date Trig Rhyolite and the HFF. These layered deposits may function as pathways for meteoric water to enter groundwater aquifers or the shallower geothermal reservoirs (Rosenberg et al., 2009). According to Graham and Worthington (1988), three separate magma bodies are responsible for forming Tauhara dacite by mixing rhyolite and two andesite compositions.

Oruanui Formation

The Oruanui Formation includes the Wairakei Breccia, Wairakei Formation and Wairakei Lapilli Tuff (Wilson, 1993; Wilson, 2001). These are all synonyms ascribed to one catastrophic eruption that occurred 26,500 years ago beneath the former Lake Taupo that produced pyroclastic flow and air fall deposits (ignimbrite and tuffs) (Wilson, 2001). Fine accretionary lapilli occur at the base of the formation in an ash tuff unit. This lithological sequence rarely exceeds 120 m in thickness at Tauhara and hydrothermally altered ignimbrite is exposed in the northwest of Wairakei (Bignall et al., 2010). It is highly permeable and consequently is able to supply shallow boreholes in Taupo Township with hot fluid and steam. However, the Oruanui formation lies at shallow levels and is unable to be productive as a geothermal reservoir (Rosenberg et al., 2009).

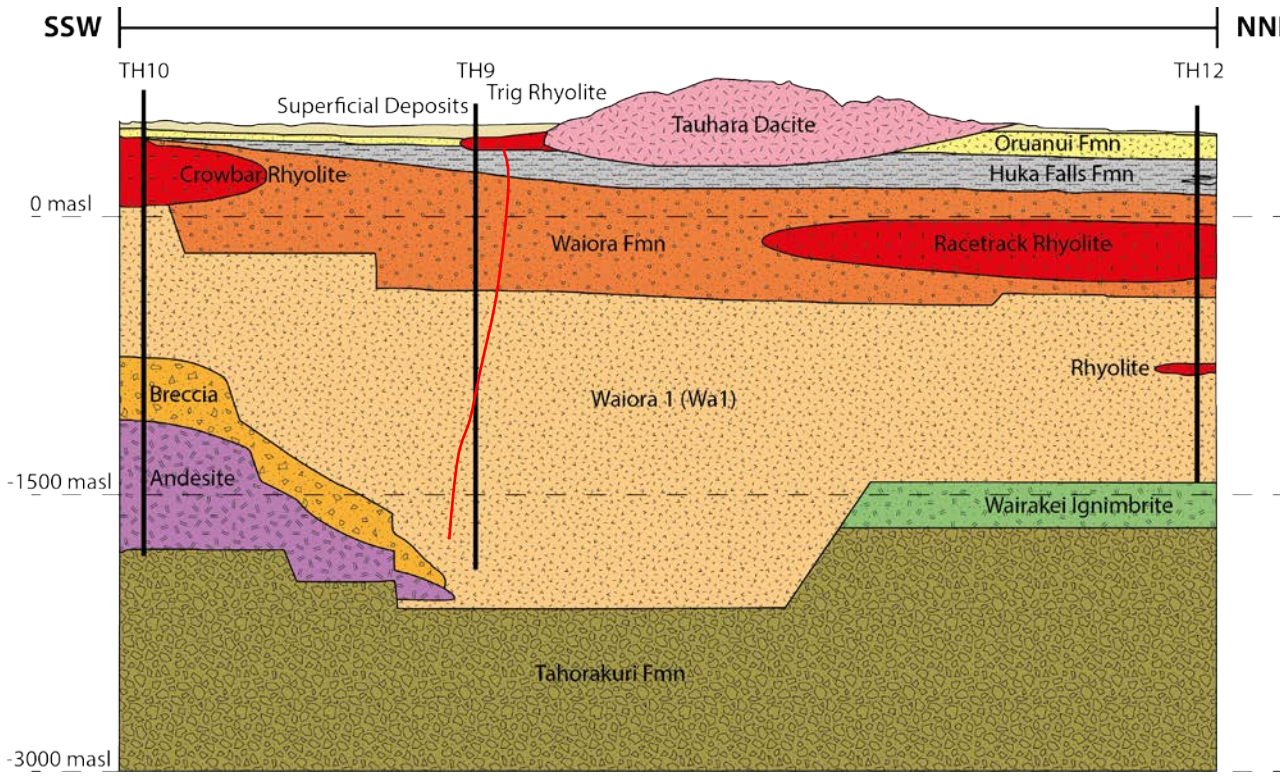

Fig. 2.10. Schematic diagram of the stratigraphic architecture of the Tauhara Geothermal Field according to the wells in this study. Red line is an interpreted rhyolite dike. (redrawn with permission from Contact Energy Ltd).

Huka Falls Formation (HFF) - Upper, Middle and Lower HFF

The Huka Falls Formation encompasses all material that sits between overlying Oruanui Formation and underlying Waiora Formation and is split into three members: the Upper, Lower and Huka Falls. An older classification scheme used by Grindley (Hu1, Hu2, Hu3, Hu4 units) to describe the Huka Falls Formation stratigraphy has been incorporated into the three members now used. The Upper and Lower members mainly consist of fine-grained lacustrine sedimentary rocks (mudstone, siltstone, sandstone) that behave as aquicludes but are locally interbedded with rhyolites (e.g. Trig Rhyolite; Grindley, 1965). The Middle HFF on the other hand encompasses pumiceous tuff and conglomerate from reworked ignimbrites and because of its high permeability it functions as an aquifer at shallower levels. The HFF examined as a whole formation is important hydrologically as it acts as an aquitard between hot fluid in the Waiora Formation and shallow groundwater (Bignall et al., 2010).

The HFF amassed in a shallow basin >50 km across that stretched from present day Lake Taupo to Waiotapu. Before the 25.4 ka Oruanui super eruption and subsequent formation of Lake Taupo, the ancient lake Huka was either one large lake or multiple small lakes in the Wairakei-Tauhara area (Cattell et al., 2015). Well TH10 is sited on the margins of the Huka Lake system (Cattell et al., 2015). The HFF is undated but is inferred to be late Castlecliffian to early Hawera Stage in age due to the pollen assemblage (Grindley, 1965) and radiometric ages of the Oruanui Ignimbrite (26.5 ka) and Kaingaroa Ignimbrite (230 ka) on either side of it (Houghton et al., 1995). It is at least 28 ka, as the Trig 9471 and Rubbish Top Rhyolites that lie within it are correlated with ~28 ka Poihipi tephra (Charlier et al., 2005). Thinly bedded siltstone megaliths correlated lithologically with the HFF were incorporated into the growing phase of the 190 ka dacitic Hipaua dome (Wilson et al., 1995) hence the HFF is at least as old as the Hipaua dome (190 ka) (Rosenberg et al., 2009).

Racetrack, Crowbar and Trig Rhyolites

Five rhyolite lava bodies and intrusions (dykes) have been intersected at Tauhara as shown in TH9 (Milicich et al., 2009) and TH18 (Ramirez et al., 2009) from drilling since 2005 onwards. In wells TH11, TH12 and TH18 the Racetrack Rhyolite occurs

beneath the Wa3-4 tuff and breccia unit. The Racetrack Rhyolite is a ~300 m thick flow-banded, porphyritic, spherulitic lava body with no other correlatives (Rosenberg et al., 2009). It is cream to grey with phenocrysts of quartz, feldspar, rare pyroxene and hornblende. A 30 m thick breccia containing spherulitic rhyolite lithics (probably incorporated Racetrack Rhyolite) overlies the Racetrack Rhyolite. The Racetrack Rhyolite lies on the northern side of Mt Tauhara (Fig. 2.11).

At the southern end of Tauhara in TH10 is the Crowbar Rhyolite Lava, also flow banded, porphyritic, spherulitic and 350 m thick (Rosenberg et al., 2009). This unit lies within the Waiora Formation tuff unit and beneath HFF siltstone. It is has phenocrysts of quartz, feldspar and rare pyroxene. The closest rhyolite is sub-aerial, cropping out on Maunganamu Hill but is not related as unlike the Crowbar Rhyolite it has hornblende phenocrysts and is quartz free (Graham & Worthington, 1988).

Both Racetrack and Crowbar Rhyolites are proposed members of the Waiora Fmn. Rhyolitic lavas and breccias are important in terms of Waikraei-Tauhara stratigraphy and hydrology. Their presence indicates prolonged local silicic volcanism before the ~0.32-0.34 Ma Wairakei Ignimbrite during the accumulation of the Waiora Formation (Crowbar and Racetrack Rhyolites) right through to recent volcanism (28 ka Trig Rhyolite) (Bignall et al., 2010).

On the western side of Mt Tauhara is the Trig Rhyolite, a grouping term for two small, young, coalesced rhyolite domes (Trig 9471 and Rubbish Tip). They have a distinctive $^{87}Sr/^{86}Sr$ isotopic signature (0.70526-0.70530), are crystal rich and have phenocrysts of plagioclase + quartz + pyroxene + hornblende + biotite (Graham & Worthington, 1988; Sutton et al., 1995). At shallow levels In TH3 rhyolite breccia was encountered and in TH9, TH11 and TH14 rhyolite lava bodies up to 100 m thick were intersected. The rhyolite lavas have a minimum volume of 0.5 km^3, an extent of ~5 km^2 and are situated beneath the Tauhara Dacite but above the HFF. Its correlation with the Poihipi tephra (~28 ka) makes it the youngest rhyolite across the Tauhara and Wairakei fields (Rosenberg et al., 2009).

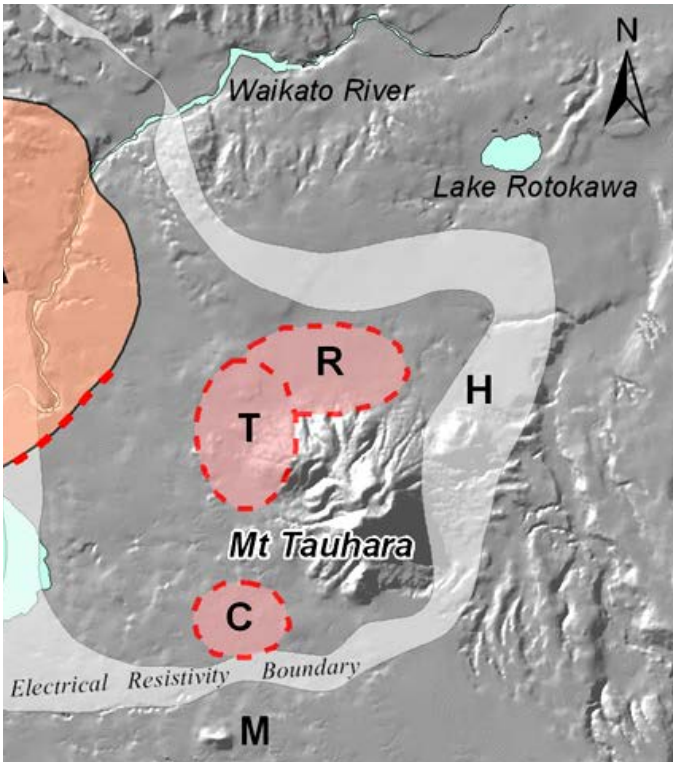

Fig. 2.11. Location of Racetrack (R), Trig (T) and Crowbar (C) Rhyolites, H=Hipaua dome, M=Maunganamu Hill. Modified from Rosenberg et al., (2009).

Waiora Formation

Thick volcanic deposits with interlayered mudstones and sandstones comprise the Waiora Formation. The Waiora Formation is laterally interbedded with rhyolite bodies such as the Crowbar and Racetrack Rhyolites. In the southeastern part of Tauhara in wells TH9 and TH10 Waiora strata is the thickest at >2100 m. Towards the west in Wairakei Waiora strata is the thinnest at ~400 m (Rosenberg et al., 2009). The Waiora Formation that is split into 5 members as described by Grindley (1965): Wa5 is ignimbrite and tuff, Wa3 and Wa4 is coarse bedded tuffs, breccias, sandstone and siltstone inter-bedded together, Wa2 is siltstone and basal member Wa1 is non-welded/welded ignimbrite that is also referred to as the Waiora Ignimbrite. Wood (1994) surmised that the Waiora Ignimbrite (Wa1) may be petrogenetically related to the Wairakei Ignimbrite.

The subdivided members can be correlated across the Wairakei and Tauhara but not all are continuous across the fields. According to Rosenberg et al. (2009) and Bignall et al. (2010), Grindley's (1965) five member classification scheme is difficult to apply at Tauhara because of the considerable variety in textures, although

it is a practical starting point from which to become familiar with the stratigraphy. As a result the only member that easily distinguished is Wa1 (Waiora Ignimbrite). The current classification is simplified further by merging Wa3 and Wa4 as Wa3-4 as proposed by Rosenberg et al. (2009).

At Tauhara, the upper layers of the Waiora Formation (Wa5) contain more fine grained muddy beds than coarse volcanic beds. Consequently the boundary is blurred between the overlying HFF making it difficult to distinguish the two formations, even though the boundary is likely spatially gradational. The highest temperatures occur in the Wa3-4 breccias but all horizons are equally productive. Wa5, the upper unit of the Waiora Formation functions as a steam aquifer at Te Mihi, Wairakei, whereas Wa2 forms aquicludes locally because of its lower permeability. The Wa1 member (Waiora Ignimbrite) is not understood completely, as its permeability mechanisms and spatial extent are unknown. However the edges of a flow unit(s) or welding zones appear to influence feed zones.

The accumulation of the Waiora Formation material began ca. 320 ka but no geochronological study has been undertaken to date the ignimbrites or lavas. Ages of the overlying HFF and constituents within the formation itself are also unknown making the duration of formation difficult to determine. Dating and genetic connections between formations and intrusions across neighbouring geothermal fields would improve understanding of hydrothermal system evolution and volcanic genesis.

Wairakei Ignimbrite – Whakamaru Group

The Wairakei Ignimbrite is a member of the >320-340 ka Whakamaru Group of ignimbrites that erupted at time when caldera volcanism was at its most intense in the TVZ (Houghton et al., 1995). Multiple flow units of the Whakamaru Group are accepted by a number of authors (Rosenberg et al., 2009). The Wairakei Ignimbrite is crystal rich, moderately welded with abundant feldspar and resorbed quartz phenocrysts 1-5 mm in size, accessory orthopyroxene, biotite and hornblende, with traces of pumice, volcanic and sedimentary lithics. At Tauhara occurs in TH12 (1425 mRSL, metres relative sea level) but is absent in TH9 and TH10 (1800 mRSL)

to the southern parts of Tauhara. This evidence indicates that from well WK305, east of the Wairakei power station the Wairakei Ignimbrite continues laterally towards the eastern edge of Tauhara field but not to the south. A wide series of fault structures is thought to control the geometry of the Wairakei Ignimbrite, explaining its absence in TH9 and TH10 and presence in TH12 as the fault set continues east across both the Wairakei-Tauhara adjoining system (Rosenberg et al., 2009).

The permeability controls, extent and thickness of the Wairakei Ignimbrite is not entirely understood as in some wells of the Wairakei field (WK305, WK307, Fig. 2.5) permeability is fracture controlled while in others there is a lack of permeability (WK121, 970 m). Other mechanisms for permeability might be from formational contacts (Bixley et al., 2009) or the Whakamaru group ignimbrites themselves which in outcrop have widely spaced 1-3 m columnar joints from which fluid flow can travel vertically and laterally at depth. Nonetheless, it appears fluid flow in the Wairakei Ignimbrite is controlled by fractures and intraformational pathways which may have been modified by tectonic strain or local hydrothermal mineral precipitation (Rosenberg et al., 2009).

Lithic crystal Breccia, Andesite Lava and Tuffaceous Sandstone

In TH10 three units (Lithic crystal Breccia, Andesite lava and Tuffaceous Sst) not previously intersected by any Tauhara well were added to the stratigraphy of Tauhara (Milicich et al., 2008). The lithic crystal breccia is a grey to cream andesitic lava breccia that is crystal rich with primary phenocrysts of pyroxene, hornblende, feldspar and rare quartz. The andesite lava itself is porphyritic, pale grey to green-pink, and like the breccia has abundant phenocrysts of feldspar, pyroxene, hornblende and rare quartz. Crystal sizes and rock texture vary throughout suggesting this is a composite of several flows.

There is no age control for the andesite because the ca. 320 ka Whakamaru ignimbrite was not intersected by TH10 and TH9 and none of the Waiora Formation strata has been dated which otherwise would give an idea of its age and relationship to other units. The spatial relationships and age are important because of the lateral connections with the Waiora Formation towards the north. In TH10, textural or

alteration mineral evidence indicating fault zones is absent, therefore feed zones are probably not fault controlled and instead linked to the lava and breccia units (Milicich et al., 2008). The Tuffaceous Sandstone was penetrated in the last 12 m of well TH10, consequently the extent and depth is not well known. It contains tuff lithics, angular to sub-rounded quartz and feldspar fragments and is moderately to highly altered (Milicich et al., 2008).

Tahorakuri Formation – Reporoa Group

The Tahorakuri Formation is yet to be penetrated by Tauhara wells but is likely to be regionally extensive (Rosenberg et al., 2009). Previously named the Ohakuri Group for all units pre-dating >320–340 ka Whakamaru Group ignimbrites at the Wairakei field (Houghton et al., 1995) it was redefined by Gravley et al. (2006) as the Reporoa Group. The Reporoa Group consists of two formations, the Tahorakuri and Waikora. The Tahorakuri formation refers to the units in between the Whakamaru group ignimbrites and the greywacke basement such as pumiceous lithic tuff and partially welded ignimbrite. It is a composite at least 650 m thick but >1100 m in some Wairakei wells, however no Tauhara wells have drilled into it. It is similar in character and origin to the volcanic and sedimentary strata in the Waiora Formation but has more andesite lava and breccia (Rosenberg at al., 2009).

Greywacke Basement

The Torlesse Terrane composed of Jurassic volcaniclastic sandstones, hosts the deep fluid and heat source critical to the geothermal systems and is the geological basement of the TVZ (Figs. 2.5, 2.7). The greywacke basement has only been intersected in the northeastern part of the Tauhara field in TH17 at ~1500 m and is yet to be intersected at Wairakei (Rosenberg et al., 2009). The suggested basement structure underneath the Wairakei and Tauhara system is a basement graben striking northeast and deepening towards the west (Bignall et al., 2010). This conclusion is based on basement surface contours, the regional basement structure (Rowland & Sibson, 2001) and drillhole data from Rotokawa and Ohaaki geothermal fields (Rae et al., 2007).

2.4 SUMMARY

The modern location and geometry of the TVZ is a result of subduction migration, slab roll-back and tectonic evolution. The TVZ is the latest expression of arc volcanism and since 340 ka it has formed into a rift system that is segmented structurally and magmatically allowing the TVZ to be subdivided into three segments: two northern and southern andesitic to dacitic segments associated with composite volcano construction and a central zone representing large scale voluminous rhyolitic volcanism and caldera formation. Volcanic hosted hydrothermal systems lie in all segments, but most of the high temperature liquid dominated geothermal systems (>250 °C) lie between the silicic calderas of Okataina and Taupo.

The TVZ represents a continental arc and back-basin littered with strike-slip faults and undergoing extension. These two factors are responsible for the multiple calderas and associated geothermal systems as extension provides a weaker zone in the crust for magma to penetrate. Many hydrothermal systems are also located above the NE to SW oriented faults as they provide permeable pathways for ascending hot fluids and therefore form individual convecting hydrothermal systems.

The geology of the Tauhara Geothermal Field is summarised below:

- Superficial Deposits and Tephra (Rosenberg et al., 2010) underlain by the Oruanui Formation. In well logs, material in the first 50 metres below the rig floor (mRF) is usually combined into surficial deposits comprising recent alluvium and tephra (Rosenberg et al., 2010).

- Below the recent alluvium and tephra, is the Oruanui Formation, a sequence of tuffs and ignimbrites that are products of a single eruption from the former Lake Taupo 26,500 years ago (Wilson, 1993; Wilson, 2001; Bignall et al., 2010).

- The Oruanui Formation is underlain by the Huka Falls Formation (HFF) which is subdivided into the Upper, Middle and Lower Huka Falls Formation

members. The Upper and Lower members mainly consist of fine-grained lacustrine sedimentary rocks (mudstone, siltstone, sandstone) that behave as aquicludes but are locally interbedded with rhyolites (e.g. Trig Rhyolite; Grindley, 1965). The Middle HFF on the other hand encompasses pumiceous tuff and conglomerate from reworked ignimbrites and because of its high permeability it functions as an aquifer at shallower levels. The HFF examined as a whole formation is important hydrologically as it acts as an aquitard between hot fluid in the Waiora Formation and shallow groundwater (Bignall et al., 2010).

- Underlying HFF is the Waiora Formation that is split into 5 members as described by Grindley (1965): Wa5 is ignimbrite and tuff, Wa3 and Wa4 is breccia, tuff, sandstone and siltstone inter-bedded together, Wa2 is siltstone and basal member Wa1 is non-welded/welded ignimbrite that is also referred to as Waiora Ignimbrite. These members are not present continuously across Wairakei and Tauhara Fields. Rosenberg et al. (2009) proposed a simplification of the Waiora Formation subdivision and grouped members Wa3 and Wa4 into Wa3-4 member which is the classification currently in use. The Waiora Formation is laterally interbedded with rhyolite bodies such as the Crowbar and Racetrack Rhyolites. The Waiora Formation is the main geothermal producing reservoir in the Tauhara hydrothermal system due to the inherent permeability of units within the thick formation. For example rhyolite intrusions cause fracturing in the country rock, cooling fractures in ignimbrites and interconnected pores in volcaniclastic units provide permeability. Feed zones in the Lithic-crystal Breccia and Andesite Lava units are not fault controlled but rather linked to the units themselves.

- Underlying the Waiora Formation is the Wairakei Ignimbrite, from the Whakamaru Group (Rosenberg et al., 2009; Bignall et al., 2010), which is crystal-rich and moderately welded. The Whakamaru Group is recognised as having multiple flow units. In some wells the Wairakei Ignimbrite is absent (TH9, TH10), but is present in TH12 suggesting that the Wairakei Ignimbrite is geometrically controlled by horst and graben fault structures (Rosenberg et

al., 2009; Bignall et al., 2010). Fluid flow in the Wairakei Ignimbrite is controlled by fractures and intraformational pathways.

- Below 1000 mRSL, the deeper stratigraphy of Tauhara is dominated by rhyolite and andesite lavas further underlain by volcanic (welded or non-welded pyroclastic units), volcaniclastic and sedimentary units of the Tahorakuri Formation (Gravley et al., 2006, Bignall et al., 2010). The underlying Jurassic greywacke basement rocks, intersected elsewhere in the Taupo Volcanic Zone, such as in Rotokawa, Ohaaki, Ngatamariki and Kawerau geothermal fields, have been intersected by only one well in the whole Wairakei-Tauhara region (well TH17, northeastern boundary of the Tauhara Field) (Rosenberg et al., 2009; Bignall et al., 2010). The Torlesse Terrane greywacke basement holds the deeper fluids and heat source critical to geothermal systems.

Chapter 3
Hydrothermal alteration

3.1 INTRODUCTION

Hydrothermal alteration minerals are formed by fluid rock interactions (at high or low temperatures) and can be used to assess the physical and chemical conditions such as temperature, rock permeability and fluid acidity (Yang et al., 2001). Many alteration mineralogy and petrographic studies have been performed in a wide variety of settings as hydrothermal alteration is different in each individual deposit, field and region. From broad scale petrographic studies of the TVZ in the North Island of New Zealand (Cole, 1978, 1979; Wilson et al., 1995; Wilson & Rowland, 2011), to large connected systems for example the Wairakei-Tauhara system (Grindley, 1965; Steiner, 1977) to individual geothermal fields such as Ngawha, Ohaaki, Mangakino, Tauhara, Kawerau and Ngatamariki (Cox & Browne, 1998; Yang et al., 2001; Fagan, 2006; Rosenberg et al., 2009; Milicich et al., 2013; Chambefort et al., 2014).

In addition to studies on various geothermal fields, ore deposits and active hydrothermal systems have long been accepted to being closely related. Epithermal deposits are thought to be the fossil equivalents of once active geothermal systems with neutral pH hot springs and geysers (Hedenquist, 1991; Hedenquist & Lowenstern, 1994; Simmons & Browne, 2000; Simmons et al., 2005). Consequently this link has permitted analogues to be drawn between active geothermal systems during numerous studies on epithermal deposits (Simpson & Mauk, 2000; Christie et al., 2006; Cocker & Mauk, 2008).

This chapter will focus on what hydrothermal alteration mineralogy is, and discuss the factors that control hydrothermal alteration. It will also detail the formation of hydrothermal systems and resulting useful hydrothermal alteration mineral associations in geothermal exploration and evolution. It links closely with the

following chapter which describes the resultant hydrothermal alteration mineralogy and relict primary mineralogy of the Tauhara Geothermal Field.

3.2 HYDROTHERMAL SYSTEMS

In the Taupo Volcanic Zone (TVZ) there are over 23 geothermal systems that discharge 10^8 tonnes of hydrothermal water annually (Bibby et al., 1995). Hydrothermal convection originates from buoyancy as a result of density differences between the column of ascending fluid and the surrounding column of cooler fluid. At depths of over 5 km, meteoric water circulates, picks up magmatic volatiles (H_2O, HCl, SO_2, H_2S, CO_2) and constituents from water-rock interaction resulting in meteoric water transforming into a near-neutral pH chloride fluid (Browne & Lloyd, 1987; Giggenbach, 1995, 1997). This interaction produces hydrothermal plumes that have physical and chemical signatures (Bibby et al., 1995; Rowland & Simmons, 2012).

The origin of hydrothermal fluid can come from multiple sources, depending on the geological and tectonic environment (Kühn, 2004; Pirajno, 2009):

- Meteoric water and near surface groundwater. Isotopic evidence shows that the fluid encountered by drill holes, at least in the TVZ is essentially meteoric.
- Formation waters or connate waters released upon compaction.
- Magmatic or juvenile waters named ‘new’ water not previously part of hydrosphere derived from cooling igneous intrusions, or expelled from subduction processes.
- Fossil water, enclosed in deep rock formations, out of contact with atmosphere such as deep fossil marine waters.
- Metamorphic fluids where hydrous minerals recrystallise into anhydrous minerals leaving leftover water to circulate.
- Seawater infiltrated at mid oceanic ridges.

Subsequently hydrothermal alteration can occur in a variety of different geologic settings for example mid-ocean ridges, orogenic terranes and volcanic environments (Fig. 3.1).

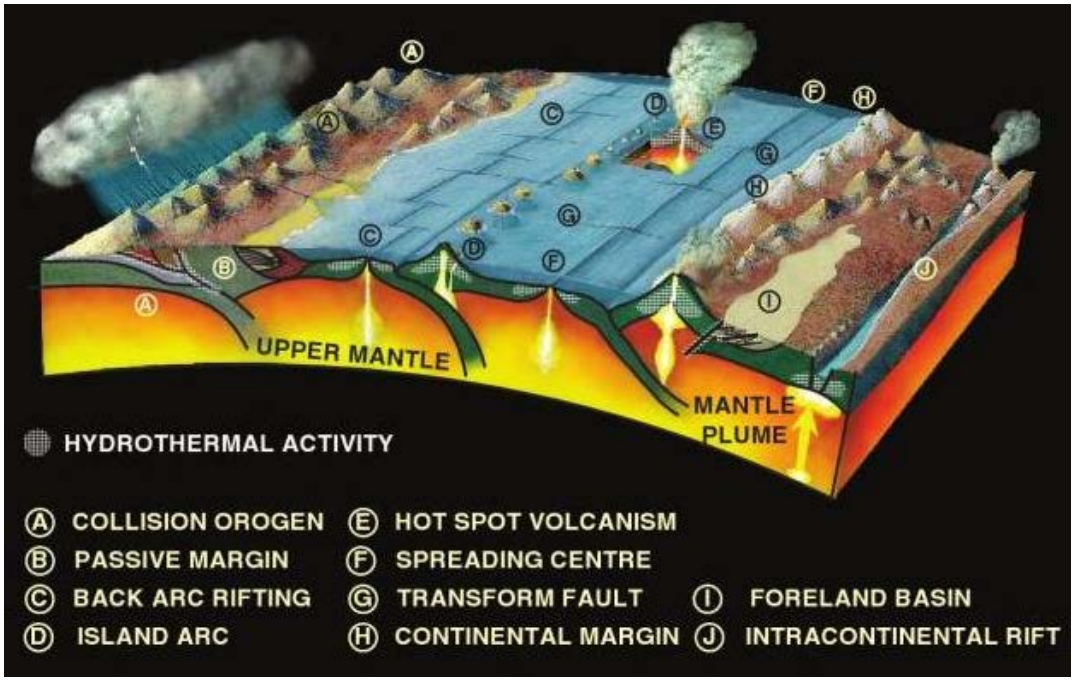

Fig. 3.1. Environments of hydrothermal activity (Pirajno, 2009).

3.2.1 Classification of hydrothermal systems

Temperatures of 275 °C or below are relatively common in active high temperature hydrothermal systems, whilst some can reach temperatures over 350 °C e.g. the Salton Sea, California (360 °C). White, Muffler and Truesdell (1971) showed that generally water dominated convective hydrothermal systems fall into three categories: high temperature (>150 °C), intermediate temperature (90 to 150 °C), and low temperature <90 °C.

Lindgren (1933) focused on classifying the deposits made by hydrothermal systems (like ore deposits) according to temperature: hypothermal describes a mineral deposit formed at great depths and temperatures of 300-500°C, mesothermal a deposit formed at moderate depths and 200-300°C temperatures, and epithermal a shallow forming vein deposit (within 1 km of the surface) at 50-200°C temperatures (Hedenquist & Lowenstern, 1994; Simmons et al., 2005).

Nicholson (1993), Pirajno (1992) and Heiken (1982) have also attempted to classify geothermal systems. Nicholson (1993) categorises geothermal systems using terms that describe the type of geothermal reservoir. Pirajno (1992) focused on

categorising according to the mineral deposits generated and Heiken (1982) utilised the geological setting where each system develops in. Kühn (2004) has combined these last three author's schemes into one (Fig. 3.2).

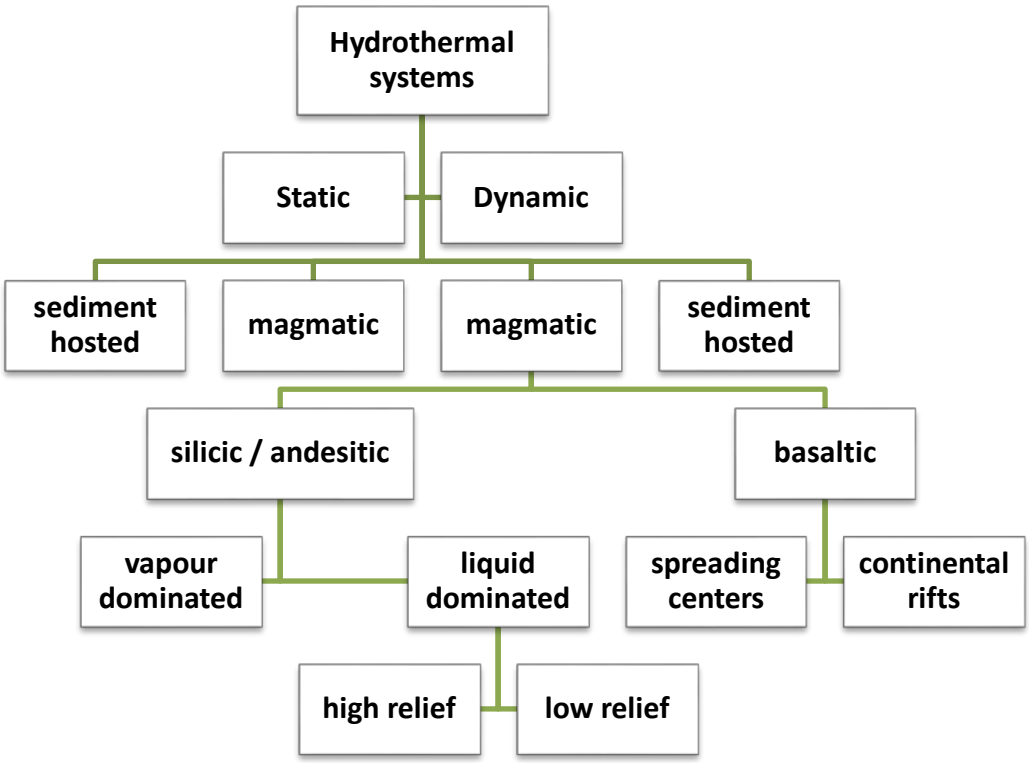

Fig. 3.2. Classification of geothermal systems (redrawn from Kühn, 2004).

3.2.2 Anatomy of a hydrothermal system

A hydrothermal system is a naturally occurring system that describes how hot fluids travel and move in the earth's crust beneath the surface, in a variety of settings. A hydrothermal system requires three fundamental elements to function: a heat source, convecting fluid and host rock to hold that convecting fluid (Pirajno, 2009). There are three aquifer zones that are hosted by rock formations in the TVZ geothermal fields (Bignall, 2009). Host rock contains meteoric groundwater at shallow levels, chloride-bicarbonate waters at depth and a chloride reservoir at 290 °C below 1000 m, which in the Tauhara Geothermal Field is the Waiora Ignimbrite.

The fluids migrate vertically, diagonally and laterally and also move at different temperatures and pressures. The heat source circulates the fluid through a system of

fractures, faults and permeable host rocks. As it migrates it mineralogically alters the host rocks, collecting minerals and metals and re-depositing them elsewhere to form veins, veinlets, vuggy textures (Browne & Ellis, 1970) or pervasively distributing minerals throughout the host rock. As the fluid moves upwards it may reach the surface and discharge as hot springs (surface manifestation), or remain subsurface and flow along permeable strata and/or structures (Fig. 3.3).

3.2.3 Magmatic high temperature systems

With the exception of Ketetahi, all New Zealand hydrothermal fields are liquid dominated (Browne & Lloyd, 1987). Based on the classification system (Fig. 3.2), the Tauhara geothermal field is a dynamic magmatic high temperature system in low relief silicic-andesitic terrain and is liquid dominated. Four settings in silicic or andesitic terrain are silicic volcanism, andesitic stratovolcanoes, highland volcanoes and volcanic islands. High temperature geothermal systems are hosted in these settings.

Liquid dominated systems are largely composed of convecting fluids. Near the surface of a system low porosity and high heat flow from convecting fluids combine to cause a steam zone to separate and develop (Henley & Ellis, 1983; Kühn, 2004). Liquid dominated systems may arise in two topographic terrains, high relief or low relief. In island arc settings, andesitic volcanoes are characteristic of high relief. Fumarolic activity, rock alteration and perched steam heated aquifers of sulphate-bicarbonate waters on volcanic slopes reveal the upflow part of the hydrothermal system (e.g. the Hakone Volcano, Japan and Kamojang system, Indonesia; Henley & Ellis, 1983). In high relief chloride water discharges are scarce due to a lower water table and are also far away from the geothermal reservoir as extensive lateral flows of hot fluid occur at distances of 20 km from the upflow zone (e.g. El Tatio, Chile) (Henley & Ellis, 1983).

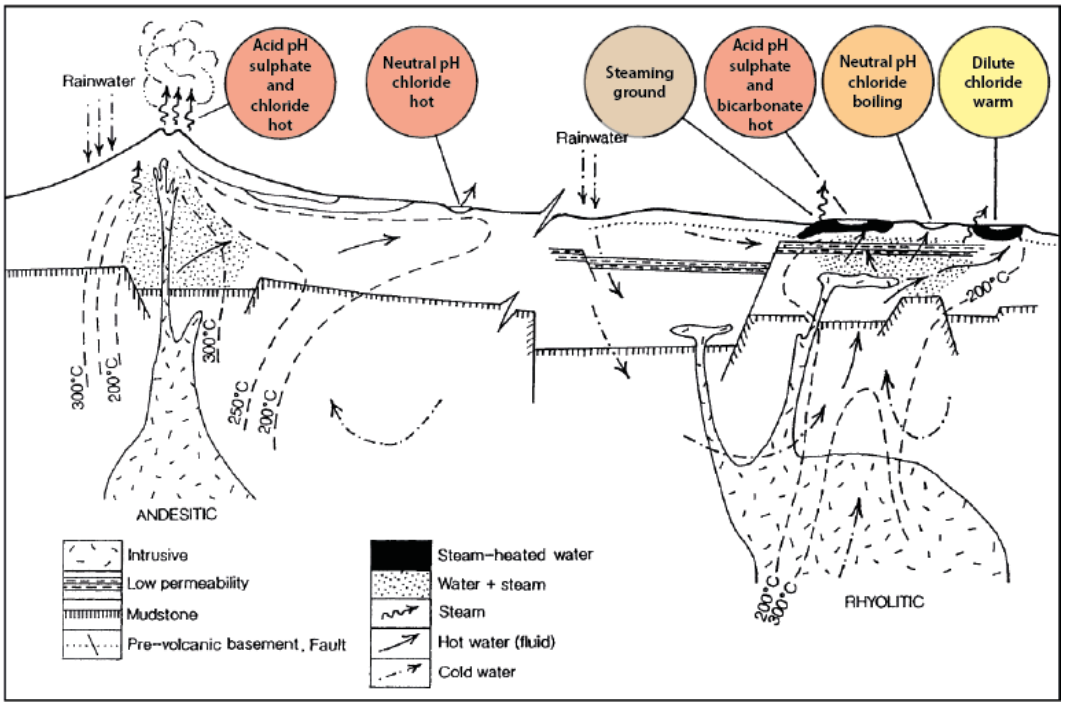

Fig. 3.3. Example of a high relief hydrothermal system in andesitic terrain and a low relief hydrothermal system in rhyolitic/silicic terrain (modified after Henley & Ellis, 1983; Hodder, 2008).

In low relief meteoric groundwater provides the recharge for the system and buried magmatic systems provide the heat source needed to drive the convective column consisting of near-neutral pH chloride water. In low relief settings, lateral flow is less extensive than high relief, consequently the surface activity like chloride hot springs, sulphate and hydrogen carbonate waters, fumaroles and steaming ground are closely situated (Henley & Ellis, 1983). These types of systems are found in NZ, USA, East Africa and Iceland.

3.3 ALTERATION MINERALOGY

Alteration mineralogy refers to the change in the host mineralogy as a result of rock and fluid (hydrothermal fluid) interaction, hence hydrothermal alteration (Allaby, 2008). Alteration occurs either isochemically or metasomatically. Fluid composition differs because the fluids contain varying types of brine (salts), gases, metals and water. The fluids carry metals in solution as different complexes, mainly involving sulphur or chlorine that are derived from an igneous source or leached out of rocks (Lagat, 2009).

When a rock is altered its mineralogy changes, the alteration (or secondary) minerals replace the original primary minerals because of the changed physicochemical conditions which occur (i.e. changes in temperature, pressure or chemical conditions; Lagat, 2009). Secondary minerals are formed as they are stable or at least metastable in these environments and seek to stay in equilibrium. As a result, the type of hydrothermal alteration minerals formed are dependent on a range of factors further outlined below. The location, extent and effect of hydrothermal alteration can be a combination of one or more of these factors (Browne, 1978).

3.4 CONTROLS ON ALTERATION MINERALOGY

A number of factors: temperature, permeability, fluid composition/pH, pressure, initial rock composition and duration of hydrothermal activity affect the formation of hydrothermal minerals. Some factors are more predominant in controlling alteration in certain geothermal fields compared to others (Browne & Ellis, 1970; Browne, 1978; Cox & Browne, 1998). For example at Ngawha, permeability plays a major role in controlling how circulating fluid and reservoir rocks interact, as well as determining what alterations form. In the TVZ, the reservoir rocks are pyroclastics and lavas compared to Ngawha in the northern tip of the North Island, where the reservoir rocks are greywackes and argillites. Greywacke and argillite have low permeability and almost no porosity but faulting at Ngawha has produced veins, joint channels and fracture zones enabling fluid to move (Cox & Browne, 1998). In contrast, TVZ geothermal systems have less veining but the pyroclasts and lavas are more permeable so fluids move via interconnected pores.

At the Salton Sea, the northernmost field in the Imperial Valley of Southern California, Muffler & White state that temperature is the main control on the low grade greenschist hydrothermal alteration assemblage that is present (Browne, 1978). Fluid composition plus temperature control the formation and distribution of hydrothermal minerals at the Cierro Prieto field in California. At the Otake field in north-central Kyushu, Japan, fluid composition closely controls alteration. Two fluids with unique chemical fingerprints have deposited minerals zoned around fractures (Browne, 1978).

3.4.1 Temperature

Temperature is considered to be one of the most significant factors in hydrothermal alteration. However, Browne (1978) suggests permeability and fluid composition are just as important as temperature. Temperature is critical because the chemical reactions that occur require elevated temperatures and at high temperatures, some minerals are thermodynamically stable. Temperatures can be distinguished by the occurrence of particular mineral assemblages (Gifkins, Herrmann, & Large, 2005). The position of the drill core or well in a geothermal field can also be deduced because certain minerals and mineral assemblages occur over a specific temperature range, thus characterising the proximal or marginal areas of a geothermal field or deposit (Browne, 1978).

3.4.2 Permeability

Permeability describes how easily a fluid moves through a rock (Allaby, 2008), typically through an interconnected network of pore spaces, fractures or joints. The permeability of a rock dictates the pathways that thermal fluids can infiltrate and move through the rock hence it controls the amount of interaction between reservoir rocks and fluids (Browne, 1970). As it moves, it hydrothermally alters the rock by replacing host minerals and precipitating secondary minerals in the spaces it moves through. Rocks with limited permeability will only be slightly altered e.g. some dense welded tuffs at Yellowstone and Wairakei remain only slightly affected because fluid access is limited (Browne, 1978).

The degree of permeability can also affect alteration type and intensity. For example, geothermal wells at Ohaaki Geothermal Field, New Zealand indicate a relationship between permeability and feldspar type. With increasing permeability, primary andesine alters to albite then to albite + adularia and finally adularia, signifying the highest permeability. Typically drillholes where there is unaltered andesine-albite are poorly permeable or non-producing, albite + adularia are moderately steam producing and adularia with abundant quartz and calcite are good steam producers (Browne, 1970). At Ohaaki, a large increase in potassium oxide (K_2O) is common in rocks situated in highly permeable zones (Browne, 1978). The relationship between

permeability and hydrothermal feldspars enables decisions to be made on the capacity of a drillhole to produce steam, the depth of production and the hydrological purpose of geological formations in the area Browne (1970).

3.4.3 Pressure

Pressures in reservoirs at depths drilled by geothermal wells rarely exceed 200 bars, which does not significantly influence the types of hydrothermal alteration minerals formed (Browne, 1978). However movement of hydrothermal fluids requires fluid pressure to exceed confining pressures (Hutchinson, 1983). This means the sum of the partial pressures of all the volatiles in the fluid such as H_2O, CO_2, CH_4 need to be considered. A change in fluid pressure also affects fluid composition (Browne, 1978). Fluid pressure indirectly affects hydrothermal alteration by controlling the depth where boiling occurs and where vapour and gases (CO_2) are lost. Hydrothermal quartz, K-feldspar and bladed calcite are typical where boiling occurs (Browne, 1978).

3.4.4 Composition

The composition of the host rock effectively determines what components will be leached to form the alteration minerals. Additionally fluid composition can be influenced by the composition of the magmatic source (Lagat, 2009). As host rock textures and porosities affect permeability, so does its chemistry influence the types of hydrothermal alteration minerals. This influence is strongest at lower temperatures (i.e., <200 °C). For example rhyolites at Yellowstone contain high silica zeolites such as mordenite, whereas lower silica zeolites, i.e. thomsonite, chabazite, occur in Iceland basalts and the andesites at Kamchatka (Browne, 1978). However, if temperatures are significantly greater than 280 °C, the stable alteration assemblage of albite, K-feldspar, chlorite, Fe-epidote, calcite, quartz, illite and pyrite results, regardless of host rock type, as is seen in the basalts of Iceland, rhyolites in New Zealand, Indonesian andesites and sandstones in the Imperial Valley (Browne, 1978; Henley & Ellis, 1983).

3.4.5 Fluid

Solutes in the natural waters can be divided approximately into two categories: Common rock-forming constituents, Si, Al, Na, K, Ca, Mg, Fe and Mn are available in abundance. Solubilities are limited by mineral-water equilibria, which favour the retention of elements in the mineral phases. A second class of soluble elements includes chloride, bromide, boric acid, arsenic, caesium which favour the liquid water phase (Ellis & Mahon, 1977).

Fluid chemistry and alteration mineralogy are closely related. Fluid composition is important as the metal complexes it carries will eventually precipitate as an ore deposit. Hydrothermal fluids both add elements to altered host rocks whilst removing others. Some of the more mobile components of a typical geothermal fluid include that are added to the host rock are: H_2O, Si, S, CO_2, K, Na, Ca, Mg, B, Cl, Li, P and others deposited as sulphides and oxides (Schwartz, 1959). Corbett and Leach (1997) state that fluid pH is one of the most important factors in alteration mineralogy as certain minerals are only stable under particular pH conditions.

Geochemical modelling of geothermal reservoir fluids using thermodynamic data has allowed us to predict and understand the distribution of alteration minerals. For example at Ohaaki geothermal field, New Zealand, high CO_2 concentrations in the fluid favours calcite deposition over epidote or wairakite (Browne, 1978). Most metals can be carried as various complexes and separate into a magmatic-hydrothermal fluid with chloride, bi-sulphide and hydroxyl-acid complexes. The mechanism by which metals concentrate in a hydrothermal fluid is not entirely understood but data available suggest that at low magmatic pressures, metals such as Cu can be scavenged from exsolving magmatic fluids (Hedenquist & Lowenstern, 1994). Estimating reservoir temperatures from the fluid chemistry is possible by the use of chemical geothermometers (e.g. silica) but these are based on the assumption that the fluid has achieved chemical equilibrium with the host rock.

3.4.6 Duration of activity, lifespan of a hydrothermal system

Hydrothermal systems are dynamic, changing due to natural evolution and with geothermal exploitation. Continuous activity at plate boundaries keeps the hydrothermal systems constantly renewed by a source of heat. However the lifespan of active hydrothermal systems is poorly constrained. Numerical modelling by Kissling and Weir (2005) demonstrated that the lifetime of TVZ geothermal fields is equivalent to the lifespan of the TVZ. Ellis and Mahon (1977) believe that many natural hydrothermal systems have been active for 10^4-10^5 years to several million years. Grindley (1965) proved that Wairakei is at least 500,000 years old while other fields such as the Great Geysir in Iceland is at least 10,000 years old and the Steamboat Springs system in Nevada, USA is 1 million to perhaps 3 million years old (Ellis & Mahon, 1977). Simmons and Brown (2007) state that the typical minimum lifetime for a geothermal system in the Taupo Volcanic Zone is over 100,000 years. Indirect evidence suggests that Kawerau has been active for >200 ka, Ohaaki ~ 300 ka and Whakarewarewa over 100 ka (Browne & Lloyd, 1987).

Thermal activity in active geothermal fields may not necessarily be continuous but rather wax and wane, with periods of activity and quiescence. Particular physical and chemical qualities of the reservoir and the geology can change during a systems life-time (e.g., temperatures, heat sources, upflow locations, outflow paths). At Kawah Kamojang (Indonesia) and Matsukawa (Japan) geothermal fields the current temperatures are 150°-250 °C yet pyrophyllite and diaspore hydrothermal minerals are interpreted as relicts of when temperatures were >310 °C (Browne, 1978). At Tui mine, New Zealand (a relict epithermal system), the progressive alteration of hydrothermal adularia to sericite then retrograde illite-montomorillonite, kaolin and adularia suggests a waning of geothermal activity (Brown, 1970).

Modern geothermal systems may also be one in a series of systems that have died and reactivated, or they may completely seal and become extinct. The Mangakino hydrothermal system has undergone substantial cooling indicating that hydrothermal systems can wax, wane or rejuvenate. Ohakuri a hydrothermal system that was active >160,000 years ago (Henneberger & Browne, 1988) and is now extinct likely died off as the heat source cooled or permeable pathways were sealed off. Milicich

et al. (2014) further showed that other TVZ geothermal systems, isolated in time, overprint one another. For example at Ngatamariki geothermal field there is evidence of two hydrothermal systems.

It is clear that hydrothermal systems and their surface manifestations are forever changing. In the TVZ, surface activity only began in 1886 at Waimangu and some hydrothermal systems may have been obliterated by volcanic eruptions as proven by tephra deposits containing clasts of silicified and hydrothermally altered rock. For example, the 1886 Tarawera eruption modified the Rotomahana hydrothermal system responsible for the formation of the Pink (Otukapuarangi) and White (Te Tarata) Terraces. Monitoring hot springs provide quantitative data of composition and temperature but these only go back a few hundred years hence geological evidence such as fluid inclusions and hydrothermally altered minerals are required in reconstructing the evolution and behaviour of a hydrothermal system.

3.5 USEFUL ALTERATION ASSEMBLAGES

Intrusive masses in volcano plutonic and volcanic settings are usually the source of the elevated temperatures. Hydrothermal systems in these settings can develop on the flanks of volcanoes, in the depressions or rims of calderas (e.g. Rotorua and Okataina calderas) or in tectonic rift grabens (e.g. Wairakei-Tauhara) (Henley & Ellis, 1983; Kühn, 2004). Igneous bodies provide the heat source needed to form convection cells with fluids. As a result, environments with these ingredients are ideal for porphyry and epithermal ore deposit formation, geothermal systems and alteration types such as potassic, propylitic, phyllic and argillic alteration (Fig. 3.4).

Table 3.1. Main mineral assemblages specifically associated with geothermal fields and epithermal deposits (fossil geothermal systems) detailing where and how they form (after Burnham, 1962; Thompson & Thompson, 1996; Gifkins et al., 2005).

MINERAL ASSOCIATION	ALTERATION	COMPOSITION	ENVIRONMENT OF FORMATION
Geothermal (epithermal)			
quartz, chalcedony, opal, pyrite, hematite	Silicic, silicification	Si enrichment	Pervasively replace rock. Occurs around fractures, veins or in permeable zones In epithermal and geothermal systems at shallow levels. Forms blanket zones at the water table below steam-heated advanced argillic alteration. Replaces or fills vugs left behind from intense leaching.
orthoclase (adularia), albite, quartz, sericite-illite, chalcopyrite, pyrite	Potassic or sodium alteration	K or Na metasomatism, H metasomatism	Around veins, fractures and permeable zones or selectively replaces plagioclase. In epithermal / geothermal systems at shallow to intermediate depths; maybe associated with boiling. Occurs in major upflow zone as ascending solutions cool. Pervasive replacement of adularia often mistaken for silicification.
muscovite, illite, illite-smectite, montmorillonite, kaolinite, quartz, calcite, dolomite, pyrite	Argillic	H metasomatism	Around veins and as replacement in permeable lithologies. With proximity to the upflow zone mixed-layer clays progress to illite. Upper part of geothermal systems there are carbonate-bearing blanket alteration zones possibly from the condensation of gases (CO_2) from deeper boiling zones.
kaolinite, alunite, cristobalite (opal, chalcedony), native sulphur, jarosite, pyrite	Advanced argillic-acid-sulphate	Ca, Mg, Na depletion, H-metasomatism	Widespread above the water (paleowater) table probably related to condensation and oxidation of gases (H_2S). Surface = mud pools, fumaroles.
quartz, calcite	Silica-carbonate	Ca, Si enrichment	In the shallow parts of geothermal systems (low temp) replacing ultramafic rocks.
kaolinite/dickite, montmorillonite, illite-smectite, quartz, pyrite	Intermediate argillic	K, Ca, Mg, Na metasomatism	Occurs as an alteration zone between advanced argillic and propylitic alteration.
chlorite, epidote, albite, wairakite, calcite, illite-smectite, montmorillonite, pyrite	Propylitic, Zeolitic alteration	Na, Mg, Ca metasomatism	Extensive regional alteration zone around epithermal and geothermal systems. Change from zeolite-rich to propylitic reflects increasing depth and temperature. CO_2 concentration influences the stability of zeolites, calcite & epidote.
sericite, quartz, pyrite, adularia, biotite, calcite, rutile	Phyllic	H-K metasomatism	Phyllic alteration spreads into potassic from increasing K-feldspar amounts, and argillic from increasing clay minerals. Outer halo from middle upflow zone.
quartz, rutile, alunite, native sulphur, barite, hematite, pyrite, jarosite	Vuggy silica, vuggy quartz		In structural zones, permeable lithologies or centre of advanced argillic zones. Common at epithermal levels but also in upper parts of porphyry systems.

There are many alteration assemblages that form in specific environments. Table 3.1 outlines common hydrothermal alteration types that are found in geothermal fields and their "frozen fossil" equivalents, low sulphidation epithermal deposits. Hydrothermal minerals form in response to the conditions experienced at the time of formation hence mineral associations provide information on hydrothermal conditions and specific forms of metasomatism at the time of deposition. Identifying past and present hydrothermal fluid channel-ways is also possible using alteration mineral zonation.

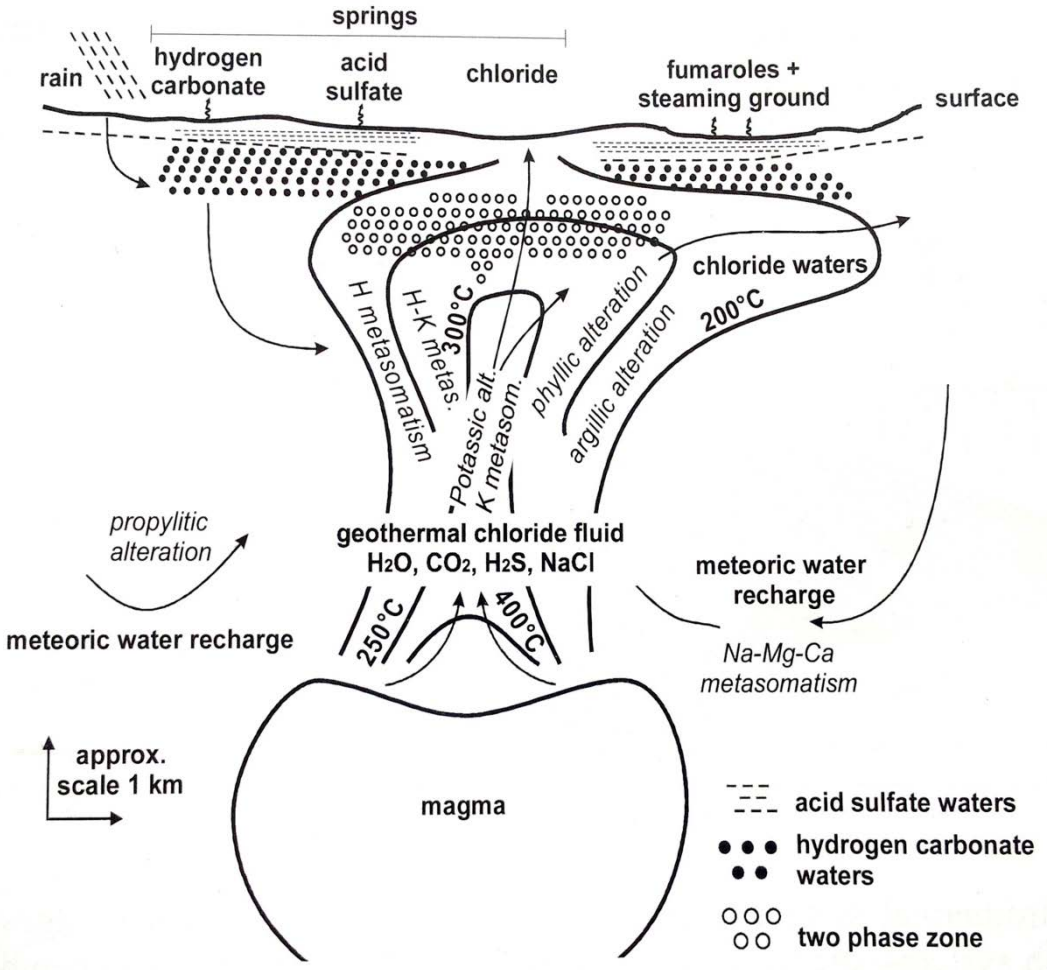

Fig. 3.4. Alteration and metasomatism processes at work in a liquid dominated geothermal system in low relief, typical in silicic volcanic terrain such as the high temperature systems in the TVZ such as the Tauhara Geothermal Field (Nicholson, 1993; Kühn, 2004).

Propylitic

Propylitic alteration occurs as extensive regional alteration halos around geothermal systems. As meteoric waters descend propylitic alteration occurs along with additional H_2O and CO_2 and some sulphur (Kühn, 2004). Meteroic water descends on the periphery of the hydrothermal system, known as the recharge zone (Fig. 3.4). The descending solutions undergo Na, Mg and Ca metasomatism and destroy K-feldspar (microcline) to produce epidote, chlorite, calcite and albite which are common mineral associations in propylitic alteration (Table 3.1). Propylitic alteration tends to be more pervasive towards the source of the heat, grading into unaltered rock with distance (Pirajno, 2009).

Zeolitic

Zeolitic alteration, an alteration style associated with propylitic alteration, and occurs at temperatures < 220°C and relates to volcanic environments even though it occurs at some distance from these (Lagat, 2009). With increasing depth and temperature, alteration changes from zeolite-rich to propylitic alteration. During the waning stages of volcanic activity or near surface environments, zeolite minerals form at low temperatures and replace the glassy matrix (Henley & Ellis, 1983; Lagat, 2009).

In New Zealand geothermal fields the calcium zeolites, mordenite-laumontite-wairakite is a typical zonation found. Mordenite forms near 50 to 100 °C, through laumonite from 150 ° to 200°C and wairakite at higher temperatures usually above 215 °C, but may form occasionally as low as 140 °C (Browne & Ellis, 1970; Browne, 1978; Henley & Ellis, 1983).

The stability of these minerals is not only temperature dependent but also relies on fluid and rock compositions. For example the amount of CO_2 in the fluid influences the stability of zeolites, calcite and epidote. At Ohaaki, if CO_2 concentrations are high, during steam separation calcite will precipitate instead of epidote and the zeolite, wairakite (Browne, 1978) whereas the low CO_2 system at Wairakei favours epidote and wairakite formation (Henley & Ellis, 1983).

Additionally, formational temperatures of epidote may be different in each field for example at Cerro Prieto field, Mexico, epidote forms >255 °C but at the Salton Sea field, California epidote is abundant at approximately 300 °C (Browne, 1978). At Reykjavik, Iceland, epidote appears at 120 °C but this is thought to be a relic of once higher temperatures (Browne, 1978).

Potassic

Potassic alteration (biotite, adularia) is a result of potassium enrichment or K-metasomatism and is usually accompanied by sulphides (chalcopyrite, pyrite, Table 3.1, Pirajno, 2009). The occurrence of adularia in shallow volcanic environments usually indicates potassic alteration. Adularia forms in areas of high permeability and if it occurs with hydrothermal biotite then it is indicative of high temperatures as hydrothermal biotite typically forms >325 °C such as at Cerro Prieto, Mexico (Henley & Ellis, 1983). Potassic alteration occurs in the major upflow zone in a hydrothermal system as ascending solutions cool (Fig. 3.4). In epithermal or geothermal systems it occurs at shallow to intermediate depths, around veins, fractures and permeable zones, selectively replaces plagioclase and maybe associated with boiling (Table 3.1). Pervasive replacement of adularia is often mistaken for silicification.

Albitic

Albitic alteration is a sub style of potassic alteration representing Na metasomatism. This type of alteration results in albite or sodic plagioclase deposition and indicates Na enrichment (Lagat, 2009; Pirajno, 2009).

Silicification

Silicification is common in epithermal and geothermal systems and involves the addition of silica (SiO_2). Circulating fluids introduce silica largely as a vein mineral by fluid flow or precipitation due to its prograde solubility (Kühn, 2004). It also redistributes silica from glass and host rock to form amorphous silica, cristobalite, chalcedony or quartz, depending on the temperature (Henley & Ellis, 1983; Lagat, 2009). Silicificaton pervasively replaces rock, fills vugs left behind

from intense leaching and occurs around fractures, veins or in permeable zones at shallow levels (Table 3.1). It can occur as "silica flooding" where microcrystalline quartz (chalcedony) replaces the rock, or forms a network of closely spaced fractures filled with quartz (Lagat, 2009). Silicification also forms blanket zones at the water table, below steam-heated advanced argillic alteration. Henley and Ellis (1983) state that steam loss near the surface combined with temperature gradients towards the margins, indicate that silica deposition is most prominent on the boundaries of the geothermal system.

Drilling in Yellowstone Park penetrated rocks that have reduced in porosity due to silica precipitation (Henley & Ellis, 1983). Pressure data between the wells showed that horizontal permeability was self-sealed by silica precipitation. In contrast at Wairakei geothermal field in the TVZ, there is little evidence of self-sealing (Henley & Ellis, 1983).

Argillic

Argillic alteration forms clay minerals from H-metasomatism that causes extreme acid leaching (Table 3.1). H-metasomatism occurs in two places in a hydrothermal system either within the primary neutralisation zone or as the next alteration halo out adjacent to the main upflow zone (Fig. 3.4, Kühn, 2004). Argillic alteration grades into phyllic alteration with proximity to the main upflow zone, and further outwards to propylitic alteration. In the upper part of geothermal systems there are carbonate-bearing blanket argillic alteration zones possibly from the condensation of gases (CO_2) from deeper boiling zones (Table 3.1).

The H-metasomatism results in base leaching of alumina-silicates and feldspars that result in silica enrichment hence there may be a gradation from an argillic zone to a silica rich zone (Pirajno, 2009). Argillic alteration typically has mineral associations of muscovite, illite, illite-smectite, kaolinite, quartz, calcite, dolomite and pyrite (Table 3.1). With proximity to the upflow mineralised zone mixed-layer clays (illite-smectite) progress to illite.

Intermediate argillic

Intermediate argillic occurs as an alteration zone between advanced argillic and propylitic alteration with a mineral association of smectite, illite, chlorite and kaolin clays (kaolinite, dickite, halloysite) (Pirajno, 2009). Potassium, Ca, Mg, Na metasomatism occurs but may not entirely leach out and K-feldspar (orthoclase) may stay unaltered (Pirajno, 2009). Within the intermediate argillic zone, zonation of minerals is possible as kaolinite occurs closer to the phyllic zone compared to smectite which occurs in the outer zones. As hydrothermal fluids pass through the neutralisation zone, Na, K, Mg and Ca increase as rock is dissolved isochemically (Kühn, 2004). Calcium and magnesium then decrease as secondary minerals form such as amphiboles and chlorite.

Advanced argillic acid-sulphate

Advanced argillic is an alteration type indicative of intense acid attack and low pH conditions where feldspars and mafic silicates are completely destroyed (Pirajno, 2009). Advanced argillic alteration is the result of H metasomatism and Ca, Mg and Na depletion. It has a mineral association of kaolinite, alunite, cristobalite (opal, chalcedony), native sulphur, jarosite and pyrite (Table 3.1). Advanced argillic alteration is widespread above the water table or paleowater table and is related to underground boiling, dissolved gases separating into the steam phase and oxidation of those rising gases to form acid condensate above the boiling zone (H_2S). It is a distinct alteration type that occurs in the steam heated zone near the surface that is responsible for mud pools and fumaroles at the surface (Fig. 3.4).

In Matsukawa, Japan and Matsao, Taiwan, rather than surficial acid waters, acid waters have been found much deeper at temperatures of 250-280 °C. The reasons for their deeper occurrence may be an influx of acid gases (SO_2) at depth or sulphur deposits at deeper levels being altered by high temperatures (Henley & Ellis, 1983). Within this alteration type, the mineral associations that typify more acidic conditions occur in the central zone of the field (kaolinite, alunite, anhydrite, pyrophyllite, quartz and pyrite) and as conditions become less acidic trending outward, montmorillonite, mica, quartz and anhydrite arise (Henley &

Ellis, 1983). The acid alteration or advanced argillic assemblage at Wairakei consists of kaolinite, alunite, gypsum, opal and hydrated iron oxides (Steiner, 1977; Henley & Ellis, 1983).

Phyllic / Sericitic

Phyllic alteration is also termed sericitic alteration and involves both K-metasomatism and H-metasomatism (Kühn, 2004). In literature, the term sericite is often used but it is more of a general varietal term for any fine grained white mica such as muscovite, illite or paragonite. In TVZ geothermal fields, illite is the main fine grained white mica. Phyllic alteration zones have typical mineral associations of illite, quartz, pyrite with minerals such as adularia, kaolinite, biotite, calcite, rutile, apatite and anhydrite (Table 3.1). Phyllic alteration extends outwards as an outer halo from the middle of the upflow zone (Fig. 3.4). It spreads into potassic from increasing K-feldspar amounts, and argillic from increasing clay minerals. At temperatures up to 200 °C, laumontite (zeolite), microcline (feldspar) combined with CO_2 produce calcite, muscovite (sericite) and silica (Kühn, 2004). From 200-280 °C, clinozoisite, microcline and CO_2 produce the same constituents as before. At higher temperatures above 280 °C wairakite and anorthite (Ca silicates) control the reaction to produce the same products.

Alunitic

Alunitic alteration is a sub style of advanced argillic alteration and is representative of hot spring environments that contain alunite which forms ledges. Alunite is associated with high SO_4 gas content probably from the oxidation of sulphide minerals (Lagat, 2009).

3.6 VECTORS TOWARDS FLUID FLOW

Recognising alteration halos and mineral zonations may provide vectors to mineralisation and hydrothermal fluid pathways (Camuti, 2008). To do this requires the use of hydrothermal alteration types described above, and noting several key aspects:

- Alteration types are locally distributed occurring either uniformly and/or pervasively through highly permeable rock, or restricted to fractures and/or narrow alteration halos in impermeable rocks.
- The distribution or extent of an alteration zone is one of the main criteria in distinguishing areas in a hydrothermal system e.g. the periphery, the main upflow zone, adjacent to the upflow zone, or where boiling occurs.
- Chemical modifications are common, e.g. in the alteration types typical of volcanic hosted massive sulphide (VHMS) deposits, disseminated pyrite, base metal sulphides, manganese-rich assemblages and zinc deposits are common (Gifkins et al., 2005).

Major element lithogeochemistry can be used to determine compositional changes in altered rocks (Corbett & Leach, 1997), especially where fluids overprint previous alteration assemblages. Thus analysing whole rock samples for elemental abundances is used to measure alteration intensity and it supports estimates of mineral proportions and alteration intensity otherwise determined visually. Insights are gained from spatial chemical variance. For example, that increases in Na_2O concentrations in volcanic rocks maybe related to increasing paragonitic and/or albite alteration. These trends have been used effectively in VHMS exploration and can be applied to the geothermal environment (see Chapter 5, this thesis). Alteration indices are then created that will yield values related to alteration intensity to guide exploration for fluid altered zones (or ore bodies in mineralised environments).

Mineral chemistry in exploration has been limited to lab based techniques such as electron microprobe and X-Ray Diffraction (XRD) analysis, however the advent of portable short wave infrared has revolutionised exploration to the point that the

instrument is pointed at a rock and it analyses the components in it. White micas, chlorites and clays in altered zones display variations in composition spatially that could be used as vectors towards permeability, feed zones (fluid pathways) and mineralisation. Remote sensing using spectral imaging is also being applied to map white mica, kaolinite, calcite, pyrophyllite and hematite to name a few, in epithermal altered zones (Simpson et al., 2004; Simpson & Mauk, 2011).

Drill cores collected at varying depths enable a pre-drilling temperature profile to be made from oxygen isotope ratios $^{18}O/^{16}O$ in the minerals (Henley & Ellis, 1983). Calcite precipitation in fissure zones and the water from it precipitated from in these permeable areas are in fact in isotopic equilibrium. Hence vein calcite is a target mineral used for $\delta^{18}O$ measurements and at Kawerau this technique was applied successfully by Blattner in 1979 (Henley & Ellis, 1983).

3.7 SUMMARY

A hydrothermal system describes how hot fluids travel within the earth's crust and occurs in hydrothermal a variety of different settings e.g. mid-ocean ridges, orogenic terranes and volcanic environments. The lifespan of a hydrothermal system ranges from 10,000 to several million years and may undergo periods of activity and quiescence, reactivation or become extinct. Hydrothermal systems may change in time and space, with more than one system operating over its lifespan or multiple upflows changing position over time.

Hydrothermal alteration refers to a change in the host rock mineralogy as a result of chemical interaction between rock and hot hydrothermal fluid. A number of factors control alteration mineralogy: temperature, permeability, fluid composition/pH, pressure, initial rock composition and duration of hydrothermal activity. One or more factors tend to dominate. Temperature is considered to be one of the most significant factors in hydrothermal alteration but permeability and fluid composition, particularly fluid pH are also important.

Hydrothermal minerals and mineral assemblages are useful in finding permeability, fluid pathways, geothermal reservoirs and hydrothermal ore deposits

because they form in response to the hydrothermal conditions experienced at the time of formation. Several exploration vectors and proximity indicators such as mineral zonation, major element lithogeochemistry, mineral chemistry and oxygen isotopes are being increasingly utilised to help determine the geohydrological structure of hydrothermal systems.

Chapter 4

Alteration mineralogy

4.1 INTRODUCTION

In hydrothermal systems, a heat source circulates fluid at different temperatures and pressures, through a system of fractures, faults and permeable host rocks where the fluid alters the rock in the process. These interactions between fluid and rock lead to changes in the host rock minerals to form secondary minerals, including clay minerals (or hydrothermal alteration minerals). The mineral species that form are broadly dependent on temperature (Browne, 1970). Thus certain minerals and/or mineral assemblages are formed under specific temperature ranges and conditions, such as permeability, pH/fluid composition, pressure and duration of interaction. These minerals are also influenced by host rock composition (Browne and Ellis, 1970; Browne, 1978).

Changes in alteration mineral associations can be used to locate hot permeable production zones or fluid flow paths related to up-flow zones in active hydrothermal systems (i.e. geothermal fields) as well as the current temperature regime and what thermal history the field has undergone. In a geothermal system mineral associations of earlier thermal events that are cooler or hotter such as intrusion related dikes must be distinguished from mineral assemblages related to current temperature or pressure regimes. High temperature (i.e. >220 °C) minerals (epidote, illite) may be overprinted by low temperature (< 150 °C) minerals (smectite) and vice versa. Consequently, alteration minerals have a significant impact on geothermal production as wells that have mineral associations in agreement with measured well temperatures and permeability are prime production targets for fluid or steam extraction.

Much of our knowledge of vectors towards mineralization in epithermal environments has been gained from studying active hydrothermal systems in geothermal fields. Alteration minerals form under certain fluid compositions,

temperatures and pressures and their distributions form mineral zonations (Browne, 1970). Epithermal ore deposits often have zoned alteration halos where chemical and mineral vectors point towards regions of fossil hydrothermal fluid upflow and therefore mineralization. In this chapter I am examining an active hydrothermal system, to identify vectors towards known fluid flow pathways and permeable zones through alteration zonation to aid exploration in geothermal fields, in this case, the Tauhara geothermal field.

This chapter describes mainly the hydrothermal alteration mineralogy and primary mineralogy in three wells (TH9, TH10, TH12) within the Tauhara geothermal field. The main aim of this chapter is to determine at what temperatures the minerals identified have formed and how this contributes to understanding past fluid flow pathways and how the geothermal field is evolving. This chapter also links closely with Chapter 5, geochemistry, to connect mineralogy and alteration types with geochemistry.

4.2 METHODOLOGY

4.2.1 Sample selection

Three geothermal wells (TH9, TH10, TH12) across the Tauhara geothermal field were targeted with 304 samples of drill cuttings and six core samples collected. Sample selection was on the basis of three GNS Science Consultancy Reports that were examined for this study (Table 4.1).

Table 4.1. Three main well reports used in this thesis.

Well	Authors	Year/Report no.	Title
TH9	MIlicich, Rosenberg, Ramirez & Kilgour	2008a/56	Geology of Exploration Well TH9 Tauhara Geothermal Field
TH10	Milicich, Ramirez & Rosenberg	2008b/80	Geology of Exploration Well TH10 Tauhara Geothermal Field
TH12	Kilgour, Rae & Milicich	2006/219	Geology of Exploration Well TH12, Tauhara Geothermal Field

Every 20 m down well rock cuttings (5-10 g) were collected. If rock cuttings at the required interval were unavailable, a sample from the closest available interval was taken. Samples were also taken five to ten metres either side of logged lithological boundaries to capture changes in lithology and at least 20 m beneath casing points to

avoid cement contamination. Hulen and Sibbett (1982) state that drill bit flakes, pieces of cement casings, drilling mud, grease or lost circulation material (LCM) such as hazel wood chips or mica (used to plug up holes when circulation is lost) and parts of the drill hole itself that has collapsed can contaminate cuttings. However these can be easily recognised amongst the cuttings, for example if there are metal drill bit flakes these are removed with a magnet. Removing metal flakes is important to avoid mis-identification of mafic minerals that are high in Fe and Mg.

Existing core was sparse as samples available were mostly cuttings, therefore only six core samples was obtained in order to make thin sections (Table 4.2, Fig. 4.1).

Table 4.2. Core samples obtained and approximate depth of collection.

Core samples	Approx. depth	Core cut in well from
TH9-C1-S1	~ 1801.5 m	Between 1801 - 1803.5 m
TH9-C2-S1	~ 2424 m	Between 2423.5 - 2425 m
TH10-C1-S1	~ 1405.5 m	Between 1403.88 - 1406.57 m
TH12-C1-S1	~ 1372.5 mRF	Between 1368 - 1370 mRF
TH12-C1-S2	~ 1372.5 mRF	Between 1368 - 1370 mRF
TH12-C2-S1	~ 1379.5 mRF	Between 1368 - 1370 mRF

Fig. 4.1. Examples of cut core section where core samples were collected from and rock cuttings at 5 m intervals in cloth bags where samples were taken every 20 m.

4.2.2 Short wave infrared spectroscopy (SWIR)

The TerraSpec® is an analytical spectral device (ASD) or spectrometer that is field-portable and uses non-destructive reflectance spectroscopy for mineral identification (Simpson et al., 2006), by measuring reflected radiation from a sample's surface. The instrument used is a TerraSpec® Hi Res 4, which measures radiation in the visible light (380 – 700 nm), and near to short-wave infrared spectra (NIR and SWIR, respectively; 700 – 2500 nm). However, it is short-wave infrared wavelengths (1300-2500 nm) that are most useful for mineral identification.

Many minerals have characteristic spectral signatures or spectra, which is the basis of the short-wave infrared spectroscopic technique. A mineral's spectral signature depends on crystallographic factors unique to each mineral species. Unique spectral signatures allow many minerals to be identified by simple pattern recognition. In a mixed sample, the absorption patterns are a combination of all the responsive minerals in the sample.

The spectrometer (TerraSpec® + wand) contains a light source that illuminates the sample allowing visible light, NIR and SWIR to be reflected off the surface. However specific wavelengths of radiation are absorbed by different types of minerals resulting in a unique spectral response (Simpson et al., 2006; AusSpec, 2010). Absorption occurs as a result of sub-molecular vibrations from the bending and stretching of covalent and molecular bonds (OH, H_2O, CO_3^{2-}, NH_4, AlOH, FeOH, MgOH) in the minerals. As a result, these bonds produce spectral absorption features that distinguish a mineral. The absorption features are at particular wavelength positions: the hydroxyl (OH) feature at 1400 nm, H_2O at 1900 nm, FeOH at 2250 nm, and $CO_3^{2-}$and MgOH at ~2350 nm (Fig. 4.2). The relative intensities of these and their wavelength position help identify minerals present in a sample. Below the baseline of the spectra, the absorption features in the reflectance spectrum are represented as minima.

The TerraSpec® is able to detect mineral species that contain the covalent and molecular bonds described above, such as clays, micas, carbonates, hydroxides as well as some sulphates and silicates (Table 4.3). Minerals not detectable are ones

that lack the necessary covalent or molecular bonds (structural OH, water and CO_3^{2-}) such as quartz and feldspar (Simpson et al., 2006). This technique is especially suited to hydrothermally altered silicate rocks as they are commonly pale in colour and reflect light well. Conversely, dark rocks absorb excessive amounts of infrared and visible light, rather than reflecting, and this produces noisy spectra. Hence rock colouration influences the quality of a spectral profile.

According to Simpson et al. (2006) the sharpness of the absorption feature and its wavelength position are a means of determining the crystallinity of many minerals (e.g., illite, kaolinite). The wavelength positions of specific features also provide information on the composition of many minerals, especially the AlOH, FeOH, MgOH and CO_3^{2-} absorptions (e.g., illite, chlorite and carbonates).

Table 4.3. Mineral groups and minerals identified by TerraSpec.

Mineral group	Mineral examples
Clays	illite, interstratified illite-smectite, smectite, chlorite, kaolinite, dickite, halloysite, palygorskite
Micas	biotite, muscovite, paragonite
Other Phyllosilicates	serpentine, talc, pyrophyllite
Epidote	Clinozoisite, zoisite
Amphibole	hornblende, actinolite
Sulphates	alunite, jarosite, gypsum
Carbonates	calcite, dolomite, ankerite, magnesite, malachite, siderite
Ammonium-bearing Minerals	buddingtonite, NH4- illites

Figures 4.2 and 4.3 show spectral profiles generated by the TerraSpec®. Raw spectral profiles are known as reflectance spectra, reflectance intensity on the y-axis and spectral wavelength in nanometers on the x-axis. The reflectance spectra are influenced by absorptions outside of the SWIR range due to ferrous iron (Fe^{2+}) at ~1000 nm and strong water and carbonate absorptions at ~2700 nm. The effect of these influences is known as the 'reflectance hull' where the background shape or continuum of the spectrum is curved (Fig. 4.2).

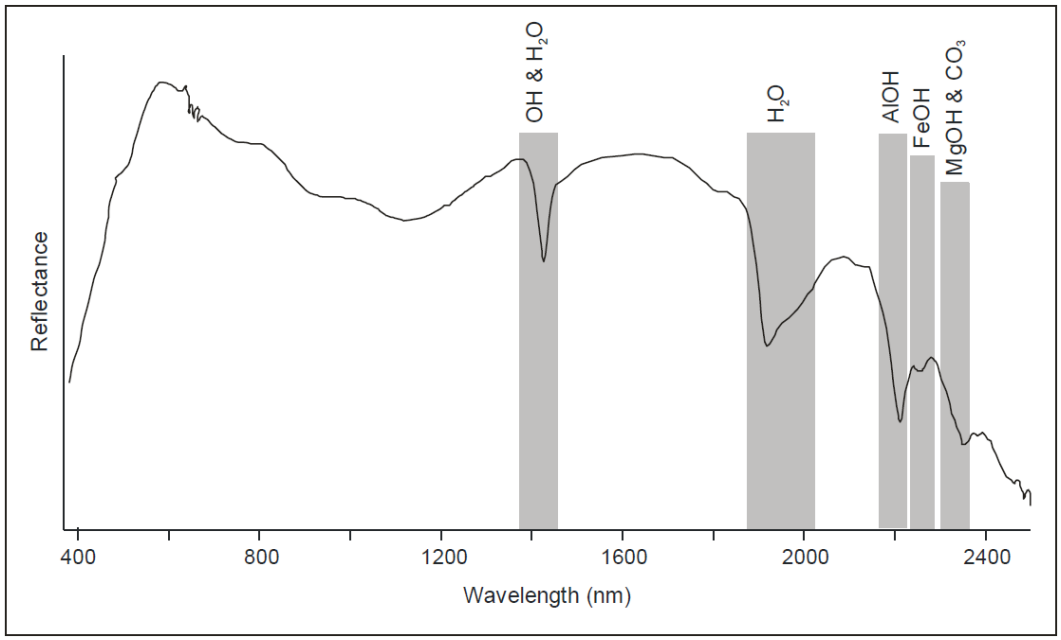

Fig. 4.2. Example of a raw spectral profile showing the wavelength positions of the main absorption features: OH ~1400 nm, water ~1400 and 1900 nm, AlOH ~2200 nm, FeOH ~2250 nm, MgOH ~2350 nm, CO_3^{2-} ~2300-2350 nm. (Simpson et al., 2006).

Because the reflectance hull distorts some absorption features that hinder accurate determination of some wavelength positions. For this reason a baseline correction termed the hull quotient is made during processing to remove the reflectance hull and enhance the spectral absorption features (Fig. 4.3). This process is effectively removing the background spectra. Both hull and reflectance spectra are ratioed resulting in a "hull quotient" spectrum. The SWIR range is best viewed using the hull quotient correction however it is worth considering both spectra when assessing what minerals are present. In the visible near infrared (< 1300 nm) range, reflectance spectra are best.

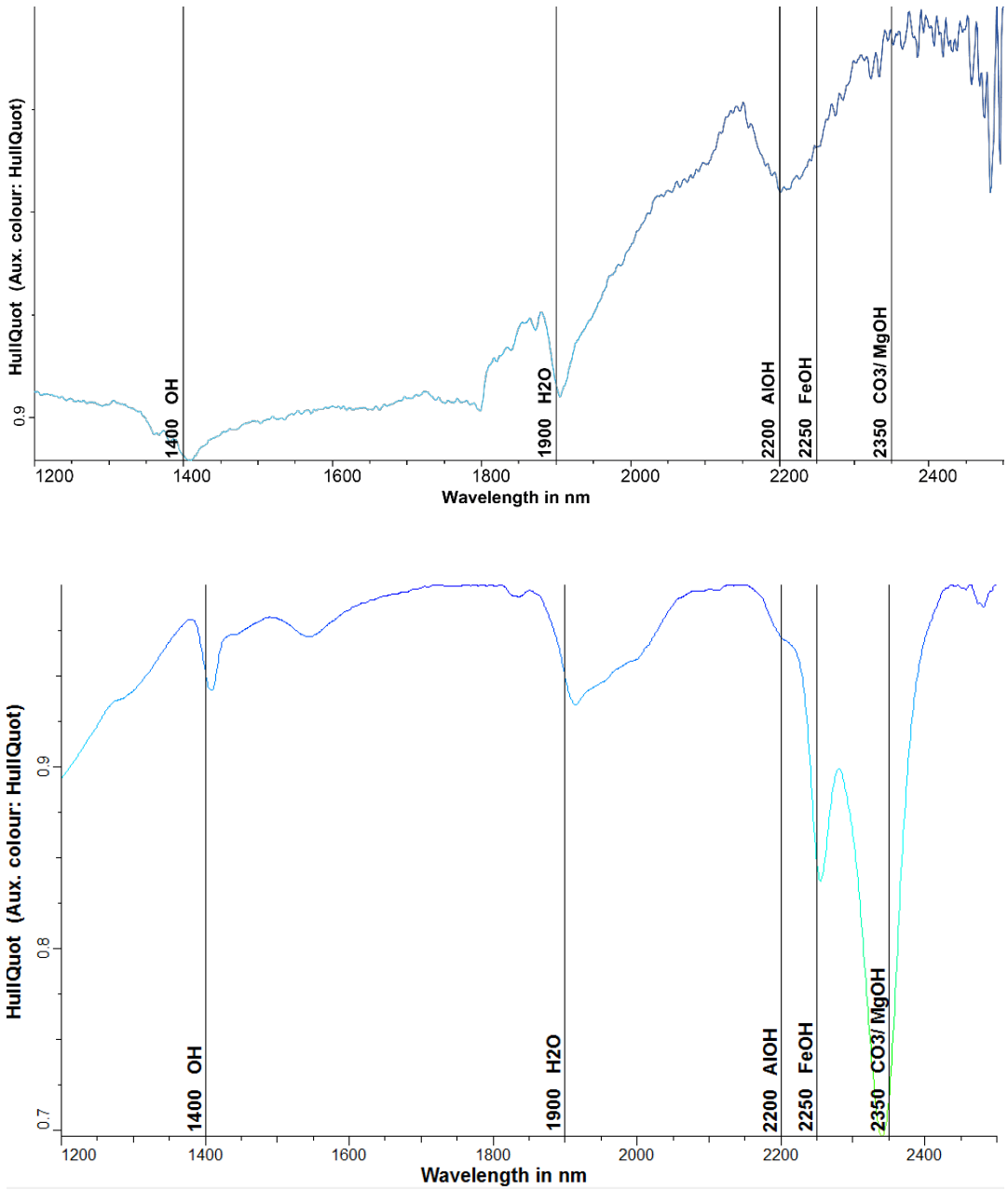

Fig. 4.3. ***Top*: Example of a noisy or poor Hull quotient spectral reflectance, which shows numerous peaks and troughs of distortion (Sample TH10 160 mRF).** ***Below*: Example of a good Hull quotient spectral profile (Sample TH10 1720 mRF) showing the main absorption features marked. Minerals in this spectrum are chlorite, epidote, minor illite and possible calcite.**

4.2.3 Short wave infrared spectroscopy (SWIR) method

To identify hydrothermally altered minerals, short wave infrared spectroscopy was performed on all 304 drill cutting samples collected across the three wells. Sample preparation for SWIR only required that the cuttings be dry. The cuttings (of each sample) were put into a porcelain spectrally inert bowl and the wand of the instrument was placed directly on the sample. Data was collected using a TerraSpec® 4 Hi-Res instrument equipped with three detectors (Fig. 4.4). Scans took 10 s each and in between each scan the cuttings were mixed to minimise heterogeneity. Three scans were taken per sample to ensure the best possible scan result. The bowl and corundum plate on the wand were wiped with a tissue after each scan (Fig. 4.4). The instrument was calibrated every hour using a white disc placed on the corundum plate until a flat spectrum with 100% reflectance was obtained. Lastly, the spectral patterns (see Appendix B on CD) were viewed and interpreted using The Spectral Geologist (TSG®) software, with a TSG spectral database of reference minerals, NASA spectral database of reference minerals and an AusSpec International Ltd manual and guide to the SWIR technique complete with reference mineral spectra (Figs 4.5a-e).

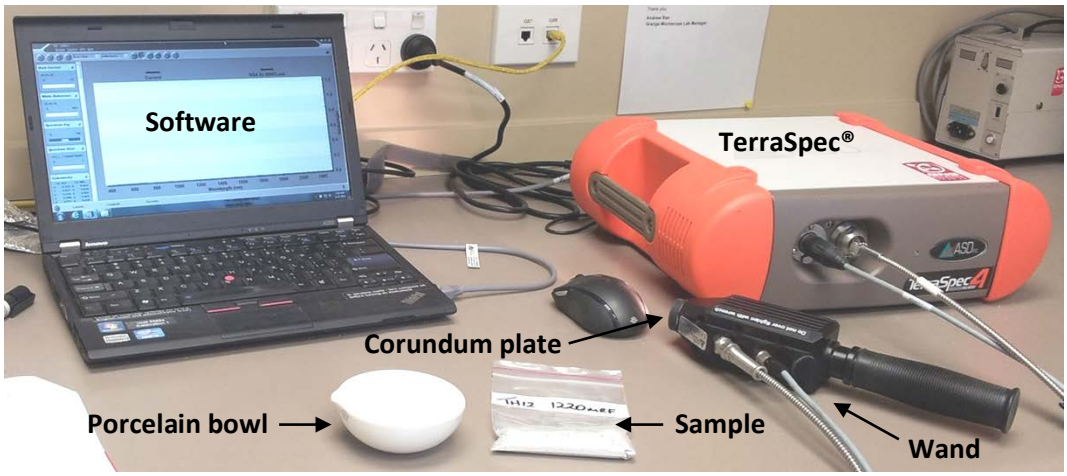

Fig. 4.4. TerraSpec® 4 Hi-Res instrument equipment and sample setup.

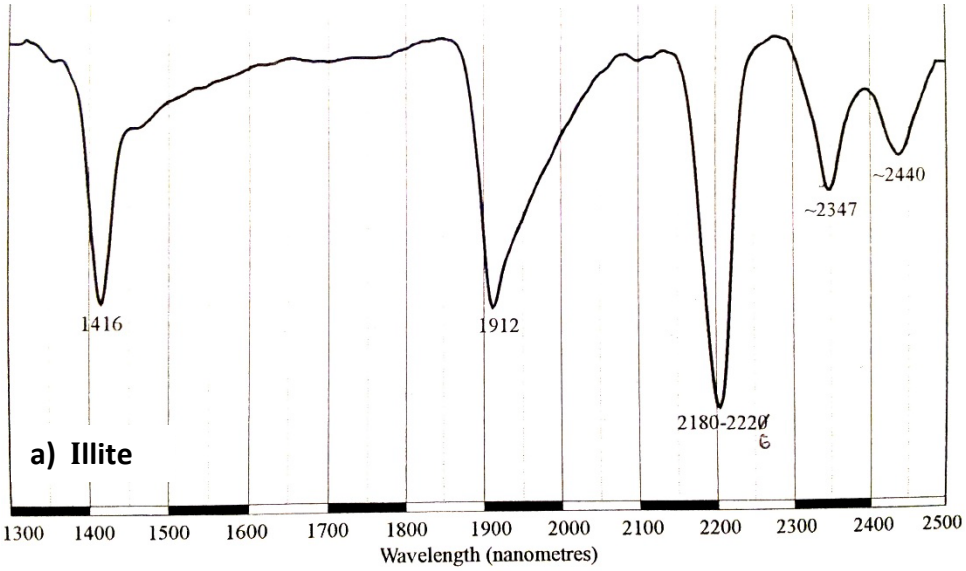
1416
1912
2180-2220
~2347
~2440
a) Illite
1300 1400 1500 1600 1700 1800 1900 2000 2100 2200 2300 2400 2500
Wavelength (nanometres)

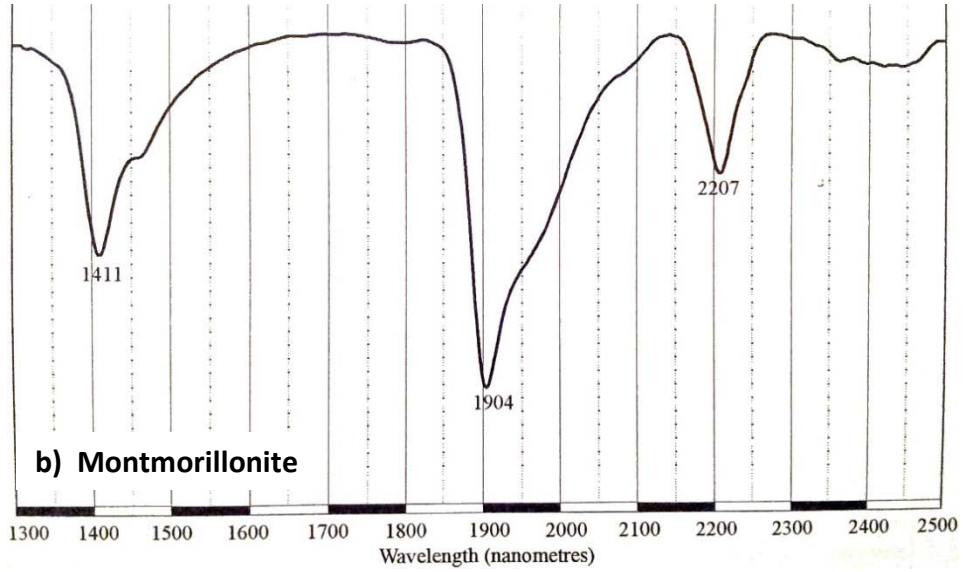
1411
1904
2207
b) Montmorillonite
1300 1400 1500 1600 1700 1800 1900 2000 2100 2200 2300 2400 2500
Wavelength (nanometres)

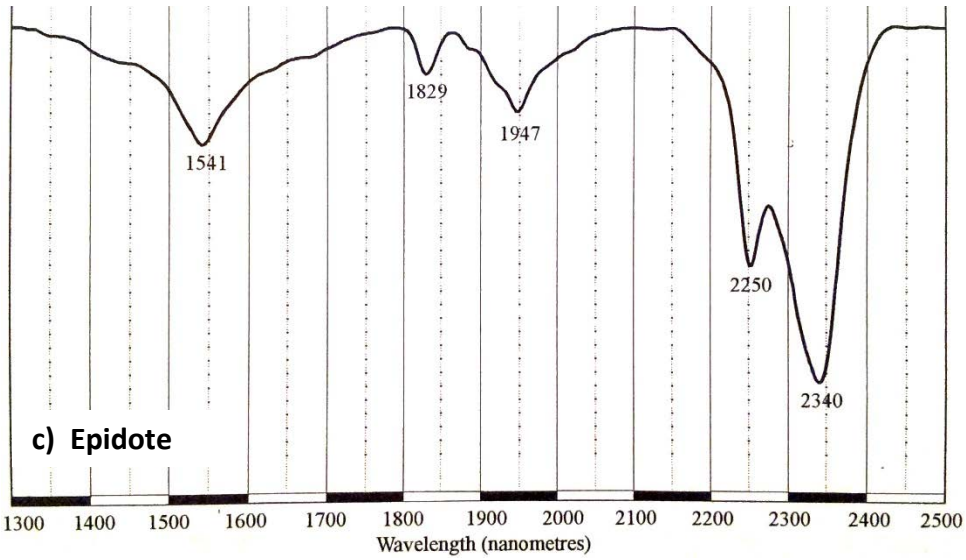
1541
1829
1947
2250
2340
c) Epidote
1300 1400 1500 1600 1700 1800 1900 2000 2100 2200 2300 2400 2500
Wavelength (nanometres)

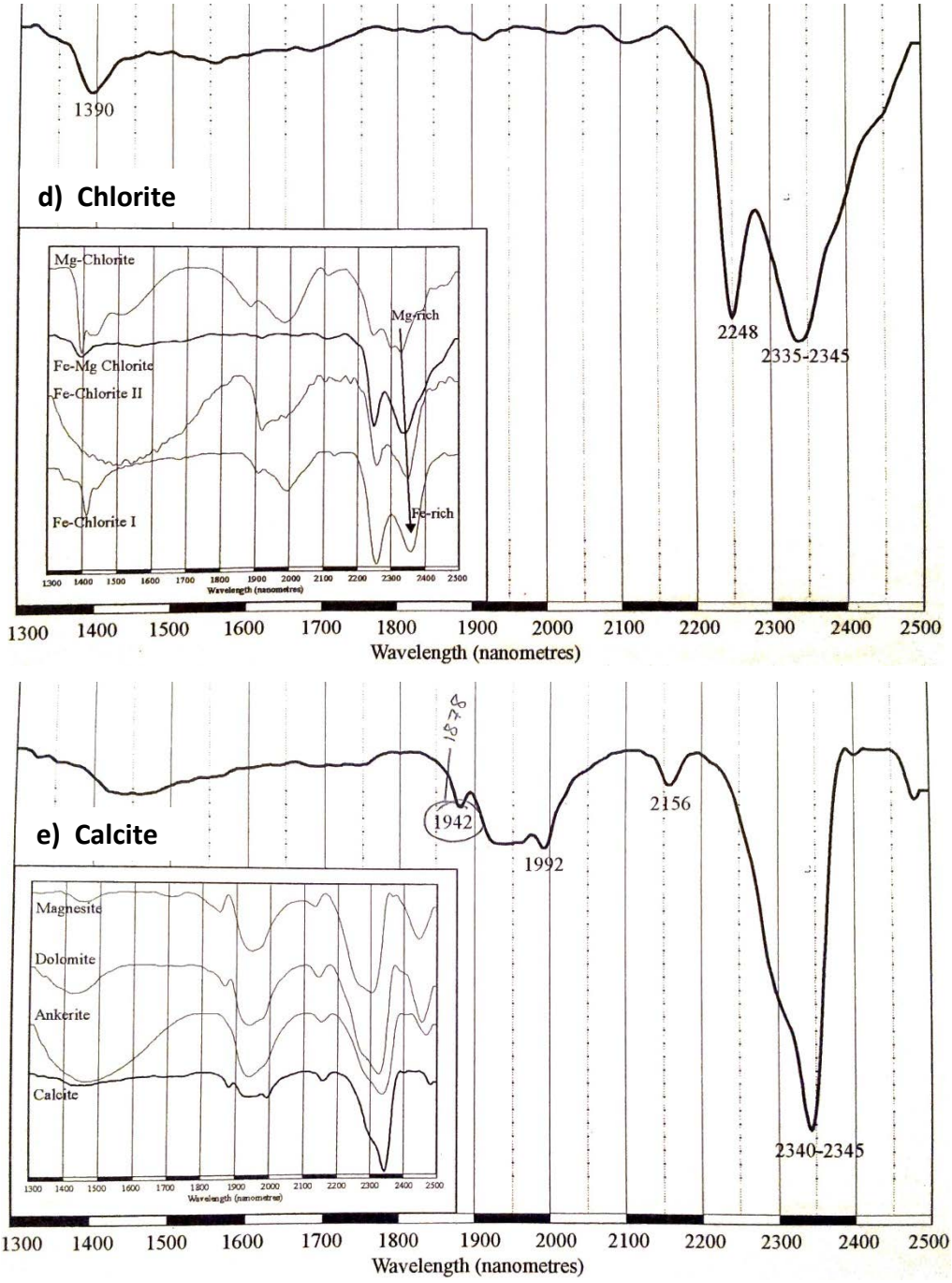

Figs. 4.5a-e. Reference spectral profiles from AusSpec International Ltd of illite, montmorillonite, epidote, chlorite and calcite showing the diagnostic features used to identify them in a mixed mineral spectrum.

4.2.4 X-ray diffraction (XRD)

X-ray diffraction is a technique used to identify and quantify crystalline compounds found in solid or powdered samples. It is particularly useful for identification of the clay minerals that have been separated as a fine fraction (< 2μm). The advent of x-ray diffraction began with Röntgen's discovery of x-rays, or Rontgenstrahlen

(Rontgen rays). Following that breakthrough, Max von Laue, Walter Friedrich and Paul Knipping proved that atomic particles in crystals are arranged in an ordered 3-dimensional repeated configuration, in the same dimensions as the x-ray wavelengths (Friedrich et al., 1912). Bragg and Bragg (1913a) further invented x-ray crystallography, describing the crystal structures of NaCl, KCl, KBr, and KI (Moore & Reynolds, 1997). The Bragg's also set the principle of Bragg's Law which explains that crystals reflect x-rays much like a mirror reflects light except that reflected x-rays interfere with one another at certain incidence angles, rather than at all angles of incidence like reflected light (Raudsepp & Pani, 2003).

According to Bragg's Law, the spacing between the parallel planes of atoms (*d*-spacing), the wavelength (λ) and diffracted angle of x-rays can be measured using an x-ray powder diffractometer. Bragg's Law is described as:

$$n\lambda = 2d\sin\theta$$

n = integer, order of diffraction — d = the interplanar spacing of atoms

λ = the wavelength of the x-rays — θ = the incident angle of the x-rays

X-ray diffraction (Brindley, 1968; Bish & Howard, 1988; Raudsepp & Pani, 2003) relies on the basis of the 3-dimensional periodic arrangements of atoms inherent in a crystal lattice (e.g., cubic, rhombic). When a monochromatic x-ray beam with a wavelength (λ) passes through the lattice structure of crystal at an angle (θ), the crystalline lattice structure behaves as a diffraction grating because the wavelength (λ) of x-rays are of the same magnitude as the spacing (*d*) of atoms in a crystal structure (~1 Å). The resulting intensities and angles of the diffracted beams returned from specific orientations of the crystal can be measured and the atomic structure in a phase can be determined (Raudsepp & Pani, 2003). Clay minerals diffract from 020 and 110 spacings and the spacings are nearly the same dimension for all of them (Moore & Reynolds, 1997). Both low and high 2 θ angles determine clay minerals whereas high 2 θ angle detect non-clay minerals i.e. feldspar, quartz, carbonates, pyrite, zeolites and Fe-oxides.

To characterise a sample, an x-ray diffraction pattern or diffractogram is produced by plotting the angular positions and intensities of the resultant diffracted peaks. The diffractogram displays peak positions (indicative of minerals present), peak heights (mineral concentrations), peak width (mineral crystallinity, size/strain) and a background curve that signifies amorphous content. The crystal structure can be further refined during processing using the Rietveld method where the recently generated diffractogram is compared to one calculated from a known crystal structure, usually sourced from an internationally recognised database of reference patterns containing ~ 70,000 crystalline phases.

4.2.5 Clay separate x-ray diffraction (XRD) method

Clay separate XRD, rather than whole rock XRD was performed on 17 samples to identify the clay mineral species of particular interest. Methodology chosen followed those in place at GNS Science, Wairakei, Taupo and those outlined by Moore & Reynolds (1997). In preparation for clay separate x-ray diffraction, 17 samples of ~3-5 g of rock cuttings were crushed by hand in a large agate mortar and pestle until a fine particle consistency was achieved . Excessive dry grinding was avoided to prevent reducing the coarse grained non-clay minerals such as quartz, and feldspar to the clay size range and obscuring the actual clay minerals present (Moore & Reynolds, 1997).

Approximately 3-5 g of powdered sample was placed in a 10 ml test tube, filled to 2 ml level, and 8 ml of distilled water with sodium hexametaphosphate (a deflocculent) was added to prevent sub-microscopic polymineralic aggregates forming (Moore & Reynolds, 1997). The deflocculent was prepared by adding 76 mg of $(NaPO_3)_6$ into 500 ml of distilled water in a beaker (or 0.15 g to 1 L distilled water) that is stirred with a magnetic stirrer. The test tube was placed in an ultrasonic bath for five minutes, shaken by hand for a minute then placed in a centrifuge and spun for two minutes at 1500 rpm, to obtain the < 2 µm fraction. The clay water mixture was pipetted onto a glass slide by sucking up the suspended clays 1 mm below the meniscus thus avoiding coarser material settled on the bottom. Enough solution was added to the slide so that the surface tension allowed a dome to form and samples were left overnight to air dry.

Two identical sets of slide samples were made, the first set was air dried while the second set was treated by glycolation in a sealed desiccator containing ethylene glycol for at least 36 hours to allow absorption of the ethylene glycol vapour. Glycolation causes smectite to expand as the glycol molecules enter the interlayer space of the swelling clay leading to the formation of a two layer structure, triggering a shift in Ångstrom position as water molecules are replaced. Glycolated samples were then analysed in small batches to prevent the vapour defusing out.

Both air dry and glycolated samples were analysed by x-ray diffraction in the 2° – 28° 2 θ angle. XRD analysis was carried out at the University of Waikato on a PANalytical Empyrean X-ray diffractometer at 45 kV and 40 mA using Cu Kα1 radiation. The mineralogy of each sample was determined from primary and secondary peak positions on graphs produced by the software Highscore Plus and the International Centre for Diffraction Data mineral reference database (ICDD Minerals PDF-4 database) (see Appendix C on CD). Other useful sources used were the USGS manual and flow chart, XRD reference charts and Brown and Brindley (1980).

4.3 ALTERATION MINERALOGY

Typically in active hydrothermal settings, the primary host minerals in a rock are replaced by a variety of alteration minerals. Hence there is a general relationship between alteration products and the original composition of the primary minerals. Early formed alteration minerals can also be destroyed and overprinted by minerals formed by later alteration processes. For example chlorite can be replaced by illite or epidote replaced by chlorite or carbonate. Minerals that are common products of hydrothermal alteration are illite, kaolinite, smectite, quartz, chlorite, adularia, albite, sulphides (especially pyrite), epidote, calcite (or other carbonates) and leucoxene (Table 4.4). Clay minerals are abundant in some geothermal fields but less so in others (Browne, 1978).

Depending on the temperature and pH of the environment, feldspars typically alter to clay minerals such as illite and smectite, as well as alunite, carbonate and epidote-zoisite. Sodic and potassic feldspars such as albite, orthoclase and adularia also occur as abundant alteration products. Minerals that commonly alter to chlorite are

the Mg and Fe-bearing minerals such as pyroxene, amphibole and biotite, however hydrothermal ferromagnesian minerals, such as epidote can also be replaced by chlorite, carbonate, pyrite, and leucoxene. Biotite is usually the first to be destroyed during alteration but in some less common, high temperature (i.e., >260°C; Reyes, 1990) hydrothermal environments it becomes a product of alteration (Schwartz, 1959; Simpson & Mauk, 2011).

Table 4.4. Common replacement products for original components as a result of alteration (after Gifkins et al., 2005). The term sericite used in this table is a varietal term often used for fine-grained muscovite, illite or paragonite (Kühn, 2004).

Original component	Typical alteration replacement products
Silicic volcanic glass	Zeolites, cristobalite, opaline silica, quartz, calcite, smectite, mixed layer clays
Mafic volcanic glass	Smectite, calcite, chlorite, epidote, Ca-rich zeolites, nontronic clays, Fe/Ti/Mn-oxides
Magnetite, ilmenite, titanomagnetite	Pyrite, leucoxene, titanite, pyrrhotite, hematite
Pyroxene, amphibole, olivine, biotite	Chlorite, illite, quartz, calcite, pyrite, anhydrite
Plagioclase	Calcite, albite, adularia, wairakite, quartz, anhydrite, chlorite, illite, kaolin, smectite, epidote, sericite
Anorthoclase, sanidine, orthoclase	Adularia, albite, sericite
Quartz	Microcrystalline quartz

Hydrothermal alteration is typically described and classified by the mineral assemblages or common mineral associations found and chemical changes involved. Gifkins et al., (2005) and Pirajno (2009) outline a four-variable approach to describe alteration in volcanic rocks: intensity, distribution, texture and mineral assemblage.

4 + 3 + 2 + 1

The intensity variable (4) can be described as subtle, weak, moderate, strong or intense and refers to the degree to which a rock has undergone alteration. For example, weak means only a few of the primary minerals have been replaced and minimal textural replacement has occurred. The distribution variable (3) uses terms such as local, regional, footwall, hanging wall, pipe or stratabound. The texture variable (2) determined by hand specimen and petrographic description includes shape, grainsize and fabric and the alteration may have altered the textures in a selective, pervasive or vein halo way. Pervasive alteration means the replacement of

most or all minerals and textures. Selective alteration refers to only certain minerals being replaced while original textures largely remain. The mineral assemblage (1) lists the minerals identifed from most abundant to least.

Another term used is alteration rank that is an indication of the temperature and permeability in a volcanic field. Studies of the types of secondary minerals formed help to define alteration rank. For example epidote indicates higher temperatures (an increase in rank from lower temperature minerals) and adularia represents higher temperatures and higher permeability (an increase from lower permeability minerals) in a hydrothermal system (Browne, 1978).

4.3.1 Mineral inferred and measured well temperatures

Direct measurements of fluid output, pressure and temperature from geothermal wells enable present-day fluid flow to be monitored. However, to decipher the geological evolution of a geothermal system one must examine the temperatures and other conditions (permeability, pressure, acidity) at which minerals form and how these have varied over geological time (Fig. 4.6). Measured well temperatures during well completion tests after heat-up periods of one month, or more, establish the current temperatures of the reservoir encountered by the well and it is useful to compare these to the inferred mineral temperatures to understand the dynamics of the hydrothermal system. The SWIR and XRD results determine the alteration mineralogy (and therefore the inferred temperatures from mineral associations), while pXRF and XRF provide information on the chemical compositions of altered host rocks. When wells are drilled in a geothermal field the natural state of the geothermal reservoir encountered by the well is disturbed. Therefore the alteration minerals can aid in understanding the pre-drilled state of the system. This section describes the alteration minerals recognised by XRD, SWIR and petrographic analysis to gain insights into the hydrothermal conditions they form under.

Kaolinite $Al_2Si_2O_5(OH)_4$

Kaolinite occurs in marginal argillic zones and forms at low pH's of 3-4 and generally low temperatures of (<150 °C) (Thompson & Thompson, 1996), although surface kaolinite in the New Zealand fields typically does not occur at temperatures

above 60 °C (Browne, 1978). Dickite usually forms at higher temperatures (<200-250 °C) (Thompson & Thompson, 1996), but is generally rare in TVZ geothermal systems. According to Browne (1978) in one well in the TVZ at Ohaaki geothermal field dickite is known where current temperatures are 140-150 °C. Once past 220°C, the abundant clay mineral assemblage is illite and chlorite. Kaolinite also forms as cool, late-stage hydrothermal overprints and is probably some distance from the upflow zone, or when the geothermal reservoir is waning. It typically replaces host mineralogy and/or fills in veins and vugs. Kaolinite is also produced from the alteration of volcanic glass or feldspars and/or K-micas (i.e., illite) under acid conditions as the following reactions demonstrate (Kühn, 2004, Pirajno, 2009, Ellis & Mahon, 1977):

$$2NaAlSi_3O_8 + H_2O + 2H^+ = Al_2Si_2O_5(OH)_4 + 4SiO_2 + 2Na^+$$

Sodic plagioclase + water = kaolinite + quartz

$$2KAl_3Si_3O_{10}(OH)_2 + 3H_2O + 2H^+ = 3Al_2Si_2O_5(OH)_4 + 2K^+$$

K-mica + water + acid = kaolinite

Smectite (Montmorillonite) $(0.5Ca,Na)_{0.7}(Al,Mg,Fe)_4[(Si,Al)_8O_{20}](OH)_4.nH_2O$

Smectite (or montmorillonite) occurs as open space fill but most commonly replaces volcanic glass and sedimentary rocks (Steiner, 1977). Smectite is a general term for swelling clays, of which montmorillonite is usually encountered in geothermal fields. Montmorillonite is an important mineral thermometer as it is stable at temperatures up to 140 °C and forms during the passage of neutral and acid fluids that can form in steam-heated environments (Browne & Ellis, 1970, Thompson & Thompson, 1996). It usually occurs above or adjacent to the upflow zone. Ca-montmorillonite dominates with depth until temperature increases above ~140°C, at which point it becomes interlayered with illite. As temperature and typically depth increases a general progression from montmorillonite to interlayered montmorillonite-illite then interlayered illite-montmorillonite and finally to illite occurs (Browne, 1970). Consequently, they are useful common geothermometers as montmorillonite forms at ~140 °C or lower and illite >210 °C (Hedenquist, 1990; Harvey & Browne, 1991).

Illite-smectite (Montmorillonite)

With increasing temperature smectite interstratifies with illite to produce interlayered illite-smectite. Interlayered illite-smectite prevails at temperatures ~140° – 210°C (Browne and Ellis, 1970). Smectite transforms to illite, by the fixation of K^+ and the substitution of Al for Si. More acidic conditions cause a reverse, converting smectite to kaolinite.

Illite $K_{1.5\text{-}1.0}Al_4[Si_{6.5\text{-}7.0}Al_{1.5\text{-}1.0}O_{20}](OH)_4$

Illite is a micaceous clay mineral that gives rock a bleached appearance in hand specimen that is easily scratched. Illite is an ideal geothermometer as it has a temperature stability range greater than ~220°C (Browne and Ellis, 1970). Neutral pH to weakly acid, CO_2 rich fluids are ideal conditions for illite formation. Illite replaces primary plagioclase and original rock components, occurs in vugs and veins and seems to increase in permeable zones as replacement in permeable lithologies.

Chlorite $(Mg,Fe^{2+},Fe^{3+},Mn,Al)_6(AlSi)_4O_{10}(OH)_8$

Chlorite forms over a wide temperature range and is common throughout and peripheral to most geothermal reservoirs. Strong chlorite alteration can impart a green tinge to the affected rocks. It is an alteration product resulting from the breakdown of ferromagnesian minerals such as biotite, pyroxene, hornblende but also volcanic (magmatic) glass. It can also precipitate in open spaces and veins (Bailey, 1988). Chlorite and quartz alteration occupy the inner alteration zone leading outward to sericite alteration in VHMS-related hydrothermal systems (Thompson & Thompson, 1996).

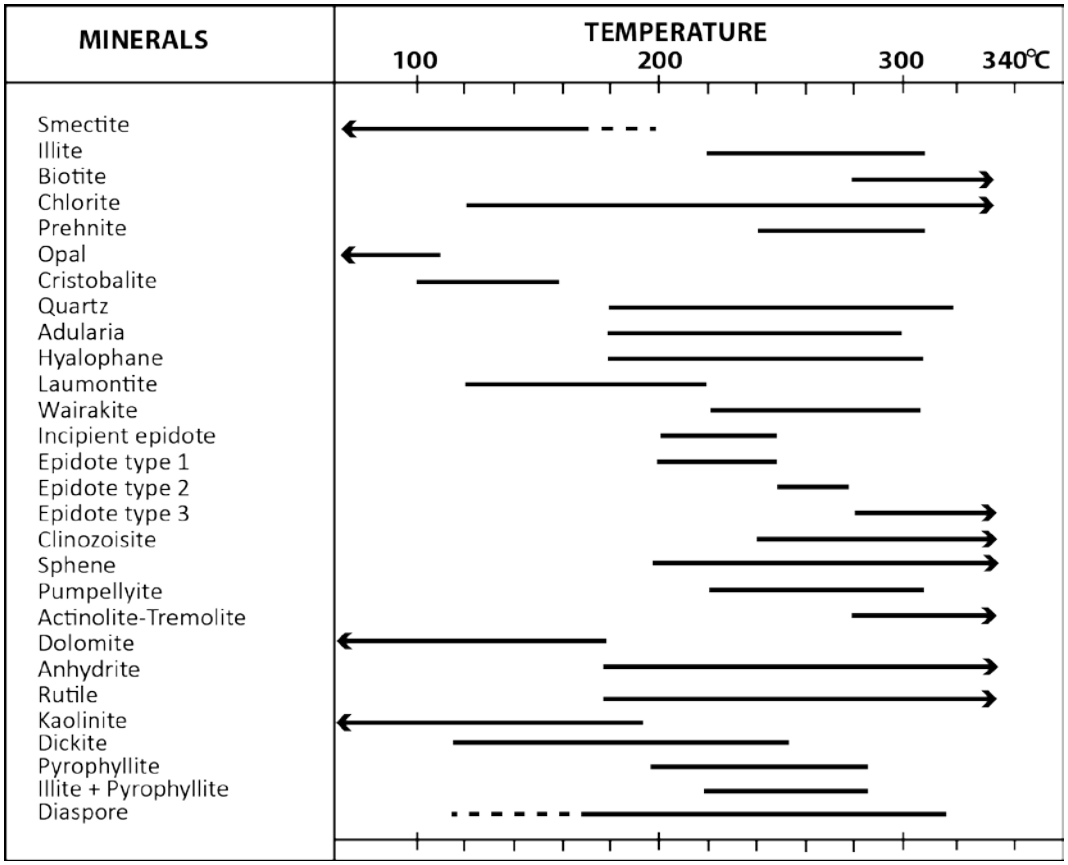

Fig. 4.6. Generalised temperature ranges of stability or formation for common hydrothermal minerals (Reyes, 1990). The different types of epidote refer to differences in crystallinity, abundance and occurrence.

Quartz SiO_2

In geothermal settings, secondary quartz is a common component of hydrothermal alteration, with primary quartz remaining for the most part, unaffected by hydrothermal alteration (Browne, 1970). Quartz is primarily composed of silica, the most abundant element in crustal rocks, and is highly soluble in high temperature fluids. Quartz is a polymorph of silica, other polymorphs encountered in geothermal fields are chalcedony, cristobalite, opal and amorphous silica (sinter) which can be used to subdivide the kaolinite zone further (Reyes, 1990).

Browne (1978) describes two wells (Y7 and Y8) from the Yellowstone National Park that illustrate the relationship of silica minerals in a geothermal field. Amorphous opal is typical of superficial sinter. In well Y7 α-cristobalite fills the groundmass and β-cristobalite occurs in veinlets. In contrast the hotter well Y8, contains chalcedony and quartz, suggesting temperature controls the distribution of silica minerals. Hydrothermal quartz precipitates over a temperature range of 180-

320 °C whereas amorphous silica, opal and cristobalite varieties stable at comparatively lower temperature and pressures, with amorphous silica stable and cristobalite stable at <160 °C and opal approximately <100 °C (Fig. 4.6, Reyes, 1990). In New Zealand fields, Browne (1978) states that cristobalite occurs frequently below 100 °C. These lower temperature polymorphs are less stable than quartz and are prone to dissolution or alkali reactivity (Broekmans, 2004). Quartz is the least soluble, that is followed by (with increasing solubility) chalcedony to cristobalite to amorphous silica.

At deeper levels in the geothermal system, silica dissolves and upon supersaturation precipitates out as a result of decreasing fluid temperatures. This silicification can cause issues with permeability as it seals fluid pathways disrupting the plumbing of the geothermal system. However Fournier and Rowe (1966) assert that at temperatures of <250 °C if a fluid supersaturated in silica ascends rapidly, quartz deposition is minimal. In contrast slow fluid ascension at hotter temperatures is favourable to precipitation of quartz, chalcedony or opaline silica due to conductive cooling. In geothermal systems the paleowater table is delineated from lateral replacement of rock by chalcedony or opaline silica (Thompson & Thompson, 1996).

Very low pH fluids or vapours that remove all other components in the rock besides primary quartz and rutile (TiO_2) are responsible for leaving residual vuggy quartz. Vuggy quartz may grade into quartz-alunite or quartz-kaolinite on the margins of an alteration zone (Thompson & Thompson, 1996). The vugs may be filled by late stage quartz, sulphides and sulphates.

Albite $NaAlSi_3O_8$

Albite, a sodic plagioclase, commonly replaces plagioclase (plagioclase by definition is Na and Ca rich) and forms above 230 °C (Browne, 1970). The replacement concentrates the residual Na, with added Na from geothermal fluid (Steiner, 1977) hence the presence of albite is indicative of Na enrichment. It also restructures the aluminosilicate tetrahedra within the plagioclase and creates vacuolisation (creation of micropores) caused by dissolution (Morad et al., 2009). At ~280 °C albite precipitates into vugs and fractures (Lagat, 2009). Depth, temperature and the

presence of primary plagioclase is suggested by Browne and Ellis (1970) to control the distribution of albite laterally and to depths over 800 m at Ohaaki Geothermal Field.

Albite is also an alteration product in propylitic alteration and is part of the sub-alteration styles of saussuritization and albitisation. Calcium rich plagioclase reacts with hydrothermal fluids to produce albite, epidote, chlorite, amphibole and calcite (Demange, 2012). Dolejš and Wagner (2008) report that at 275 °C, anorthite is replaced by epidote and excess Al is drawn into muscovite formation from K-feldspar (microcline):

$$4CaAl_2Si_2O_8 + 2KAlSi_3O_8 + Fe_2O_3 + 3H_2O$$
anorthite + microcline + iron oxide + water

$$= 2Ca_2FeAl_2Si_3O_{12}(OH) + 2KAl_2[AlSi_3O_{10}](OH)_2 + 2SiO_2$$
= epidote + muscovite + quartz

Morad et al. (2009) noted that in areas where ferromagnesian minerals are minor, albitisation occurs more readily because epidote formation is restricted due to the limited availability of iron and magnesium:

$$Na_2CaAl_4Si_8O_{24} + 4SiO_2 + 2Na^+ = 4NaAlSi_3O_8 + Ca^{2+}$$
andesine + quartz + sodium = albite + calcium

Albite replaces andesine above 230 °C and andesine may be completely replaced by adularia or adularia and albite (Wohletz & Heiken, 1992). Conversely where ferromagnesian minerals are common, propylitic alteration dominates enabling secondary ferromagnesian minerals (e.g., chlorite and epidote) to form. At the expense of plagioclase, the Si, Fe, Mg and K constituent ions are portioned into albite, epidote and sericite (illite) (Morad et al., 2009).

1.0 plagioclase (andesine) + 0.3 biotite + 2.2 H^+

=

0.6 albite + 0.2 epidote + 0.2 sericite + 0.7 H_4SiO_4 + 0.3 Fe^{2+} + 0.7 Mg^{2+} + 0.2 K^+

In thin section, albite has a variety of habits, appearing as tabular, cloudy, patchwork, chessboard, polysynthetic twinning or irregular crystals. Often the twinning maybe

inherited from the primary plagioclase it replaced. Mineral inclusions of iron oxide also point to the cloudy appearance of albite (Macintosh et al., 2000). Irregular textured albite is distributed along fractures and vein halos but towards the core alteration zone it is more pervasive resembling true potassic alteration. Conversely, the margins or weak mineralisation elsewhere results in patchwork or chessboard albite (Thompson & Thompson, 1996).

Adularia **$KAlSi_3O_8$**

Adularia is a high temperature (240-265 °C at Wairakei, Steiner 1970, 1977), near-neutral alteration mineral found in many geothermal reservoirs (Browne, 1978). Adularia is a K-feldspar that along with quartz and less common albite, replace host-rock minerals in permeable rocks and vein margins. At Ohaaki, its occurrence coincides with areas of high permeability making it a good indicator of high permeability as well as boiling in geothermal fields (Browne, 1970; Browne & Ellis, 1970; Steiner, 1970). The feldspars in the aquifer rocks directly correlate with the degree of permeability. With increasing permeability the feldspar type changes from andesine, to albite, albite + adularia and then adularia (Browne, 1978) which indicates the zone of highest permeability. At Ohaaki andesine (the most common feldspar) alters at temperatures of 70-290 °C to quartz, clay, calcite, albite or adularia depending on permeability.

Permeable areas in the central upflow zone of Ohaaki from ~100–1000 m depth are where adularia predominates. The relationship between feldspar types illustrates an increasing enrichment in K, as a result of K-metasomatism that is governed by cooling and CO_2 exsolution due to boiling and an increase in pH (Macintosh et al., 2000). In the deeper peripheral environment albite dominates due to Na-metasomatism influenced by heated inflowing waters. This knowledge is useful in geothermal production as the presence and abundance of adularia is related to bore output (Thompson & Thompson, 1996; Macintosh et al., 2000).

Consecutive replacement of plagioclase to albite then adularia might be caused by a decrease in temperature and an increase in the a_{K+}/a_{H+} ratio as albite dominates at temperatures of ~300° C whereas adularia stabilises at ~250° C. Sources of

potassium may be chloritised biotite (Morad et al., 2009) or an assemblage containing illite (a K-mica) and quartz:

$$KAl_2AlSi_3O_{10}(OH)_2 + 6SiO_2 + 2K^+ = 3KAlSi_3O_8 + 2H^+$$
K-mica (illite) + quartz = adularia

Reaction of chloritised biotite with simultaneous formation of adularia (K-feldspar) (Dolejš & Wagner, 2008).

$$5K(Mg,Fe)_3[AlSi_3O_{10}](OH)_2 + 3KAl_2[AlSi_3O_{10}](OH)_2 + 9SiO_2 + 4H_2O = 3(Mg,Fe)_5Al_2Si_3O_{10}(OH)_8 + 8KAlSi_3O_8$$
biotite + sericite + quartz = chlorite + adularia

Thus the growth of adularia removes excess potassium ions from the fluid. Fluid mixing and subsequent release of CO_2 or ionic diffusion derived from micropores in albite are reasons suggested to cause the replacement of albite by adularia (Parry, 1998; Caussiux et al., 2006). Overall the main mechanism in feldspar replacement is dissolution-precipitation reactions. In thin section, plagioclase replaced by adularia forms pseudomorphs made up of overlapping crystals that produce an uneven, or undulose extinction (Lagat, 2009). Adularia itself is commonly replaced by illite.

Epidote $Ca_2(Al,Fe)_3Si_3O_{12}(OH)$

Epidote forms at very high temperatures in excess of 230 °C (Browne & Ellis, 1970; Reyes, 1990; Thompson & Thompson, 1996), and its presence in geothermal wells is a good geothermometer. As temperatures increase so too does the size and prismatic nature (degree of crystallinity), abundance and occurrence of epidote crystals (Reyes, 1990, Fig. 4.6). In drill cuttings it has a characteristic pistachio-green colour (Steiner, 1977) and in thin section a high relief with distinctively high birefringence. It often occurs with calcite and wairakite to replace calcic-plagioclase (andesine), forms pseudomorphs by replacing ferromagnesian minerals (hypersthene, hornblende), deposits in veins and fractures and is accompanied by chlorite and mica clays to replace glassy silicic groundmass (Steiner, 1977). Where CO_2 rich fluids occur epidote is vulnerable to calcite replacement therefore requires low CO_2 concentrations to remain stable (Browne, 1978). The mineral assemblage characteristic of propylitic alteration or saussuritization is produced when Ca-rich plagioclase like anorthite reacts with hydrothermal fluid and is replaced by Na-rich

albite, epidote, chlorite, amphibole and calcite (Thompson & Thompson, 1996; Barker, 2014).

Wairakite $CaAl_2Si_4O_{12}.2H_2O$

Wairakite, a zeolite, is widespread in many geothermal systems and forms between temperatures of 200-250 °C making it a valuable geothermometer (Steiner, 1977; Browne & Ellis, 1970). Another zeolite that forms at lower temperatures is laumontite. For wairakite to remain stable, aqueous CO_2 must be at low concentrations to avoid replacement by calcite, which is also true for epidote. The occurrence of wairakite is indicative of moderate permeability. In thin section, wairakite has low or negative relief and distinctive sets of perpendicular twin lamellae. It occurs in altered volcanic and sedimentary rocks as open space fill (vugs, veinlets) or replacing Ca-plagioclase and volcanic glass (Steiner, 1977; Thompson & Thompson, 1996). Steiner (1977) reports that it has been identified in most TVZ geothermal fields, including Tauhara, Ohaaki, Kawerau, Te Kopia and Waiotapu, and in geothermal fields in Japan and Russia.

Calcite $CaCO_3$

Calcite is distinctive in thin section as it has extremely high birefringence, displaying pastel colours. Calcite forms from the replacement of typically plagioclase and silicic glass (Steiner, 1977; Simmons & Christenson, 1994). It remains stable over a wide temperature range 160-300 °C, depending on CO_2 concentrations in aqueous solutions however it is vulnerable to quartz replacement (Simmons & Christenson, 1994; Thompson & Thompson, 1996). Calcite has inverse solubility with temperature where it becomes less soluble as temperature increases. This is the reason why calcite precipitates from fluids that are heated and then dissolves upon cooling unlike quartz which precipitates upon cooling.

In rocks with low porosity and permeability where sub boiling CO_2 rich fluids and calcium alumina-silicates are present, calcite infills voids or replaces calcite bearing minerals like Ca-plagioclase (anorthite), zeolites, epidote and volcanic glass.

$$CaAl_2Si_2O_8 + CO_2 + H_2O = CaCO_3 + 2(\text{H-Al-silicate})\ Al_2Si_2O_5(OH)_4$$

anorthite + carbon dioxide + water = calcite + kaolinite

Hydrothermal calcite is highly sensitive to boiling in geothermal systems. A decrease in confining pressure, and loss of steam removes dissolved CO_2, and other gases, causing calcite to deposit:

$$Ca^{2+} + 2HCO_3^- = CaCO_{3(s)} + CO_{2(g)} + H_2O$$
Calcium + bicarbonate = calcite + carbon dioxide + water

Platy calcite (lattice textured calcite) in particular is very diagnostic of CO_2 exsolving and boiling zones. It forms an approximately ~300 m thick vertical column within the two-phase upflow zone (Nicholson, 1993; Simmons & Christenson, 1994; Kuhn, 2004). Simmons and Christenson (1994) found that calcite precipitation and distribution is an indication of temperature, pressure, CO_2 concentration in the fluid and fluid movement through a boiling geothermal system.

Pyrite **FeS_2**

Pyrite has a clear cubic habit and is opaque in thin section. Pyrite occurs in geothermal systems in three ways:

1) by replacing magnetite or ferromagnesian minerals, rich in iron:

Magnetite to pyrite

$$Fe_3O_4 + 6H_2S \leftrightarrow 3FeS_2 + 4H_2O + 2H_2$$

Magnetite becomes unstable at temperatures greater than 150 °C while pyrite is being formed (Steiner, 1977). Cubes of pyrite enclose magnetite relics or make up pseudomorphs of ferromagnesian minerals.

2) disseminated pyrite forms from iron in altered rocks that have been argillised:

Iron oxides in glass and silicate minerals to form pyrite

$$FeO + 2H_2S \leftrightarrow FeS_2 + H_2O + H_2$$

3) or it deposits from geothermal fluid along veinlets or fractures. Steiner & Rafter (1966) showed isotopically that geothermal fluid is the source of sulphur in pyrite.

4.3.2 X-ray diffraction results

X-ray diffraction (XRD) analysis identified montmorillonite, kaolinite, chlorite, illite and quartz, along with the feldspars, albite, orthoclase and minor anorthoclase, sanidine and microcline. Identified minerals are shown in Table 4.5. Because clay separate XRD was performed rather than whole rock XRD, the presence of epidote was not detected. Its presence was established visually by logging and thin section petrography. Although short wave infrared does recognise epidote, it needs to be present in large quantities in order for it to register on the spectrometer. Nevertheless, the minerals present are indicative of argillic or intermediate argillic alteration, propylitic or zeolitic alteration and possibly adularia alteration according to Table 4.5.

The presence of montmorillonite and kaolinite at shallower levels in TH9 and TH10 is indicative of low temperature acid alteration suggesting a flux of cooler water is encountered in this area beneath the Huka Falls Formation. This is compatible with the Huka Falls acting as a cap or aquitard to the system. Beneath this, samples are clearly in the illite zone, except for in TH10 where illite appears to be poorly developed. Chlorite, illite, quartz and albite are common at intermediate levels in all the wells representing an increase in alteration rank, which is followed by chlorite, illite and adularia at the deepest levels. Chlorite is common in the deeper parts for all the wells.

Interestingly, the mineral assemblage in TH10 lacks illite at deeper levels (2100-2305 mRF) suggesting that the aluminium needed to form illite has been scavenged by albite. The reverse is seen at 1620 mRF where illite is present but albite absent. However the lack of illite may also be related to pH or host rock chemistry.

Table 4.5. Minerals identified by clay-separate XRD analysis from three wells, TH9, TH10, TH12 from the Tauhara Geothermal Field.

Minerals / Well depth		Montmorillonite	Kaolinite	Chlorite	Illite	Quartz	Plagioclase feldspars	→ Albite	Alkali / K-feldspars	→ Orthoclase	→ Anorthoclase	→ Sanidine	→ Microcline	Cristobalite	Zeolite
TH9	350 mRF	✓	✓											?	
TH9	720 mRF			✓	✓	✓		✓							
TH9	940 mRF			✓	✓	✓		✓				✓			
TH9	1100 mRF			✓	✓			✓		✓					
TH9	1540 mRF	?		✓	✓			✓		✓					
TH10	520 mRF	✓	✓			✓								?	
TH10	880 mRF			✓	✓	✓		✓							
TH10	1240 mRF			✓		✓		✓							
TH10	1620 mRF			✓	✓	✓									
TH10	2100 mRF			✓		✓		✓							
TH10	2305 mRF			✓		✓		✓							?
TH12	240 mRF	✓			✓	✓									?
TH12	390 mRF	✓			✓	✓							✓	?	
TH12	1040 mRF	?		✓	✓	✓		✓							
TH12	1160 mRF			✓	✓			?		✓	✓				
TH12	1240 mRF			✓	✓	✓		✓							
TH12	1380 mRF			✓	✓	✓				✓					

4.3.3 Terraspec mineralogy (SWIR)

The results of the SWIR analyses are tabulated and described below (Table 4.6). In order to understand the distribution of minerals detected by SWIR and XRD and the resulting mineral inferred temperatures and subsequent thermal evolution in the system, the results of both analyses were plotted downhole for each well (Figures 4.7a, 4.7b and 4.7c). Downhole plots also allowed discrepancies between the two techniques to be ascertained.

Table 4.6. Summary of SWIR alteration mineralogy for wells TH9, TH10 and TH12.

Depth (mRF)	TH9
60 – 320	smectite
340 – 540	illite-smec, kaolinite at 350, 400 & 420
560 – 900	illite, minor chlorite, calcite
920 – 1280	smectite, strong H_2O
1300 – 2415	illite-smec or illite, common chlorite and calcite

Depth (mRF)	TH10
70 – 760	illite-smec, kaolinite at 360, 460 & 520
620 mRF +	chlorite and calcite appear
740 – 1180	illite, with calcite and chlorite
1200 – 2332	strong calcite and chlorite, subordinate AlOH (2210 nm) feature that is often seen as subtle asymmetry suggestive of illite-smec or illite, 1640 mRF onwards is epidote

Depth (mRF)	TH12
40 – 410	mainly illite-smec
420 – 1020	mainly illite, with local illite-smec
1040 – 1400	mainly illite-smec, local smectite at approx. 1200 mRF, from 1040 mRF with depth is calcite and chlorite

TH9 well

From 60 – 320 mRF in TH9 smectite dominates with illite-smectite from 340 – 540 mRF (Fig. 4.7a). Kaolinite is distinct at 350 mRF and is also present at 400 and 420 mRF where it is recognised in profiles by a subtle asymmetry. Illite predominates from 560 – 900 mRF along with minor chlorite and suspected calcite. From 920 – 1280 mRF the SWIR spectra resembles the profile of smectite. Cuttings from 1300 – 2415 mRF have illite-smectite/illite together with common chlorite and calcite. From 920-1280 mRF SWIR profiles have the appearance of smectite but XRD indicates illite. When discrepancies like this arise, the clay XRD identified mineral (in this case illite) is always favoured because the clay is concentrated rather than surface analysed.

The contradictory spectra are dominated by a water feature suggesting the presence of additional water (possibly from fluid inclusions) that has resulted in a SWIR mis-identification. Further work is presently underway to better determine the source of

the excess water in the SWIR profiles and to recognise spectral characteristics that could be used to distinguish when excess water is an issue.

TH10 well

Interlayered illite-smectite prevails over 70 – 760 mRF in TH10 (Fig. 4.7b) with rare kaolinite appearing at 360, 460 and 520 mRF. From 620 mRF chlorite and calcite appear with illite present from 740 – 1180 mRF. Strong calcite and chlorite dominate from 1200 – 2332 mRF and illite-smectite or illite is suspected to also be present in these samples, but is only seen as a subtle asymmetry obscured by strong spectral responses for chlorite and calcite. Only some samples below 1200 mRF have stronger profiles and appear mostly to be of illite. Epidote is identified in samples below 1640 mRF and is reported from binocular observation as present in low concentrations.

TH12 well

In well TH12 (Fig. 4.7c) illite-smectite dominates from 40 – 410 mRF. Generally illite with local illite-smectite occurs over 420 – 1020 mRF. Interlayered illite-smectite predominates from 1040 – 1400 mRF onwards with local apparent smectite around 1200 mRF. From 1040 mRF onwards chlorite and associated calcite are present. Beyond 1040 mRF the clay identified by SWIR is illite-smectite / smectite, but from XRD is illite. Again, SWIR spectra appear to have excess water (fluid inclusion / intra-crystalline) resulting in the mis-identification of illite.

4.3.4 SWIR alteration mineralogy and hydrothermal conditions

The distinction between smectite, illite-smectite and illite is based on the determination of the AlOH / H_2O ratio (aluminium hydroxyl/water ratio) that is used as a crystallinity index to indicate white mica crystallinity. According to Simpson et al., (2013) the hull quotient ratio for AlOH / H_2O has an accuracy of 94% and is preferred over the raw AlOH / H_2O ratio. The boundaries are <0.76 for smectite, interlayered illite-smectite is 0.76 and 0.96 and illite is >0.96. This generally distinguishes the clays but there can be some overlap, for example interstratified illite-smectites with a high percentage of illite (>80 %) can be categorized as illite.

Likewise interstratified illite-smectites with a high percentage of smectite (>80 %) will plot within the smectite field. Generally, the AlOH / H_2O ratio decreases with increasing amounts of smectite (Simpson et al., 2013). Figures 4.7a, 4.7b and 4.7c present hull quotient ratio boundaries (red lines) and illustrate the distribution of smectite, illite-smectite, illite and epidote down well, and can be used to infer the temperatures of hydrothermal fluids that formed these minerals (Browne, 1978).

Trends in the aluminium hydroxyl and water ratio (AlOH / H_2O) also seem to coincide with some of the locations of feed zones, namely in TH9 and TH12 (Figs. 4.7a and 4.7c) as there is a lack of data points in TH10. In TH9 (at ~ 970, 1500, 1850 mRF) and TH12 (at ~ 1060, 1120, 1225, 1320 mRF) the AlOH / H_2O ratio decreases from an illite zone or interlayered illite-smectite zone (>0.76) to a smectite zone (<0.76). In TH9 at 2140 and 2330 mRF there are also clear breaks in the AlOH / H_2O ratio which appear to correlate with the two feed zone locations at the bottom of that well.

In TH10 there is an obvious gap from approximately ~ 1200 to ~ 1600 mRF. The gap in the data is due to fluid inclusions or inter-crystalline water as the spectral profiles in this area have a very broad water feature that distorts the spectral response. Fluid inclusions are also the reason for a smaller gap at deeper levels from ~ 1950 – 2250 mRF where the spectral profiles show broad water features.

Smectite generally forms at temperatures of <150 ºC, illite-smectite 150 – 210 ºC, illite >210 ºC and epidote >250 ºC (Browne and Ellis, 1970). In TH9 there is a sequence of smectite to illite-smectite to illite with increasing depth and in TH10 and TH12 a general sequence of illite-smectite to illite. Both indicate a prograde sequence with depth. However in TH9 (920 – 1300 mRF) and also TH12 (below 1050 mRF) the interpretations of SWIR spectra suggest smectite or illite-smectite in contrast to illite identified from XRD.

In TH12 at ~ 1200 mRF (Fig. 4.7c) SWIR indicates smectite, whereas XRD identified illite. Once again XRD is preferred as it has fewer ambiguities generated by smectite interlayering and potential trapped fluid. Hence illite formation

temperatures are >210 ºC (Browne, 1978). In TH9 measured well temperatures of >240 °C below ~772 mRF and >280 °C above ~952 mRF do not correlate with mineral associations identified by SWIR but are in agreement with the petrography in this study and Rosenberg et al., (2010) where the presence of epidote, wairakite, adularia and albite were noted, implying permeable conditions and formation temperatures of at least 240 °C (Browne and Ellis, 1970).

The appearance of illite-smectite at the top of TH12 and TH10 suggests formation temperatures of <210 °C, leading to an increase in formation temperature (>220 °C) down well with the presence of illite (Browne, 1978). In TH12 formation temperatures seem to decrease to <210 °C (Browne and Ellis, 1970) as illite-smectite appears then decreases further to <140 °C (Browne and Ellis, 1970) from an interval of smectite-dominated rock at ~1200 mRF. The alteration mineralogy at depth is not consistent with the measured well temperatures of 280 °C at 4 weeks heat up in TH12 at ~820 m depth implying that fluid temperatures may have only recently increased because the illite-smectite should have transformed to illite at the modern fluid temperature.

In TH12, but more obviously in TH10 due to the presence of epidote, the hydrothermal alteration appears to increase in intensity from an argillic to a propylitic alteration type down well, from a hydrothermal mineral association of illite-smectite / illite, chlorite, epidote and calcite. Epidote occurrence implies formation temperatures of >250 °C (Rosenberg et al., 2010). TH10 mineral inferred temperatures seem to generally correlate with measured well temperatures.

SWIR is ideal for rapid identification and cost effective data acquisition. While a well is drilled clay minerals can be identified, then used to infer formation temperatures and give insights on the geohydrology of the reservoir. Ideal samples that will produce reliable results are those with minimal volcanic glass (as these produce a spectral profile similar to smectite) and intercrystalline water (Simpson et al., 2013).

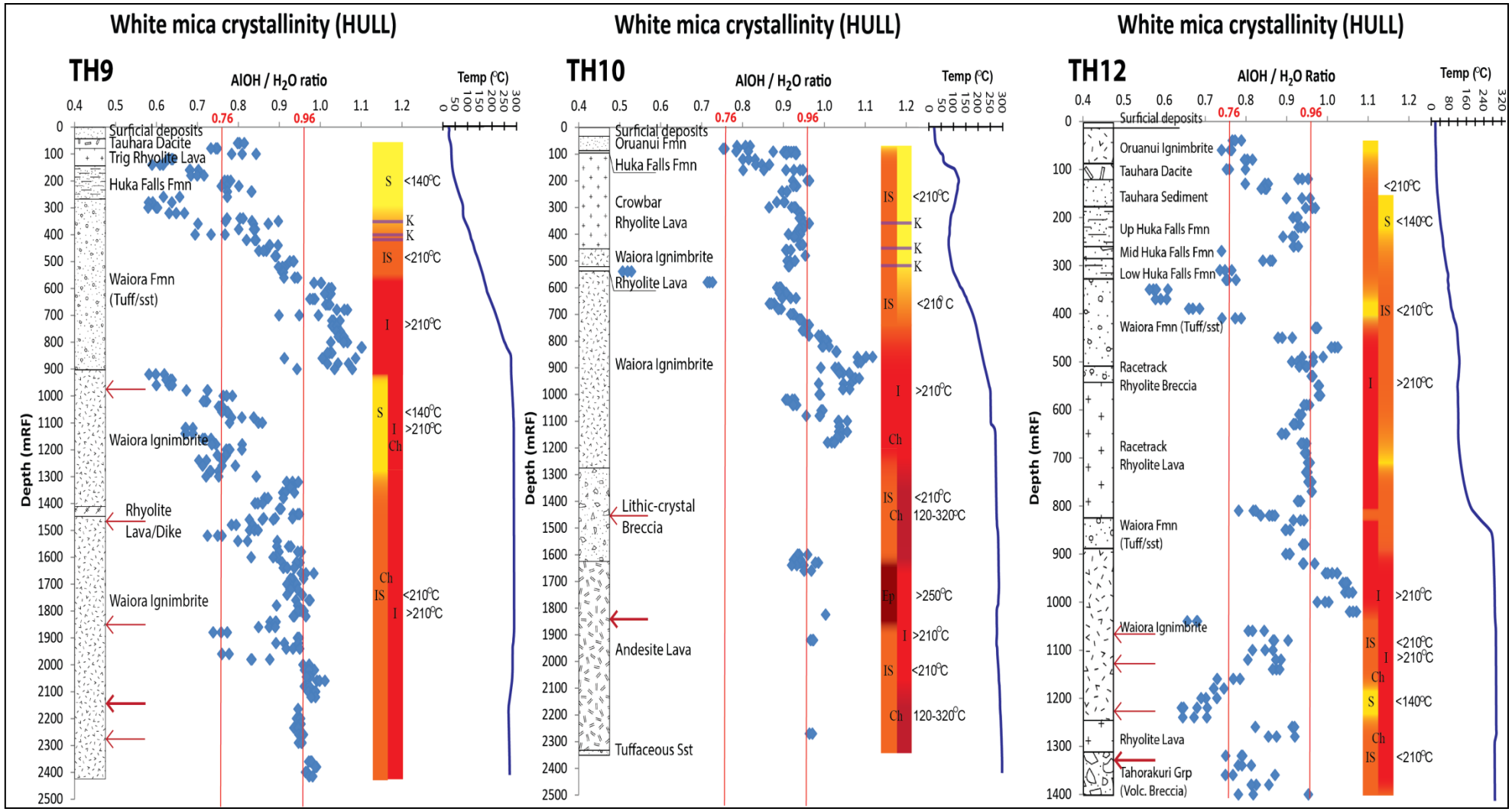

Figs. 4.7a, 4.7b, 4.7c. Plotted SWIR samples per well. The blue diamonds are SWIR data plotted as AlOH/H_2O ratio against depth (mrF=metres below rig floor). Red arrows are recognised feed zones. Red column is minerals identified from SWIR on the left and XRD on the right with their corresponding inferred temperatures. K= kaolinite, S=smectite, IS=illite-smectite, I=illite, Ep = epidote. Blue line is measured well temperatures a) TH9 - 30 day heat up, b) TH10 - 28 day heat up and c) TH12 – 4 weeks heat up (Measured temperature data and feed zones from Contact Energy Ltd).

4.4 ALTERED PRIMARY MINERALOGY

During alteration, primary mineralogy and textures are either completely or partially replaced to produce new hydrothermally altered minerals and textures. The type of hydrothermally altered minerals that occur in the Tauhara geothermal field according to the XRD and SWIR results shown previously, were described earlier in the chapter. A thin section of a rock produces a snapshot of alteration intensity and textural overprinting relationships. Studying alteration textures provides insights into the order of mineral genesis (paragenesis) and alteration stages in a system (Gifkins, et al., 2005), and hence patterns of fluid flow, the physical chemistry occurring and alteration system evolution.

4.4.1 Textures

Alteration produces textural destruction and either creates new textures or preserves relicts of the original textures. These textural changes are a result of modifications to shape, form, grainsize and orientation of clasts or minerals in the rock. Other changes involve the precipitation of minerals that infill open spaces and along fluid pathways.

Common alteration textures outlined by Gifkins et al., (2005) are:

1) Replacement (metasomatism) – original minerals and/or glass is replaced by new minerals e.g. pervasive, selective, disseminated, pseudomorph, microcrystalline, cryptocrystalline, spheroid, vein-halo
2) Infill – minerals are precipitated into open spaces such as cavities, pore spaces or in veins from solution. Infill can be incomplete, massive, layered, fibrous, prismatic, layered, crustiform
3) Dissolution – existing minerals or glass is dissolved and removed by solution, successive replacement minerals may occur. Examples of dissolution are solution seams, stylolites, corrosion vugs and veins.
4) Recrystallisation (static or dynamic) – existing minerals or grains are recrystallised into new minerals or grains accompanied by a morphological change. Dynamic recrystallisation incorporates an additional change in orientation. Examples of recrystallisation include

foliation, lineation and layering that produce microscopic textures such as granoblastic, poikiloblastic, porphyroblastic, perlitic, gneissic, schistose.

5) Deformation – primary minerals or textures are rotated, compressed, milled, comminuted, fractured, broken or modified. Examples are fiamme, foliated, lineated, augen schistose and eutaxitic. Deformation in volcanic deposits is usually a result of tectonic forces, welding (in ignimbrites) and compaction during burial.

4.4.2 Pseudotextures

Pseudotextures are textures that obscure the true primary volcanic textures making identification of initial volcanic facies difficult. Overprinting alteration (polyphase) and partial destruction of initial textures result in false textures (McPhie et al., 1993). Pseudotextures come in two categories: 1) pseudoclastic textures which encompass pseudogranular, false thinly bedded volcaniclastic and the most common pseudobreccia, or 2) false pyroclastic textures such as false shards, false pyroclasts or a false eutaxitic texture (Gifkins et al., 2005). False massive textures are produced by intense pervasive alteration while polyphase alteration produces false-clast supported textures.

Alteration occurs in different stages, intensities and duration producing alteration minerals of varying proportions and types thereby differing colours and textures. False breccia and pyroclastic textures result from two-phase alteration where complete replacement is achieved by the first alteration phase (phyllosilicate alteration) while the second alteration phase (quartzo-feldspathic alteration) replacement is incomplete, enabling relics of the former phase to be preserved. As a result, the primary glass and crystalline areas end up with different colours and alteration mineralogy. Often the glassy matrix is altered to phyllosilicate assemblages and crystalline domains altered to quartzo-feldspathic assemblages.

Volcanic glass is then widely replaced preferentially and pervasive alteration saturates the matrix (McPhie et al., 1993). Following this, alteration is focused on fractures and moves progressively through the matrix and unaltered sections.

Advanced alteration eventually shifts into clasts which enhances the pseudoclastic-pseudomatrix appearance.

Not all pseudotextures are created equal because the outcome depends on the original texture and composition of the rock. Mottled and patchy alteration distribution from the colour and preservation of primary minerals give pseudobreccia and pseudoclastic facies a polymictic (of varying clast type) appearance. The recrystallisation of spherulitic or micropoikilitic groundmass textures produce pseudogranular textures that look like fine-grained well sorted sandstones. Flow banding, creates a false thin-bedded volcaniclastic texture (Allen, 1988) because darker phyllosilicates replace glassy bands and cryptocrystalline bands change to a quartzo-feldspathic assemblage with polycrystalline phenocrysts. Pseudoclastic and finer grained textures are also aided by fracturing of phenocrysts resulting from deformation.

4.4.3 Petrography methodology

Detailed rock description and petrographic analyses for each well were completed by Kilgour et al. (2006), and Milicich et al. (2008a, 2008b) therefore the following results are from my own observations and serve to supplement the mineralogy retrieved by SWIR and XRD. Minerals not identified during this study but were recognised in well reports are included.

Although available core from the three wells are sparse, six thin sections of drill core were made. One core sample from TH10, two core samples from TH9, and three core samples from TH12 were collected (Table 4.2). Core samples were cut with a rock saw Struers Discoplan - TS into smaller blocks in order to fit them onto a standard petrographic glass slide (27 x 46 x 1.2 mm). The glass slides were pre-frosted to obtain an even surface in which to mount the block. Because the rock was cut on the saw at a slow speed, only grinding by hand using 600 grit aluminium oxide (Al_2O_3) powder on a glass surface was needed to make the block as flat as possible.

The core blocks, a prepared mixture of 2-part Hillquist resin and the frosted glass slides were placed on a hot plate set at 60 °C for 3 hours. Heating the resin reduces the viscosity allowing air bubbles to escape and enables the blocks to be easily mounted on to the glass slides. Once mounted and set overnight, the blocks were ground down to a thickness of ~30 microns. The ideal interference colours of straw yellow-white for feldspars/quartz under cross-polarised light were used to achieve the correct thickness. A Buehler twin grinder-polisher with a 1200 grit silica carbon paper (SiC) was used for the final grinding stage, followed by the same polisher with polishing pads and a 0.3 µm alumina polishing powder to obtain the smoothest surface and eliminate the need for a coverslip.

4.4.4 Petrography results (thin section and hand specimen)

TH9 well, Core 1 **~1801.5mRF**

Fig. 4.8. TH9 core 1, hand specimen, Waiora Ignimbrite, ~1801.5 mRF. Above: Brecciated texture of various clasts in vitroclastic matrix. Below: Chlorite, pyrite and quartz lined joint face.

The first core sample from TH9 at ~1801.5 mRF is from a lithic-rich ignimbrite termed the Waiora Ignimbrite. It is whitish pinky grey with a brecciated texture. Clasts consist of pumice, tuff, angular xenoliths, minor feldspar and quartz crystals and chloritised fiamme in a vitroclastic matrix. The rock is densely welded but has joint fractures that are visibly lined with chlorite, pyrite and quartz, therefore the lines have self-sealed to some degree, inhibiting permeability

(Milicich et al., 2008a). It is also intensely altered, and a clearly zoned phenocryst in hand specimen can be seen (Fig. 4.8, black arrow).

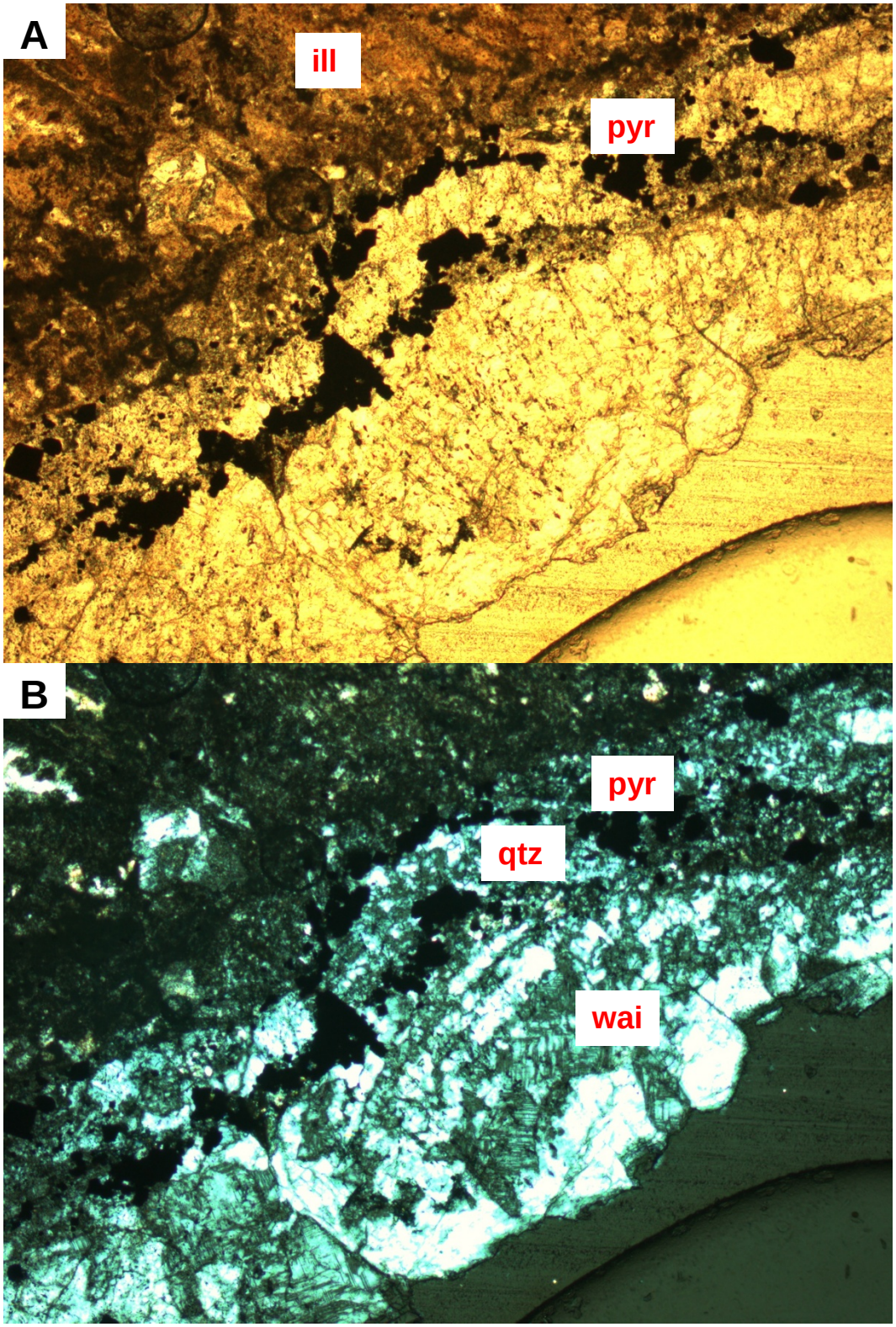

Fig. 4.9. Wairakite (wai) infilling vein fracture along with quartz (qtz) and pyrite (pyr). Illite alteration zone before leading towards vein. 5x magnification, A=PPL, B=XPL.

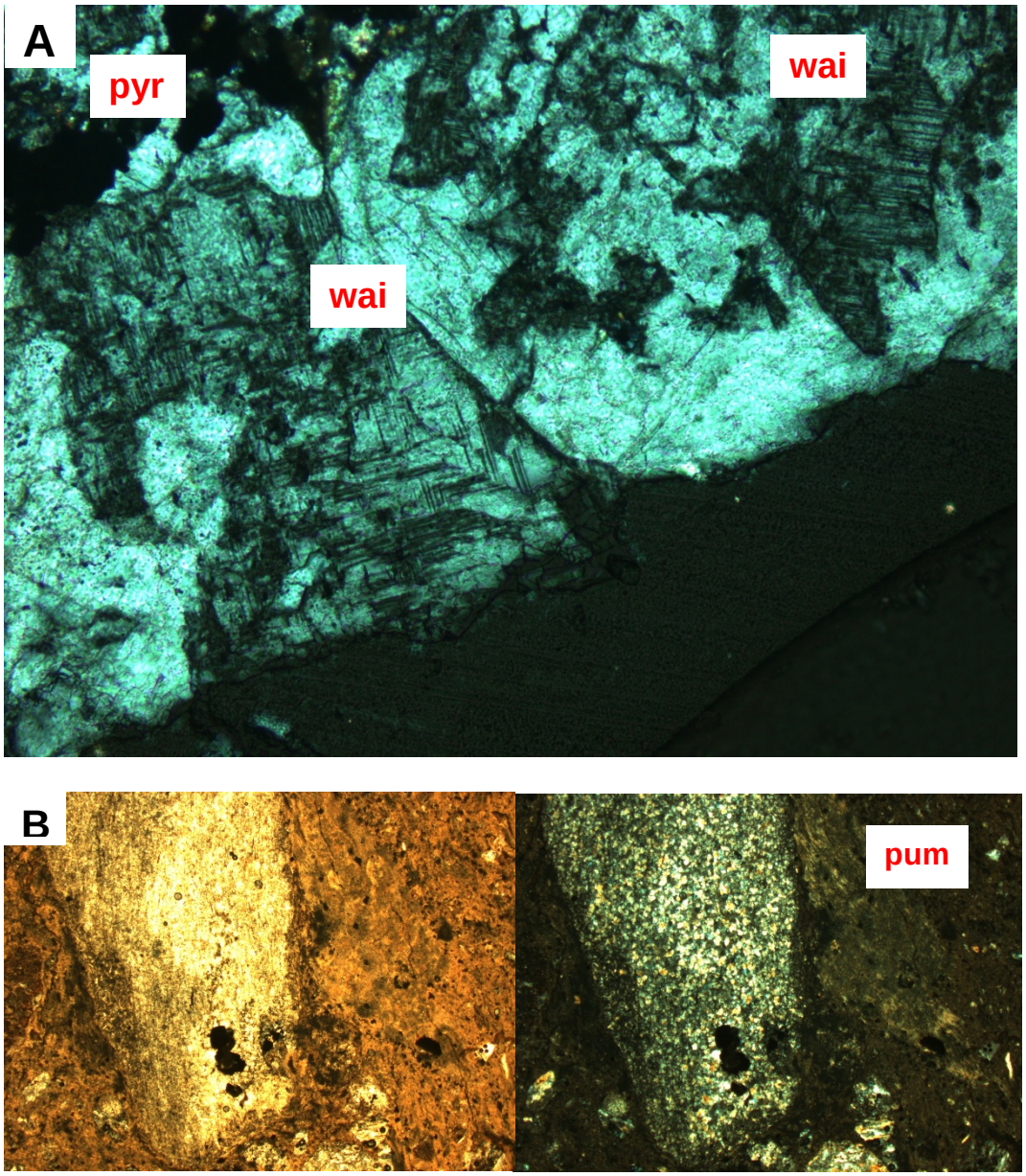

Fig. 4.10. A: Close up of wairakite infilling vein with quartz and pyrite (pyr). 10x magnification, XPL. B: Tuff lithic recrystallised to quartz, pumice clast subjected to clay alteration (pum). 2.5x magnification, PPL on left, XPL on right.

In thin section, the clasts of pumice are chloritised, and the tuff lithics have been recrystallised to quartz or smeared by illite. Wairakite appears as open space fill but more so as vein infill in hydrothermal quartz veins that are lined with pyrite. Zoned alteration is seen towards veins beginning with illite, quartz-pyrite where pyrite is particularly concentrated in vein selvedges followed by wairakite. Primary plagioclase is replaced by simple twinned albite and/or radiating acicular epidote. The groundmass has been altered from vitrophyric to completely

chloritic with minor quartz. Opaque pyrite and hematite are also disseminated throughout the sample.

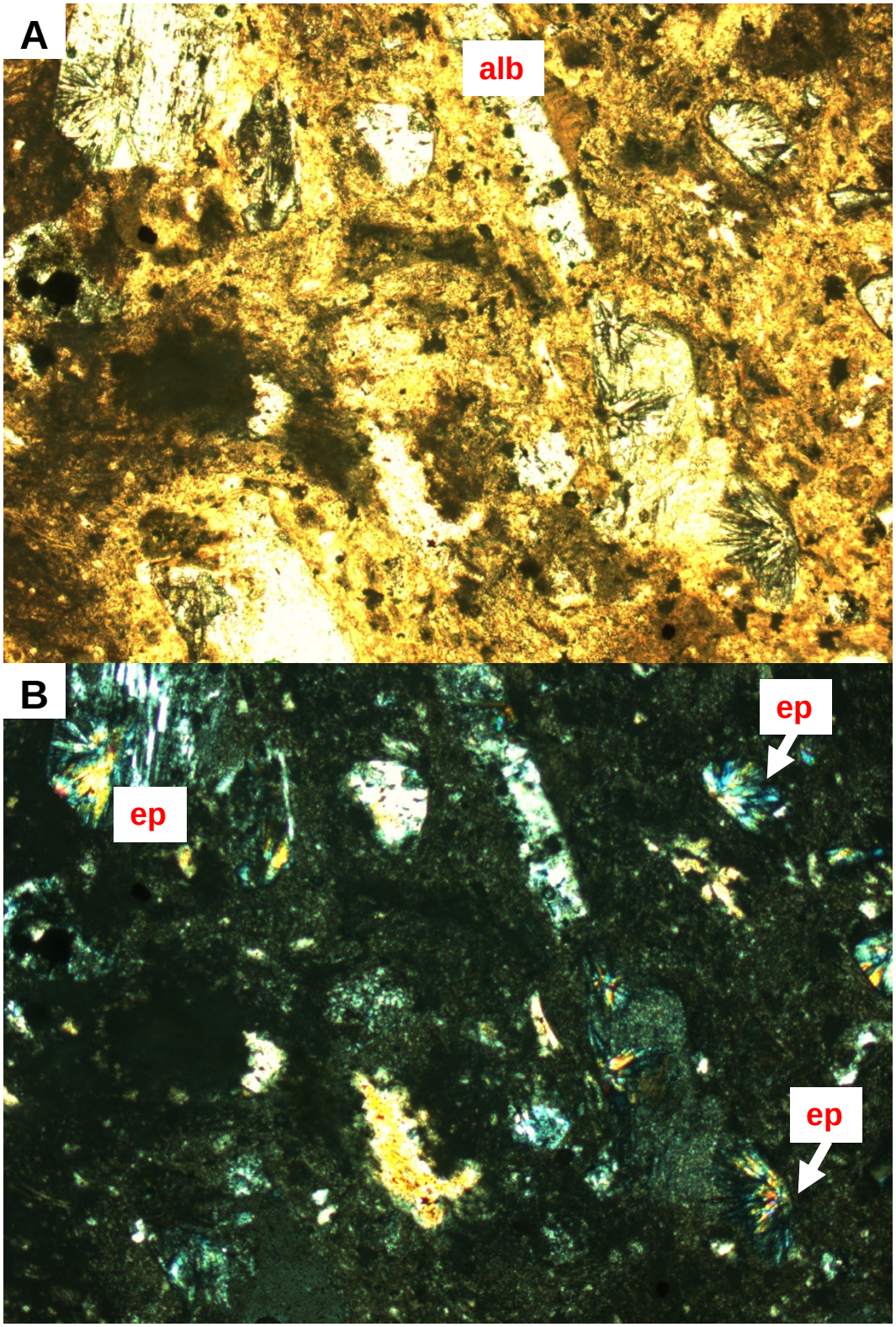

Fig. 4.11. Simple twinned albite plagioclase and radiating acicular epidote needles replacing primary plagioclase in a vitreous chloritic groundmass. Opaques are pyrite and hematite. 2.5x magnification, A=PPL, B=XPL.

TH9 well, Core 2 **~2424mRF**

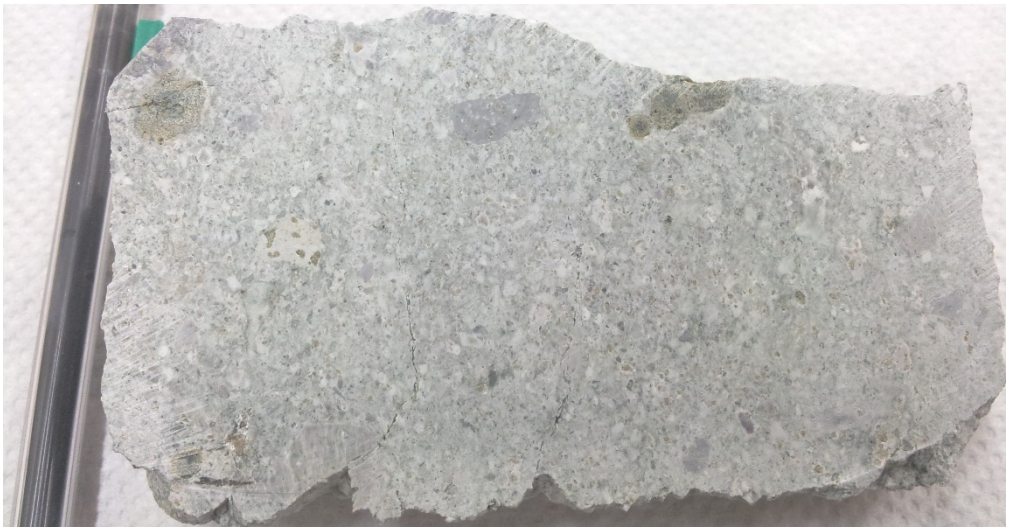

Fig. 4.12. TH9 core 2, hand specimen, Waiora Ignimbrite, ~2424 mRF. Brecciated texture of lithic rich ignimbrite in vitroclastic matrix.

The second core sample is from the same formation as previous (Waiora Ignimbrite) except this sample was retrieved from a deeper level at 2424 mRF. The rock is greyish green indicating some pervasive chlorite alteration, crystal rich, brecciated and very strongly altered. Smaller (<10 mm) purple andesite lithic clasts (compared to the earlier sample) and phenocrysts of epidote, quartz and feldspar are observed. There are also darker patches of dark green chlorite. Most of the visible clasts and phenocrysts are angular and veining is absent.

In thin section, the main phenocrysts and xenoliths are crystal-lithic tuffs, lava clasts, quartz and feldspar. The lithics are replaced by quartz, illite, epidote and chlorite. Some quartz phenocrysts remain but the feldspars are completely altered to albite, epidote and adularia (Milicich et al., 2008a). Quartz, illite and chlorite plus traces of epidote, has replaced the vitrophyric groundmass. There is also a reaction rim of ilmenite or rutile rim around an opaque mineral, perhaps titanomagnetite.

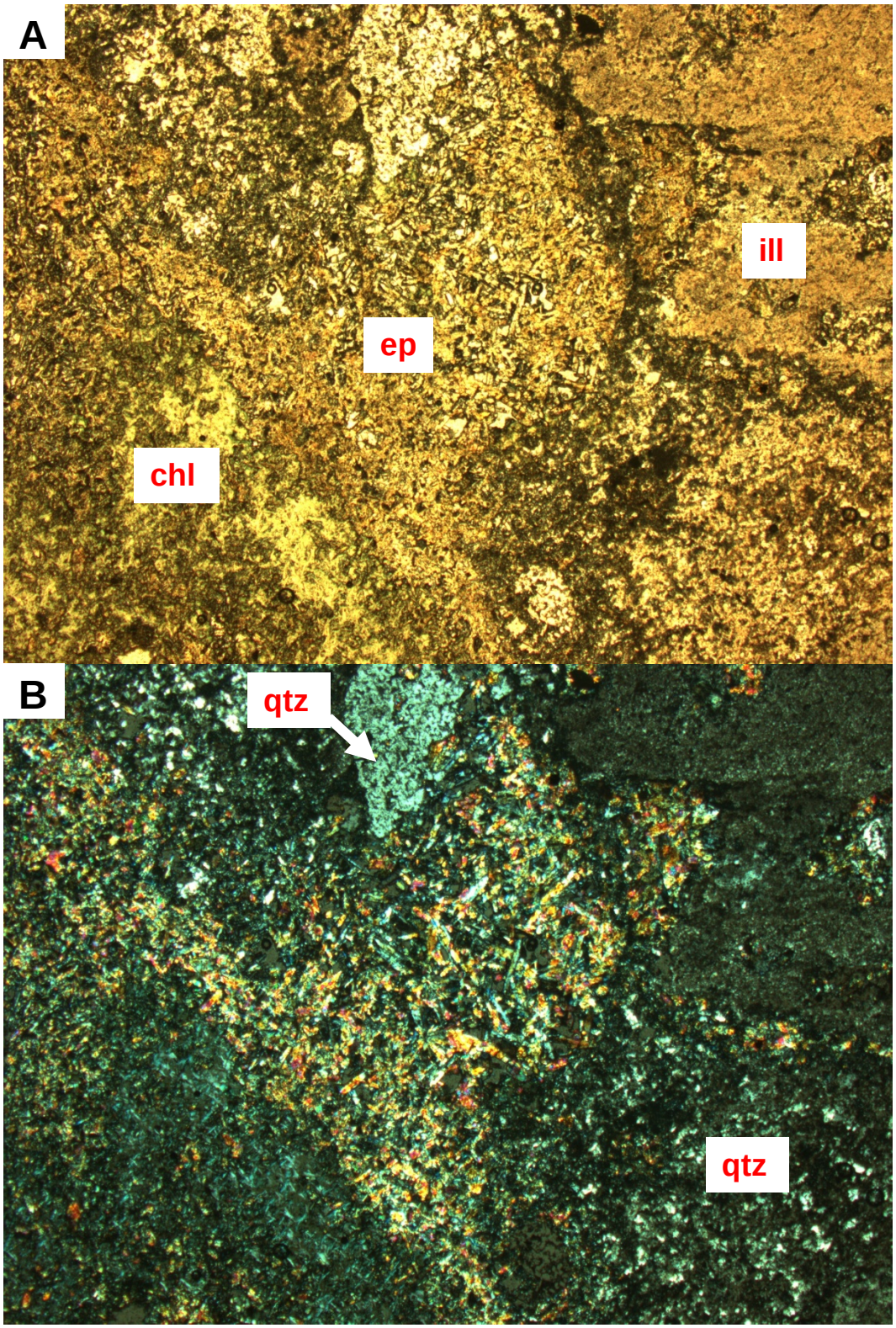

Fig. 4.13. Intense alteration to produce chlorite (chl), epidote (ep), quartz (qtz) and illite (ill). 2.5x magnification, A=PPL, B=XPL.

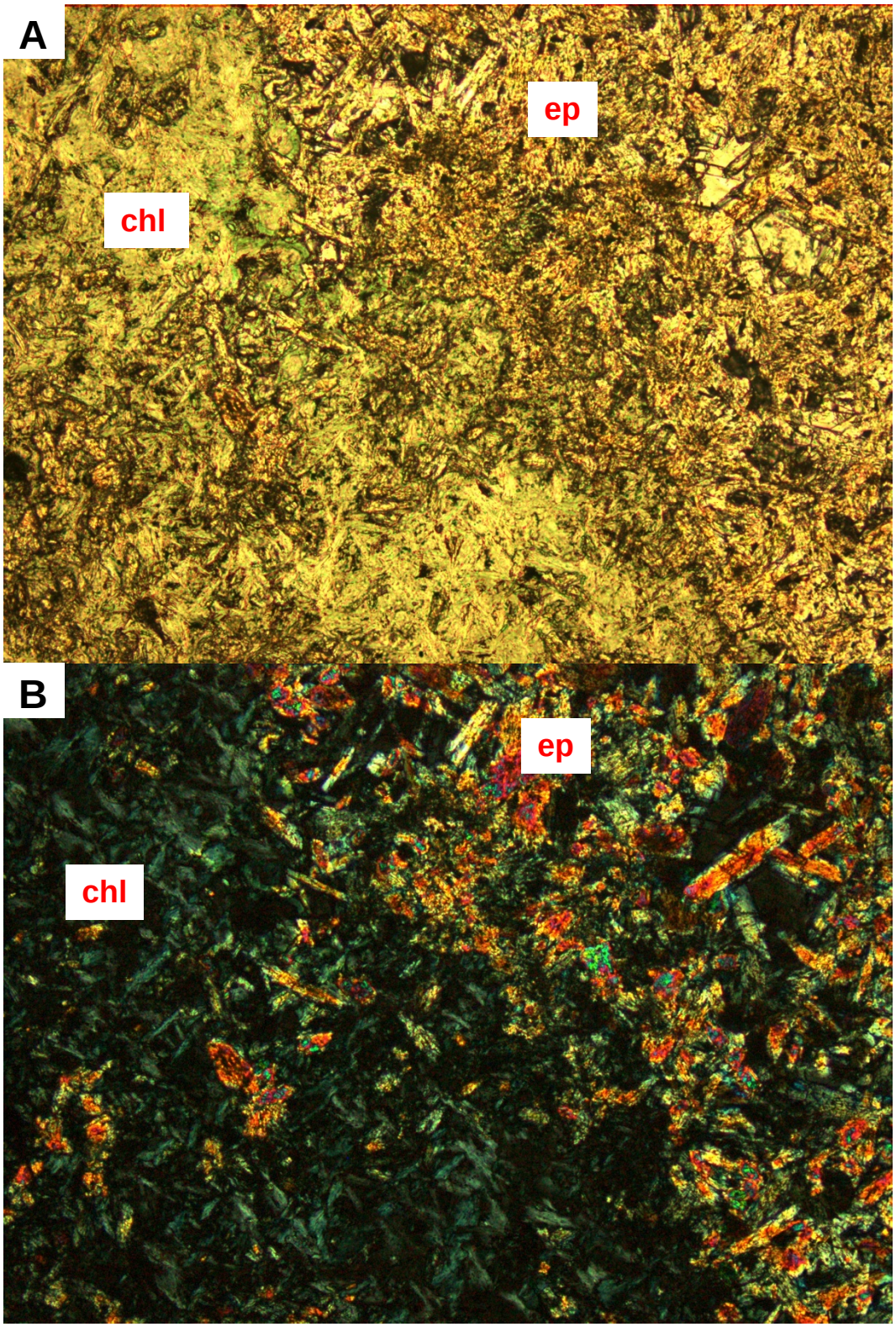

Fig. 4.14. Close up of replacement by chlorite (chl) and epidote (ep). 10x magnification, A=PPL, B=XPL.

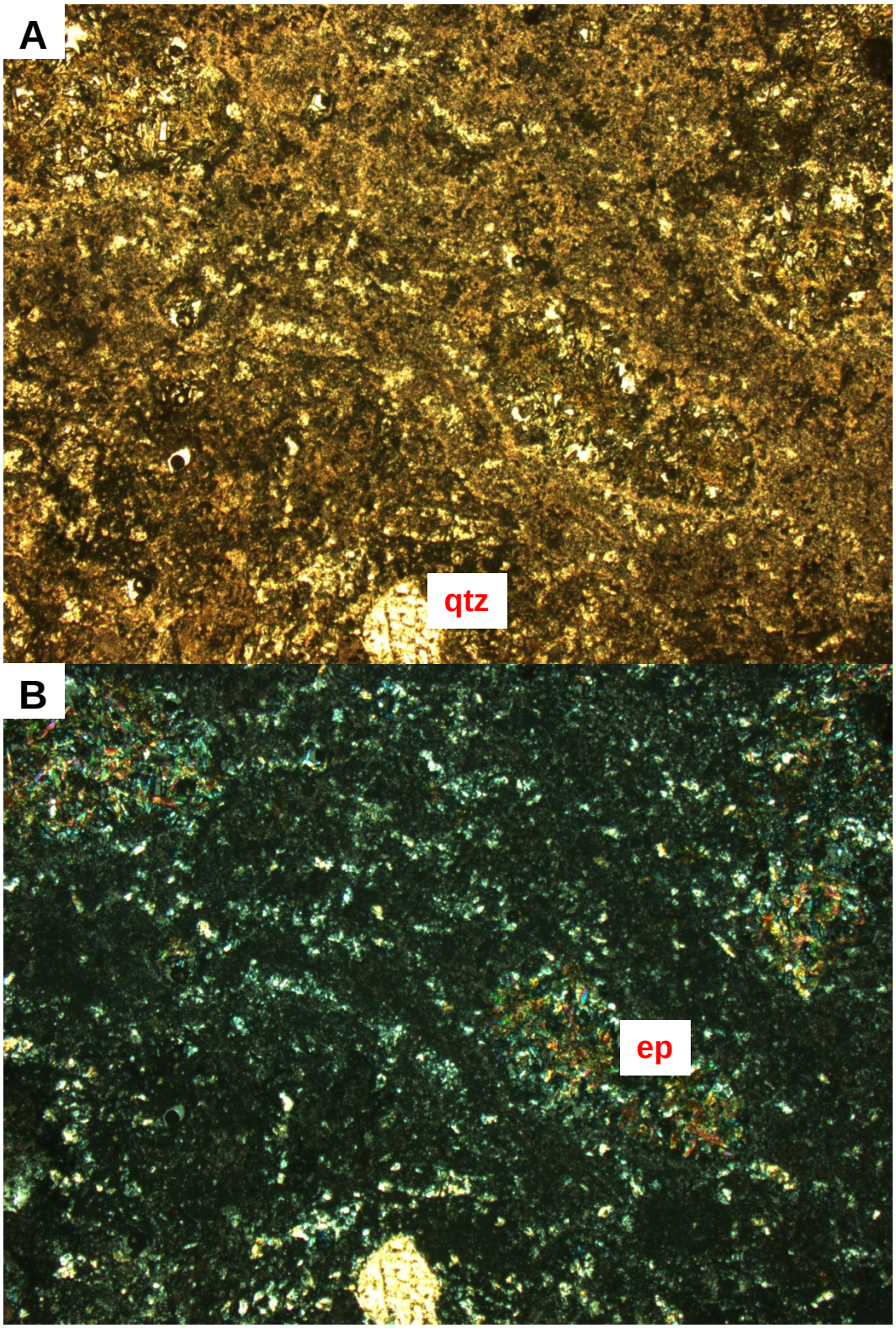

Fig. 4.15. Pseudomorphs of epidote with chlorite rims and a quartz phenocryst in a groundmass of quartz and illite. 2.5x magnification, A=PPL, B=XPL.

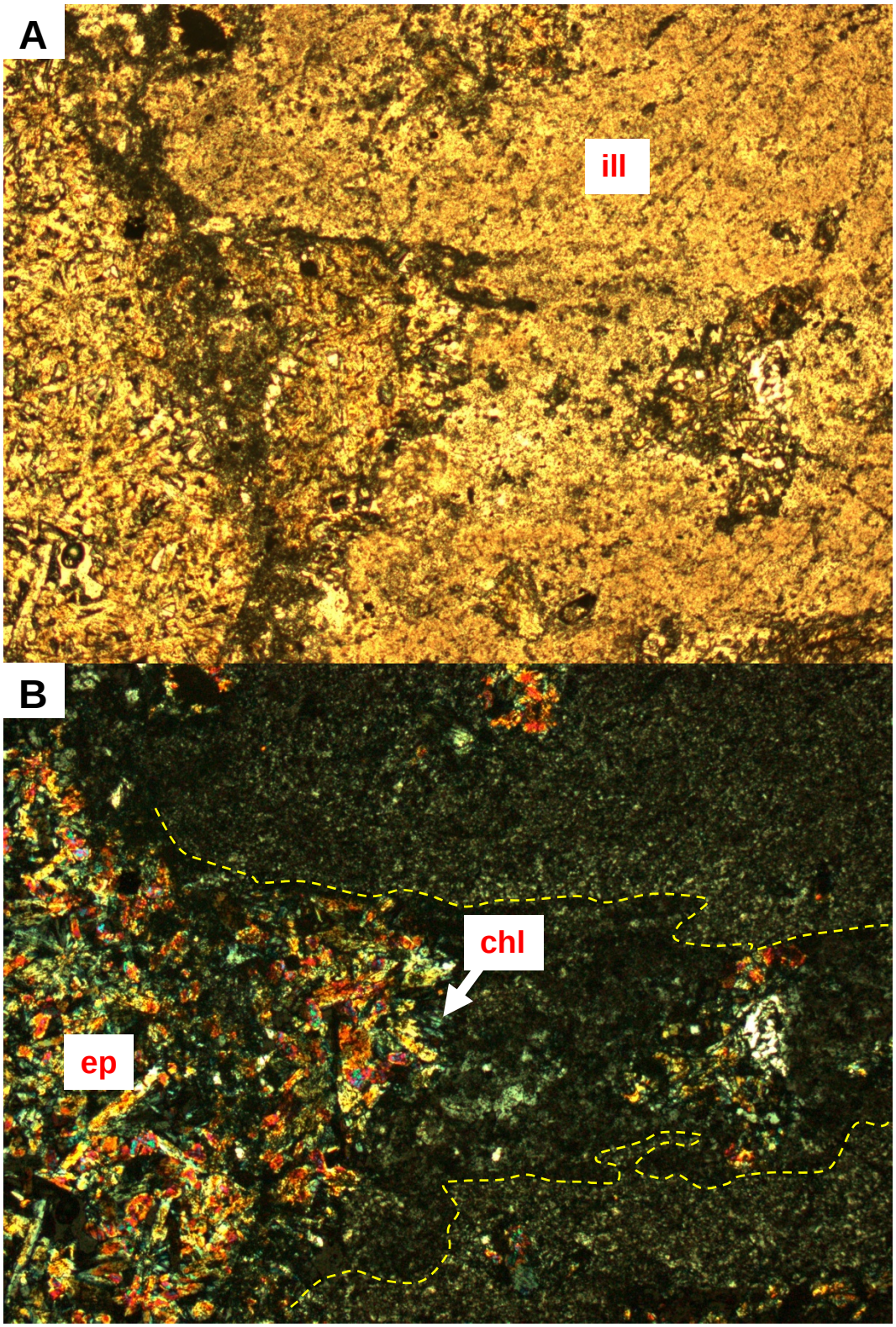

Fig. 4.16. Large epidote pseudomorph chloritised in an illite (ill) groundmass. 5x magnification, A=PPL, B=XPL.

TH10 well, Core **~1405.5 mRF**

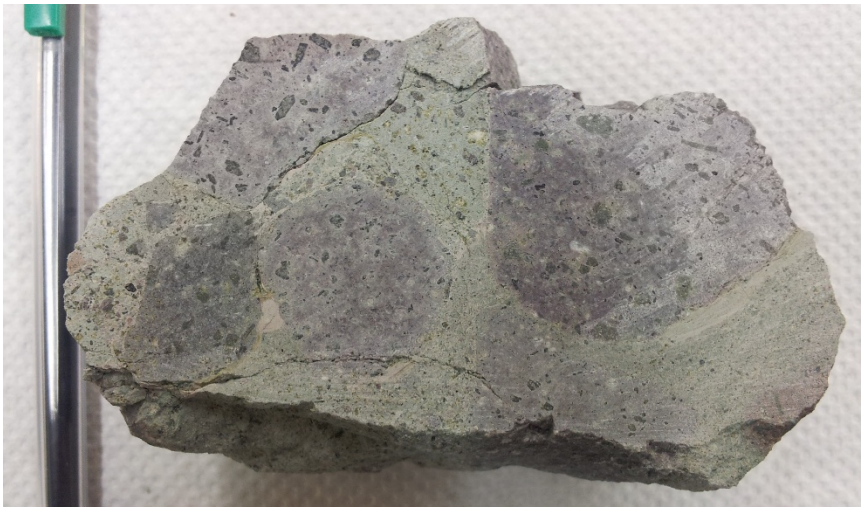

Fig. 4.17. TH10 core sample hand specimen, lithic crystal breccia ~1405.5 mRF with large purple andesite lava lithics in a pale green matrix.

The core sample from TH10 at ~1405.5 mRF is from a lithic-crystal breccia that is moderately to highly altered. The rock is pale green with large crystal rich purple andesite lithic clasts. The green tinge to the rock or matrix is likely from chloritic alteration. The larger purple lithic clasts contain visible quartz crystals and darker lithics. Phenocrysts were probably feldspars and pyroxenes or amphiboles based on their shape. The andesite lithic clasts are large, at 2-5 cm and contain selectively altered subhedral to anhedral (<2 mm) plagioclase. Some plagioclase phenocrysts show compositional zoning and large sieve textures. The original plagioclase has been partially replaced by albite or adularia and in some cases chlorite and epidote. Amphiboles or pyroxenes have been replaced by epidote and have black alteration rims and a skeletal texture. Epidote is also beginning to replace primary feldspars, infilling phenocrysts. The groundmass is microcrystalline with feldspar laths and minor quartz that at times is weakly trachytic. The groundmass has been altered to produce secondary quartz, albitised feldspar laths, chlorite and epidote.

The green rock matrix contains ferromagnesian minerals such as amphibole and pyroxene and is replaced by epidote. Epidote also partially replaces the feldspar laths and the matrix while any larger feldspars crystals are susceptible to albite or adularia replacement (Milicich et al., 2008b). The matrix also contains opaques such as magnetite and some pyrite. Thin or thick (~0.1-0.5 mm) irregular epidote

veins also cut through the matrix (Fig. 4.21). Of note are two epidote veins that cross-cut a previous vein that is most likely illite or chlorite.

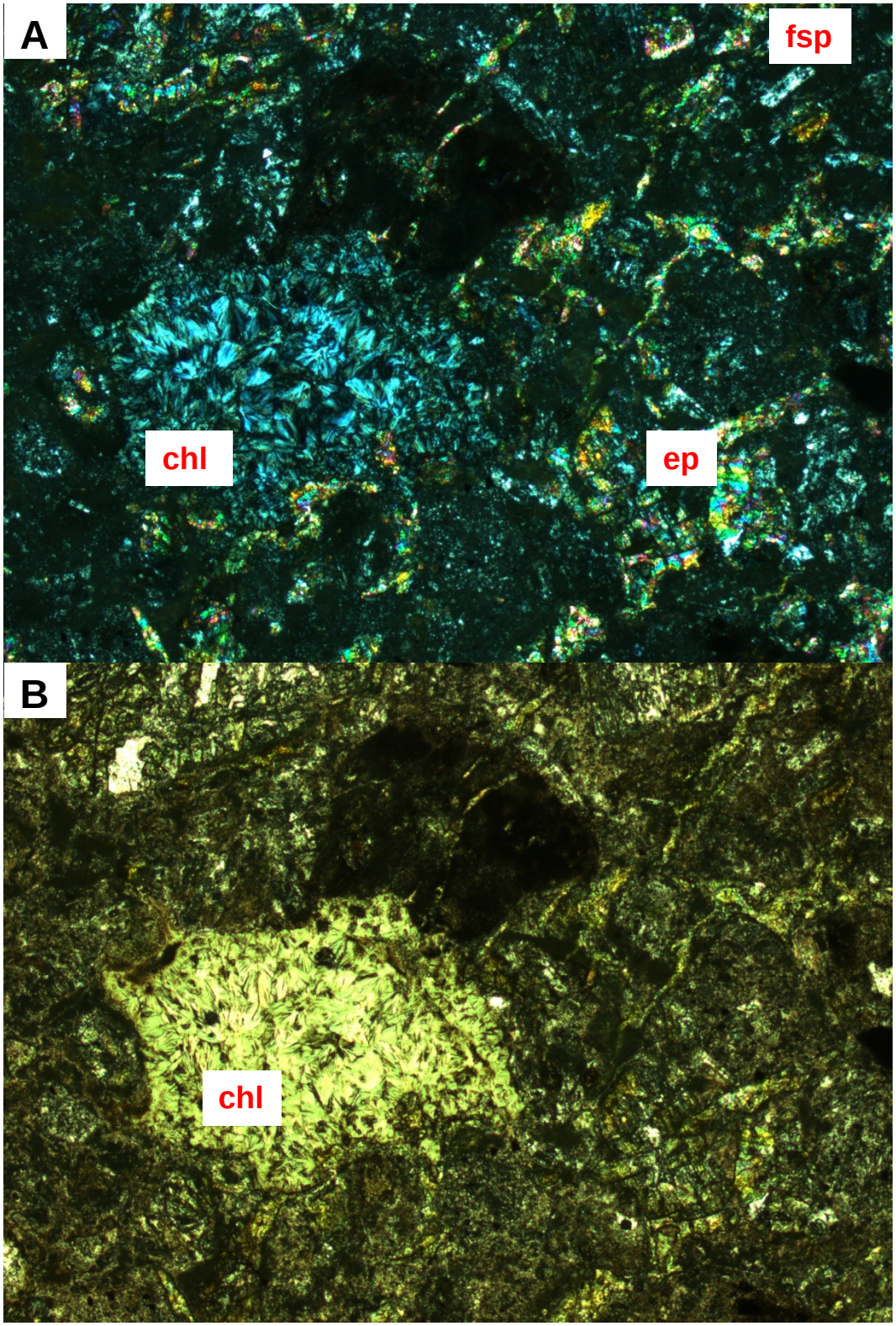

Fig. 4.18. Chlorite (chl) and stringy epidote (ep) veinlets replacing groundmass and ferromagnesian minerals. (fsp=feldspar). 5x magnification, A=XPL, B=PPL.

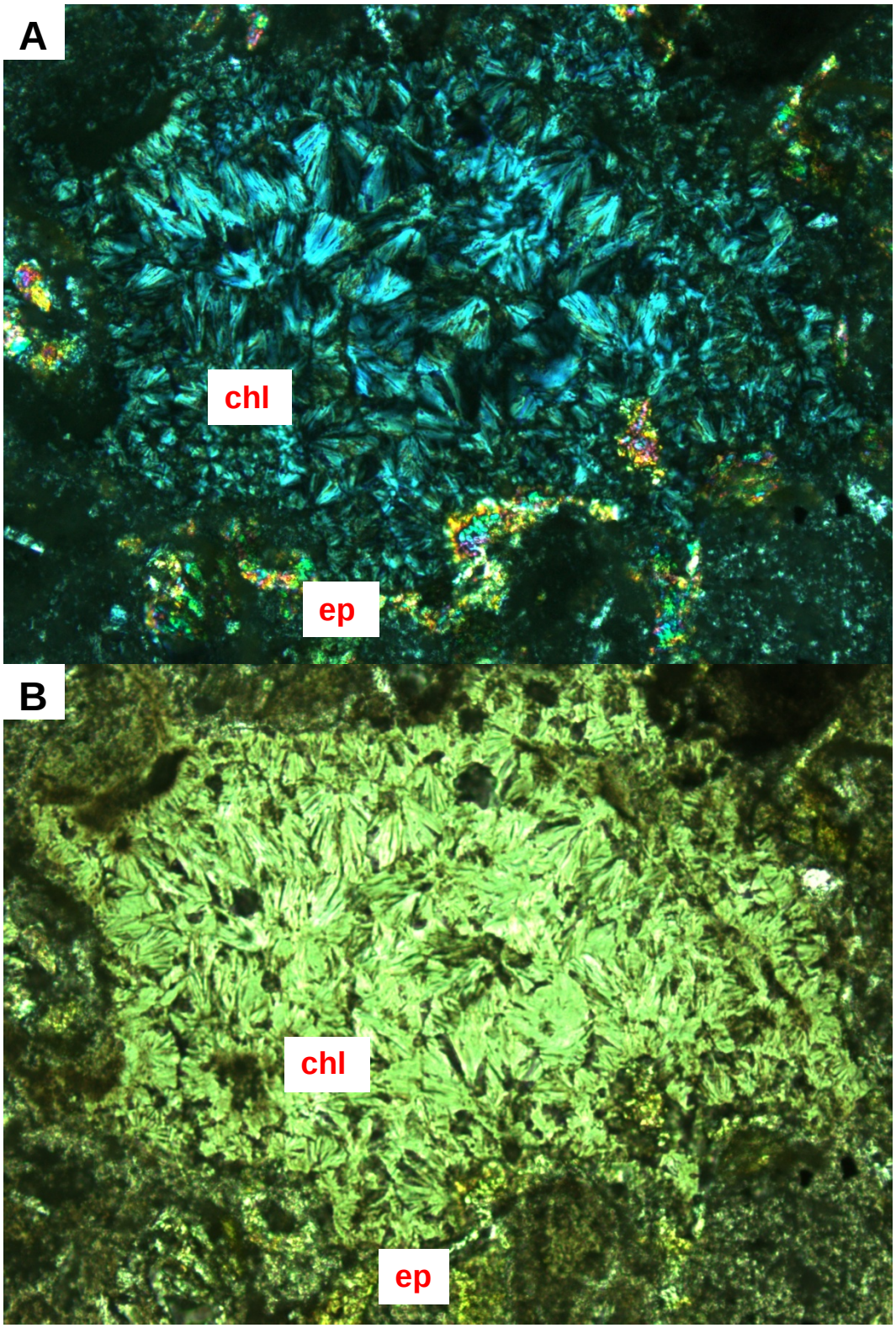

Fig. 4.19. Close up of replacement, possibly vug fill by chlorite (chl) and epidote (ep). 10x magnification, A=XPL, B=PPL.

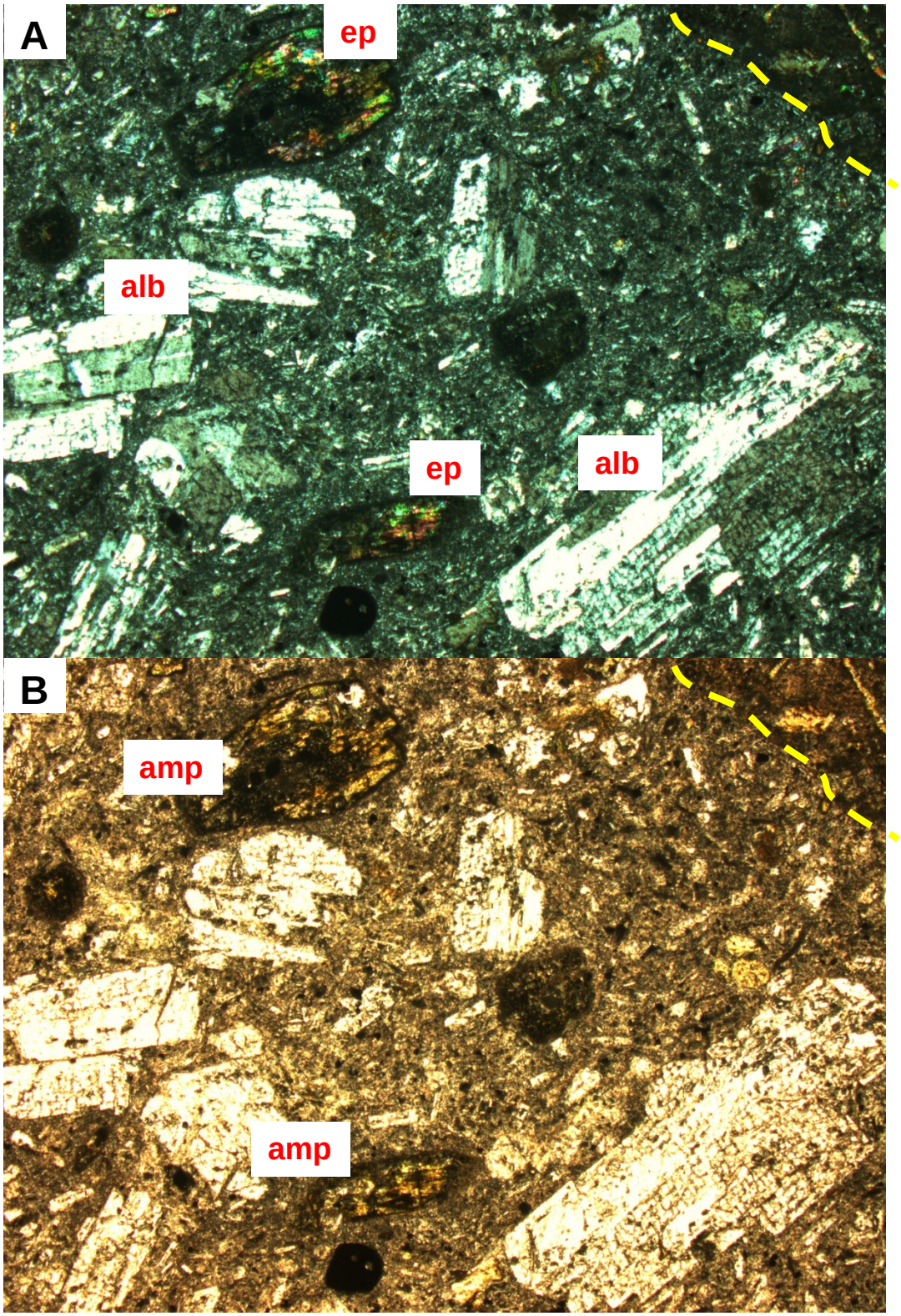

Fig. 4.20. Purple andesite lava lithic to the left of yellow line, right side is the green matrix. Andesite lava lithic: Albite (alb) partially replaces plagioclase, amphibole (amp) with black alteration rims that originate from decompression during magma ascent, (Devine et al., 1998) are replaced by epidote (ep). Groundmass has secondary quartz and albitised feldspar laths and chlorite. 2.5x magnification, A=XPL, B=PPL.

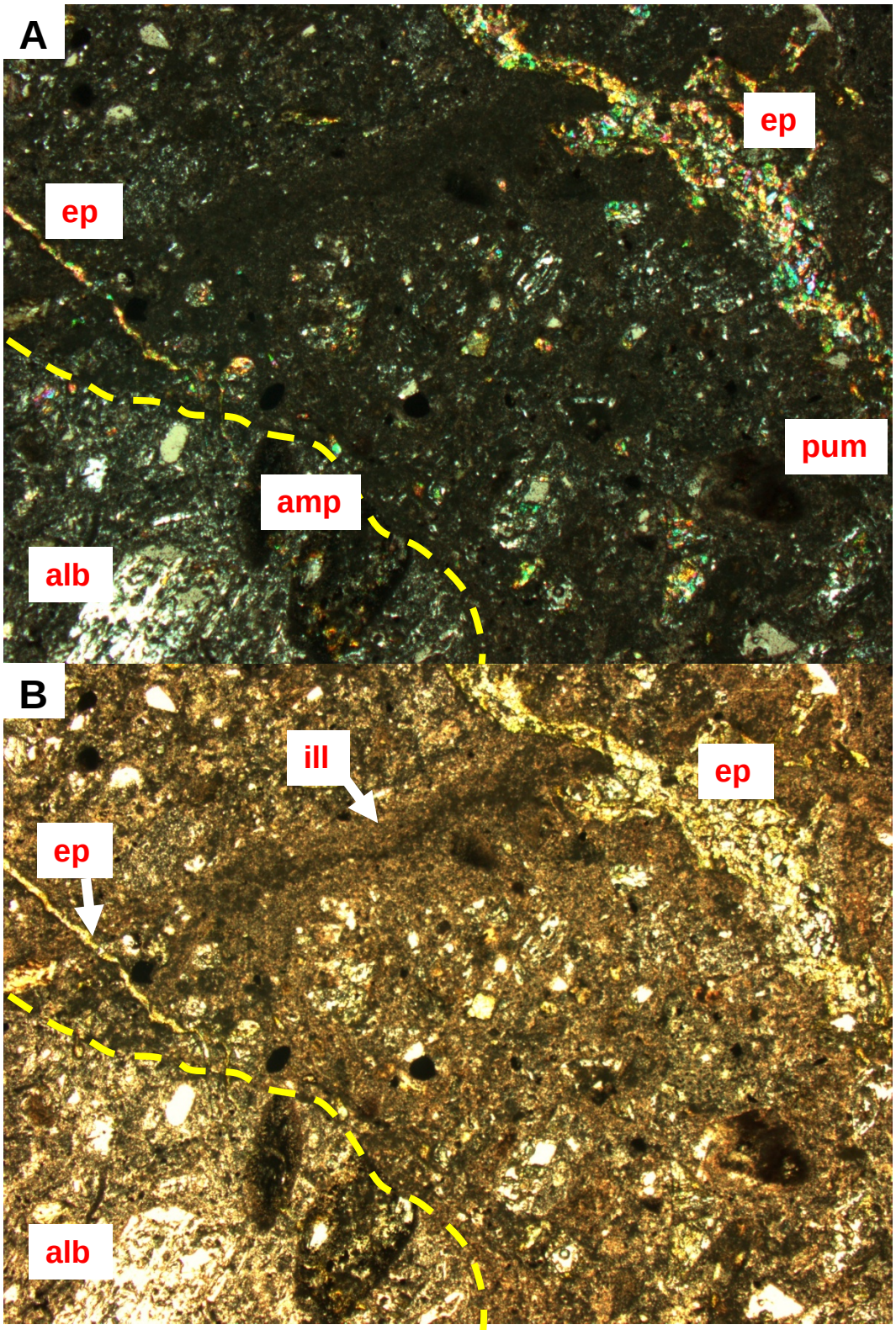

Fig. 4.21. To the left of the yellow line is the purple andesite lava lithic, to the right is the green matrix. Epidote and epidote veins completely replaces amphiboles (amp) and groundmass. Groundmass is altered by quartz, albite and chlorite. An illite (ill) vein is overprinted by an epidote vein. Altered pumice clast (pum). 2.5x magnification, A=XPL, B=PPL.

TH12 well, Core 1 Sample 1 ~1370.5 mRF

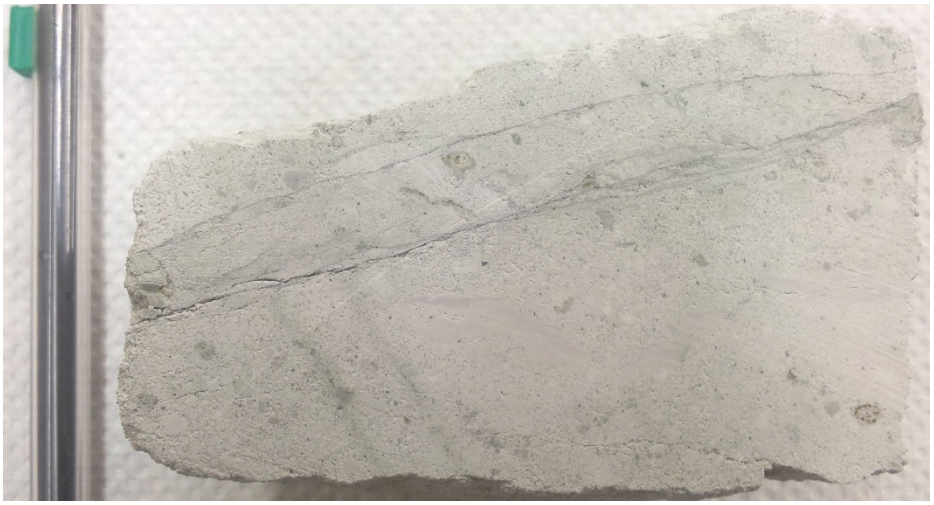

Fig. 4.22. TH12 core 1, sample 1, hand specimen, volcanic breccia from the Waiora Formation showing veining that has produced small fractures.

The first core sample from TH12 at ~1370.5 mRF is an intensely altered volcanic breccia from the Waiora Formation. It is off white in colour tinged with pastel green and is clay rich. Chlorite veining (<1 mm) and clay veining (<4 mm) is evident along with visible epidote and pyrite. Clasts are sub-angular to sub-rounded, 1-8 mm in size and are dark grey xenolithics, altered pumice or fragments altered to epidote. Epidote also appears in small vugs. The clasts are held in a massive chlorite and clay altered matrix.

In thin section, epidote and quartz have replaced pumice and rhyolitic clasts (Kilgour et al., 2006). Illite pseudomorphs are common, and together with quartz, pyrite and chlorite have replaced siltstone clasts. Plagioclase has been altered to adularia, albite, quartz and wairakite with fine acicular needles of epidote while quartz phenocrysts have been altered to a mosaic of finer quartz. Fine chlorite veinlets and clay-microcrystalline quartz veinlets are observed in thin section. The groundmass consists of quartz, illite, chlorite, wairakite, adularia, fine epidote and disseminated pyrite. Illite alteration is found throughout, and leucoxene is described by Kilgour et al. (2006).

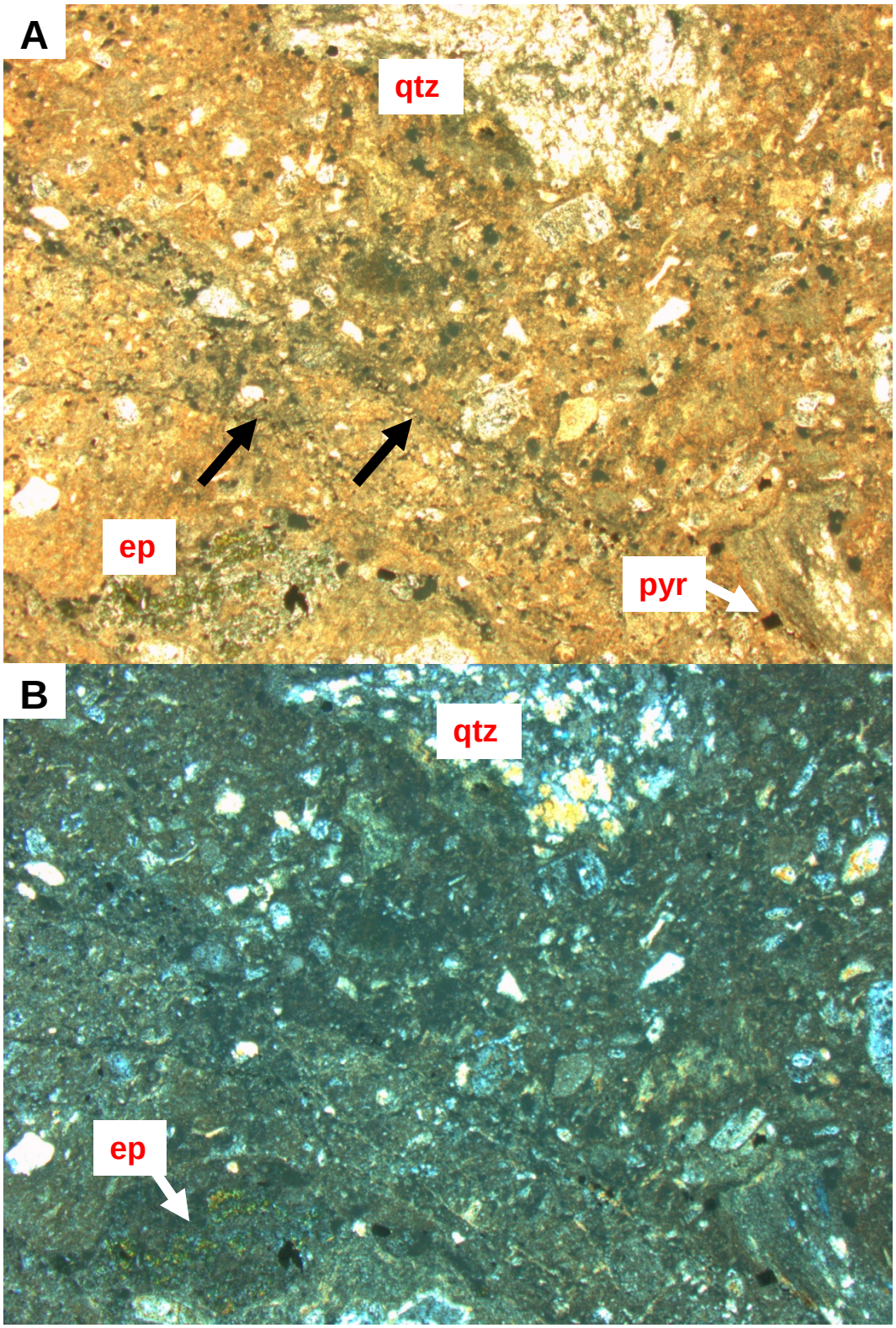

Fig. 4.23. Epidote altered pumice clast and quartz phenocryst, chlorite veins (black arrows), and the groundmass of quartz, illite, chlorite and disseminated pyrite. 2.5x magnification, A=PPL, B=XPL.

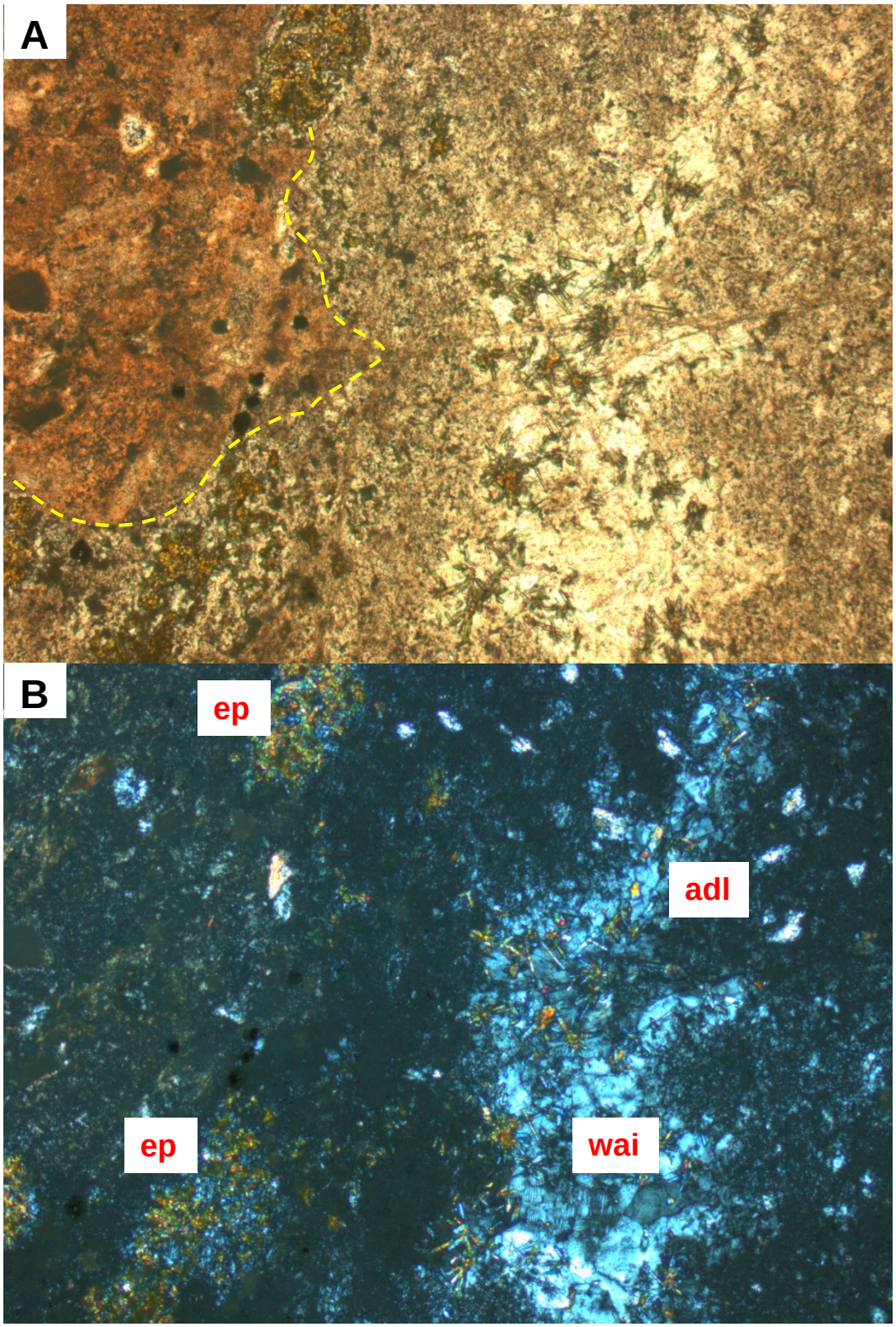

Fig. 4.24. Large siltstone clast (left of yellow line) altered to illite and quartz, with epidote altered pumice clasts in a groundmass of wairakite, adularia and fine acicular epidote. 5x magnification, A=PPL, B=XPL.

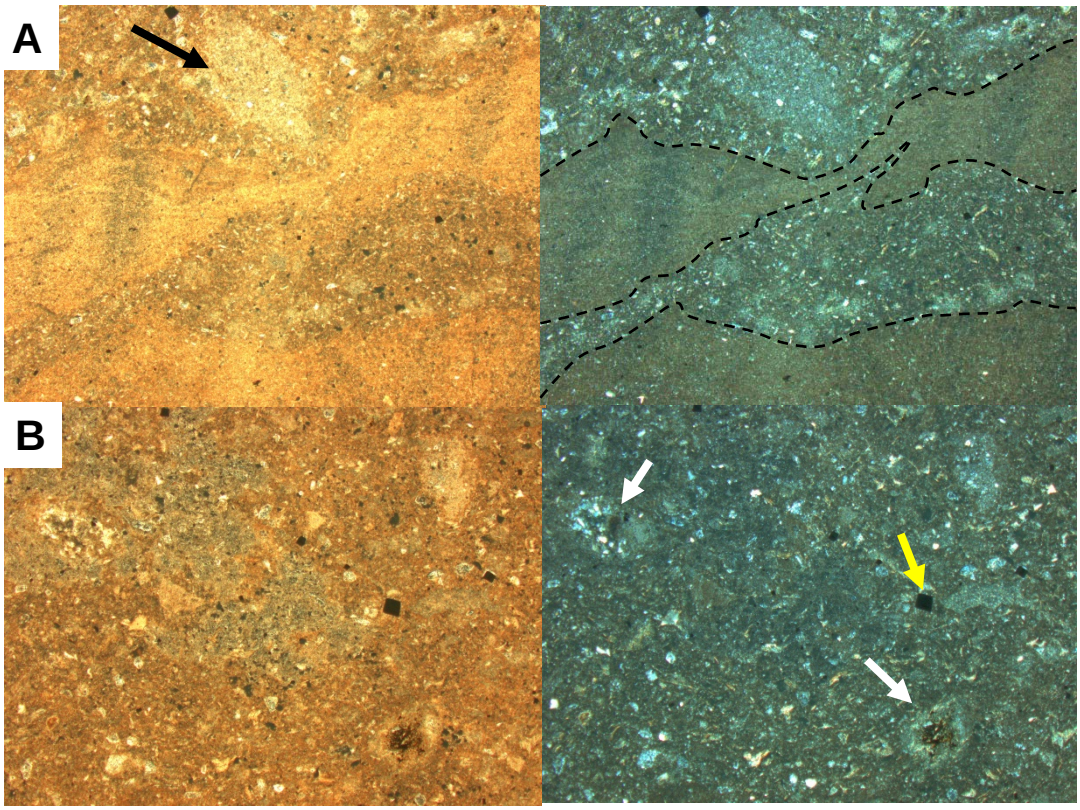

Fig. 4.25. A: Clay-microcrystalline quartz veinlets (outlined black dashed line) with an illite+quartz pseudomorph (black arrow), 2.5x magnification, left=PPL, right=XPL. B: Groundmass texture, with epidote-quartz pseudomorphs (white arrows) and pyrite (yellow arrow) 2.5x magnification, left=PPL, right=XPL.

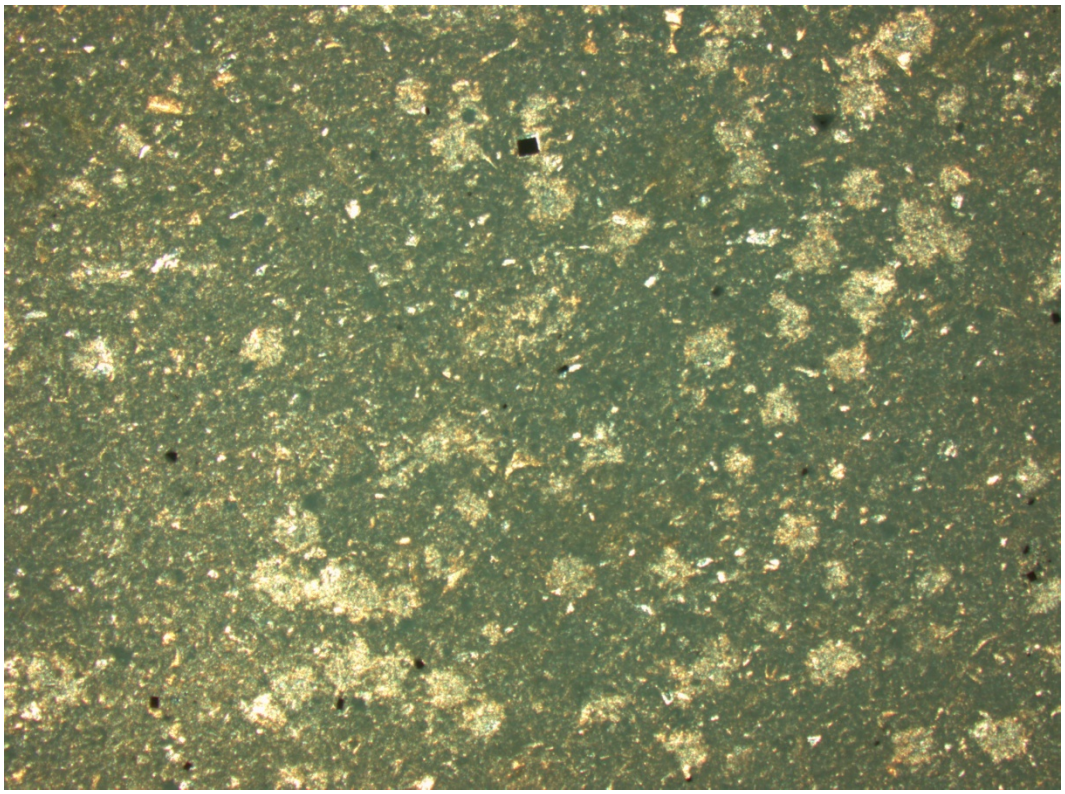

Fig. 4.26. Mottled pseudotexture from illite alteration. 2.5x magnification, PPL.

TH12 well, Core 1 Sample 2 ~1372 mRF

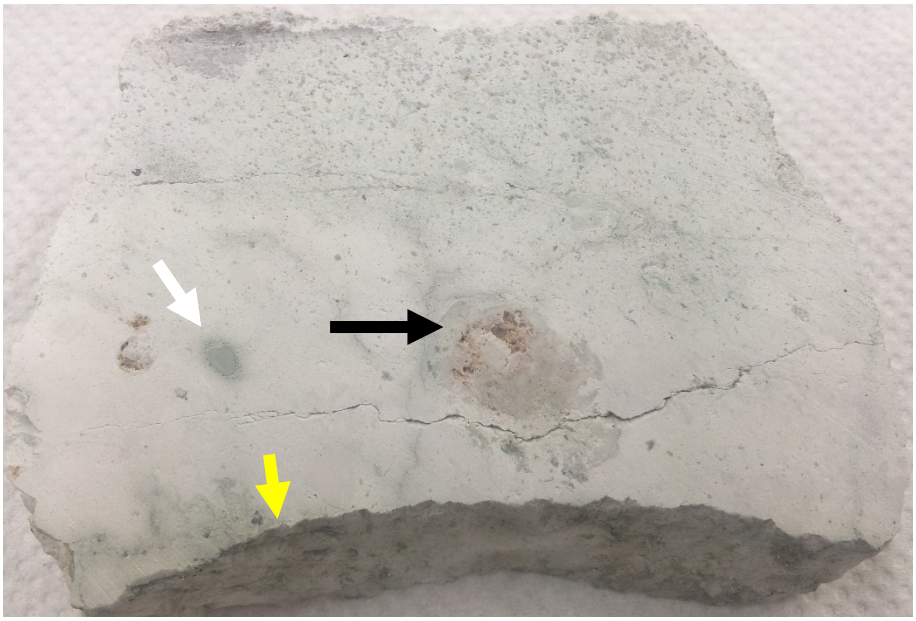

Fig. 4.27. TH12 core 1, sample 2, hand specimen, volcanic breccia from the Waiora Formation displaying distinct vugs (black arrow), fractures, chlorite and pyrite lined vein (yellow arrow) and chloritic clast (white arrow).

The second sample from the first core at TH12 (~1372 mRF) is relatively close to the first (~1370.5 mRF) and is a volcanic breccia from the Waiora Formation. It is a white pastel green shade, crystal and clay rich leaving a clay residue and has undergone intense alteration. Crystals in hand specimen are quartz, pyrite, and feldspar. There are small vugs or cavities (15 mm) of quartz coated with clay. Distinct chlorite patches and chlorite-pyrite veining are evident. Darker lithics are smaller (<1 mm) compared to the earlier sample. The matrix is the same massive chlorite and clay altered matrix as before.

In thin section, little of the primary mineralogy is left, as most have been replaced by pseudomorphs of alteration minerals. Feldspars are completely altered to albite and epidote. There are abundant pseudomorphs of illite that have probably replaced pumiceous or siltstone clasts. Most of the sample has been subjected to chlorite and illite alteration. Fine quartz veinlets are present, <0.1 mm wide. There is also the development of vuggy textures of quartz. Quartz, illite and chlorite make up the majority of the groundmass.

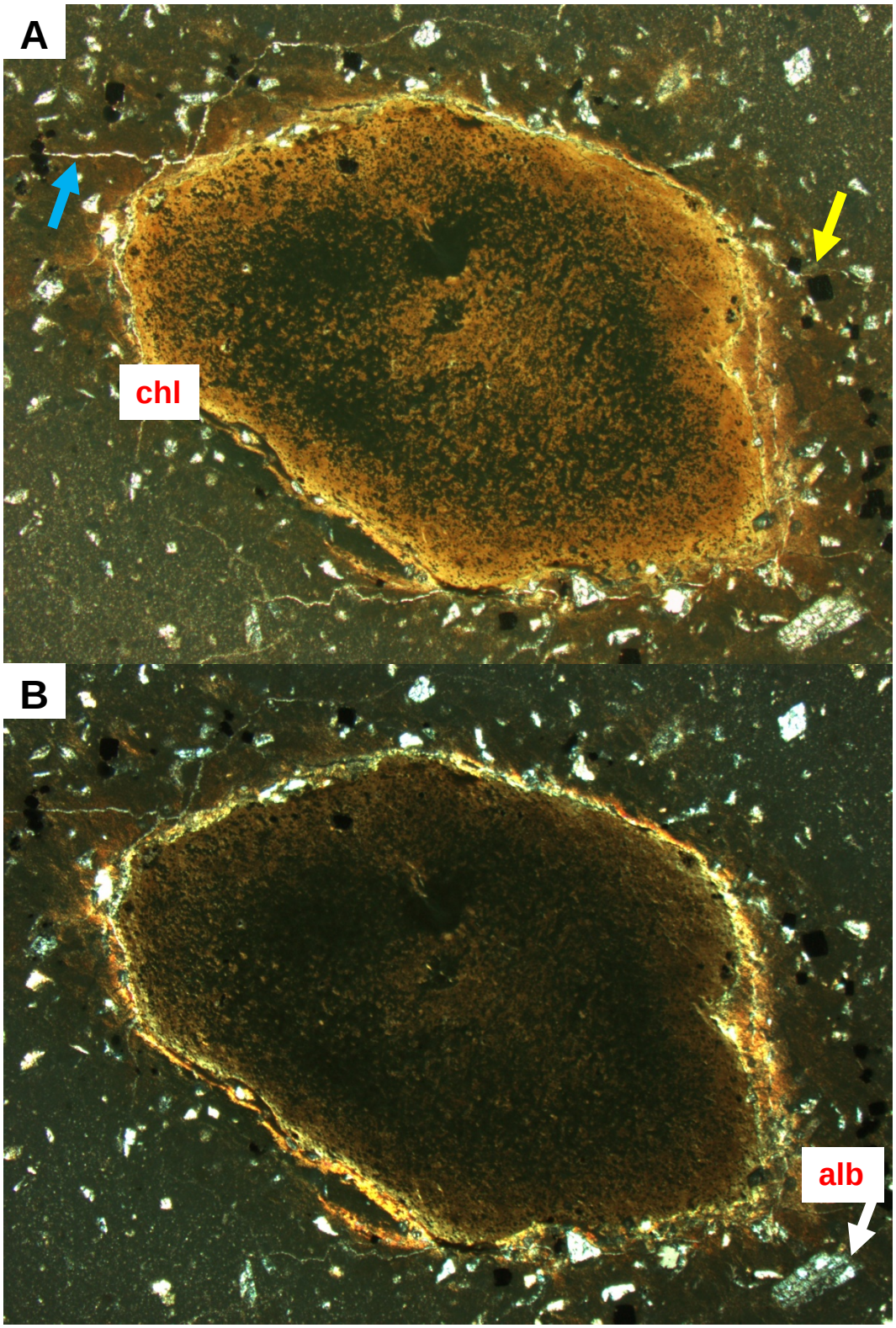

Fig. 4.28. Large chlorite altered clast seen in hand specimen and now in thin section, showing fine irregular fractures (blue arrow), pyrite (yellow arrow). 2.5x magnification, A=PPL, B=XPL.

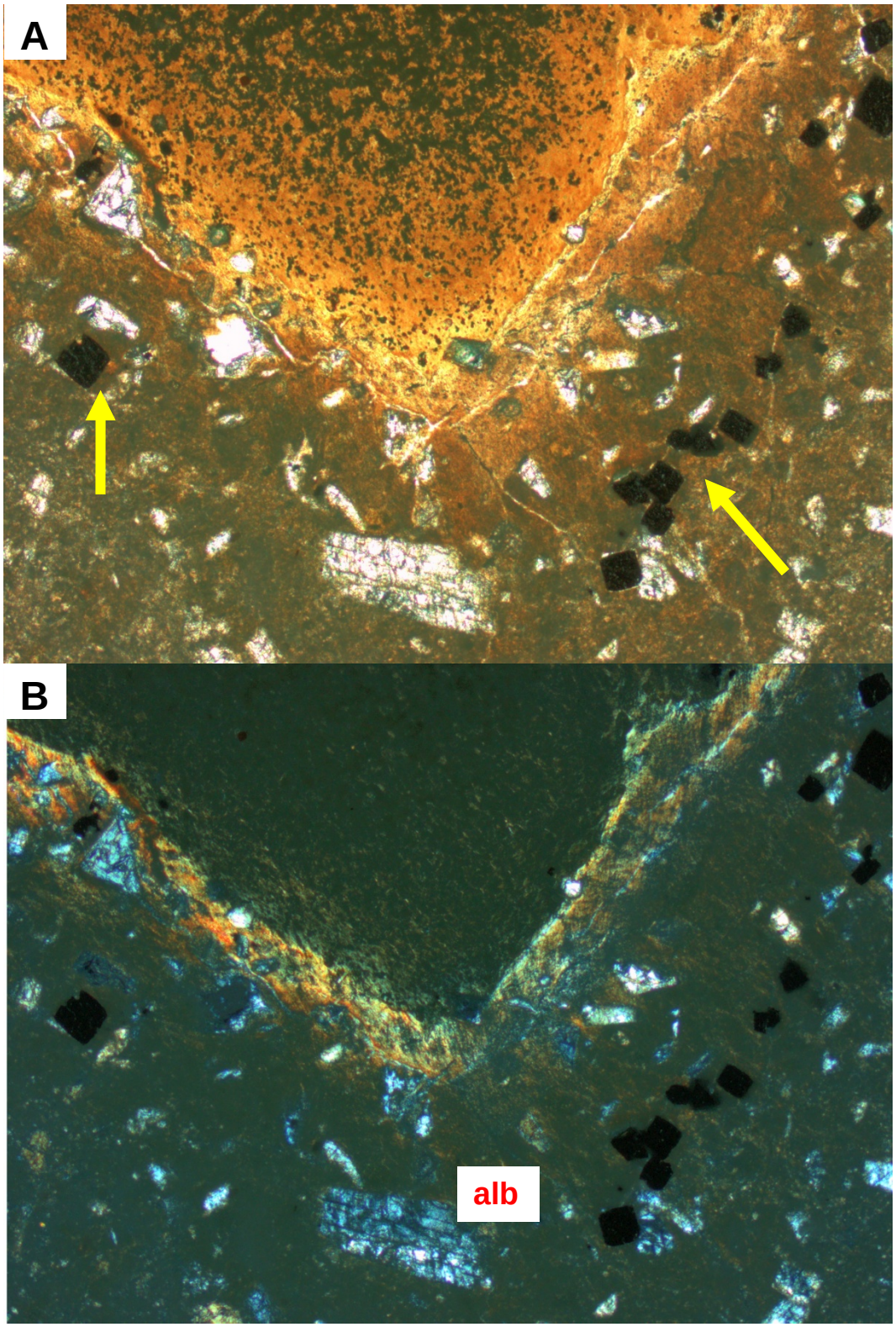

Fig. 4.29. Close up of chlorite altered clast, pyrite concentrated around rim. 5x magnification, A=PPL, B=XPL.

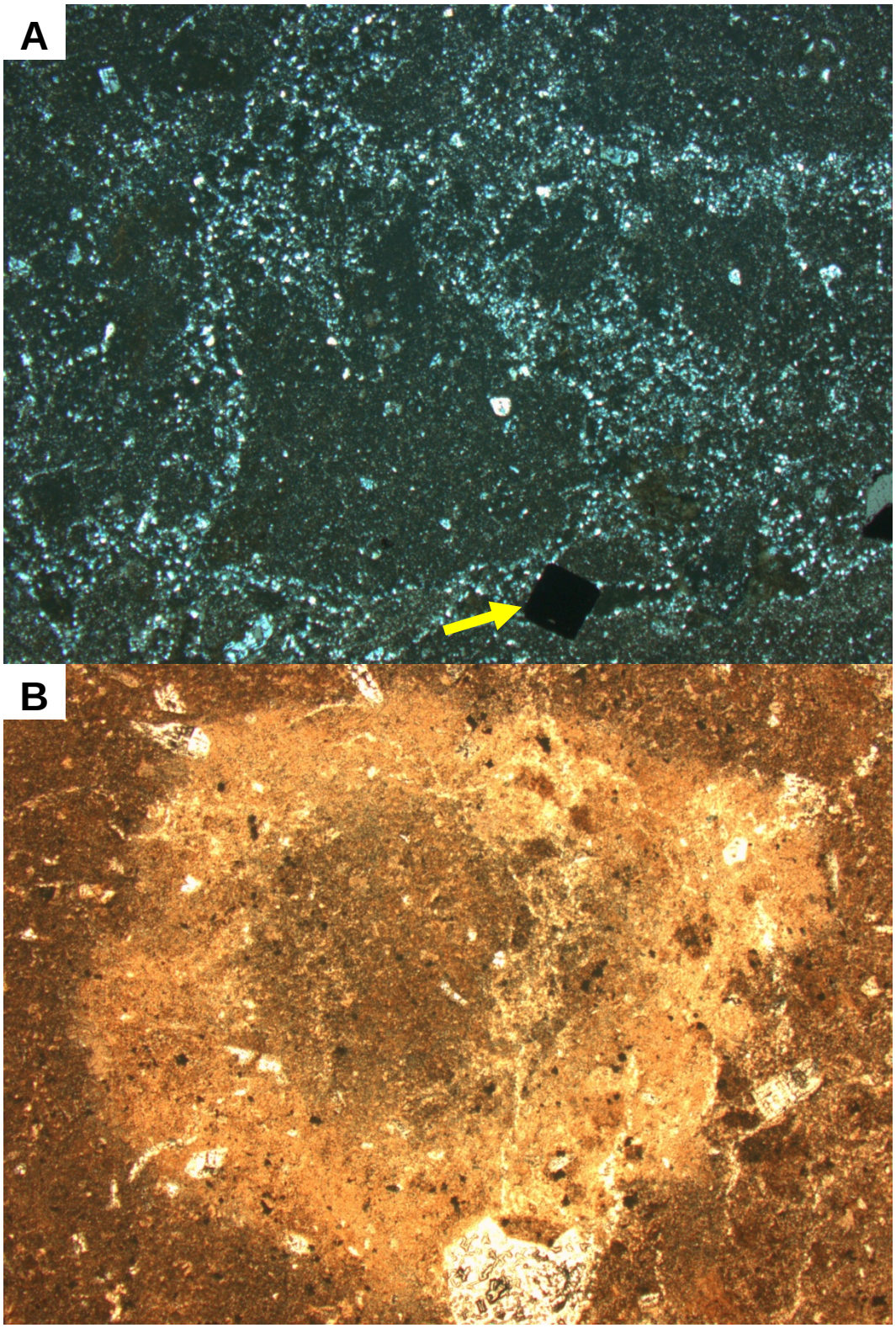

Fig. 4.30. A: vuggy quartz, cubic pyrite (yellow arrow) 2.5x magnification, XPL. B: illite pseudomorph, replacing pumice clast 2.5x magnification, PPL.

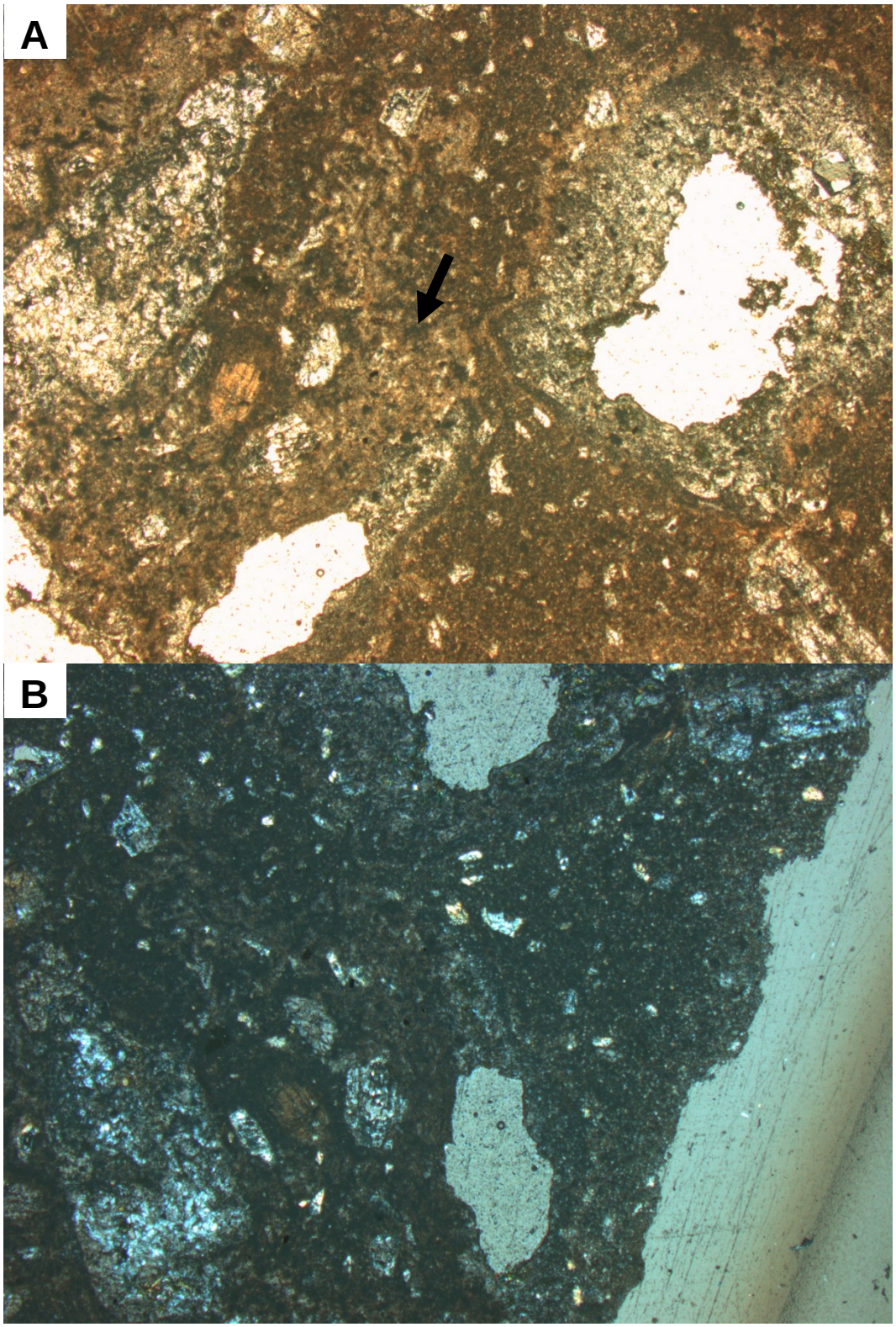

Fig. 4.31. Sieved plagioclase with minor epidote replacment, clay altered pumice clast (black arrow) with a microcrystalline quartz-feldspar groundmass overprinted by illite. 2.5x magnification, A=PPL, B=XPL.

TH12 well, Core 2 **~1899 mRF**

Fig. 4.32. TH12 core 2, hand specimen, partially welded ignimbrite, Whakamaru Group ignimbrite, ~1899 mRF. Circle surrounds pumice clast.

The sample from the second core taken from TH12 at 1899 mRF depth is from a partially welded crystal rich ignimbrite called the Whakamaru Ignimbrite. Quartz is very abundant and phenocrysts are visible in hand specimen (5 mm largest). No visible epidote crystals were observed in hand specimen. Angular lithics are weakly altered, 2-30 mm in size and consist of rhyolite or andesite lava and greywacke (Kilgour et al., 2006). The matrix is a fine ash that has undergone chlorite and clay alteration. The edges of the core seem to be more pervasively

chlorite altered than the centre. Pumice clasts are chloritised and moderately flattened (3 cm in size).

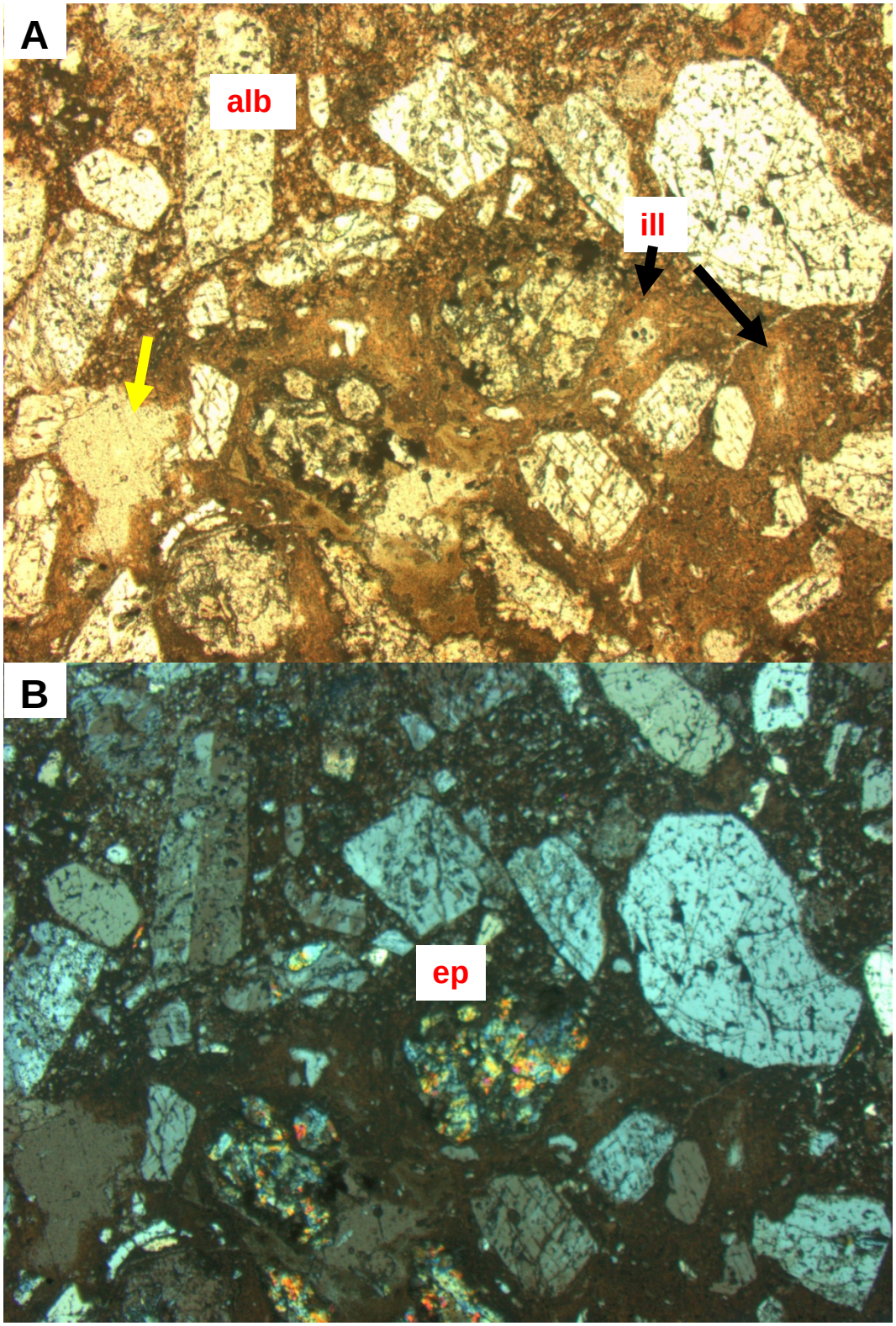

Fig. 4.33. Simple twinned plagioclase completely replaced by albite and epidote, illite rimmed phenocrysts (black arrows). Vug rimmed with illite (yellow arrow). Quartz phenocrysts are fractured. 2.5x magnification, A=PPL, B=XPL.

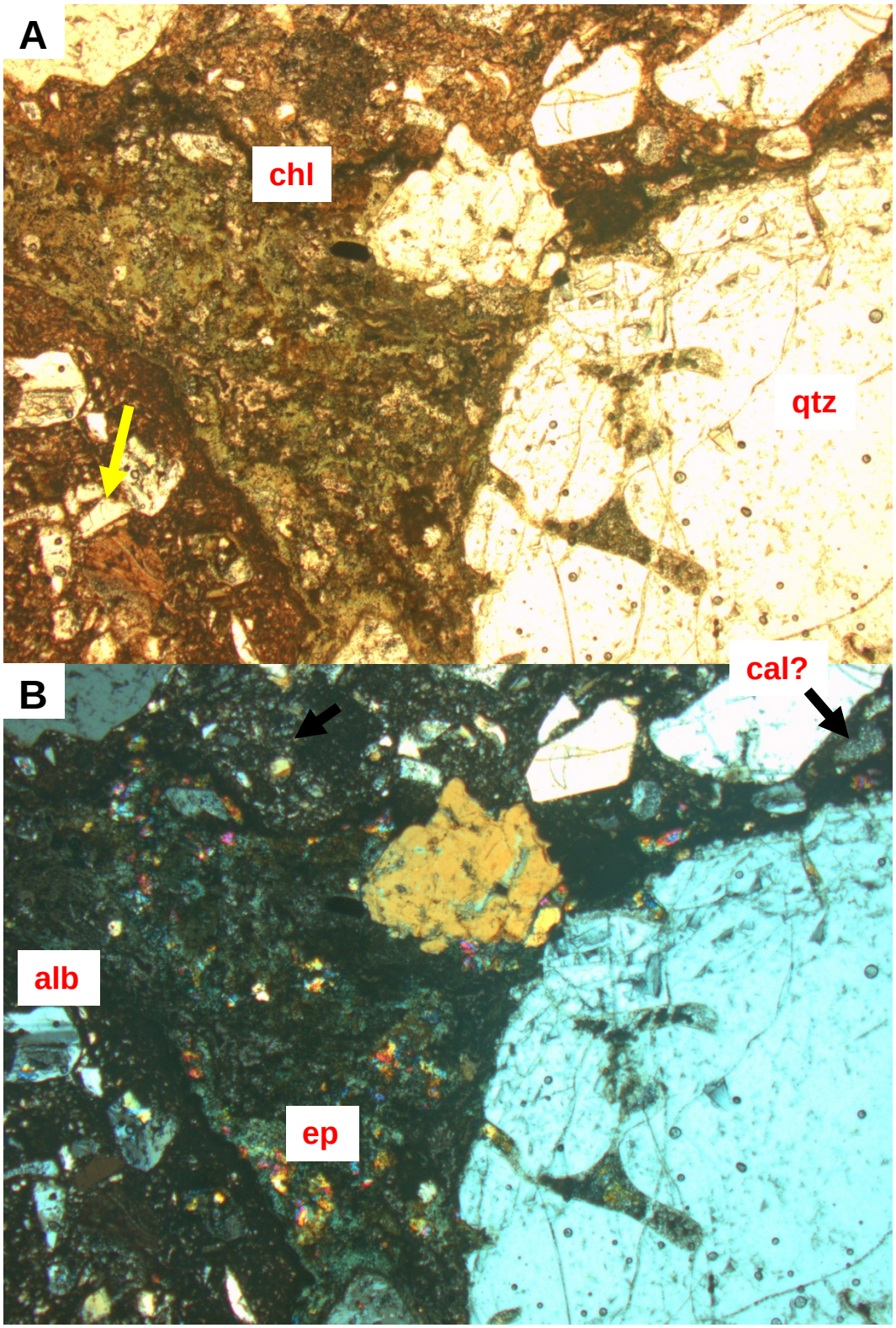

Fig. 4.34. Embayed quartz clast with chlorite and epidote altered tail. Possible calcite (cal, black arrow). 2.5x magnification, A=PPL, B=XPL.

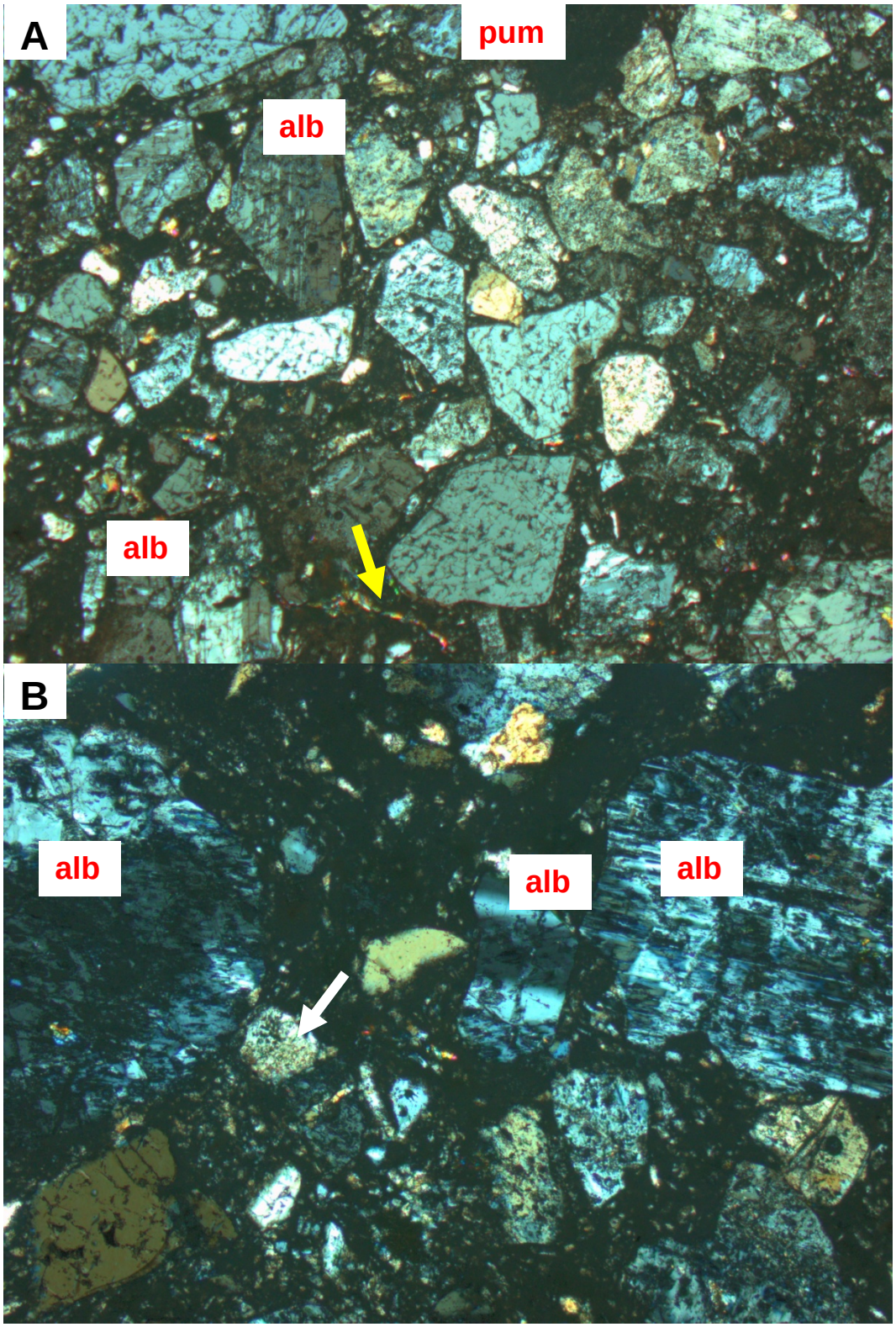

Fig. 4.35. A: Albite (alb) replacing plagioclase, pumice clast (pum), epidote vein (yellow arrow). B: Albite (alb) replacing plagioclase. Dissolution fabric (looks like small air bubbles, white arrow). Illite altered groundmass. 2.5x magnification, A=XPL, B=XPL.

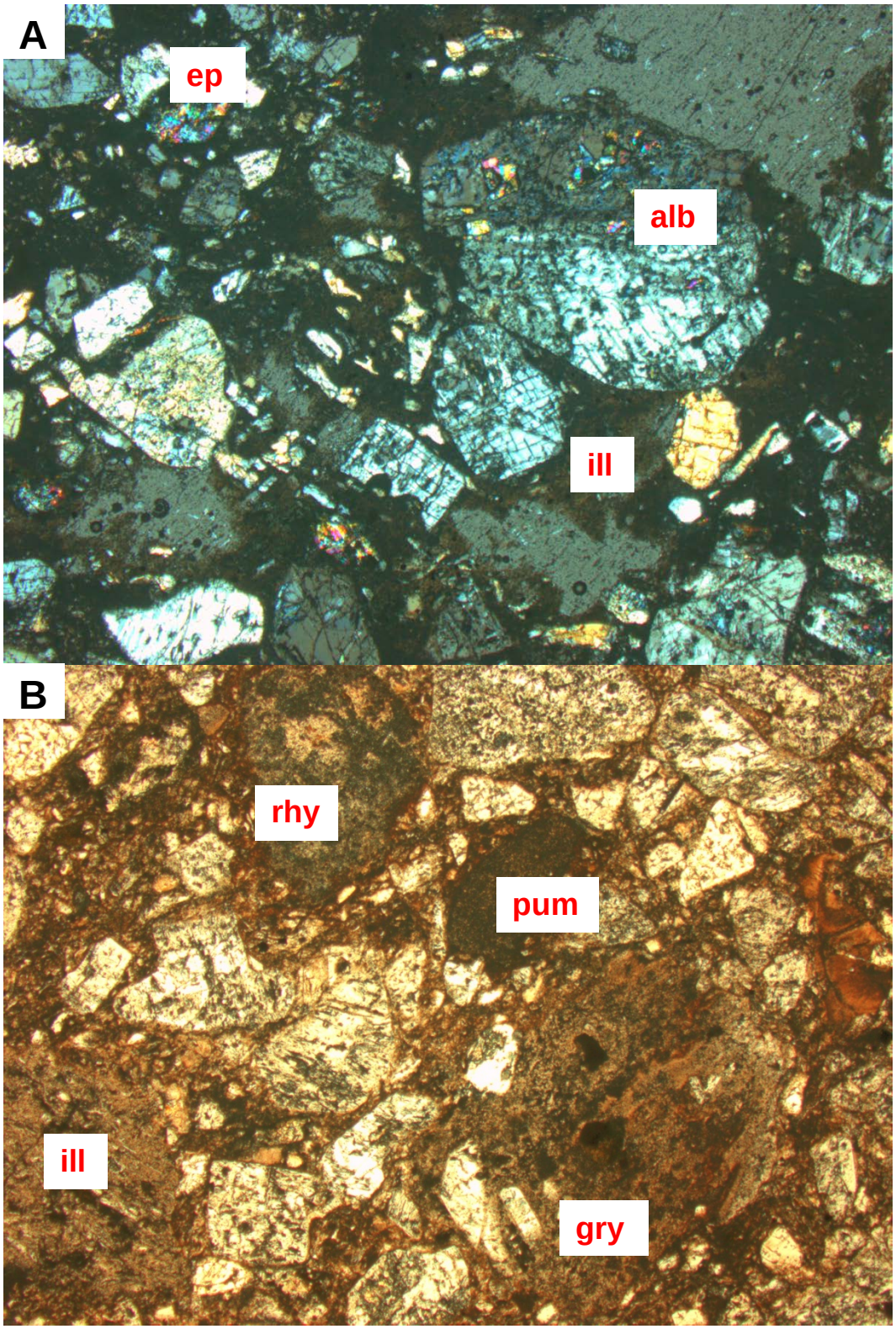

Fig. 4.36. A: Albite (alb) and epidote replacing plagioclase, fractured quartz, illite surrounding vugs. 2.5x magnification, XPL. B: Illite pseudomorph (ill), greywacke clast (gry) pumice fragment (pum), rhyolite lava clast (rhy). 2.5x magnification, PPL.

Crystals make up 30% of the thin section, with large fragmented and embayed quartz crystals (6 mm) the most abundant phenocryst. Quartz may be sieved or cleavage and rimmed textures. Plagioclase feldspars (<2 mm) are the next abundant crystal along with ferromagnesian minerals (<0.5 mm). Feldspars are partially replaced to albite, epidote, illite and according to Kilgour et al. (2006), also wairakite, adularia and calcite. Epidote completely replaces ferromagnesian minerals (pyroxene or amphibole). The rhyolite, pumice and greywacke clasts have been partially or completely altered to mostly illite, quartz, chlorite, calcite and leucoxene but also epidote, albite and pyrite. The groundmass is fine grained, composed of secondary minerals and even smaller lithics that have been subjected to illite and chlorite alteration. Illite pseudomorphs, vugs rimmed with illite and very small epidote filled veins are seen in thin section. Kilgour et al. (2006) suggest that fragmentation of quartz and plagioclase crystals occurred during or after alteration by small faulting episodes.

4.4.5 Petrographic summary

The main hydrothermally altered minerals identified in thin sections across all three wells are albite, adularia, wairakite, quartz, chlorite, epidote, illite, pyrite, and perhaps calcite, leucoxene and ilmenite. These have replaced original minerals such as plagioclase, ferromagnesian minerals such as amphiboles and possible pyroxene, and magnetite. The most common phenocrysts are plagioclase and quartz, with some of the quartz showing embayments (caused by magmatic processes such as reactions with the melt) or fracturing from deformation. There is a variety of clast types: rhyolite or andesite lava, siltstone (greywacke), tuff lithics and pumiceous fragments most of which are angular to sub-rounded and have been altered to varying degrees. Pumice clasts are chloritised, with some moderately flattened to produce fiamme.

The alteration minerals recognised suggest an alteration association consistent with propylitic alteration but with components of argillic or intermediate argillic alteration. Argillic or intermediate argillic shares the alteration minerals illite-smectite, quartz, and pyrite indicating temperatures of <210 °C. Ca, Mg and Na metasomatism is evident but potentially K-metasomatic changes in the form of

adularia as well. Propylitic alteration to epidote, chlorite, albite, calcite and pyrite is a higher temperature assemblage due to the presence of epidote (>250 °C) and results from Ca-Mg metasomatism. Propylitic or potassium mineral associations prevail at deep levels in high-temperature water areas (Ellis & Mahon, 1977). In contrast, zeolites and montmorillonite clays are common at shallower, cooler levels. Additional adularia alteration (K-feldspar (adularia), quartz, sericite-illite, pyrite) is also evident. Most rock samples have undergone chlorite alteration owing to the pale green shade observed and illite/sericitic alteration that is easily observed in deeper samples (TH9 2424 mRF, TH12 ~1900 mRF).

Epidote veining cutting through the matrix is observed in all three wells. In TH10 at 1405.5 mRF, mineral paragenesis is evident where an epidote vein cuts across a previous illite or chlorite vein. This cross-cutting suggests prograde alteration with depth where a higher temperature association (epidote vein, >250 °C) has overprinted a lower temperature association (illite vein, >210 °C). However this may not be the case as epidote and illite can also co-exist at the same temperatures. In TH9 1801.5 mRF, vein or joint fractures are lined with quartz, chlorite, pyrite and wairakite, however veining is absent deeper in the well (2424 mRF). The presence of adularia and wairakite are indicative of permeability. Veins in TH12 (1370 mRF) are much thinner and are chlorite or clay-microcrystalline quartz. At deeper levels (TH12, 1900 mRF) are rare smaller epidote veins.

Vugs, the result of dissolution of silica, are present in TH12 at ~1300 mRF, and are lined with wairakite, adularia, quartz and/or coated with clay while at deeper levels (1900 mRF) weak vuggy textures of quartz have developed. In TH12 vugs are rimmed with illite and pseudomorphs of illite are abundant, the result of replacement. Deformation has impacted on quartz and plagioclase phenocrysts in TH12 that is probably caused by small faulting episodes (Kilgour et al., 2006).

4.5 DISCUSSION

4.5.1 Mineral stability in other TVZ geothermal fields

The temperature of the fluid, both inflow and outflow, is not constant in the life of a geothermal system due to waxing, waning and replenishment of subsurface geothermal activity (Milicich et al., 2014). This concept is corroborated by findings from other authors such as Henneberger and Browne (1988) and their research on the extinct hydrothermal system of Ohakuri (active >160,000 years ago). Fagan et al. (2006) also reported that the geothermal system at Mangakino has undergone substantial cooling. Therefore as the temperature regime changes so too does the mineral assemblage, as the minerals try to maintain equilibrium with the hydrothermal fluid.

4.5.2 Minerals in equilibrium

The temperature stability and consequently mineral stability changes between each geothermal system. Hedenquist and Browne's (1989) research from the Waiotapu geothermal system revealed a principal alteration assemblage of quartz, albite + adularia, with minerals such as chlorite, pyrite calcite, zeolites, epidote, pyrrhotite, sphene, leucoxene, apatite and minor sulphides variably distributed. Surficial alteration by acid sulphate, steam-heated waters produced a clay assemblage of kaolinite, cristobalite, alunite and smectite. At shallow subsurface levels a later overprint of white mica is developed. The assemblages and measured well temperatures showed a shallow reservoir with fluids at 225 °C. Deep chloride fluids from depths of ~1500 m ascend and boil at temperatures of at least 300 °C to 230 °C accounting for the albite-adularia assemblage. A later overprint of white mica at shallow levels indicates cooling, where albite-adularia alteration has stabilised to white mica influenced by the CO_2 rich dilution. The deep chloride fluids are diluted and capped by CO_2 rich steam-heated water which also occurs on the system margins.

The Ohaaki geothermal system yielded a similar hydrothermal mineral assemblage of quartz-albite-illite-adularia-calcite-chlorite and pyrite at 260 °C (600-800 m depth) (Hedenquist, 1990). As at Waiotapu, Ohaaki also has

kaolinite, smectite (Ca-montmorillonite), illite-smectite, cristobalite as well as siderite, leucoxene and mordenite on the cooler margins of the system. The current mineral assemblage at Ohaaki reflects the present temperature regime of ~305 °C (Browne & Ellis, 1970). At Kawerau, hydrothermal minerals are also in equilibrium with fluids. Mineral assemblages reflect a surficial acid alteration zone, followed by a neutral pH assemblage (wairakite, epidote, quartz, calcite, illite suggesting temperatures >240 °C, Bignall et al., 2010).

4.5.3 Thermal events and overprinting

The Kawerau geothermal system has experienced a series of overprinting thermal events (Milicich et al., 2014b). Wairakite-prehnite alteration in the southern end of the geothermal system has been overprinted by a modern assemblage of calcite, calcite, quartz, calc-silicates, illite and adularia. Textural evidence indicates epidote (250-290 °C) deposition was followed by chalcedony (<190 °C) implying a cooling period in the north of the geothermal system. Likewise at the Mangakino geothermal system, Fagan et al. (2006) showed that calcic plagioclase is replaced by adularia, which in turn is replaced by illite, thus suggesting separate thermal events. The cause was rhyolite dome emplacement in the east resulting in high temperature minerals (epidote, wairakite) subsequently replaced by lower temperature minerals such as clays.

At depth in the Ngatamariki geothermal system, Chambefort et al. (2014) reports that some hydrothermal alteration is in equilibrium with high temperature neutral pH fluids that produce a high temperature assemblage of illite, chlorite, epidote and pyrite. However in the northern part of the field, biotite, magnetite and rare K-feldspar, quartz, pyrophyllite/muscovite, andalusite and topaz are artefacts of advanced argillic and potassic hydrothermal alteration at high temperatures (Lewis et al., 2013). Thus two hydrothermal systems or events are said to have occurred at Ngatamariki (Chambefort et al., 2014). A magmatic intrusion surrounded by a contact metamorphism halo caused the first associated fluid-rock interactions and alteration, and the present day convective system.

At Ngawha, the only other high temperature geothermal system outside of the TVZ, Cox and Browne (1998) state that replacement alteration is minor in the host rocks, instead it is focused in veins within the relatively impermeable reservoir rocks. The vein focused alteration along with temperature, are major contributing factors for alteration at Ngawha. Measured temperatures compared to mineral inferred temperatures show that in the south/southeastern areas of the field hotter temperatures had occurred in the past, usually a 20-30 °C increase but in some places 50-80 °C. However, now the system is cooler due to an eastern inflow of cool groundwater triggering a change in hydrology inside the reservoir (Cox & Browne, 1998). Other indications of previous hotter fluid movement are along the Mangatawai Fault (fault permeability) and in deeper parts of wells where epidote abundance and crystal size indicate temperatures >280 °C compared to measured temperatures of 270°C.

4.5.4 Alteration Mineralogy of the Tauhara Geothermal Field

For the alteration mineralogy by SWIR, interpretation of spectral profiles have identified an alteration association of kaolinite, smectite, illite-smectite, illite, chlorite and epidote reflecting both argillic and propylitic alteration types. SWIR alteration mineralogy was validated by XRD, as XRD also identified montmorillonite (smectite), illite-smectite, illite, kaolinite and chlorite as well as hydrothermal feldspars albite and orthoclase (adularia). Hence XRD also suggests argillic or intermediate argillic alteration and propylitic alteration as well as potential adularia alteration according to Table 4.5. The distribution of calcite was predominantly identified by HCl application, well logs and petrography. Wairakite and pyrite was confirmed in this study by petrography and the presence of wairakite correlated closely with known feed zones.

The wells are all from separate areas of the geothermal field (TH9 - west, TH10 - southwest, TH12 - northeast) and logically from different areas of the hydrothermal system. Table 4.7 is a summation of the hydrothermal minerals identified from each analysis. Lines were drawn arbitrarily to look for common minerals across the analyses and correlate them to principal mineral associations,

alteration zones/alteration type and the likely temperature regime operating in that part of the geothermal field.

The main alteration zones identified downhole across the three wells are:

1) Beige zone: a shallow zone of argillic to intermediate argillic alteration consisting of smectite, kaolinite, quartz, illite-smectite, calcite, pyrite and perhaps cristobalite and zeolite.
2) Orange zone: with increasing depth, an increase in alteration intensity where the mineral assemblage consists of illite, chlorite, illite-smectite, quartz, albite and calcite with minor epidote and pyrite. This is a transition zone where propylitic alteration begins to dominate.
3) Red zone: at the deepest level is a more intense propylitic alteration zone with an assemblage of illite, chlorite, epidote, quartz, albite, adularia, wairakite and pyrite.

Table 4.7. Summary table of minerals identified across all XRD, SWIR and petrographic analyses combined with reported logged minerals. The table is divided into sections based on the most common minerals across each analysis.

	XRD	SWIR	Petrography	Well logs
TH9	***350*** = montmorillonite, kaolinite, cristobalite?	***60-540*** = smectite, kaolinite, illite-smectite		***100-800*** = clay, pyrite, Fe-oxides
	720-940 = chlorite, illite, qtz, albite, sanidine	***560-900*** = illite, chlorite, calcite ***920-1280*** = smectite		***800-1450*** = chlorite, epidote, pyrite, qtz
	1100-1540 = chlorite, illite, albite, adularia	***1300-2415*** = illite, illite-smectite, chlorite, calcite	***~1405*** = epidote, chlorite, albite, adularia, pyrite, illite, groundmass qtz	***1450-2400*** = clay, chlorite, epidote, calcite, pyrite, qtz, wairakite, vein
TH10	***520*** = montmorillonite, kaolinite, qtz, cristobalite	***70-620*** = kaolinite, illite-smectite		***100-350*** = clay, chlorite, calcite, pyrite, Fe-oxides, qtz ***350-550*** = clay, pyrite, Fe-oxides, qtz
	880-1620 = chlorite, illite, qtz, albite	***620-1180*** = illite, chlorite, calcite	***~1801*** = epidote, chlorite, wairakite, qtz-pyrite, illite, albite	***550-1200*** = clay, chlorite, calcite, pyrite, qtz
	2100-2305 = chlorite, qtz, albite, zeolite	***1200-2332*** = chlorite, calcite. Trace illite or illite-smectite ***>1640*** = epidote	***2424*** = epidote, illite, qtz, chlorite, albite, adularia, ilmenite?	***1200-2300*** = clay, chlorite, epidote, Fe-oxides, qtz, vein
TH12	***240-390*** = montmorillonite, illite, qtz, cristobalite, zeolite	***40-410*** = illite-smectite		***50-150*** = smectite, chlorite, calcite, pyrite, Fe-oxides ***150-450*** = clay, pyrite
	1040-1160 = chlorite, illite, qtz, albite, adularia, anorthoclase, ***1240-1380*** = chlorite, illite, qtz, albite, adularia	***420-1020*** = illite ***1040-1400*** = illite-smectite, smectite at 1200, chlorite, calcite	***1370-1372*** = chlorite, epidote, pyrite, illite, wairakite, adularia, albite, qtz ***1899*** = albite, epidote, illite, wairakite, adularia, calcite, pyrite	***450-825*** = clay, chlorite, calcite, Fe-oxides, qtz, pyrite ***825-1050*** = illite, chlorite, calcite, pyrite, qtz ***>1050*** = illite, chlorite, calcite, epidote, qtz, wairakite

These findings are in agreement with previous hydrothermal alteration studies at the Tauhara which reveal increased alteration intensity with depth. The presence of epidote indicates temperatures in excess of 250 ºC (Rosenberg et al., 2009; 2010). The Oruanui Formation and Huka Falls Formation are affected by an argillic alteration association (smectite, calcite ± pyrite, ± illite-smectite) at shallow levels. Interlayered illite-smectite, hydrothermal quartz, calcite and pyrite followed by minor illite, chlorite and epidote indicate an increase in alteration rank and intensity. As depth increases propylitic alteration becomes the dominant style represented by chlorite, quartz, epidote, albite, adularia, wairakite and titanite.

Rosenberg et al (2009) and Bignall et al (2010) state that the propylitic assemblage (adularia, albite) on the western side of the Wairakei-Tauhara system has been overprinted by an illite-calcite assemblage indicating a decrease in temperature or pH of the fluid, although this overprint is not seen on the eastern side of the field. According to Kilgour et al. (2006) there is some evidence for the overprint in TH12 and petrography in this study reveals a strong pervasive illite alteration in the core sample of TH12 (~1899 mRF) that supports this suggestion.

4.5.5 Temperature stability at Tauhara geothermal field

Tauhara geothermal field has a segregation of alteration zones similar to other geothermal fields of the TVZ: shallow meteoric groundwater aquifer, chloride-bicarbonate waters at depth and a chloride geothermal reservoir at high temperatures >280 °C at depths of over 1000 m (Bignall, 2009). Overall mineral inferred temperatures are somewhat cooler than the measured well temperatures (Fig. 4.37).

The shallow argillic zone containing smectite, kaolinite, and cristobalite comprise the acid sulphate argillic alteration zone which changes outward with depth towards illite and illite-smectite. Above the groundwater table, H_2S is oxidised to produce kaolinite and cristobalite (low temperature, acid stable minerals) from steam percolating towards the surface. At Tauhara, kaolinite is present at depths of ~400 mRF in TH9 towards the west of the field and ~500 mRF in TH10 at the

southern end (Fig. 4.37). This deeper occurrence contrasts with other New Zealand systems where kaolinite lies at surficial levels of 50-100 m (Hedenquist, 1990). In the Jigoku area of Japan, Hayashi in 1973 reported that a funnel shaped zone of alunite, kaolin, pyrophyllite reaches depths of 380-1000 m, but the mechanism for such deep acid alteration is not clear (Kiyosaki, 2003). A zone of alteration comprising these minerals, occurs above low-sulphidation systems, but may extend downward along fractures (White & Hedenquist, 1995; Pirajno, 2009), accounting for their occurrence at deeper levels. Reyes (1990) findings also support the fracture theory. In Phillipine wells, permeable horizons can be correlated with surface mapped structures that are also connected to alteration assemblages at depth which show acid sulphate alteration or alteration from cooler fluids (Reyes, 1990). Acid altered areas on the surface that are cut by structures (such as fractures) typically allow acid fluids to percolate to depths as deep as 500 m below the surface. These descending steam heated acid waters may produce an assemblage of kaolinite, dickite, pyrophyllite + illite, quartz, opal, cristobalite, pyrite with temperature and distance from the flow path. This same mechanism is the reason why kaolinite is found at deeper levels (~500 m) at Tauhara.

In all wells there is a prograde sequence of alteration (smectite, illite-smectite, illite) with depth where hydrothermal intensity increases. This sequence is best recognised in TH9. The mineral association is illite, chlorite, illite-smectite, quartz, albite and calcite with minor epidote and pyrite. This is likely a transition zone where propylitic alteration begins to dominate. Evidence of mineral paragenesis to support this finding is in the core sample from TH10 where an epidote vein (>250 °C) crosses and overprints a previous illite/sericite vein (illite vein, ~210 °C). This finding suggests there is currently late stage, hotter fluids in TH10 and it is potentially closer to productivity or the major upflow zone in south Tauhara. However illite and epidote can co-exist at the same temperature. Ellis & Mahon (1977) also state that in high temperature water systems, propylitic or potassic mineral associations predominate at deeper levels. Mineral inferred temperatures also generally agree with measured well temperatures in TH10 hence TH10 is a prospective area for geothermal production as reiterated by Rosenberg et al. (2010).

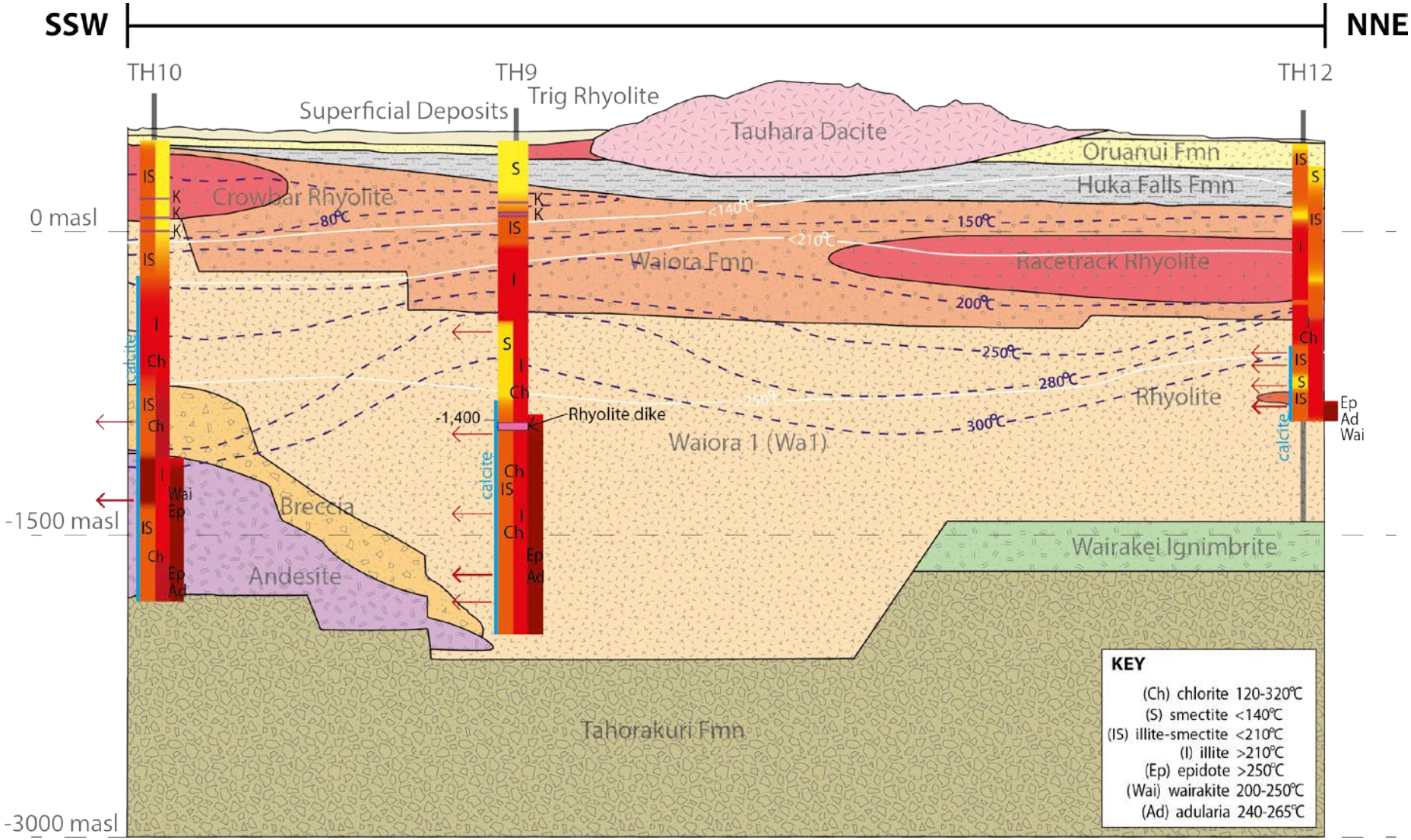

Fig. 4.37. Schematic diagram of mineral inferred temperatures (white isotherms) and measured downhole temperatures (dashed blue isotherms) overlying geology. Red arrows are feed zones. Each well column is split into three, the left side is SWIR identified minerals, the middle column XRD identified minerals, the right side is petrographic identified minerals. Geology redrawn by permission from Contact Energy.

In contrast, the alteration mineralogy in TH12 is inconsistent with the measured well temperature of 280 °C at a depth of ~820 m. This inconsistency implies a possible recent increase of fluid temperature, as the illite-smectite is yet to transform to illite at the modern fluid temperature. However there is a late stage overprint of illite-calcite at the bottom of the well (~1900 mRF) over a previously higher temperature assemblage of epidote according to Kilgour et al. (2006). This overprint is supported by the abundance of illite in the core sample from ~1899 mRF which contains illite pseudomorphs, common illite rimmed vugs and pervasive illite alteration of the groundmass suggesting temperatures may have cooled in this area. Perhaps this well is more marginal to the upflow zone compared to wells TH10 and TH9.

Well TH12 also contains deformed quartz and plagioclase phenocrysts that are highly fractured and are probably caused by small faulting episodes. TH12 is near an upthrusted block of greywacke Torlesse basement (Kilgour et al., 2006) that may be the source. Alternatively blind faults at depth with no surface manifestation (Rosenberg et al., 2009; Bignall et al., 2010) may provide fluid conduits to allow a change in the temperature regime in this area of the field. Figure 4.37 shows that the feed zones (red arrows) in TH12 are congregated around the ~50 m thick rhyolite lava therefore its emplacement may also have provided fluid flow pathways.

It is also important to answer one of the objectives in determining if there was an alteration halo pointing to the rhyolite dike at 1440 mRF in TH9. Epidote, pyrite and vein material were recognised either side of 1440 mRF (1360-1380 mRF, 1455-1460 mRF) but other hydrothermal alteration minerals (illite, chlorite) analysed by SWIR did not show any appreciable halo.

Chapter 5
Geochemistry

5.1 INTRODUCTION

Much of our knowledge of vectors towards mineralization in epithermal gold and silver deposits has been gained from studying active hydrothermal systems in geothermal fields. Browne (1970) pioneered the idea that alteration minerals were formed under certain temperature and pressure conditions, and that their distribution is zoned. Epithermal deposits often have zoned alteration halos where chemical and mineral variations point towards fossil fluid flow and therefore precious metal mineralization. In this chapter, I am examining samples from an active hydrothermal system, to distinguish lithological variations that may not be apparent from logging of cuttings, and identify geochemical vectors towards known fluid flow pathways and permeable zones that can assist with geothermal exploration, and potentially epithermal gold and silver exploration.

Portable x-ray fluorescence (pXRF), a technique initially created for remote planetary exploration and adopted widely by the mining industry, is a powerful instrument that enables rapid chemical testing and real-time decisions to be made during drilling programmes (Le Vaillant et al., 2014). In this chapter, the pXRF technology is applied to samples from the three wells of the Tauhara geothermal field to establish how effective it is in identifying lithology, stratigraphic units, hydrothermal metasomatism and fluid flow pathways. If successful, the technique will be valuable to companies and researchers in the geothermal industry.

This chapter describes the geochemistry of 304 samples collected over three wells (TH9, TH10, TH12) across the Tauhara geothermal field with the aim of identifying and quantifying chemistry of geothermal cuttings. The alteration types, alteration associations, fluid movement zones are inferred using alteration indices and the alteration box plot. Quantifying alteration using molar element ratio plots and alteration indices provided an indication of constituents lost and gained in exchange

reactions, mineral stoichiometries and minerals formed. This chapter links very closely to Chapter 4 which describes the alteration mineralogy (secondary mineralogy) and what remains of the primary mineralogy. It also links with Chapter 2 which provides a background to alteration mineralogy for the reader.

5.2 METHODOLOGY

5.2.1 Sample selection

Three GNS Science Consultancy Reports form the basis of sample selection in this study.

Table 4.1. Three main well reports used in this thesis.

Well	Authors	Year/Report no.	Title
TH9	MIlicich, Rosenberg, Ramirez & Kilgour	2008a/56	Geology of Exploration Well TH9 Tauhara Geothermal Field
TH10	Milicich, Ramirez & Rosenberg	2008b/80	Geology of Exploration Well TH10 Tauhara Geothermal Field
TH12	Kilgour, Rae & Milicich	2006/219	Geology of Exploration Well TH12, Tauhara Geothermal Field

As reiterated in Chapter 4, a total of 304 samples were collected down hole from three geothermal wells across the Tauhara Geothermal field (TH9, TH10, TH12). Samples of rock cuttings (5-10 g) were collected every 20 m down well. Where no rock cuttings at the required interval existed, a sample from the closest available interval was taken. Samples were also taken five to ten metres either side of logged lithological boundaries to capture changes in lithology and at least 20 m beneath casing points to avoid cement contamination. According to Hulen and Sibbett (1982) cuttings can be contaminated by; parts of the drillhole that has collapsed, drill bit flakes, pieces of cement casings, drilling mud, grease or lost circulation material (LCM) such as hazel wood chips or mica (used to plug up holes when circulation is lost). However these can be easily recognised amongst the cuttings and can be removed for example, if there are metal drill bit flakes these are removed with a magnet. It is important to remove these so that anomalous readings of Fe do not interrupt the geochemistry. Whole rock geochemistry was performed by portable x-ray fluorescence (pXRF) and lab-based traditional x-ray fluorescence (XRF) in order to determine rock types and alteration type.

5.2.2 X-ray fluorescence spectrometry

X-ray fluorescence is used to identify the elemental composition of a sample rapidly and quantify how much of each element is present in a sample. In x-ray fluorescence spectrometry a material (usually powdered rock) is bombarded with high energy γ rays to emit secondary fluorescent x-rays (Fig. 5.1).

The nucleus of an atom contains protons (+ charge) and neutrons (non-charge) with electrons grouped in shells around the outside. An x-ray tube produces x-rays that irradiates the sample. These x-ray photons, or electrons with enough energy, knock out electrons within the innermost K or L orbitals surrounding the nucleus. When an electron is knocked out, an electron from the outer LII, LIII or M orbitals moves in to restore stability and emits a secondary x-ray photon known as x-ray fluorescence that may then be used to measure the concentration of a specific element.

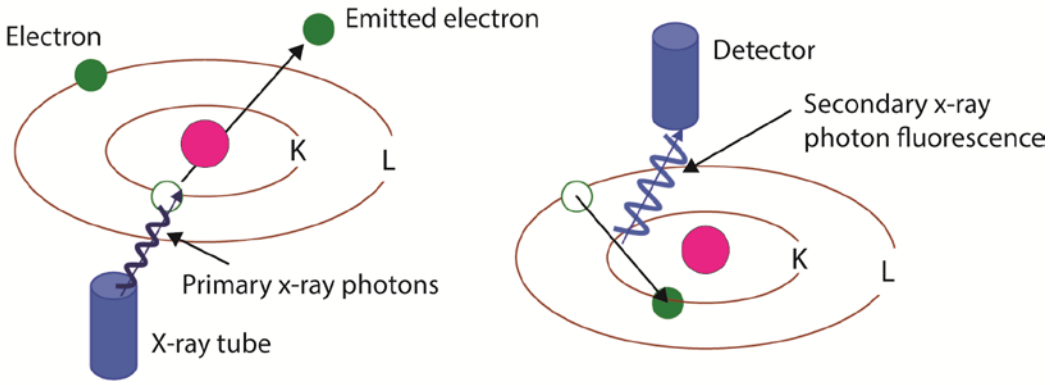

Fig. 5.1. Schematic diagram illustrating how x-ray fluorescence works (modified from the InnovX-XRF manual).

5.2.3 Portable x-ray fluorescence (pXRF)

The theory behind pXRF is the same as XRF, but the x-ray source and detector are contained within a handheld device (Fig. 5.2). The Innov-X Olympus Delta gun has a Rhodium (Rh) anode x-ray tube and a silver (Ag) anode. The tube generates an x-ray beam that interacts and triggers the atoms in the sample to fluoresce. The fluorescence releases a comprehensive spectrum of x-rays (Brehmstrahlung x-rays) and a line spectrum of defined peaks (Goodale et al., 2012). The individual atoms in

the sample are characterised by the x-ray energy via energy dispersive spectroscopy (EDS, Shindo & Oikawa, 2002).

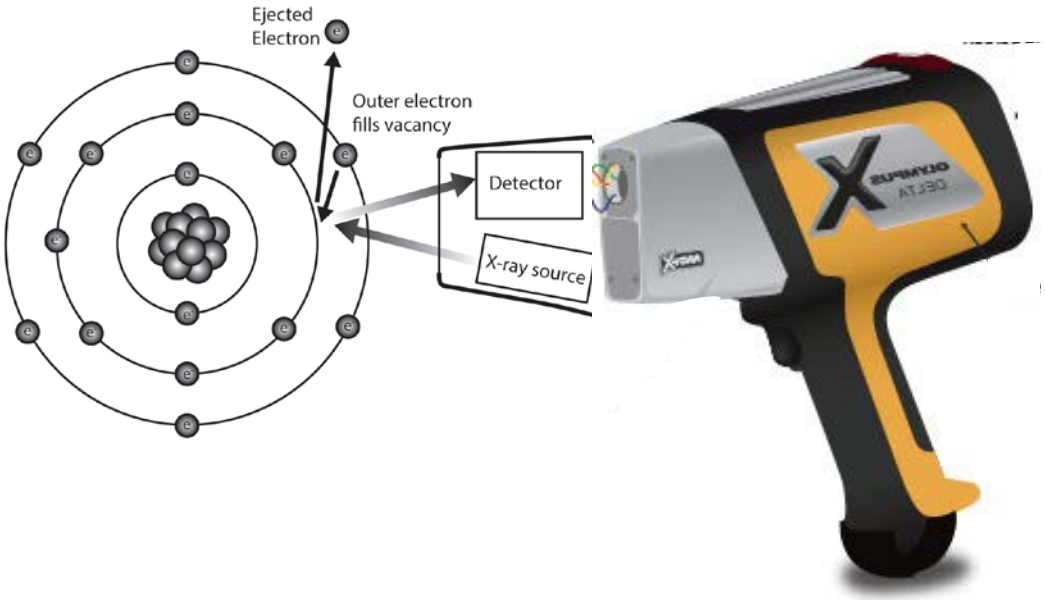

Fig. 5.2. Diagram showing how the unit works. Unit emits x-rays to excite atoms in the sample, X-rays displace inner shell electrons and outer shell electrons substitute in to fill the void emitting fluorescence as it does so (Gazley & Fisher., 2014).

From the unit, the x-rays penetrate into the sample at submillimetre depth but this varies by atomic weight with each element (Gazley & Fisher., 2014). Measured concentrations also decrease if the sample penetrated is not thick enough. Heavier elements are less affected by this. Data generated by individual instruments differ from one another so for consistency the same instrument should be used throughout sampling (Goodale et al., 2012; Brand & Brand, 2014). Recorded measurements can also be affected by sampling uncertainty, surface irregularities, weathering effects and the depth of x-ray penetration (Potts et al., 1995, 2006; Jones et al., 2005; Brand & Brand, 2014).

pXRF was performed on all 304 rock cutting samples, the average grain size is 1 – 6 mm. The raw cuttings used in pXRF and lab XRF were not cleaned of drill bit scrapings or LCM, only drilling mud. Sample preparation for pXRF utilised a SC-4331 sample cup be covered with a thin polypropylene film LS-240-2510 (both manufactured by Premier Lab Supply) with a locking ring placed on top to hold the film in place. The thin film (polypropylene or Mylar) enabled the secondary x-rays emitted from the sample to return to the detector, while allowing the sample to be

analysed with minimal exposure of x-rays to the operator using a lead-lined bench top stand. A small sample (1/2 teaspoon of cuttings) is then placed inside, and a 10c Australian coin is used to gently compress the sample. A piece of paper cut to the coin size is placed on top and cotton wool used as filler keeps the sample in place while the cap is pressed on. For samples that were too coarse, a small amount of dry grinding with an agate mortar and pestle was used.

An Innov-X Delta 50 keV Handheld XRF Analyser gun (Olympux Innov-X 50 KV DP4050CX) manufactured by Olympus was set to "Geochem mode" and mounted in a benchtop stand. Concentrations of major and trace elements were recorded by Innov-X Delta Advanced PC software. The following elements were analysed; Nd, Pr, Ce, La, Ba, Y, Al, Si, P, S, Cl, K, Ca, Ti, V, Cr, Mn, Fe, Co, Ni, Cu, Zn, As, Se, Rb, Sr, Zr, Nb, Mo, Ag, Cd, Sn, Sb, Ta, W, Au, Hg, Pb, Bi, Th, U. 304 samples were analysed by pXRF with each scan taking 60 s. The speed of analysis allows for a greater number of samples can be analysed compared to traditional XRD and XRF. CAL checks, instrument calibrations were made every 30 or so samples. See Appendix E (on CD) for the raw pXRF data. Rock standards were not run for pXRF, however traditional laboratory XRF was used as calibration to correct the concentration of elements within samples.

Table 5.1. Olympus Innov-X Delta 50 keV handheld XRF analyser specifications.

Instrument Model	Innov-X Delta
Tube current	10 - 50 µA
Tube voltage	10 - 50 kV
Mode of operation	Geochem
Analysis time	60 s, 30 s per filter (2 filters)
Calibration used	Factory
Nature of material	Rock chips/cuttings
Sample container	Sample cup SC-4331 with film TF-160-255

5.2.4 X-ray fluorescence methodology (XRF)

Traditional laboratory based x-ray fluorescence (XRF) calibrated to international standards, was performed on 45 out of the 304 samples. In order to check the accuracy of the pXRF results, 45 samples (15 from each well) representative of the different logged formations downhole based on stratigraphy from the three aforementioned well reports were selected for traditional lab-based XRF. See

Appendix D for list of XRF samples. A Spectro X-Lab 2000 polarising EDS XRF instrument located at the University of Waikato was used for the XRF analysis. Major elemental oxides were determined on fused discs and trace elements were verified on pressed pellets. The elemental oxides and trace elements analysed are; S, Cl, V, Cr, Co, Ni, Cu, Zn, Ga, Ge, As, Se, Br, Rb, Sr, Y, Zr, Nb, Mo, Sn, Sb, Te, Ba, La, Ce, Nd, Hf, Ta, Tl, Pb, Bi, Th, U. Full elemental data is in Appendix D (on CD).

A tungsten carbide mill was used to crush the samples to the consistency of talcum powder and homogenise them in preparation for XRF. The mill components holding the sample and spatula were cleaned with ordinary tap water and dried in between samples to reduce cross contamination. The fine powdered rock was then made into fused discs and pressed pellets for major and trace element analysis.

5.2.5 Major element analysis

0.28 – 0.30 g of sample was mixed with 2.50 – 2.55 g of flux type LM100 (pure 100% Lithium Metaborate suitable for andesites of > 57% SiO_2 and rhyolites) in a platinum alloy crucible. The flux is designed to melt silica hence a sample with high SiO_2 content requires a matching flux. The flux was manufactured at XRF Scientific Ltd, Perth, Australia. The sample was then step heated in a Bradway Fusion Furnace at 15 minute intervals through five temperature stages (650°C, 720°C, 780°C, 825°C, 1000°C). At the final 1000°C temperature stage the furnace shaker is turned on and when the 15 minutes is up, a pinch of ammonium iodide (NH_4I) is added to aid pouring and prevent the melt from sticking to the crucible.

Platinum tipped tongs are used to pour the sample onto a graphite disc sitting on a hot plate set at 230°C, where it is gently pressed. The melt is step cooled to glass discs where the temperature is lowered 50°C every hour to allow the glass to anneal, preventing thermal and mechanical shock. Once cool to the touch, the samples are trimmed in order to fit into the XRF sample holder. Platinum crucibles were cleaned in the fume hood with boiling 36% HCl solution and then rinsed 4-5 times in tap water, 3 times in distilled water and 3 times with ultrapure water before being boiled in ultrapure water for 1 hour in a separate clean beaker and set aside to air dry.

5.2.6 Trace element analysis

For preparation of pressed pellets for trace element analysis 5 g of powdered sample was mixed with ~ 13-15 drops of PVA binder in a paper cup. The sample was stirred with a wooden spatula then poured into a labelled metallic container and placed into a cylinder and plunger that is inserted into a pneumatic press. The powder was compressed into the container at 90 bar. The surface of the pressed pellet must be flat and smooth so it does not expand or fall out when inserted upside down into the XRF sample holder. The cylinder and plunger are cleaned with acetone in preparation for the next sample. All samples were dried at ~ 70°C for 2 hours to evaporate the PVA binder before analysis and their weights recorded.

5.2.7 Loss on ignition

Loss on Ignition (LOI) is the final step in completing XRF analysis and was performed on each of the 45 samples. Firstly the empty crucibles are heated to 1100°C for an hour and their initial empty weight recorded. After cooling ~ 2 g of powdered sample is put into a silica crucible, placed in the furnace, heated up to 1100°C and remains at that temperature for 1 hour. The crucibles (with the sample) are placed in a desiccator and cooled for 10 minutes before weighing. The difference in weight is calculated (see below) and LOI determined in wt %. Samples were run twice as fresh flux was required to eliminate potential moisture issues in the previous batch. LOI values are presented in Appendix D (on CD).

$LOI\ (wt\ \%) = 100 \times [(n_2 - n_3) / (n_2 - n_1)]$

n_1 = weight of crucible

n_2 = weight of sample (crucible + sample)

n_3 = dry weight

wt % = difference in weight

5.3 pXRF vs TRADITIONAL XRF

5.3.1 Choosing the correct correlation

The Spearman correlation coefficient was developed in 1904 by Charles Spearman (Spearman, 1904) and is a rank based, non-parametric (distribution-free) statistic that measures the strength of monotone association between two variables (Hauke & Kossowski, 2011). The Spearman correlation coefficient does not measure the linear relationship between two variables like the Pearson's product-moment correlation co-efficient rather it evaluates how well the arbitrary monotonic function describes the relationship between two variables. Data is converted to ranks before calculating the coefficient. The advantage of ranking data is that assumptions on the frequency of distribution of the variables are not necessary and it can be used for variables on an ordinal level enabling the correlation between any variables possible.

Whereas the Pearson's product-moment correlation coefficient (Pearson, 1896) assumes that the variables are linear and normally distributed, which is only really true for quantitative or interval scale variables. Hence the Spearman correlation coefficient is usually used when the distribution of data is not normally distributed or the Pearson's correlation coefficient is inadequate (Hauke & Kossowski, 2011). Consequently, the Spearman's correlation coefficient proved to be better and was used in this study as it ranks your data (removing the influence of outliers) and was more suitable to my data which is non-parametric.

5.3.2 Correlation between pXRF and lab XRF

In order to assess the efficacy and reliability of data generated by pXRF it was plotted against internationally standardised laboratory XRF data to see how well they correlated. All available correlation plots and the raw correlation table can be found in Appendix E (on CD). Table 5.2 illustrates the comparison between elements in 45 samples that were analysed by both pXRF and lab-based XRF.

Comparison of the two XRF techniques reveals that many elements show strong, positive correlations (Spearman Rho correlation coefficient ($\mathbf{r}_s$) values > +0.8). For instance, Ba ($\mathbf{r}_s$ = 0.93) and Zr ($\mathbf{r}_s$ = 0.89) are both well correlated (Table 5.2). The presence of outliers can potentially skew correlations hence the Spearman rank correlation method was used as it is more robust against outliers (Rollinson, 1993). For example, Pb has a correlation coefficient of $\mathbf{r}$ = 0.93 using the Pearson's product moment correlation method, however due to its sensitivity to outliers it produced a higher misleading correlation. In contrast the Spearman rank correlation method gave a more reliable correlation coefficient for Pb of $\mathbf{r}_s$ = 0.68 (Fig. 5.3). Removing the two outliers in the Pb data and running the Pearson correlation coefficient again gave $\mathbf{r}$ = 0.65, in closer agreement to Spearman's method.

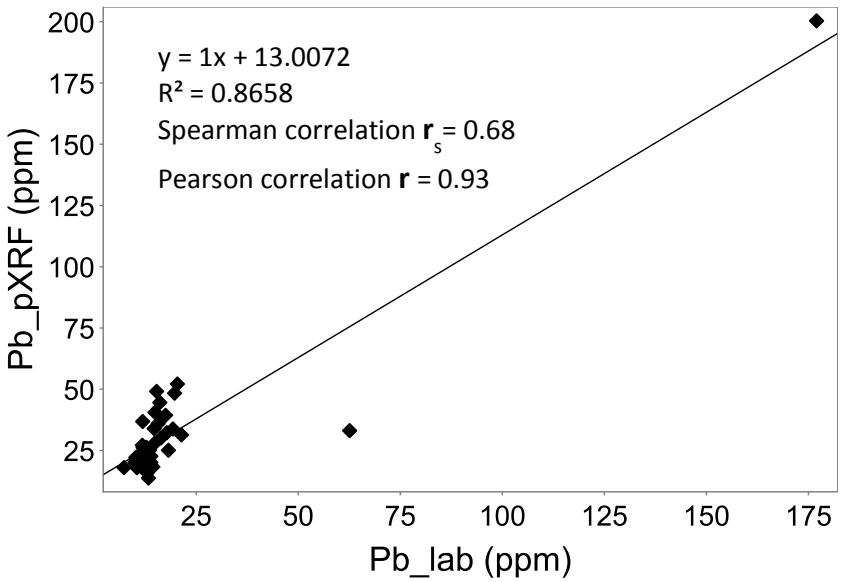

Fig. 1.3. Correlation plot of Lead.

Yttrium and Rb are also well correlated (0.89, Figs 5.4, 5.5) whereas Al is poorly correlated (0.17; Fig. 5.6). Elements with strong positive correlations of at least 0.80 are As, Ba, Ca, K, Nb, Rb, Sr, Y, and Zr (Table 5.2). Ti has a +1 correlation but the basis of this relies on detection by pXRF of Ti in only four samples. Elements with moderate correlation ($\mathbf{r}_s$ = 0.5 – 0.8) are Mn, Mo, Pb, S, Si, Zn and Fe. Elements showing a lack of correlation ($\mathbf{r}_s$ < 0.5) are Al, Cr, Cu, Sb, Ta and Th. Sn has a perfect negative linear relationship at -1, yet is based on detection in only three samples by pXRF, so this result is meaningless.

Piercey and Devine (2013) found excellent correlation between traditional XRF and pXRF for S, K_2O, CaO, TiO_2, MnO, Fe_2O_3, Co, Cu, Pb, Rb, Sr, Ba, Zr, Nb, U, As and Mo; moderate correlation for Aluminium (Al_2O_3), SiO_2, and Zn and poor correlation for MgO, P_2O_5, V, Cr, and Ni. Consequently the poor correlations I found between pXRF and laboratory XRF for S and Mo may be related to low Mo concentrations and/or the fact that in our study the pXRF data was collected from cuttings rather than the powdered rock used in Piercey and Devine's (2013) study.

These findings suggest that pXRF is reliable in measuring the concentration of many elements (As, Ba, Ca, K, Nb, Rb, Sr, Y, Zr, Mn, Mo, Pb, S, Si, Zn, Fe), particularly ones important in hydrothermal alteration, but is not as effective for other elements (Al, Cr, Cu, Sb, Ta, Th). A reason for this variance is likely due to subtle differences in techniques as pXRF performs poorly for light elements particularly ones below the atomic number 17, such as Mg, Al, Si, P, S, Cl. The lack of a vacuum or Helium purge unit in the gun to help with the detection of light elements is the most likely cause of the poor comparison of these elements.

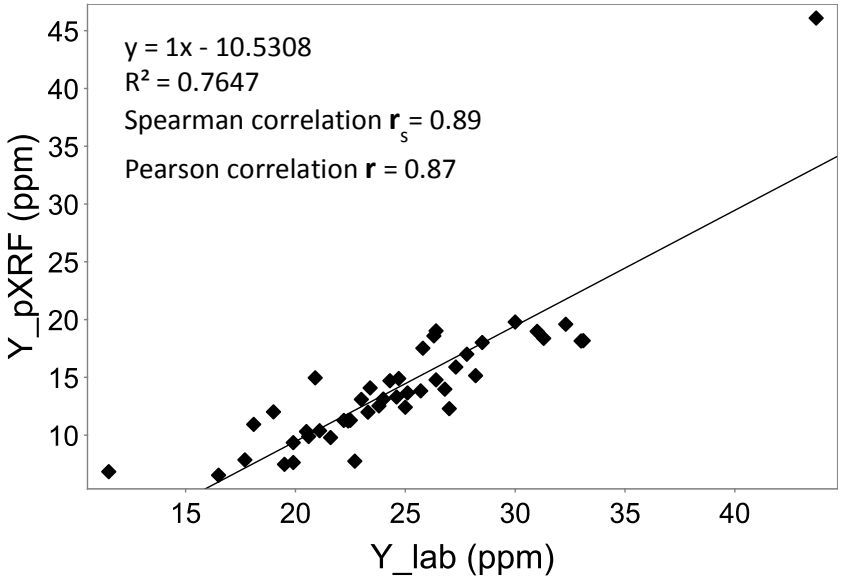

Fig. 5.4. Correlation plot of Yttrium.

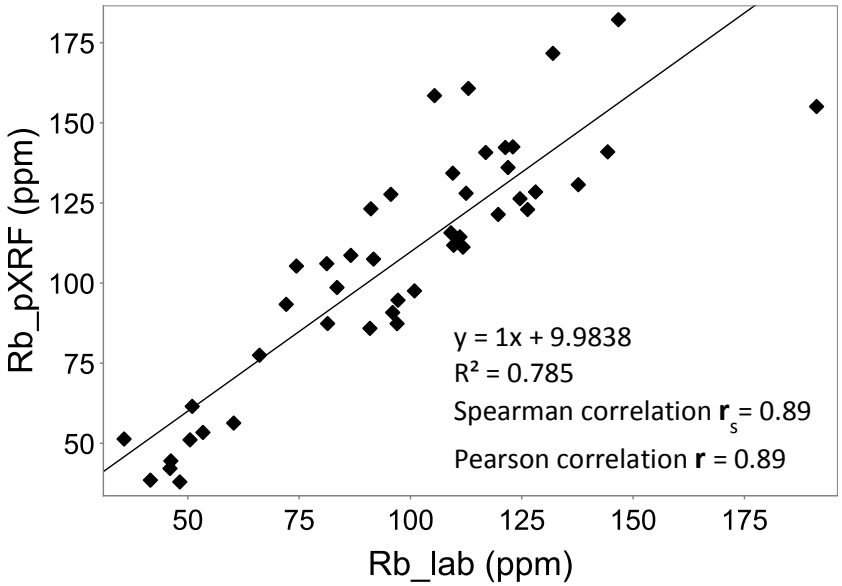

Fig. 5.5. Correlation plot of Rubidium.

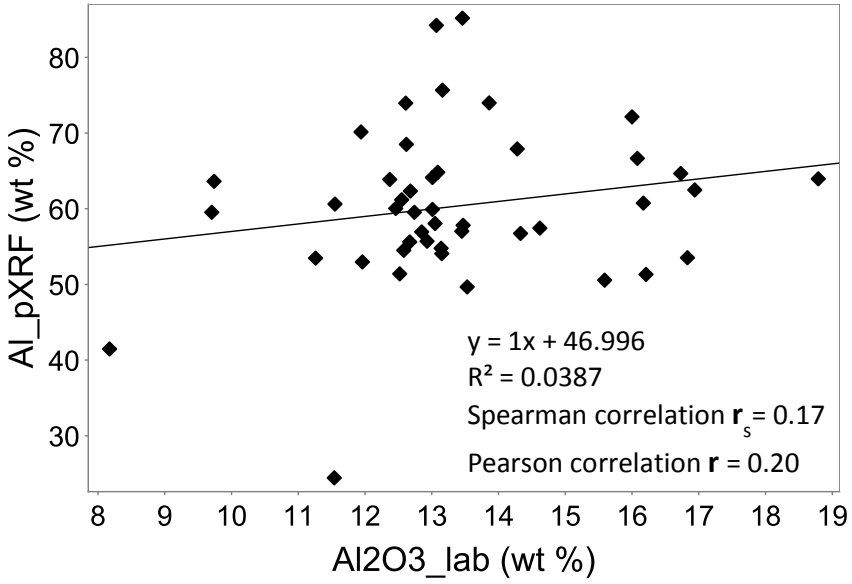

Fig. 5.6. Correlation plot of Aluminium.

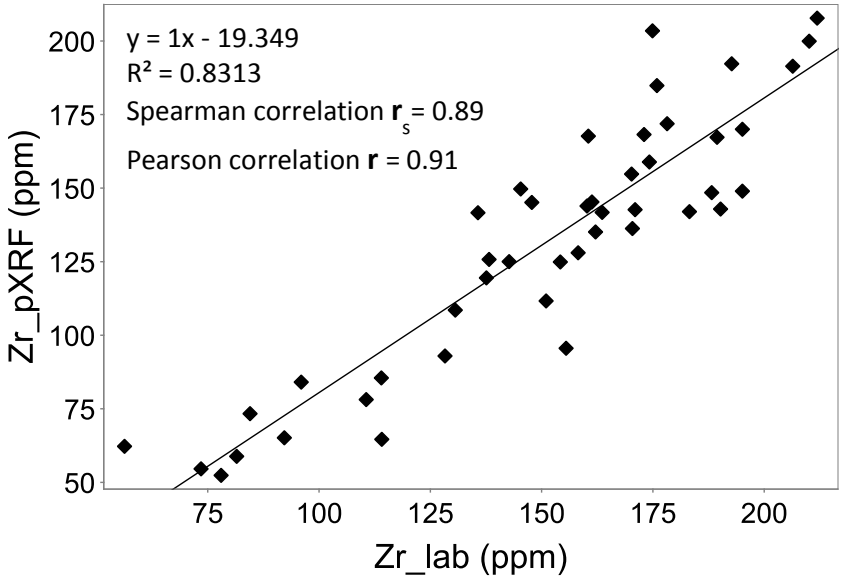

Fig. 5.7. Correlation plot of Zirconium.

Table 5.2. Lab based XRF and portable XRF correlation matrix (Spearman rank correlation coefficient) of 13 selected elements.

SPEARMAN	As-pXRF	As-lab	Al-pXRF	Al2O3-lab	Ba-pXRF	Ba-lab	Ca-pXRF	CaO-lab	Fe-pXRF	Fe2O3-lab	K-pXRF	K2O-lab	Nb-pXRF	Nb-lab	Pb-pXRF	Pb-lab	Rb-pXRF	Rb-lab	Si-pXRF	SiO2-lab	Sr-pXRF	Sr-lab	Y-pXRF	Y-lab	Zr-pXRF	Zr-lab
As-pXRF	1	0.86	-0.096	0.067	-0.39	-0.33	0.35	0.23	0.16	0.19	-0.39	-0.37	-0.11	-0.14	0.37	0.19	-0.027	-0.33	0.041	-0.35	0.22	0.11	0.14	0.064	0.072	0.024
As-lab	0.86	1	-0.26	-0.21	0.12	0.14	-0.21	-0.28	-0.14	-0.19	0.077	0.12	0.21	0.24	0.27	0.43	0.23	0.17	0.16	0.15	-0.23	-0.29	0.2	0.31	0.17	0.24
Al-pXRF	-0.096	-0.26	1	0.17	-0.098	-0.037	-0.026	0.014	0.036	-0.0053	0.15	-0.17	-0.03	-0.032	-0.065	-0.25	0.081	-0.094	0.26	-0.011	0.17	0.042	0.17	0.12	0.34	0.2
Al2O3-lab	0.067	-0.21	0.17	1	-0.45	-0.39	0.37	0.6	0.66	0.51	-0.36	-0.29	-0.38	-0.35	0.15	-0.093	-0.33	-0.33	-0.51	-0.65	0.36	0.56	-0.32	-0.29	-0.31	-0.3
Ba-pXRF	-0.39	0.12	-0.098	-0.45	1	0.93	-0.57	-0.57	-0.71	-0.68	0.74	0.75	0.61	0.7	-0.12	0.29	0.67	0.71	0.34	0.53	-0.55	-0.51	0.54	0.59	0.51	0.6
Ba-lab	-0.33	0.14	-0.037	-0.39	0.93	1	-0.52	-0.53	-0.52	-0.58	0.76	0.79	0.61	0.72	-0.047	0.36	0.7	0.73	0.38	0.44	-0.49	-0.5	0.6	0.65	0.59	0.66
Ca-pXRF	0.35	-0.21	-0.026	0.37	-0.57	-0.52	1	0.83	0.46	0.67	-0.5	-0.49	-0.41	-0.55	0.26	-0.039	-0.37	-0.45	-0.47	-0.69	0.61	0.63	-0.22	-0.32	-0.35	-0.44
CaO-lab	0.23	-0.28	0.014	0.6	-0.57	-0.53	0.83	1	0.54	0.63	-0.49	-0.51	-0.53	-0.62	0.075	-0.08	-0.46	-0.5	-0.51	-0.79	0.6	0.71	-0.37	-0.41	-0.48	-0.56
Fe-pXRF	0.16	-0.14	0.036	0.66	-0.71	-0.52	0.46	0.54	1	0.71	-0.57	-0.49	-0.41	-0.41	0.25	-0.03	-0.63	-0.61	-0.44	-0.65	0.47	0.55	-0.27	-0.28	-0.33	-0.33
Fe2O3-lab	0.19	-0.19	-0.0053	0.51	-0.68	-0.58	0.67	0.63	0.71	1	-0.6	-0.61	-0.61	-0.64	0.2	-0.027	-0.63	-0.65	-0.5	-0.73	0.54	0.66	-0.34	-0.39	-0.47	-0.5
K-pXRF	-0.39	0.077	0.15	-0.36	0.74	0.76	-0.5	-0.49	-0.57	-0.6	1	0.81	0.62	0.53	-0.052	0.25	0.82	0.73	0.66	0.52	-0.61	-0.66	0.54	0.49	0.57	0.48
K2O-lab	-0.37	0.12	-0.17	-0.29	0.75	0.79	-0.49	-0.51	-0.49	-0.61	0.81	1	0.64	0.63	-0.15	0.28	0.79	0.9	0.34	0.46	-0.73	-0.68	0.43	0.49	0.45	0.51
Nb-pXRF	-0.11	0.21	-0.03	-0.38	0.61	0.61	-0.41	-0.53	-0.41	-0.61	0.62	0.64	1	0.84	0.076	0.36	0.62	0.53	0.46	0.55	-0.53	-0.62	0.78	0.68	0.76	0.72
Nb-lab	-0.14	0.24	-0.032	-0.35	0.7	0.72	-0.55	-0.62	-0.41	-0.64	0.53	0.63	0.84	1	-0.042	0.36	0.54	0.56	0.31	0.5	-0.56	-0.58	0.75	0.82	0.74	0.86
Pb-pXRF	0.37	0.27	-0.065	0.15	-0.12	-0.047	0.26	0.075	0.25	0.2	-0.052	-0.15	0.076	-0.042	1	0.68	0.023	-0.21	0.043	-0.28	0.15	0.12	0.33	0.19	0.16	0.02
Pb-lab	0.19	0.43	-0.25	-0.093	0.29	0.36	-0.039	-0.08	-0.03	-0.027	0.25	0.28	0.36	0.36	0.68	1	0.28	0.21	0.062	-0.022	-0.22	-0.15	0.45	0.48	0.29	0.34
Rb-pXRF	-0.027	0.23	0.081	-0.33	0.67	0.7	-0.37	-0.46	-0.63	-0.63	0.82	0.79	0.62	0.54	0.023	0.28	1	0.89	0.5	0.45	-0.47	-0.58	0.49	0.49	0.58	0.52
Rb-lab	-0.33	0.17	-0.094	-0.33	0.71	0.73	-0.45	-0.5	-0.61	-0.65	0.73	0.9	0.53	0.56	-0.21	0.21	0.89	1	0.27	0.48	-0.59	-0.6	0.3	0.41	0.36	0.46
Si-pXRF	0.041	0.16	0.26	-0.51	0.34	0.38	-0.47	-0.51	-0.44	-0.5	0.66	0.34	0.46	0.31	0.043	0.062	0.5	0.27	1	0.61	-0.34	-0.62	0.47	0.3	0.56	0.33
SiO2-lab	-0.35	0.15	-0.011	-0.65	0.53	0.44	-0.69	-0.79	-0.65	-0.73	0.52	0.46	0.55	0.5	-0.28	-0.022	0.45	0.48	0.61	1	-0.61	-0.79	0.27	0.23	0.39	0.36
Sr-pXRF	0.22	-0.23	0.17	0.36	-0.55	-0.49	0.61	0.6	0.47	0.54	-0.61	-0.73	-0.53	-0.56	0.15	-0.22	-0.47	-0.59	-0.34	-0.61	1	0.87	-0.32	-0.42	-0.34	-0.41
Sr-lab	0.11	-0.29	0.042	0.56	-0.51	-0.5	0.63	0.71	0.55	0.66	-0.66	-0.68	-0.62	-0.58	0.12	-0.15	-0.58	-0.6	-0.62	-0.79	0.87	1	-0.41	-0.46	-0.49	-0.46
Y-pXRF	0.14	0.2	0.17	-0.32	0.54	0.6	-0.22	-0.37	-0.27	-0.34	0.54	0.43	0.78	0.75	0.33	0.45	0.49	0.3	0.47	0.27	-0.32	-0.41	1	0.89	0.83	0.8
Y-lab	0.064	0.31	0.12	-0.29	0.59	0.65	-0.32	-0.41	-0.28	-0.39	0.49	0.49	0.68	0.82	0.19	0.48	0.49	0.41	0.3	0.23	-0.42	-0.46	0.89	1	0.79	0.88
Zr-pXRF	0.072	0.17	0.34	-0.31	0.51	0.59	-0.35	-0.48	-0.33	-0.47	0.57	0.45	0.76	0.74	0.16	0.29	0.58	0.36	0.56	0.39	-0.34	-0.49	0.83	0.79	1	0.89
Zr-lab	0.024	0.24	0.2	-0.3	0.6	0.66	-0.44	-0.56	-0.33	-0.5	0.48	0.51	0.72	0.86	0.02	0.34	0.52	0.46	0.33	0.36	-0.41	-0.46	0.8	0.88	0.89	1

5.3.3 Correcting pXRF

pXRF is a relatively new field technique not generally applied to geothermal research or description of lithologies or hydrothermal alteration, and is a rapid version of the more traditional laboratory x-ray fluorescence. Due to the absence of suitable standards for pXRF, 45 laboratory XRF samples were used as calibration and validation for the pXRF data utilising a selection of samples from across the geothermal wells. pXRF data was plotted against laboratory XRF in scatter plots to ascertain a linear relationship between the concentration of elements measured by pXRF and those measured by traditional XRF by a simple regression analysis. Simple linear regression fits a straight line (termed the line of best-fit) through a set of points (n) in order to minimise the sum of squared residuals of the linear regression model (also known as the least squares estimator). The sum of squared residuals is the vertical distance between the data points and the fitted line.

The equation for a regression line is $y = \beta x + \alpha$ where y is the predicted score, β is the slope of the line, and α is the y-intercept (or alternatively $y = mx + c$). IoGAS-64 advanced geochem exploratory data analysis software was used to perform the simple regression, and data was then re-plotted in Microsoft Excel to display both original and corrected data on one scatter plot. The pXRF raw concentrations were divided by the slope of the line β to get the corrected pXRF corrections (Figs. 5.8-5.11, Table 5.3). For example for Rb (Fig. 5.8), Rb_pXRF and Rb_lab were plotted against one another and the equation for the original regression line is $y = 1.2231x + 12.211$. All raw pXRF concentrations were then multiplied by the slope or correction factor (1.2231) and re-plotted against the Rb_lab again to give a new corrected regression line and R^2 coefficient of determination value (measures how close the data is to the fitted line).

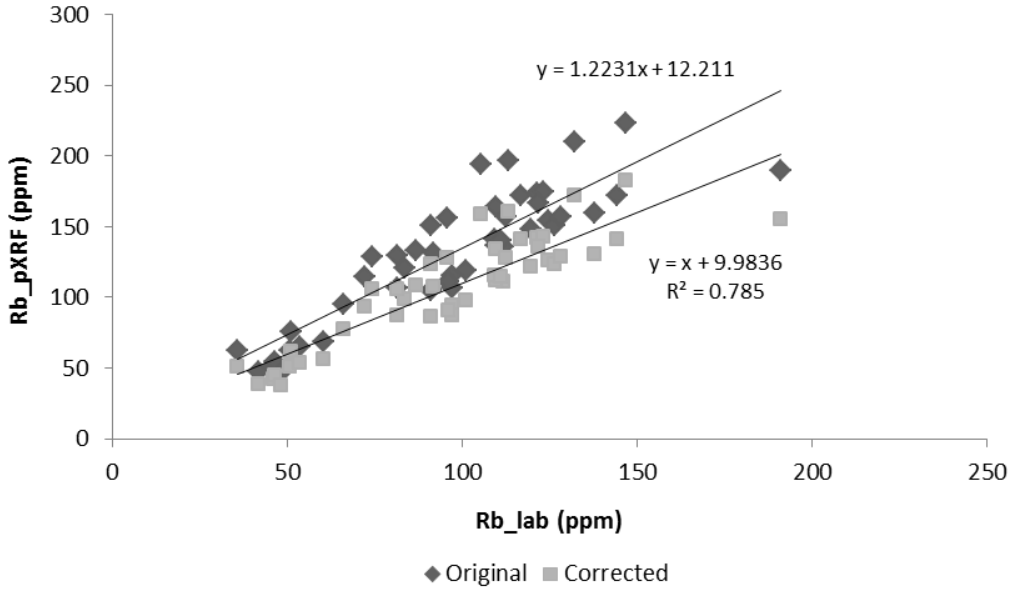

Fig. 5.8. Rubidium, pXRF original data and corrected data against lab XRF.

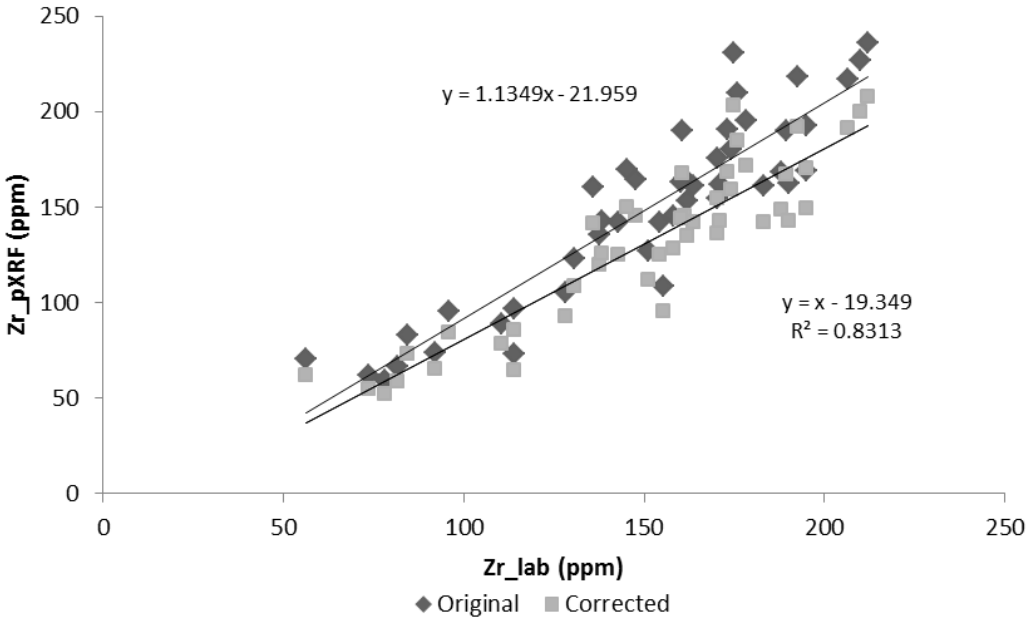

Fig. 5.9. Zirconium, pXRF original data and corrected data against lab XRF.

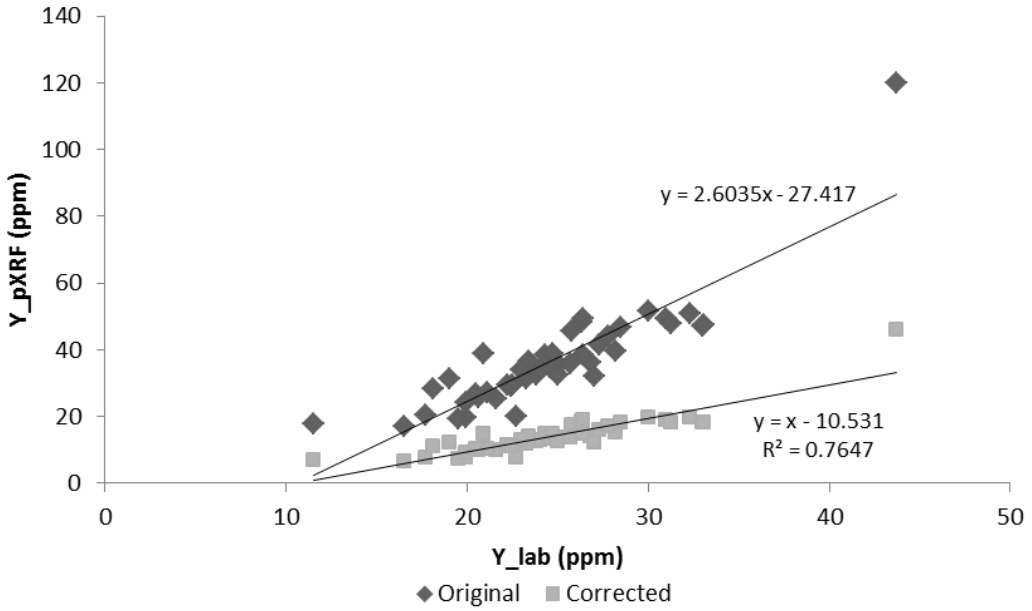

Fig. 5.10. Yttrium, pXRF original data and corrected data against lab XRF.

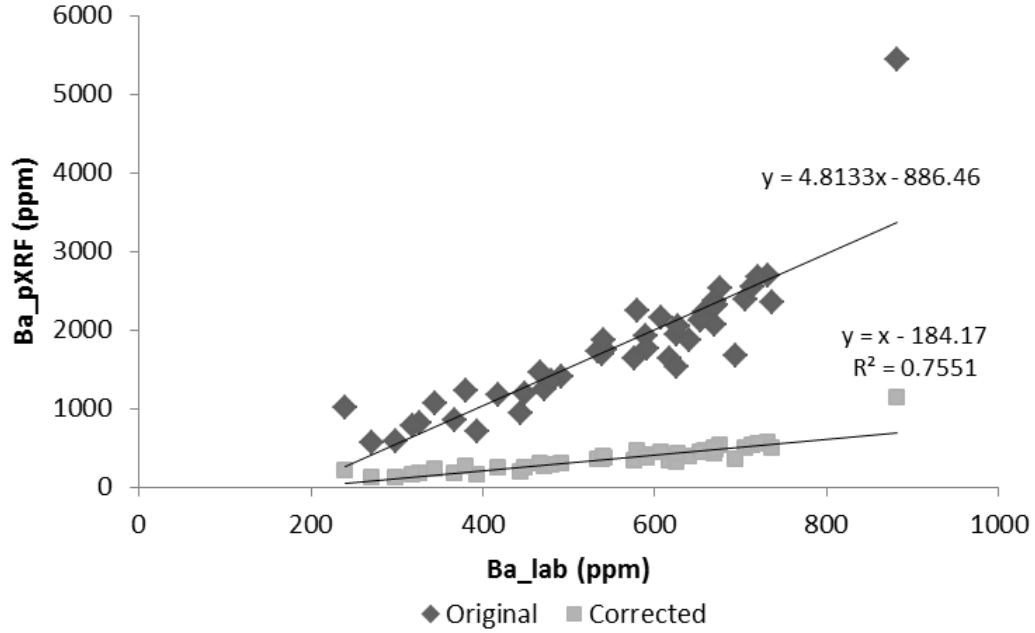

Fig. 5.11. Barium, pXRF original data and corrected data against lab XRF.

Table 5.3. Correction factors for each element detected via pXRF and lab XRF.

Element	Correction Factor						
Al	996.511	wt%	0.09965	Rb	1.223		
As	0.775			S	0.712		
Ba	4.813			Sb	-0.015		
Ca	9091.574	wt%	0.90916	Si	6852.029	wt%	0.68520
Cr	-2.412			Sn	-0.926		
Cu	0.472			Sr	1.045		
Fe	10536.604	wt%	1.05366	Ta	7.721		
K	9635.617	wt%	0.96356	Th	0.768		
Mn	11238.071	wt%	1.12381	Ti	109868.804	wt%	10.98688
Mo	0.591			Y	2.604		
Nb	20.942			Zn	0.639		
Pb	0.739			Zr	1.135		

This type of linear correction using simple regression analysis was applied to each element detected via the two pXRF and lab XRF methods across the entire dataset subsequently each element has its own correction factor (Table 5.3). The corrected pXRF data and plots of the original and corrected slopes can be found in Appendix E (on CD). The elements Ba, Cr, Nb, Ta, Y and Ti have a larger correction factor compared to the other elements. Fe, Mn, Rb, Sr and Zr have correction factors at ~1.0. The elements Al, As, Ca, Cu, K, Mo, Pb, S, Sb, Si, Sn, Th and Zn did not require much of a correction as they have correction factors < 1.0. The data is now considered reliable however when correcting and applying correction factors apparent outliers can be removed, or diminished. It is important to note that since we are comparing between fairly similar rock types with similar bulk compositions, even if pXRF results are not calibrated against lab XRF results, relative changes in elemental concentrations measured by the pXRF method are likely to be very robust. However, if you wish to compare pXRF results against results obtained by other methods (e.g. ICPMS), then XRF results must be calibrated against certified reference materials.

In this research, laboratory XRF was performed on crushed powder, whereas pXRF is directly on to rock chips with no sample preparation other than standard cleaning. Discrepancies between the concentrations measured by the two techniques may be explained by the material type analysed as chips will be more heterogeneous compared to the pulverised samples (Morris, 2009).

Sample heterogeneity is always a possibility in geochemical analyses (Gazley & Fisher, 2014). The size of the analysis window in a pXRF analyzer is 10 mm, so a sample analysed of that size cannot be assumed to representative of the surrounding rock. The same applies to rock cuttings used in this thesis. There are high concentrations of an element in single-phase minerals (e.g. As in arsenopyrite) so for best results, homogenisation to a powder is ideal. The cuttings averaged 1 mm in size (fine) in most samples therefore for pXRF it was deemed unnecessary to grind them. However, it is important to note that a large grain (e.g. 2-3 mm) of a mineral such as arsenopyrite would give an artifically elevated concentration of As for that interval compared to the true As concentration.

The "nugget effect" (Clarke, 2010) describes random errors from sampling procedures as well as variability in the sample or lithological unit itself. The term originates from the differences incurred when a gold sample has a nugget in it but the adjacent one does not so the analysis of samples may not represent the composition of the bulk material due to uneven distribution. It is important to consider what the data is being used for, that is, 'fit for purpose'. For example is the data being used for ore exploration where assay concentrations require accurate values for commercial purposes, or are relative trends required to characterise geological units or hydrothermal alteration in geothermal fields such is the case in this research.

5.4 TRADITIONAL XRF LITHOGEOCHEMISTRY

Rocks are classified based on their chemical composition with most classification schemes utilising major element data derived from XRF analysis. Elements typically used and listed as oxides in a chemical analysis are; Si, Ti, Al, Fe, Mn, Mg, Ca, Na, K, and P. Bowen (1928) first attempted to classify a magma series by suggesting silica enrichment indicated the evolution of the magma, whereas Fenner (1931) believed it was Fe enrichment. Most volcanic rocks are extremely abundant in the element oxide SiO_2, which is controlled by how much differentiation occurs in the magma chamber (resulting in magmas with varying silica concentrations) making it extremely useful diagnostically. However, in geothermal areas Si is commonly

changed in the original rock through processes of hydrothermal alteration, so it cannot be reliably used to differentiate rock types or magmatic processes.

The total alkalis versus silica diagram ($Na_2O + K_2O$ vs SiO_2) or TAS diagram by Le Maitre et al. (1989) (Rollinson, 1993) is a general igneous rock classification diagram that has been widely used to classify volcanic rock types. The silica content on the x-axis reflects the magma evolution from primitive to more evolved, so the TAS diagram is divided into ultrabasic, basic, intermediate and acidic volcanic arc rocks. The y-axis (Na_2O+K_2O) distinguishes alkaline from subalkaline types based on the concentrations of Na_2O and K_2O. Irvine and Baragar (1971) applied a curve to the TAS diagram to separate the rocks into two magma series either alkaline or sub-alkaline magma series even though most volcanic arc lavas classify in sub-alkaline. Further subdivision is achieved using the K_2O vs SiO_2 diagram developed by Peccerillo & Taylor (1976) and Rickwood (1989). Both a volcanic series and a rock type are able to be assigned using this diagram. The volcanic series is based on K_2O concentrations and enabling separation into shoshonitic, high-K calc-alkaline, calc-alkaline and tholeiitic series; it also indicates the degree of enrichment of large ion lithophile elements (LILE). Rock types are split into basalt, basaltic andesite, andesite, dacite and rhyolite by silica content and therefore degree of differentiation.

However, the TAS diagram (Le Maitre et al., 1989) or the K_2O vs SiO_2 diagram by Peccerillo and Taylor (1976) are not suitable for altered, weathered or metamorphosed volcanic rocks due to the mobilisation of alkalis and is intended for fresh volcanic rocks only. Therefore modified volcanic rock diagrams (Winchester & Floyd, 1977; Pearce, 1996) have been developed that use proxies based on trace element data, particularly the immobile elements Nb, Y, Zr, Ti. As differentiation in magma progresses, trace element concentrations change predictably (Winchester & Floyd, 1977). The regular variation of these immobile element ratios and their abundance in various rock groups replicate the magma evolution shown by the standard major element indices. The trace elements chosen must be robust against alteration, easily measured, and in concentrations great enough to be able to distinguish between magma types and rocks derived from the same magma (but subsequently evolved).

Floyd and Winchester (Floyd & Winchester, 1975, 1978; Winchester & Floyd, 1976, 1977) identified rock type using their Zr/TiO_2 vs Nb/Y diagram approach which Pearce (1996) then updated with boundaries using statistical parameters based on a considerably larger dataset (Hastie et al., 2007). Because of the ever present effect of alteration and weathering of volcanic rocks, immobile elements serve as substitutes where the Nb/Y ratio functions as a proxy for alkalinity (Na_2O+K_2O) and Zr/TiO_2 acts as a proxy for silica, making it a useful replacement to the TAS classification diagram. Pearce and Cann (1973) first noted that alkalinity in basalts was indicated by the Nb/Y ratio. The higher the Nb/Y ratio (represented by sub-alkalic to alkalic compositions on the diagram) is reflected in the higher Nb content found in alkaline suites whilst the basic to acid composition changes as Zr/TiO_2 increases.

In addition, there is no equivalent for the K_2O vs SiO_2 diagram by Perrecillo and Taylor (1976) except for the Th-Co diagram developed by Hastie et al. (2007). Th and Co behave similarly to K and Si, during subduction zone processes and stay immobile during weathering. Th replicates the characteristics of K_2O such as its incompatibility, enrichment over subduction zones, assimilation and fractional crystallization. The only element to be slightly compatible in copying the change from basic to acid compositions displayed by SiO_2 is Co which decreases instead of increasing during fractional crystallisation. Therefore Co is gradually removed from volcanic island arc rocks during this process, reflecting the evolution of basalt to rhyolite. According to Hastie et al. (2007) the diagram works well with rocks that have been subjected to hydrothermal alteration, metamorphism or intense weathering in tropical regions. Rock classification and volcanic series was attempted using the Th-Co diagram however it plotted the samples as andesite, basaltic andesite or basalts of the high-K/shoshonitic series which is not consistent with the following rock classification diagrams in the next section below.

5.4.1 Rock classification using trace elements

The rock classification diagrams used in this thesis rely on the 45 samples analysed by XRF for two reasons. Firstly, sodium is too light to be analysed by pXRF and cannot be used anyway as the alkalis Na_2O and K_2O are highly mobile during

alteration. Secondly, the bulk of pXRF samples have concentrations of Ti which are below the pXRF detection limit. Consequently the Ti concentrations analysed by XRF were used instead to ensure accurate Ti calibration.

Ratios of immobile elements unlikely to change during alteration are ratios of high field strength (HFS) elements (e.g. Zr/Ti, Nb/Y), which are a key component used to classify metamorphosed and altered volcanic rocks. These classification diagrams recognise the original rock type, magma series and tectonic setting of a sample or suite of samples despite extensive alteration (Winchester & Floyd, 1977). Hence the most reliable rock classification diagrams are the ones by and Pearce (1996, Fig. 5.12) and Winchester and Floyd (1977, Fig. 5.13).

Figure 5.12 shows that both the ignimbrites (Waiora and Oruanui) and rhyolite samples plus most of the Waiora Formation samples plot in the rhyolite/dacite section, whereas the andesite lava, lithic-crystal breccia, tuffaceous sandstone samples are in the andesite/andesite basaltic portion. The red point (TH10 1240 m) that is part of the Waiora Ignimbrite but clearly plots in the andesite/andesite basaltic area in both Figures 5.12 and 5.13 suggests that this sample is more andesitic in composition. Such compositional variation is supported by pXRF data that show an obvious break in element concentrations at a similar place (~1200 m) in the down hole trends of the elements Rb, Zr, Y, Sr, K, Ba (Fig. 5.20). Therefore the boundary of these formations requires refinement geochemically, as it cannot be determined by visual inspection alone, and that the TH10 1240 m sample likely belongs in the lithic-crystal breccia formation.

Figure 5.13 plots the samples very similarly to Pearce's 1996 version except the blue Tauhara Dacite, red ignimbrite and orange Waiora Fmn samples are now all included in the rhyodacite/dacite portion of the diagram in contrast to Pearce's (Fig. 5.12) where they plot in the upper andesite basaltic/andesite section bordering the rhyolite dacite area. The fact that it is so close to the rhyolite/dacite segment in Pearce's diagram implies that the way the boundaries have been constructed is the likely cause.

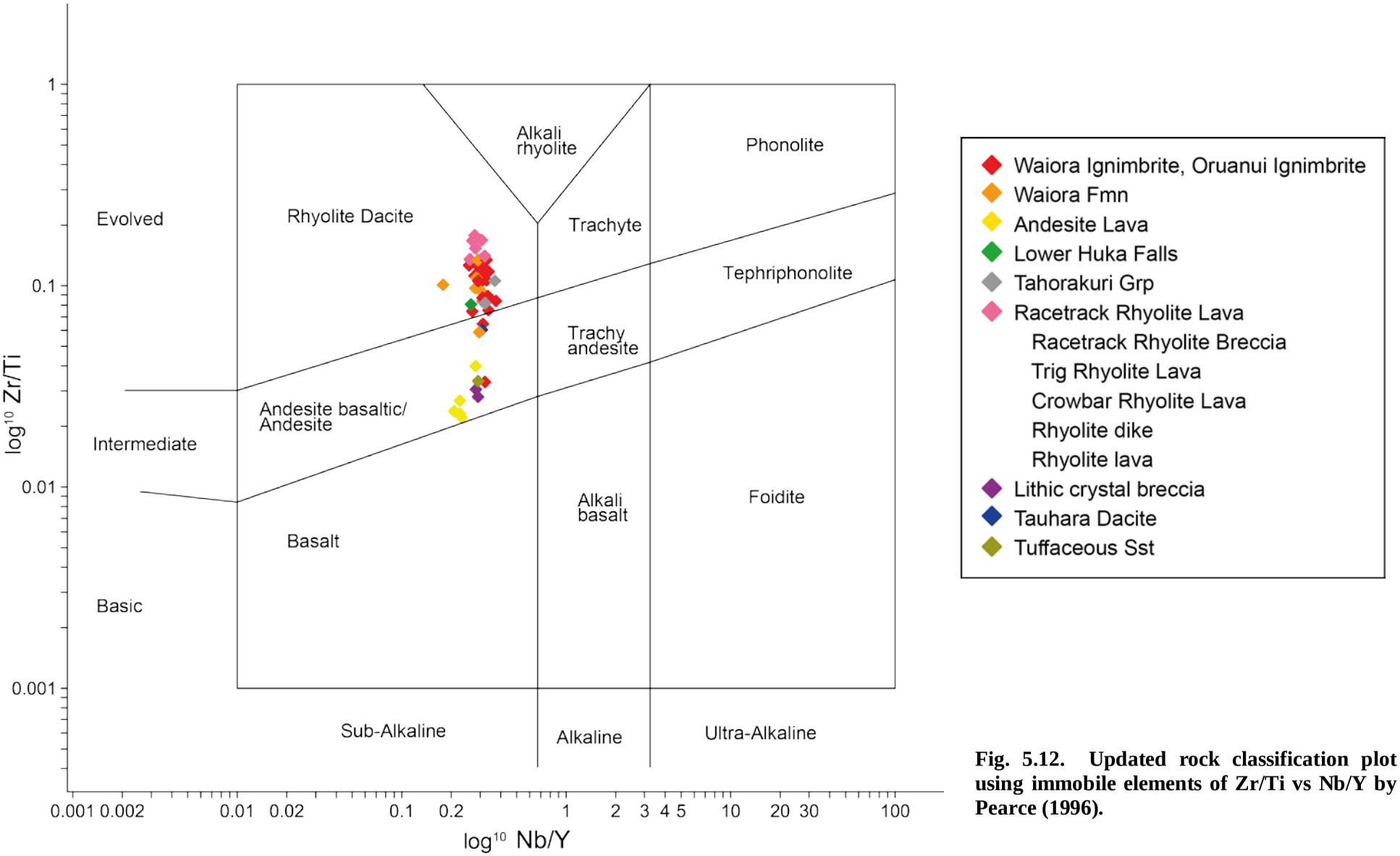

Fig. 5.12. Updated rock classification plot using immobile elements of Zr/Ti vs Nb/Y by Pearce (1996).

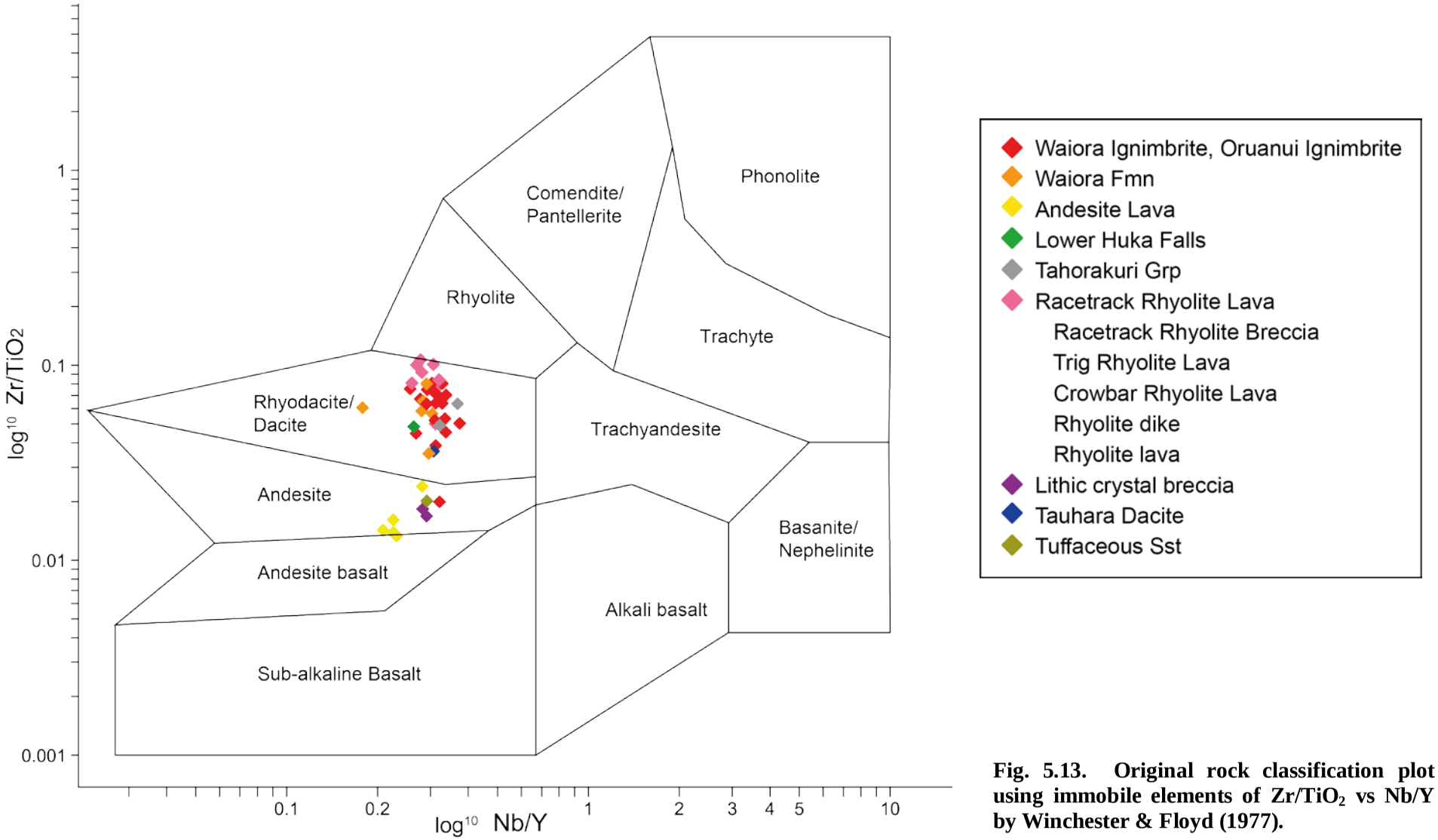

Fig. 5.13. Original rock classification plot using immobile elements of Zr/TiO_2 vs Nb/Y by Winchester & Floyd (1977).

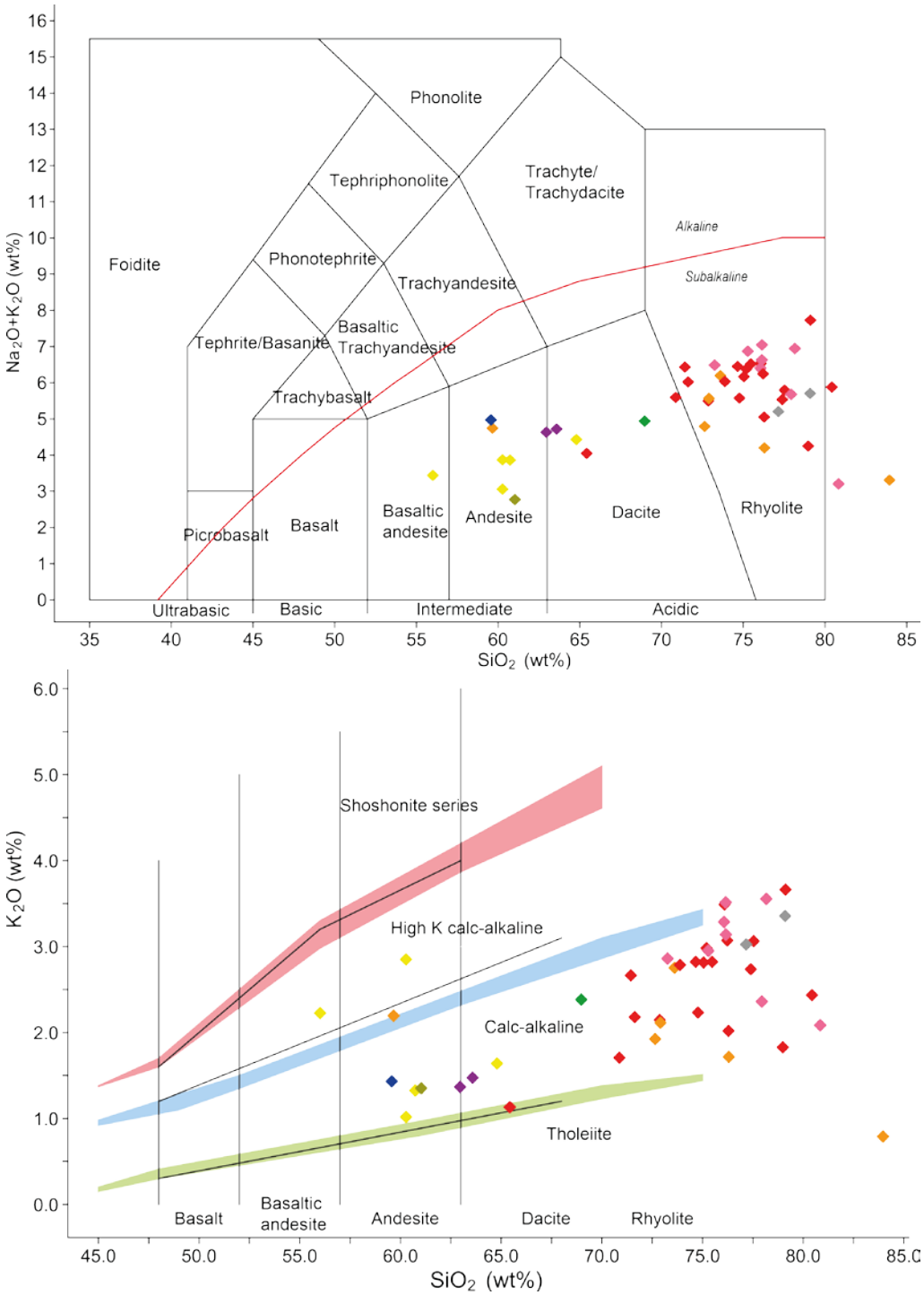

Fig. 5.14. *Above*: TAS diagram by Le Maitre et al. (1989), with alkaline-subalkaline curve (red line) over top by Irvine and Baragar (1971). *Below:* K_2O vs SiO_2 diagram by Peccerillo and Taylor (1976). Compared to the former diagrams where the samples are noticeably discriminated in clusters, in the major element based TAS diagram, samples are highly scattered. The large scatter of samples in this diagram suggests these samples, mainly the red ignimbrite, pink rhyolitic and orange Waiora Fmn samples, have been affected by hydrothermal alteration. The scatter is also reflected in Peccerillo and Taylor's K_2O vs SiO_2 diagram where the samples are also widely spread due to hydrothermal alteration although most of them still classify as sub alkaline calc-alkaline.

Discriminating between tectonic environments using trace elements

Rocks have certain geochemical signatures that signify the tectonic environments they originate from. Pearce and Cann (1971, 1973) first identified these signatures in the early 70's and were able to differentiate rocks from within plates, volcanic arcs and the ocean floor (Rollinson, 1993). Specific geochemistry can be used to distinguish individual tectonic environments, for example, basalt chemistry is best used to identify types of ocean ridge environments, granite geochemistry distinguishes types of collision zones, basalts and granites are able to characterise an intraplate setting and sedimentary rock chemistry is used to ascertain passive continental margins. Volcanic arc environments are the most versatile and can be recognised by all three discriminant analyses.

Nevertheless, discrimination diagrams should not be used explicitly but rather serve as having an association towards a particular tectonic environment. This recommendation is important because attempting to reconstruct the tectonic environment of Archean rocks using a discrimination diagram based on modern volcanic rocks will produce spurious results (Rollinson, 1993). Discrimination diagrams are also better used with a suite of samples, to highlight the multiple or mixed environments inherent in the suite. Furthermore, discrimination diagrams may provide information about the process operating in an environment or link process to the tectonic environment which is more useful.

The diagram that seems to correspond most successfully to the samples in this thesis is the La-Y-Nb diagram of Cabanis and Lecolle (1989) (Fig. 5.15). The La-Y-Nb diagram is a tool for distinguishing volcanic series and discovering crustal mixing or contamination. Its only drawbacks are that it has not been widely tested comparative to other trace element discrimination diagrams and Cabanis and Lecolle (1989) used a smaller number of samples in which to construct it compared to other authors. Metamorphosed or highly altered rocks may also be distorted at the La apex due to the potential mobility of La under hydrothermal conditions. Elemental concentrations are in ppm as La/10, Y/15, Nb/8 at the three apexes of the triangular diagram. The results in this diagram indicate that the

volcanic series the samples belong to is calc-alkaline, and the chemical data is consistent with the known tectonic setting of an arc to back arc.

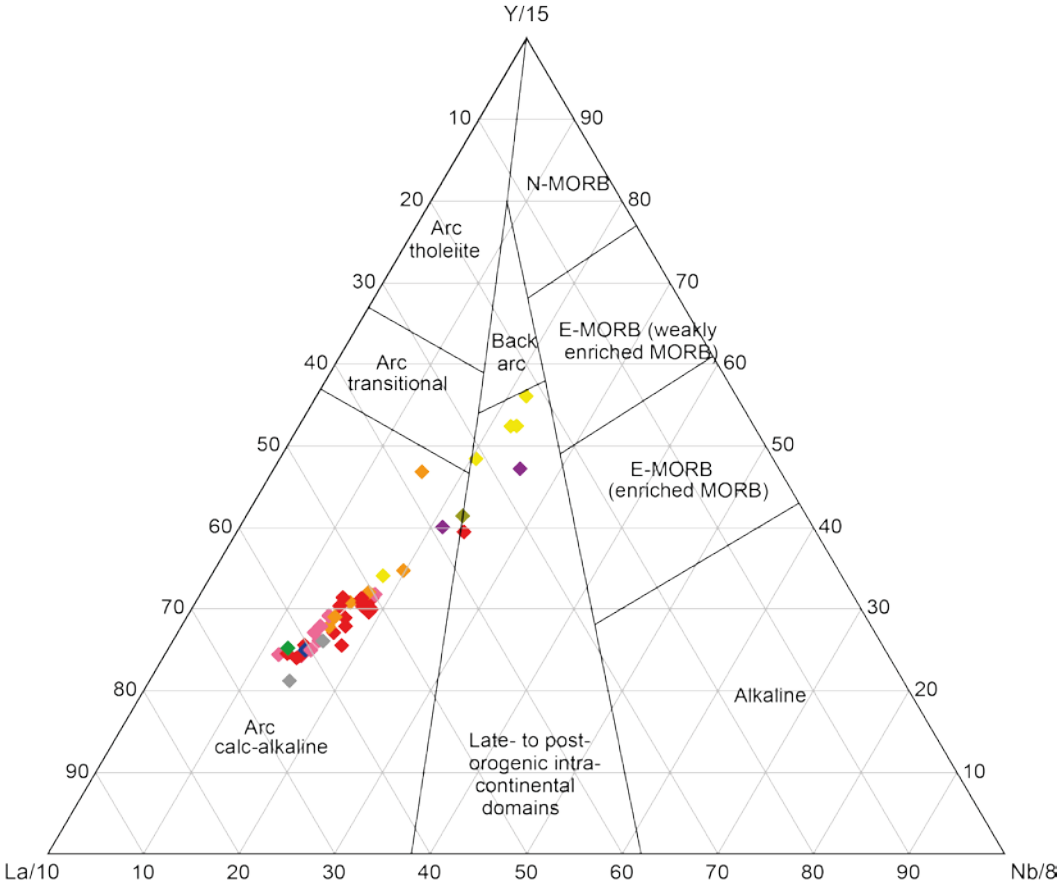

Fig. 5.15. The La-Y-Nb diagram of Cabanis and Lecolle (1989) that distinguishes volcanic series and tectonic setting.

5.4.2 Earlier geochemical data

The Tauhara geothermal field samples presented in the earlier rock classification diagrams are placed in the context of earlier geochemical data of other rocks in the TVZ. As Figures 5.16 and 5.17 illustrate, the rock units are clustered in two distinct areas, the andesite/andesite basaltic sector and the rhyolite/dacite segment. It is well known that the Taupo volcanic center (TVC) is largely rhyolitic and the Tongariro volcanic center (TgVC), predominantly andesitic (Wilson et al., 1995). The Pokai Ignimbrite, Matahina Ignimbrite, Kaharoa Ignimbrite, and Taupo rock units are placed in the rhyolite dacite area in which most of the Tauhara samples also plot. With the exception of the remaining Tauhara samples that plot in the andesite area and are probably the samples from the andesite lava formation. The Rotokawa and Tongariro rock units also lie in the andesite/andesite basaltic area.

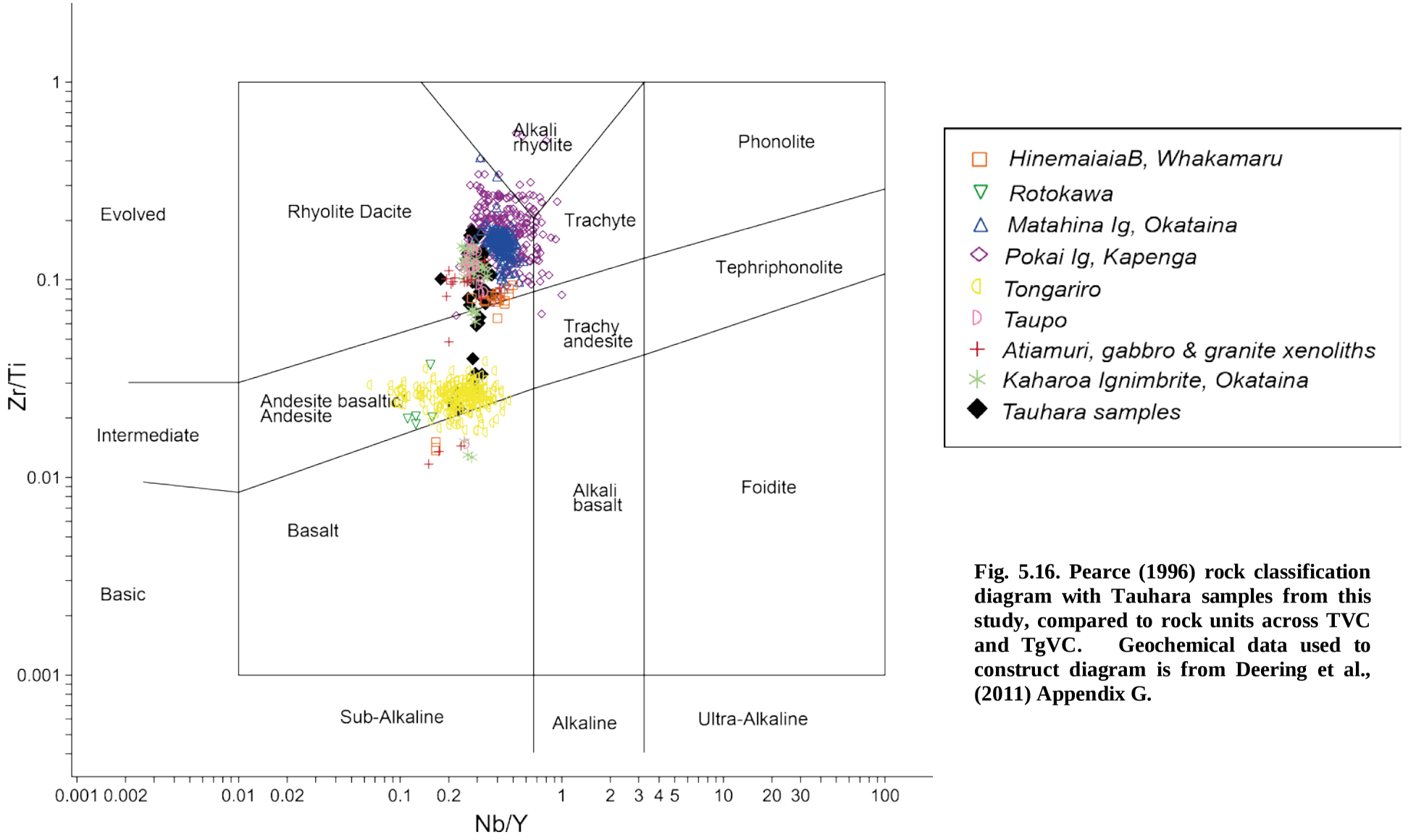

Fig. 5.16. Pearce (1996) rock classification diagram with Tauhara samples from this study, compared to rock units across TVC and TgVC. Geochemical data used to construct diagram is from Deering et al., (2011) Appendix G.

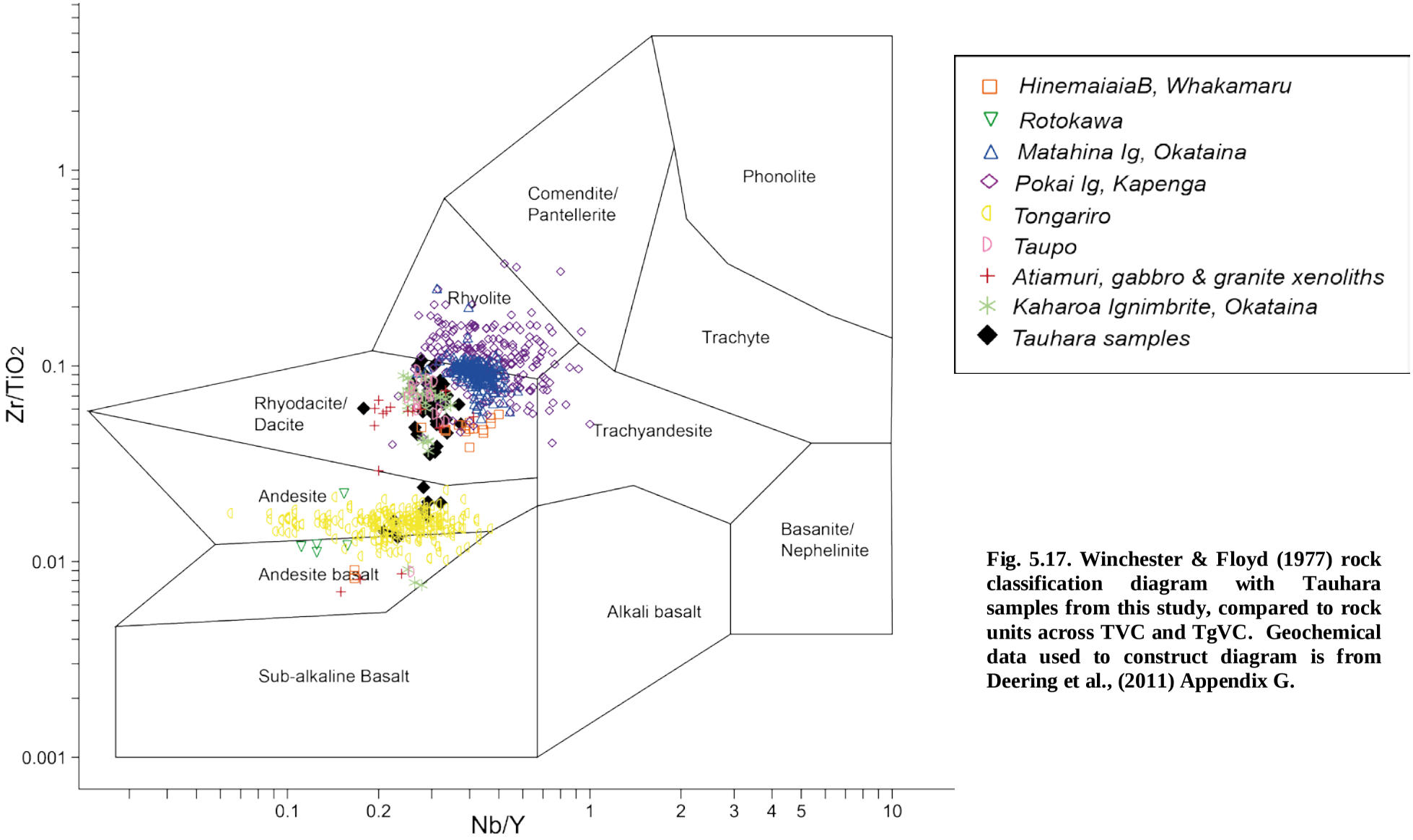

Fig. 5.17. Winchester & Floyd (1977) rock classification diagram with Tauhara samples from this study, compared to rock units across TVC and TgVC. Geochemical data used to construct diagram is from Deering et al., (2011) Appendix G.

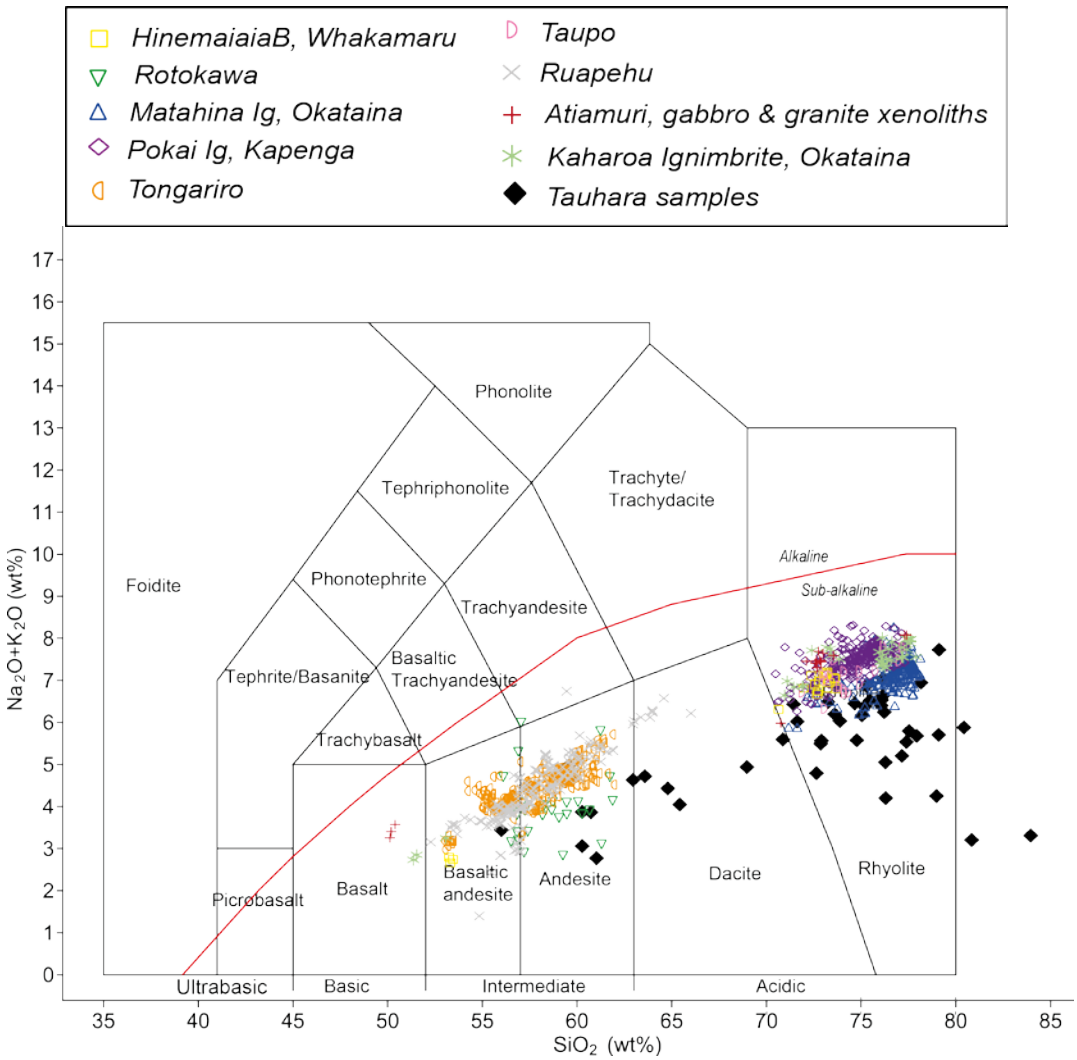

Fig. 5.18. TAS diagram by Le Maitre et al. (1989), with alkaline-subalkaline curve by Irvine and Baragar (1971) showing the Tauhara samples compared to other geochemical rock units of the TVC and TgVC from Deering et al. (2011).

In Figure 5.18 above the comparative rock units are in two distinct tight clusters, unlike the large spread shown by the altered samples from Tauhara. As mentioned previously this type of diagram is not suitable for altered rocks.

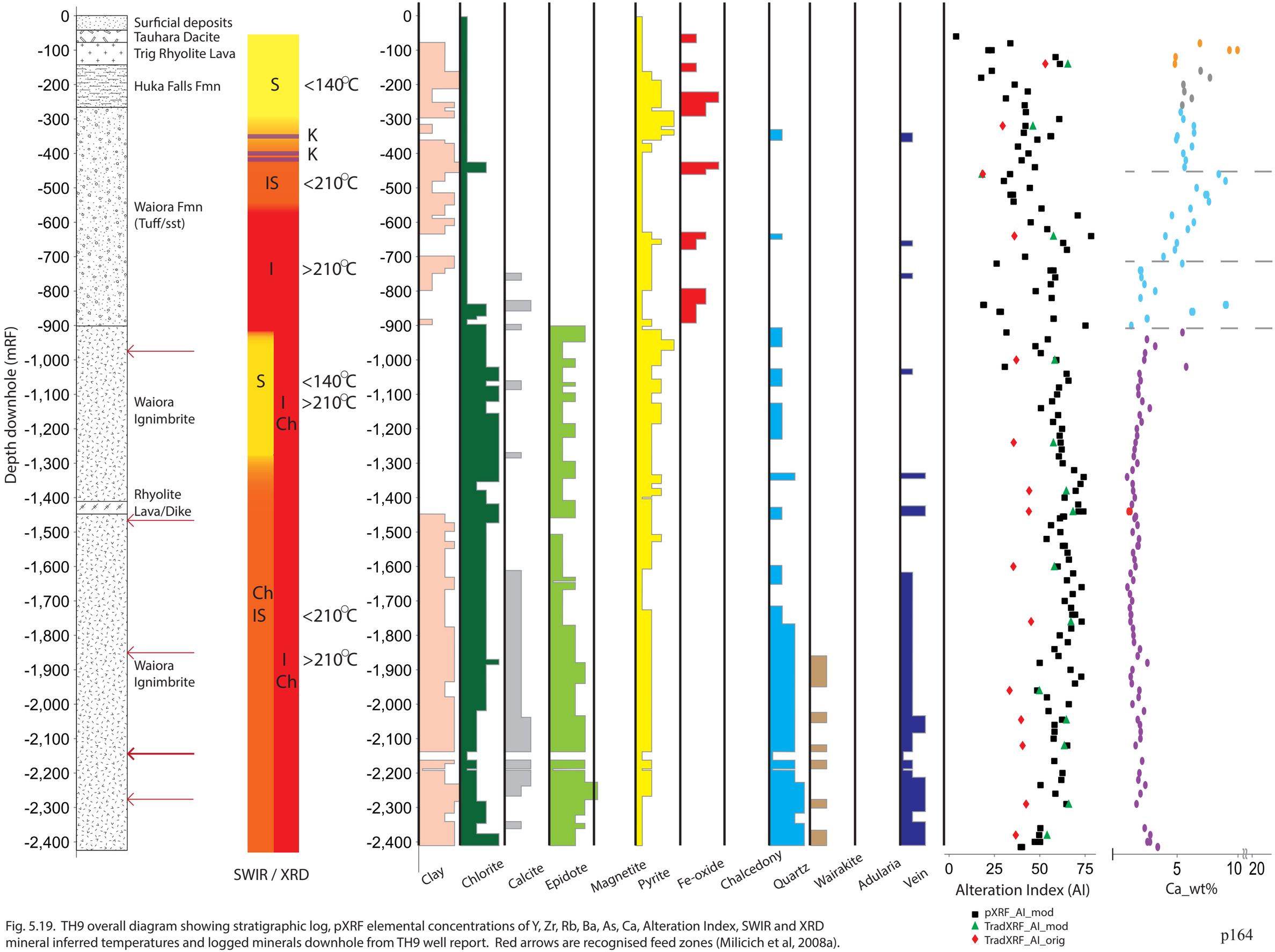

Fig. 5.19. TH9 overall diagram showing stratigraphic log, pXRF elemental concentrations of Y, Zr, Rb, Ba, As, Ca, Alteration Index, SWIR and XRD mineral inferred temperatures and logged minerals downhole from TH9 well report. Red arrows are recognised feed zones (Milicich et al, 2008a).

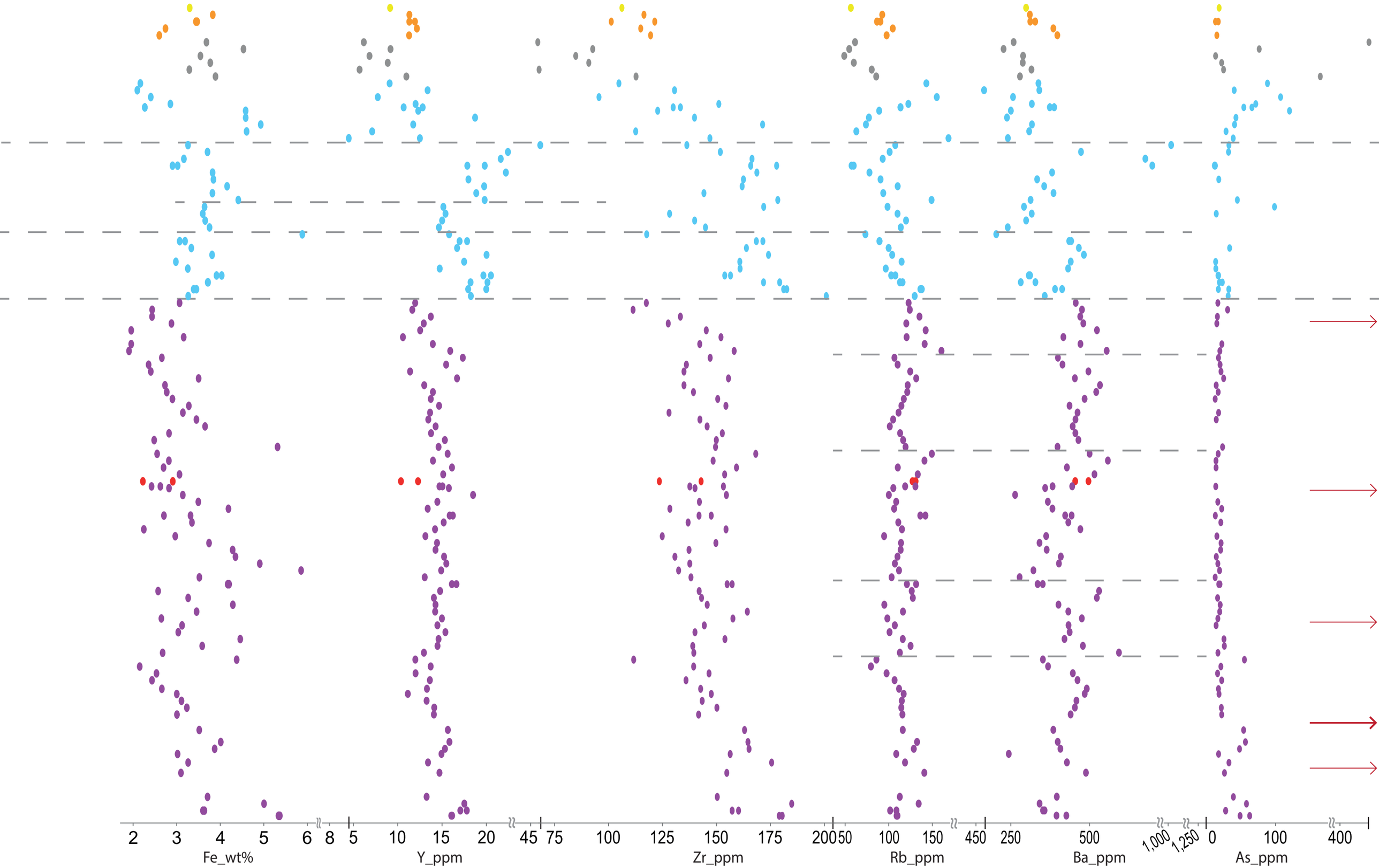
2
3
4
5
6
8
5
10
15
20
45
75
100
125
150
175
200
50
100
150
450
250
500
1,000
1,250
0
100
400
Fe_wt%
Y_ppm
Zr_ppm
Rb_ppm
Ba_ppm
As_ppm
Dacite lava (Tauhara Dacite)
Rhyolitic lava (Trig Rhyolite Lava)
Volcaniclastic sed (Huka Falls Fmn)
Tuffaceous rock (Waiora Wa3-4)
Waiora Ignimbrite (Waiora Ig Wa1)
Rhyolite dike (Hypabyssal intrusive)

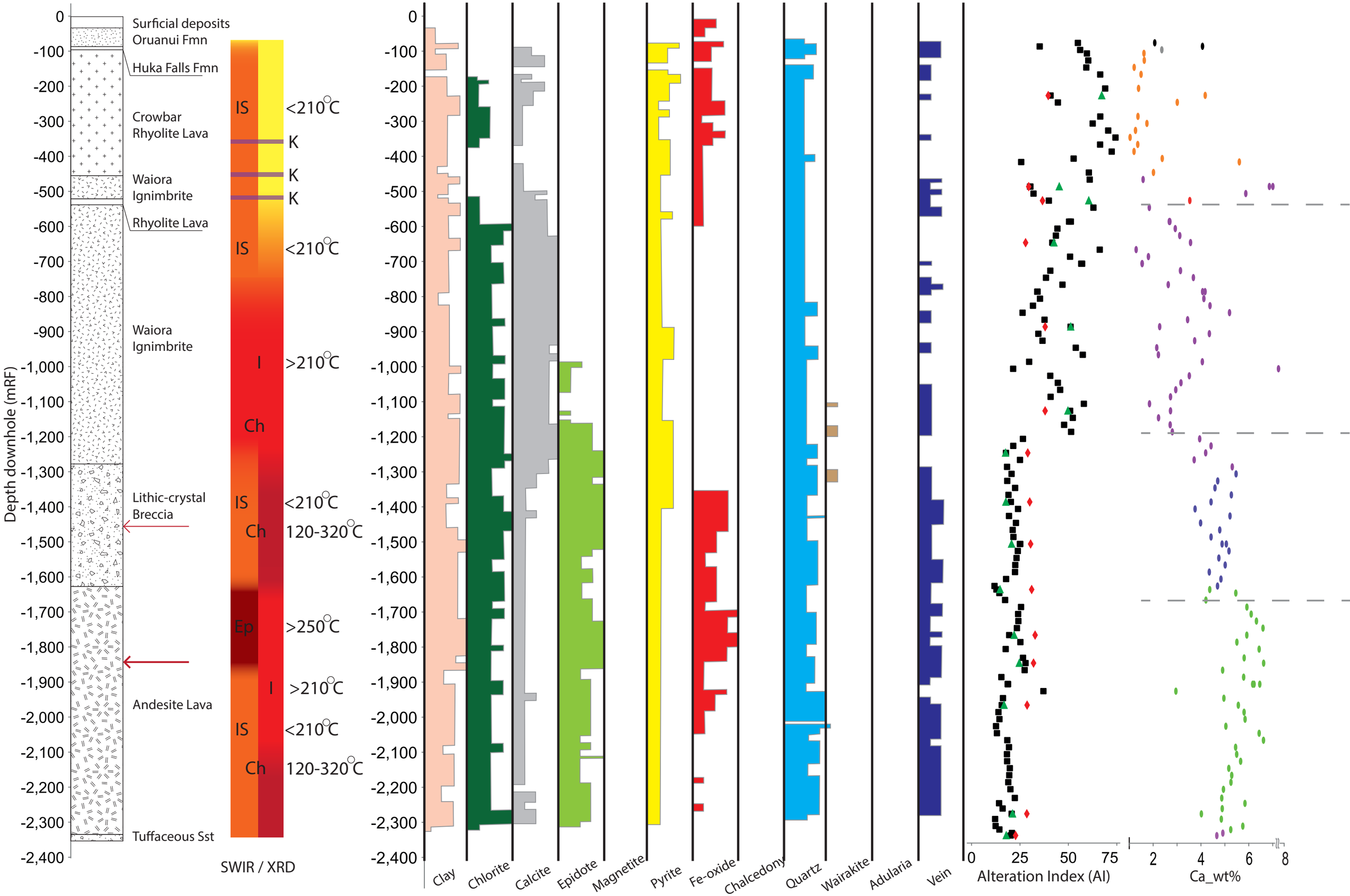

Fig. 5.20. TH10 overall diagram showing stratigraphic log, pXRF elemental concentrations of Rb, Zr, Y, Sr, K, Ba, Alteration Index, SWIR and XRD mineral inferred temperatures and logged minerals downhole from TH10 well report. Red arrows are recognised feed zones (Milicich et al, 2008b).

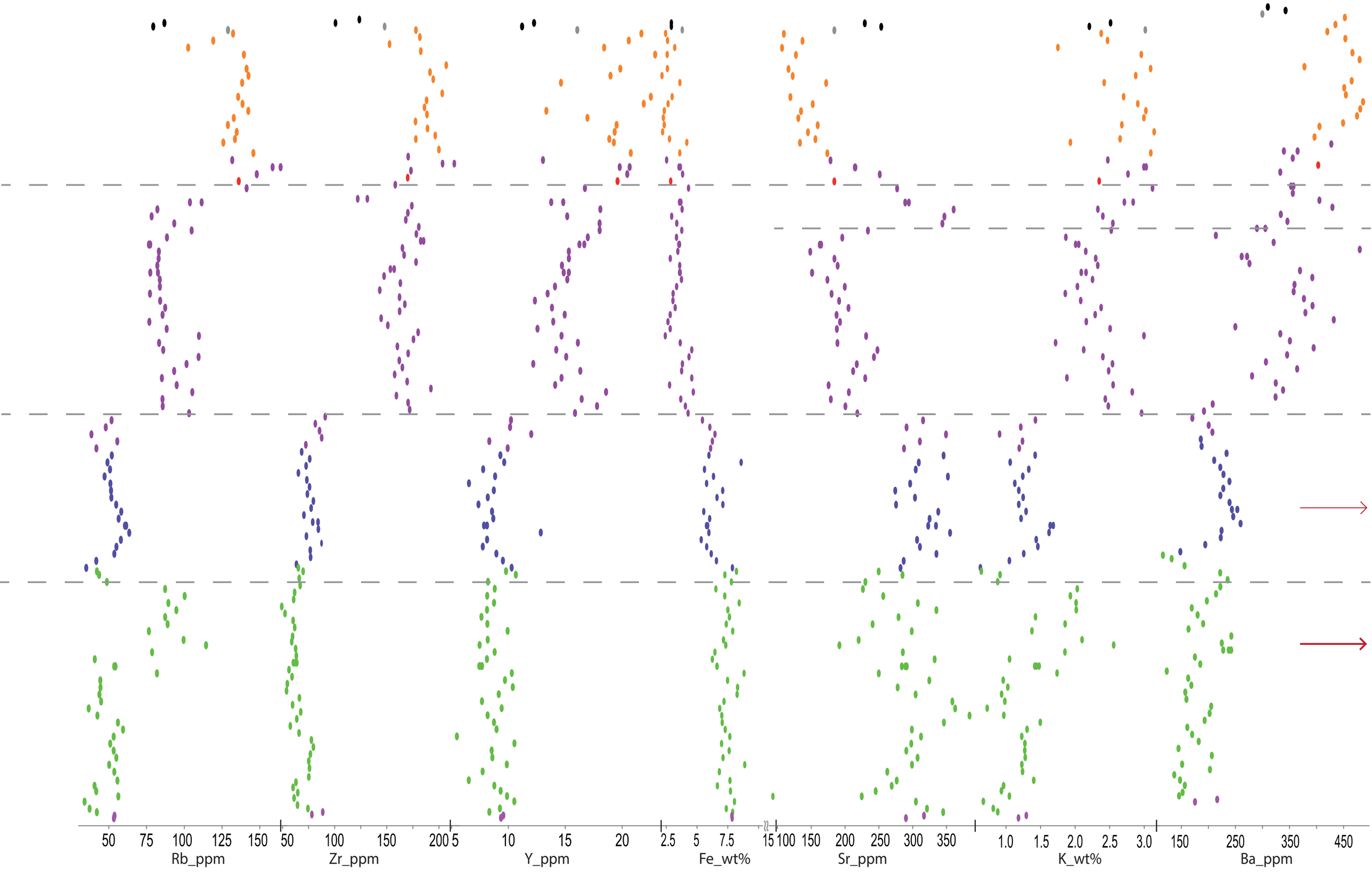
50
75
100
125
150
Rb_ppm
50
100
150
200
Zr_ppm
5
10
15
20
Y_ppm
2.5
5
7.5
15
Fe_wt%
100
150
200
250
300
350
Sr_ppm
1.0
1.5
2.0
2.5
3.0
K_wt%
150
250
350
450
Ba_ppm
Surficial deposits (Oruanui Fmn)
Volcaniclastic sed (Huka Falls Fmn)
Rhyolitic lava (Crowbar Rhyolite Lava)
Waiora Ignimbrite (Waiora Ig Wa1)
Rhyolitic lava (Rhyolite Lava)
Lithic-crystal Breccia
Andesite Lava
Tuffaceous rock (Tuffaceous Sst)

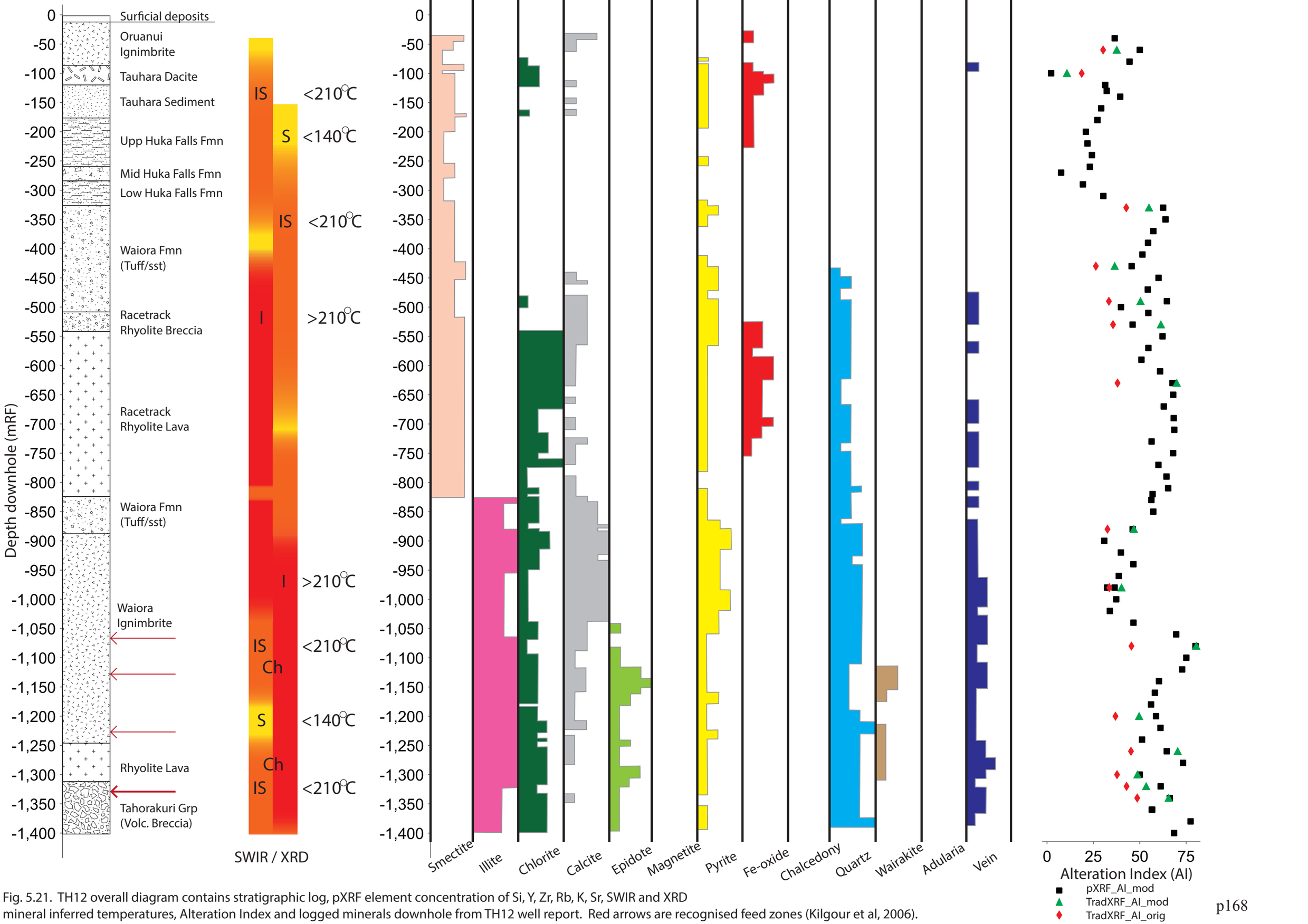

Fig. 5.21. TH12 overall diagram contains stratigraphic log, pXRF element concentration of Si, Y, Zr, Rb, K, Sr, SWIR and XRD mineral inferred temperatures, Alteration Index and logged minerals downhole from TH12 well report. Red arrows are recognised feed zones (Kilgour et al, 2006).

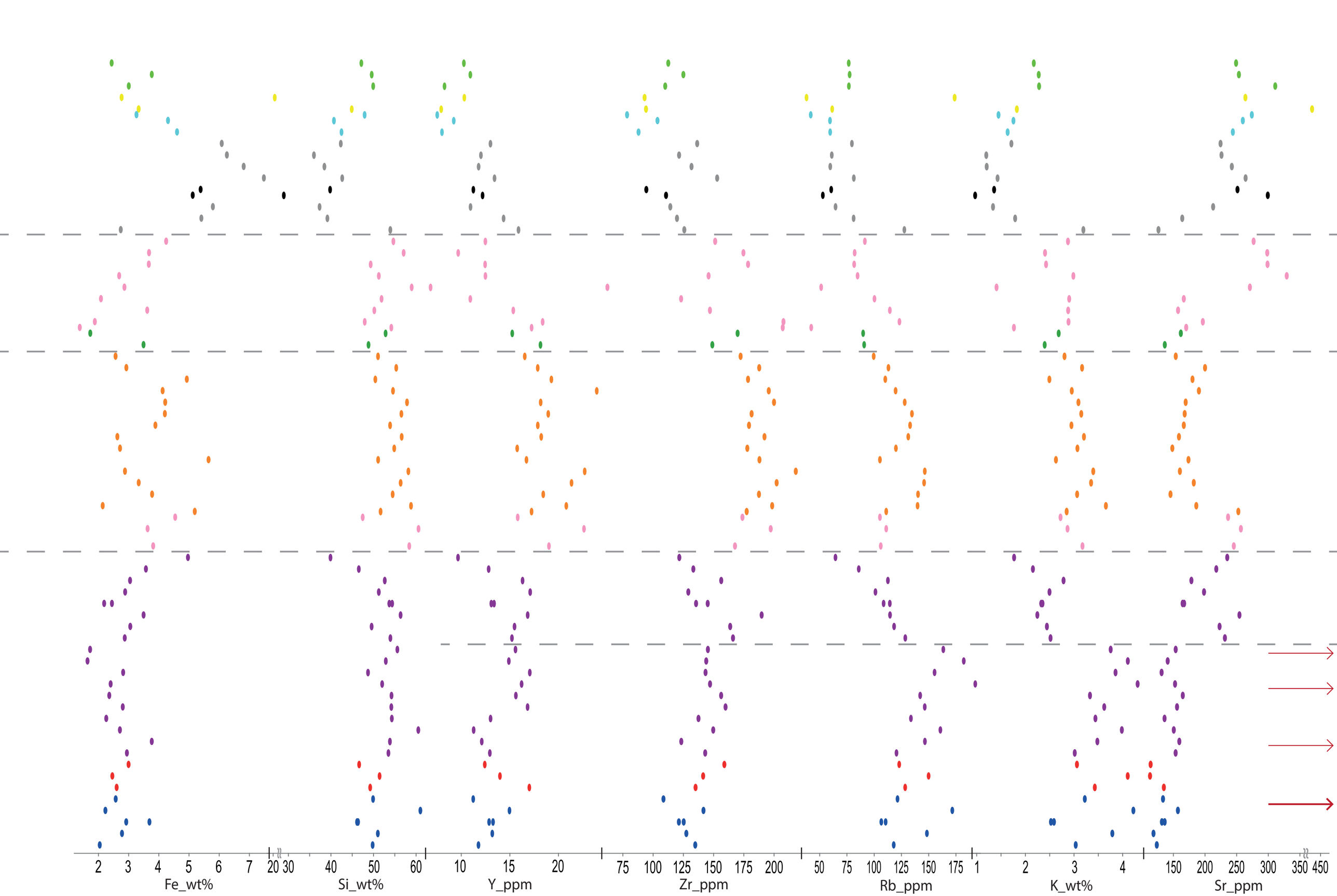
2 3 4 5 6 7 20 30 40 50 60 10 15 20 75 100 125 150 175 200 50 75 100 125 150 175 1 2 3 4 150 200 250 300 350 450
Fe_wt%
Si_wt%
Y_ppm
Zr_ppm
Rb_ppm
K_wt%
Sr_ppm
Non-welded ignimbrite (Oruanui Ig)
Dacite Lava (Tauhara Dacite)
Dac, Rhy, Zst, Sst (Tauhara Sed)
Volcaniclastic sed (Upp Huka Falls)
Lithic-tuff Breccia (Mid Huka Falls)
Volcaniclastic sed (Lower Huka Falls)
Waiora Fmn tuff-sst (Waiora Wa3-4)
Rhyolite breccia (Racetrack Rhyolite Breccia)
Rhyolite lava (Racetrack Rhyolite Lava)
Waiora Ignimbrite (Waiora Ig Wa1)
Rhyolitic lava (Rhyolite Lava)
Volcanic Breccia (Tahorakuri/Ohakuri Grp)

5.4.3 pXRF concentrations and lithogeochemistry downhole

It is widely understood that alteration varies with proximity towards hydrothermal fluid flow pathways and ore mineralization in epithermal districts (Warren et al., 2007). Patterns produced by variation in concentration can be more important than individual data values alone. Construction of simple downhole plots of elements enables geochemical trends to be unravelled that show this variation (Gifkins et al., 2005; Peter et al., 2009). In Sack and Lewis's (2013) study they noticed that even though the elements As, Ba, Ca, Co, Cu, Fe, K, Mn, Pb, Rb, S, and Sr were not present in abundances above the lower limit of detection they still gave an indication of hydrothermal alteration intensity based on how they were distributed. Consequently their low abundance and concentrations at or below the calculated limit of detection (LOD) are still informative. The overall Figures 5.19, 5.20 and 5.21 (TH9, TH10, TH12) display selected downhole element plots next to stratigraphy, predominant logged mineralogy and the alteration index in order to reveal geochemical anomalies or trends across analyses that may provide insights into past fluid conduits or hydrothermal system evolution.

High field strength elements (HFSE) such as Y, Zr and Nb are elements that remain relatively immobile during hydrothermal alteration. On the other hand, elements which move as fluids migrate through permeable areas in rocks during hydrothermal alteration are large ion lithophile elements, such as Rb and Ba. Potassium and Ca are also highly mobile during alteration therefore concentrations can vary widely in altered rocks. Elements that were analysed but were too widely scattered to show any discernable trends (such as Ti) are not mentioned in this section.

TH9 well

Yttrium concentrations increase from ~ 5 ppm to ~ 22 ppm between 440 and 480 mRF with another change in concentration also occurring at approximately 900 mRF, which correlates with the logged transition between the Waiora Formation and the Waiora Ignimbrite (Fig. 5.19). The clear change in concentrations of Y and Zr, both immobile HFS elements unlikely to be moved by hydrothermal alteration, are ideal in recognising formation boundaries that may be harder to

ascertain visually. Rubidium, Ba and Sr, are relatively mobile elements more affected by hydrothermal alteration. However, all of the elements exhibit the same step change in concentration at the formation boundary. Rb concentrations are variable, but show an increase in average concentration from ~ 100 ppm in the Waiora Formation to 130 ppm in the Waiora 1 ignimbrite (Wa1). Barium concentrations increase with depth from approximately 200-600 ppm to the base of the Waiora Formation.

Yttrium displays another change in concentration picked up geochemically (grey dashed lines) that likely represent slight changes in lithology such as sub units which cannot be recognised by visual logging alone. There is also an interesting "zig zag" trend within the 1000 m thick Waiora Ignimbrite unit (shorter dashed lines, Waiora Ignimbrite) that is displayed by Rb, Ba and to some extent Y. This trend in the chemical data suggests some internal stratigraphic variation, perhaps individual flow packages or zones that have undergone variable alteration. Subsequently this trend merits further investigation as there may be useful information about the eruptive and magmatic history of this unit which has not been previously identified.

Potassium increases with depth from 0 to 900 m, and then remains approximately constant at around 2.75 wt % to the bottom of the well. Calcium concentrations are relatively constant at ~ 1.5 wt %, but concentrations as high as 9 wt % occur at ~ 840-860 mRF which is likely related to an increased abundance of hydrothermal calcite that is also reflected in well logs from 835-860 mRF and detected by 10 % hydrochloric acid. An increase in Ca concentration occurs between 1.5 % and 2.5 % towards the bottom of TH9. Arsenic displays constant concentrations of ~15 ppm, but outliers as high as 150 ppm are seen within and below the Huka Falls Formation (cap of system) and at the bottom of TH9 at locations which correlate with recognised hydrothermal feed zones.

TH10 well

Rubidium, Zr, Y, Sr, K, Ba, Si, Ca, Fe and Nb all show a clear change in concentration between 1180 and 1200 m, which is ~ 85 m above the logged transition between the Waiora 1 ignimbrite (Wa1) and a lithic-crystal breccia (Fig. 5.20). The immobile element Zr correlates so well with formation boundaries, that it appears the boundary between lithological units is 85 m above the transition inferred from logging, or, is possibly a previously unrecognized sub unit. This pattern is also reflected in the concentration of Rb. As evidenced, many of the elements analysed by pXRF show this obvious change and generally correlate with the lithological transitions identified by traditional logging of cuttings, hence rapid geochemical analysis can be successfully used to refine and identify formations boundaries, and could supplement the traditional logging done in "real time" during geothermal drilling.

At ~1860 mRF, there is a large increase in Rb concentration which is the location of a recognised main feed zone (Contact Energy Ltd). Potassium and Ba show an increase at the same location whilst Sr shows a decrease. The mobility of Rb, K and Ba may reflect enhanced potassic hydrothermal alteration and the formation of adularia, while Sr removal is consistent with the destruction of Ca-bearing plagioclase (as Sr substitutes for Ca). Therefore, it is likely that andesine (Ca-bearing plagioclase) has been altered and replaced by adularia. Rubidium also shows other distinct changes in concentration down hole which generally correlate with logged formation boundaries (Fig. 5.20). However, some distinct Rb changes occur which do not appear to correlate with recognised formation boundaries (~1660 mRF), and instead is likely linked to hydrothermal alteration. Such changes in Rb concentration suggest hydrothermal fluids once passed through these areas as indicated by the Rb metasomatism.

Potassium and Ca also seem to generally correlate with formation boundaries down hole. Sulfur displays elevated concentrations at the top of the Crowbar Rhyolite Lava and Huka Falls Formation, and is below detection limit for most samples within the well. Arsenic is elevated at the base of the Huka Falls

Formation which is the cap for the deeper aquifer/reservoir and minor increases around recognised hydrothermal feed zones are also measured.

TH12 well

Silica is in higher concentrations from the top of the Waiora Formation with depth down hole displaying an obvious break at the boundary of the Huka Falls and Waiora Formations (330 mRF), reflecting the change in lithology from lake sediments to volcaniclastic rocks. Yttrium (HFS, immobile element) ranges between 8 and 24 ppm with changes in concentration appearing to correlate with transitions between logged formations. This correlation is also replicated by the immobile element Zirconium.

Barium is widely scattered but generally increases in concentration with depth. Potassium displays two clear changes in concentration down hole, a major change at 1050 mRF where K ppm increases in the middle of the Waiora 1 ignimbrite (Wa1) which correlates closely with a recognised feed zone and a minor break at 330 mRF, where the Huka Formation (lacustrine sediments) transitions into the underlying volcaniclastic rocks (Fig. 5.21). Changes in Ca concentration with depth are similar to K and mirror that of Sr. Rubidium displays a clear break at 1050 mRF where it is elevated in concentration, there seems to be some permeability here in this region as the mobile elements K, Sr and Rb are also fluctuating; whereas Sr has increased, Rb has decreased in concentration. These changes are close to the recognised feed zone (Fig. 5.21, Contact Energy Ltd). Alternatively there may be internal stratigraphic variations or changes in lithology to account for the variation.

In general, there is significantly more variation in the immobile elements (Zr, Y, Nb) then would be expected if the formations were all the same lithology. The implication of this is that subtle changes in lithology (representing subunits) are not easily recognised by visual logging alone. Thus rapid inexpensive geochemistry data collected via pXRF may be very beneficial in identifying and refining lithological packages. Consequently, this study concludes that:

- pXRF data downhole is able to recognise geochemical trends on the basis of variations in elemental concentrations that relate to lithology and alteration.
- Immobile elements (Y, Zr, Nb) are suitable for identifying lithology packets, refining formation boundaries, distinguishing subunits or subtle lithology changes.
- Elevations in mobile element concentrations (Ba, K, Ca, As, Rb and Pb) indicate feed zones, suggest permeable zones and may reflect intensity or type of hydrothermal alteration.
- It is reliable for measuring many elements (both HFSE and LILE) in hydrothermal cuttings which do not need to be prepared beyond being washed and dried.
- It is rapid and inexpensive and placed directly onto cuttings therefore could be used in real time to assess which formation the rig is currently drilling through, or determine changes in lithology during drilling.

5.5 LITHOGEOCHEMISTRY AND MINERALOGY

5.5.1 Alteration Index and Carbonate Chlorite Pyrite Index

Alteration intensity describes the intensity of hydrothermal alteration rocks have undergone, i.e. how completely the rock has reacted under alteration to produce new minerals and textures. It also indicates the abundance of new minerals, but not the actual mineral species themselves (Gifkins et al., 2005). Textural and compositional changes are closely associated to alteration intensity and the degree of metasomatism or conversely, the original textures and minerals may be preserved, or a mixture of both. Evaluations of alteration intensity are made qualitatively or quantitatively. Qualitative estimates rely on four parameters that are defined petrographically:

- the extent of destruction to the original minerals
- how much of the original textures have survived
- the pervasiveness of alteration and resulting textures
- the abundance of new alteration minerals

Quantitative estimates are based on alteration indices that comprise multiple components or normalised ratios derived from lithogeochemical compositional data. The alteration indices characterise hydrothermal mineral associations but in a geochemical format and is a tool to help quantify alteration intensity, differentiate alteration styles and identify mineral exploration vectors (Gifkins et al., 2005). Technology transfer to the geothermal industry from mining and application of quantitative alteration indices to active geothermal fields is uncommon (Bogie & Lawless, 2000) therefore it was trialled on the samples obtained in this thesis.

The formula alteration indices generally follow is the numerator is elements gained and the denominator is elements lost. In multi component and normalised indices the same components can be both in the numerator and the denominator such as the alkali index $K_2O/Na_2O + K_2O + CaO$ by Date et al. (1983). Some indices have a gradient of alteration intensity that is quantified by multiplying by a factor of 100. The Ishikawa Alteration Index (1976) below is a good example of these features and is probably the most commonly used alteration index.

$$\text{Alteration Index (AI)} = \frac{100\ (MgO + K_2O)}{(MgO + K_2O + CaO + Na_2O)}$$

Plagioclase-destructive hydrothermal alteration systems are where it is most beneficial, as the AI is representative of constituents that are gained during alteration such as chlorite and sericite ($MgO + K_2O$), and those that are lost when volcanic glass and Na-plagioclase are destroyed ($Na_2O + CaO$). The AI is graded into a 0 to 100 range where values > 60 are associated with intense hydrothermal sericite and chlorite alteration reflected by high MgO and K_2O contents. High CaO or Na_2O contents are characterised by low AI values (< 30) resulting from intense calcite or albite alteration that is linked to regional metamorphism or diagenetic alteration (Gifkins et al., 2005). Loss of Na and Ca is a major chemical change when plagioclase is broken down, so many studies use Na loss as a measure of alteration intensity rather than AI (Date et al., 1983).

There are two limitations to using the AI: firstly carbonate alteration (e.g. addition of carbonate minerals) is not considered and chlorite is not separated from rocks that are sericitised. For this reason, another geochemical index was developed by Large et al. (2001) termed the chlorite-carbonate-pyrite index.

$$\text{Chlorite Carbonate Pyrite Index (CCPI)} = \frac{100\ (FeO + MgO)}{(FeO + MgO + Na_2O + K_2O)}$$

The CCPI identifies the influence of chlorite, Fe-Mg carbonates and pyrite that become more common in altered zones as one gets closer to an ore deposit or hydrothermal fluid. Albite, K-feldspar and sericite is destroyed and replaced by Fe-Mg chlorite. High FeO and MgO contents are indicated by high values of CCPI. These high values may suggest intense alteration to produce chlorite, Fe-Mg carbonates, pyrite, magnetite or hematite, minerals that are rich in Fe or Mg. One drawback is that it is not appropriate for mafic rocks, because compositionally they are high in FeO and MgO content which affects the CCPI, influencing CCPI values to > 50. Lower CCPI values ranging from 10-50 are typical of felsic rocks such as rhyolite and dacite, as they are more evolved.

The rocks analysed in this research were largely rhyolitic or andesitic in composition so the CCPI was deemed to be applicable to the rocks in this study. In combination with the AI, it effectively distinguishes altered zones that are rich in sericite, chlorite and/or carbonate using a x-y bivariate plot created by Large et al. (2001), called the alteration box plot.

The geochemical analyses of 1734 unaltered rocks from modern volcanic arcs established the least altered box in the middle, where least altered volcanic rocks plot (Large et al., 2001). More intensely altered rocks plot outside of the box. As alteration intensifies, more intensely altered rocks plot gradually further outside of the box. Rocks move towards a certain direction, that movement is controlled by the alteration assemblage, and subsequently the alteration process (Large et al., 2001). A limitation is that the AI and CCPI indexes do not include SiO_2 hence quartz or silica alteration cannot be measured. However, it is able to link

alteration intensity with mineral associations and to lithogeochemistry enabling hydrothermal alteration zones to be discriminated.

The box plot differentiates between hydrothermal alteration assemblages related to ore deposits and alteration resulting from diagenetic albite or K-feldspar + albite assemblages. Mineralogy, lithogeochemistry and alteration is easily connected and visualised which can assist researchers in determining vectors towards mineralisation, both in zoned alteration systems in ore deposits, but potentially in active hydrothermal systems where hotter temperatures and/or enhanced permeability occur. Plotted around the perimeter of the box plot are mineral types such as phyllosilicates, feldspars and carbonates. Large et al. (2001) discovered that 10 different mineralogical trends could be discerned on the box plot.

Trends one to six are related to hydrothermally altered ore deposits in felsic and mafic volcanic rocks;

1) sericite alteration - usually concentrated at the edges of the alteration halo
2) footwall sericite + chlorite $\pm$ pyrite alteration
3) chlorite $\pm$ sericite $\pm$ pyrite alteration - in footwall chlorite dominated zones
4) chlorite + carbonate alteration – near massive sulfide lenses in footwall
5) sericite + carbonate alteration – near hanging wall of ore deposits or along strike in the host rocks
6) K-feldspar + sericite – uncommon, develops locally in footwall felsic volcanic rocks

Trends seven to ten are unrelated to mineralisation but rather diagenetic processes;

7) Albite + chlorite alteration – typical of seawater-volcanic rock interaction at low temperatures
8) Epidote + calcite $\pm$ albite alteration – in intermediate and mafic rocks
9) K-feldspar + albite alteration
10) Paragonitic sericite + albite alteration

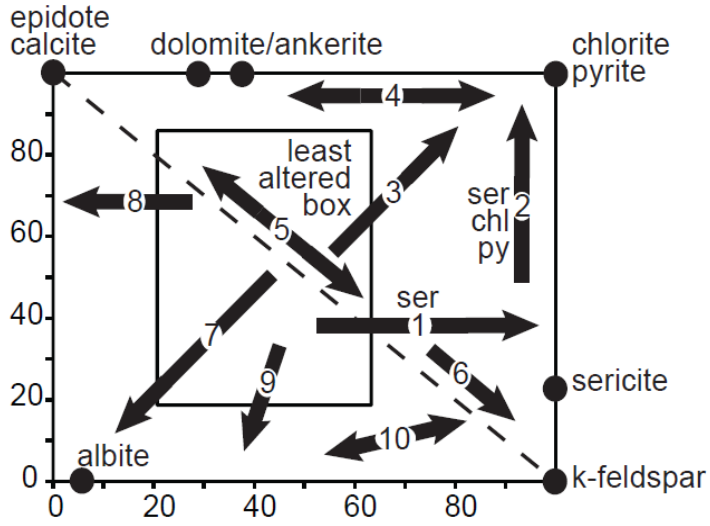

Fig. 5.22. Alteration box plot (Large et al., 2001; Sack & Lewis, 2013). Hydrothermal alteration trends are in the upper right side above the dashed line (1-6), diagenetic alteration trends are in the lower left below the dashed line (7-10).

5.5.2 Epithermal deposits and the Tauhara geothermal field

In porphyry and epithermal districts the spatial and inherited relationships between intrusions and altered zones is recognised (Bogie & Lawless, 2000; Gifkins et al., 2005) and similar relationships occur in VHMS environments. To clarify, a VHMS deposit is rich in metallic sulfide minerals for example Cu-Ni sulfides and Cu-Zn-Pb sulfides that are hosted by volcanic terrain. Even though the AI and CCPI were originally constructed from volcanic hosted massive sulfide deposits (VHMS) as a tool in exploration mining and research (Ishikawa et al., 1976; Large et al., 2001), the alteration styles can probably be applied to other ore deposit types such as low or high sulfidation epithermal or porphyry deposits.

Epithermal and porphyry ore deposits are widely accepted to be the fossil equivalents of geothermal systems (Warren et al., 2007) (Fig. 5.23). Epithermal ore deposits are vein deposits that form at shallow levels (within one kilometre of the surface) by ascending solutions at temperatures of (50-200°C). Gold and silver are examples of valuable minerals in epithermal deposits. The Martha Mine in Waihi, New Zealand is an example of a low-sulfidation epithermal Au-Ag deposit (Castendyk, 2003). Porphyry ore deposits usually occur as large Cu deposits with disseminated chalcopyrite and other sulfides that form around steep

igneous stocks, intermediate to acid in composition. They stretch across 3-8 km in depth range, show concentric zones of alteration minerals and have extensive alteration halos (Allaby, 2008).

Because Au is absent in the samples and minimal Ag detected the present hydrothermal system at Tauhara probably requires a larger mass flux of fluid over a longer timeframe in order to accumulate the quantities of Au-Ag typical of epithermal deposits. Alternatively, conditions suitable for formation of Au-Ag veins do not occur at Tauhara, or drilling has yet to intercept such a vein.

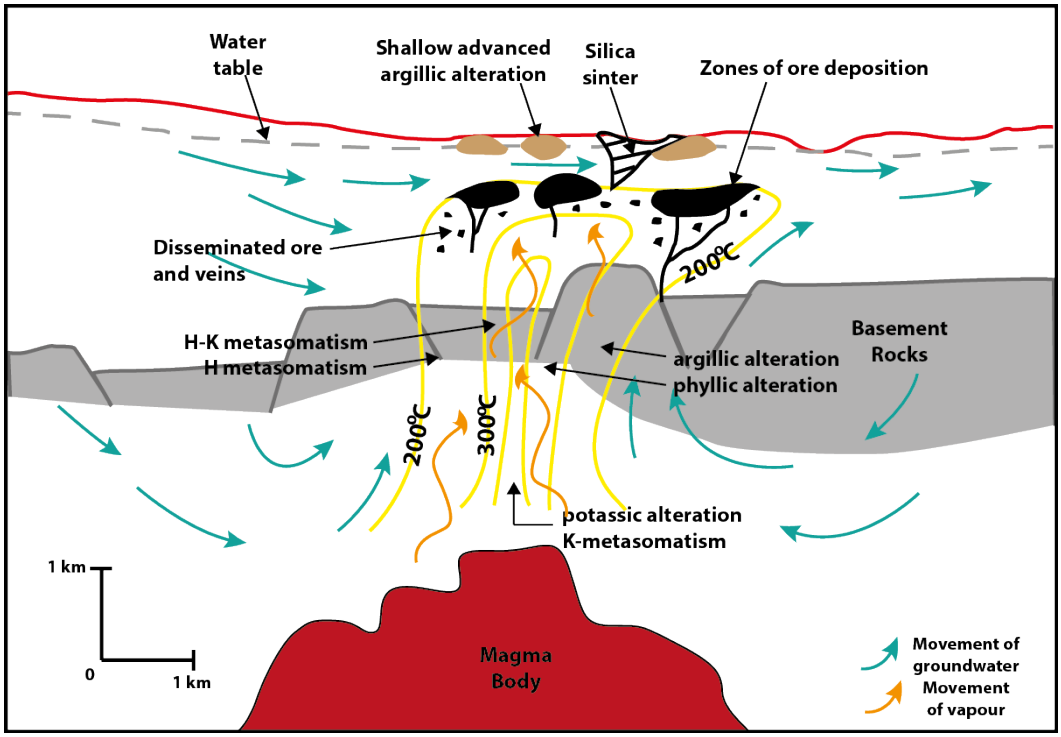

Fig. 5.232. An example of epithermal ore deposition in an active hydrothermal system (redrawn from Henley & Ellis, 1983; Wohletz & Heiken, 1992; Kühn, 2004).

5.5.3 Modified Alteration Index and Carbonate Chlorite Pyrite Index

To accommodate the fact Na and Mg are too light to be analysed by pXRF, the AI and CCPI were adjusted, based on the formula presented in Sack and Lewis's (2013) paper. The reliable elements analysed by pXRF were used and the alteration box plot by Large et al. (2001) was modified in order to enable alteration trends to be visualised.

The modified formulae employed for AI and CCPI;

$$\text{Modified Alteration Index (AI)} = \frac{100\,(K)}{(K + Ca)}$$

Original AI = 100 (MgO + K_2O) / (MgO + K_2O + CaO + Na_2O)

$$\text{Modified Chlorite Carbonate Pyrite Index (CCPI)} = \frac{100\,(Fe + Mn)}{(Fe + Mn + Ca + K)}$$

Original CCPI = 100 (FeO + MnO) / (FeO + MnO + Na_2O + K_2O)

This modified index does under estimate albite alteration (a diagenetic trend) due to the removal of Na and chlorite alteration (a hydrothermal trend) due to Mg removal (Sack & Lewis, 2013). The abundance of chlorite indicated on well logs can give an idea of Mg content. The modified AI formula does over estimate AI, yet effects and trends of hydrothermal alteration can still be scrutinised. The reason why Na is replaced by Ca in the modified CCPI formula is because it behaves similarly to Na.

The Alteration Index downhole in all three wells is illustrated in Figures 5.19, 5.20 and 5.21 and is summarised in Table 5.4. The pXRF and labXRF data where the modified AI formula was applied correlate highly with one another. In contrast, the unmodified formula had lower values (indicating lower degrees of hydrothermal alteration). As mentioned by Sack and Lewis (2013) the modified AI does slightly over estimate AI values compared to the traditional AI formula.

In well TH9 the Alteration Index is > 60 from 1000 mRF onwards plus potassium is higher reflecting more intense sericitic and chlorite alteration. Clays are converted to chlorite where the AI is highest (~ 1400 mRF) at the rhyolite dike, suggesting there may be some fluid movement along the margins of the dike where the intrusion has caused fracturing. The high AI value (~ 75) suggests that there is an alteration halo around the dike which is consistent with one of the specified questions tested in my aim.

In well TH10 higher AI values are seen from 0 – 1100 mRF indicating sericitic or chlorite alteration, logged mineralogy shows both sericitic and chlorite abundance. Over 1100 mRF the AI values are lower (< 30) and CaO is high in the pXRF downhole plots resulting in calcite or albite alteration. In comparison logged calcite abundance decreases from ~1250 mRF onwards, indicating albite alteration rather than calcite alteration.

In well TH12 the AI exhibits clear breaks at ~350, 875 and 1050 mRF. The breaks at 350 and 875 mRF correspond closely to mapped lithology breaks and is consistent with Y and Zr immobile elements but is perhaps more obvious in Fe, Si and K. The break at ~1050 mRF is more evident in mobile elements (Rb, K, Sr) and matches the location of a recognised feed zone. From 350 – 875 mRF, AI values are approximately 60, suggesting sericitic and chlorite alteration has increased or is intense in this section. The logged mineralogy also supports this as chlorite is most abundant in this section. AI values then decrease indicating albite or calcite alteration. The logged mineralogy supports calcite alteration showing increases in calcite, illite and pyrite. AI values increase again to ~70 from 1050 mRF onwards where logged epidote and illite is most abundant along with minor wairakite. Epidote has a high formation temperature (> 240°C), suggesting fluids are hotter and alteration more intense in this area.

Table 5.4. Summary of alteration index values downhole and interpreted alteration types occurring.

Well	Alteration Index	Depth (mRF)	Alteration
TH9	>60	>1000	Sericitic, chlorite
TH10	>60 <30	0 – 1000 >1100	Sericitic, chlorite Albite
TH12	~60 <60 ~70	350 – 875 875 – 1050 >1050	Sericitic, chlorite Calcite, albite Intense sericitic, chlorite

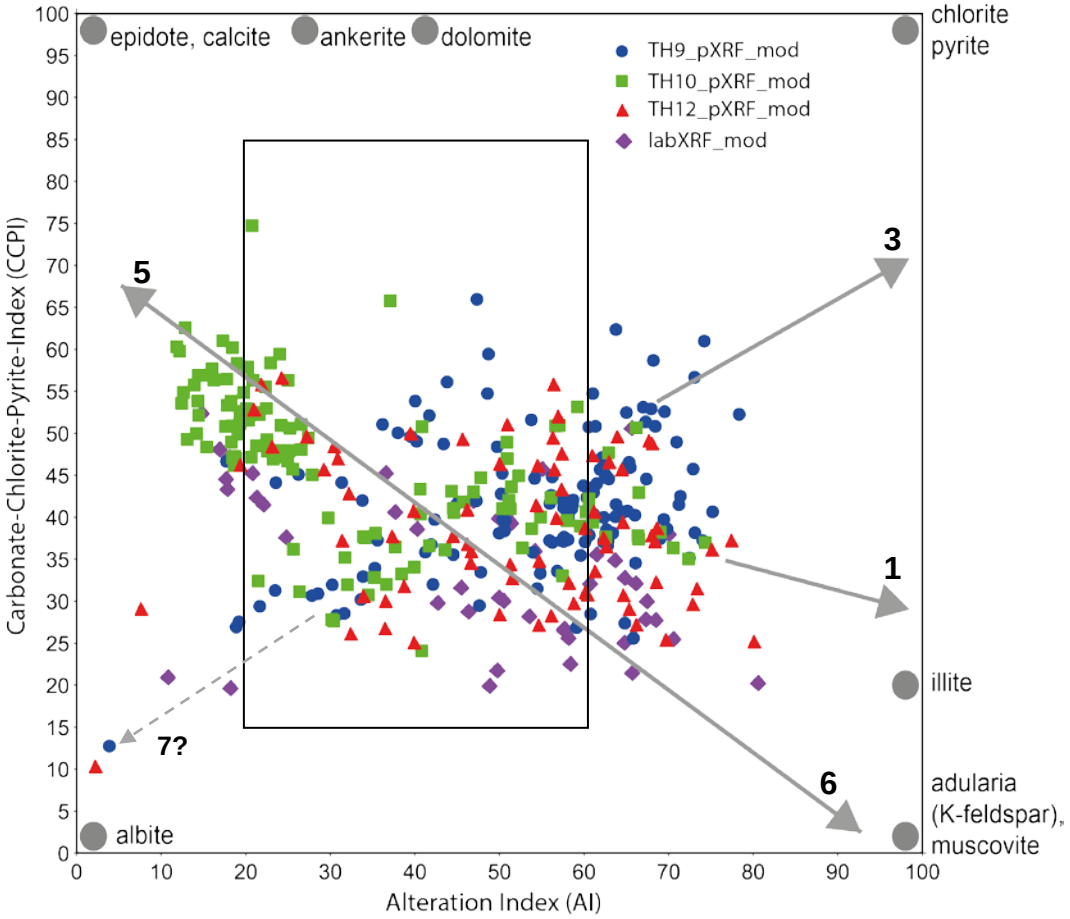

Fig. 5.24. Alteration box plot using the modified AI and CCPI formulae from Sack and Lewis (2013). Both pXRF values across all wells and traditional laboratory XRF values are plotted.

Figure 5.24 illustrates four hydrothermal alteration trends in the Tauhara data set on the modified alteration box plot.

1. Trend towards the illite (sericite) mineral on the right perimeter of the box plot indicating **sericite alteration**
3. Trend towards chlorite and pyrite in the upper right corner suggesting **chlorite ± sericite ± pyrite alteration** found in chlorite dominated zones
5. Trend towards the epidote and calcite minerals in the upper left corner suggesting **sericite and carbonate alteration**
6. Trend towards the adularia (K-feldspar) and muscovite minerals in the bottom right corner implying **K-feldspar and sericite alteration**

7?. Potential diagenetic trend towards albite mineral in the bottom left corner indicative of **albite and chlorite alteration**

The dominant mineral types identified (Fig. 5.24) are indicative of intermediate argillic (K, Ca, Mg, Na metasomatism), argillic (H-metasomatism) and propylitic (Na, Mg, Ca metasomatism) alteration associations. According to Gifkins et al. (2005) these alteration associations are commonly found in epithermal and porphyry deposits and their environment of formation is geothermal, low sulfidation epithermal, high sulfidation epithermal or porphyry-Cu environments.

The trends are more evident in some wells relative to other wells. Each well has the modified formula applied to both pXRF and lab XRF data. Well TH10 shows three trends (1, 3, 5) and perhaps a fourth (7). Well TH9 shows trend 1, 3 and potentially 7. TH12 seems to show two trends (5, 6) and traditional laboratory XRF (purple diamonds) also demonstrates the same two trends (5, 6). As traditional laboratory XRF does analyse Na and Mg, the original formula was applied and described with the original alteration box and original indexes below (Fig. 5.25). The original data depicts a trend towards epidote and calcite in the upper left corner suggesting sericite and carbonate alteration.

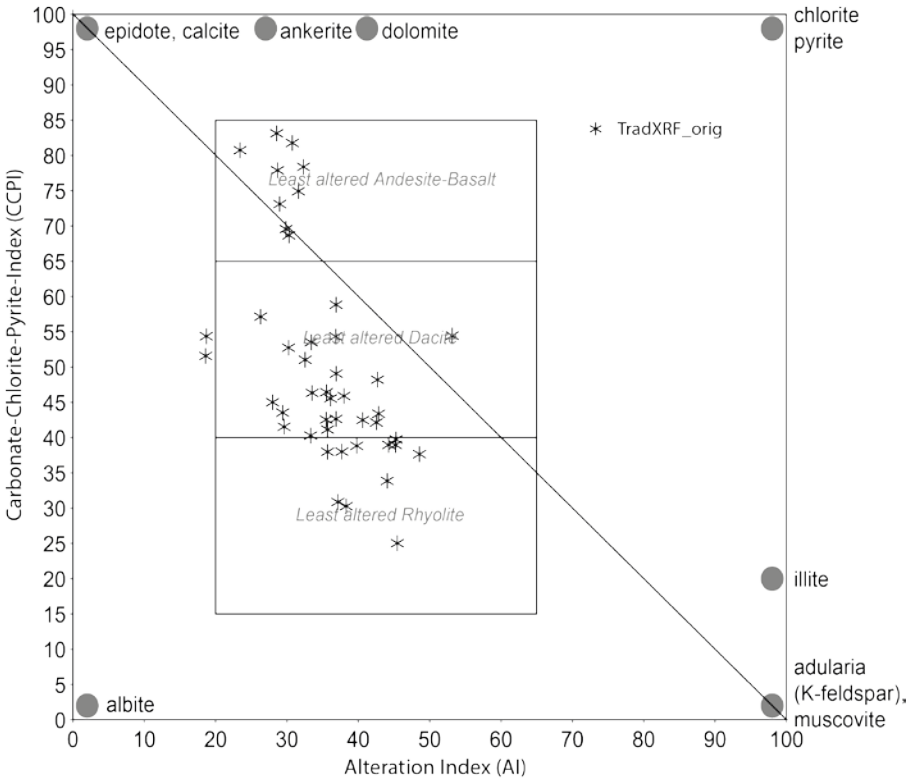

Fig. 5.25. Alteration box plot (Large et al., 2001) with original lab XRF data displaying the trend towards epidote and calcite in the upper left suggesting sericite and carbonate alteration.

Bivariate scatter plots of Alteration Index and CCPI values for pXRF and lab XRF were constructed to compare instruments and establish how effective the pXRF instrument performed. In Figure 5.26, the Alteration Index shows that the linear model or regression line explains most of the variability and fits the sample well (R^2 = 0.81). Additionally the correlation co-efficient (Pearson) shows a very excellent correlation (**r** = 0.9) indicating the pXRF performs well for the AI.

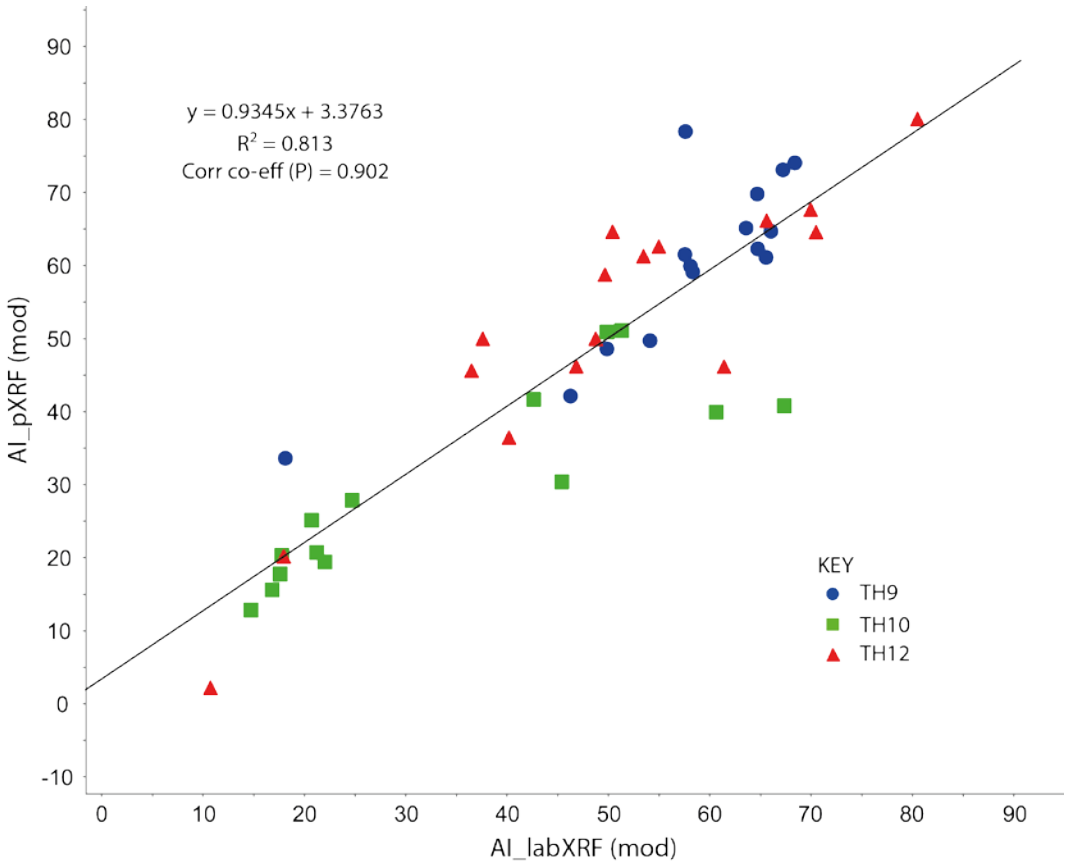

Fig. 5.26. Comparison between pXRF and lab XRF for the Alteration Index.

In contrast Figure 5.27 depicting the CCPI comparison, the correlation co-efficient is less (**r** = 0.67), the linear model is not as close a fit and explains variability less suggesting pXRF is less suitable for CCPI. Moreover CCPI values for pXRF are higher compared to the lab XRF counterparts.

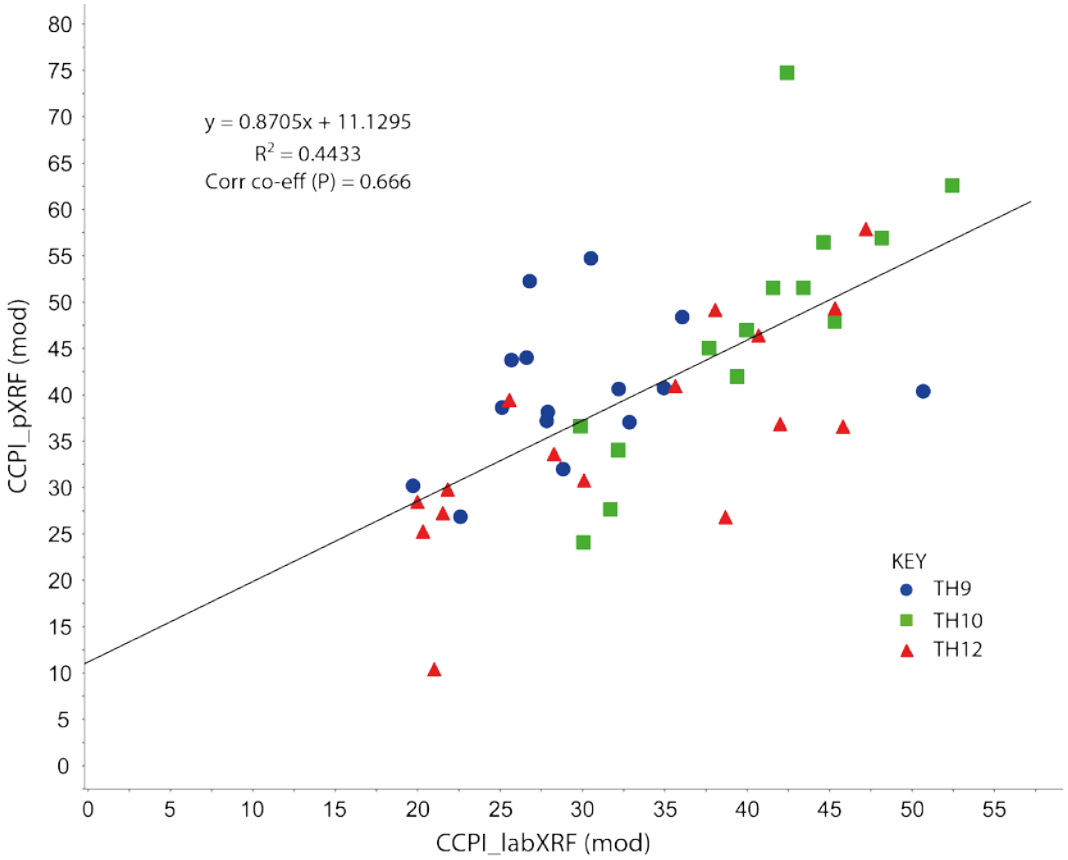

Fig. 5.27. Comparison between pXRF and lab XRF for the Carbonate-Chlorite-Pyrite Index.

5.5.4 Molar element ratio plots

Molar ratios are used to determine the moles of product formed from a certain amount of reactant or how much reactant is needed to make another reactant consequently they are important in quantitative chemistry. Assorted element ratios have been used by a variety of authors to assess the intensity and nature of alteration (Pearce, 1968; Barrett & MacLean, 1991; Stanley & Madeisky, 1994; 1996; Davies & Whitehead, 2006). The most common is using immobile elements or 'conserved' elements to plot mobile elements against (Na, K, Mg). Gresens equations (1967) and Pearce element ratios (1968) were among the earliest examples and have since been adapted to study alteration in ore deposits. In this thesis they have been extended to epithermal environments such as the Tauhara geothermal field.

The chemical and mineralogical compositions related to alteration of rhyolites and rhyodacites are easily illustrated by alkali-alumina and MgO-alumina molar ratio plots (Davies & Whitehead, 2006; Figs. 5.28, 5.29) commonly known as MER (molar element ratio) diagrams. Alteration signatures are also classified in this way and these two plots allow the alteration mineralogy for each sample to be visualised graphically (Halley, 2014). Na_2O loss from highly altered rhyolites is also clearly illustrated by alkali-alumina plots. The mobile alkalies are ratioed against Al_2O_3, an elemental oxide generally accepted as being relatively immobile (Jenner, 1996).

Alkali-alumina plots are able to overcome the problems associated with selecting the right precursor compositions required for mass-balance calculations. They also interpret the mobility of Na_2O, K_2O, and MgO much like mass balance calculations. Molar element ratio plots are a viable alternative to such calculations, particularly if the original composition of the sample cannot be determined as it is too intensely altered (Davies & Whitehead, 2006).

Two good examples of molar ratio plots are Davies & Whitehead (2006) akali-alumina ratio plot and Stanley & Madeisky's (1996) molar element ratio plot (Fig. 5.28). Stanley and Madeisky's (1996) plot is derived from Pearce element ratios (PER) which are used primarily to avoid the effects of closure. Closure is mathematically derived by trying to constrain the sum of all element concentrations to 100 %. Although examination of concentration ratios may simplify data interpretation, the variations in molar ratios are linked to both chemical reaction stoichiometries and mineral formulae (Stanley, 2011). The two plots are very similar except the axes are switched so the plots were merged to give Figure 5.29.

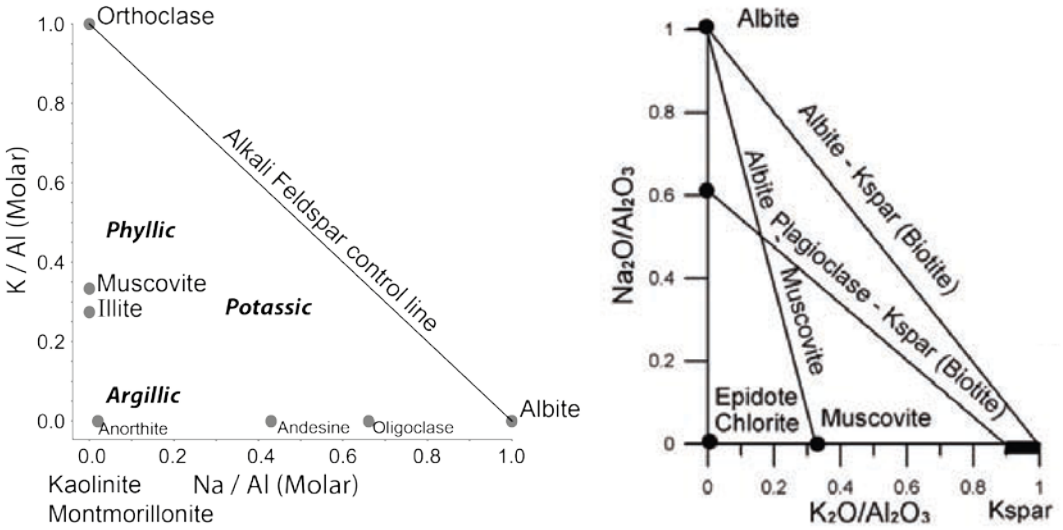

Fig. 5.28. Left: Feldspar Na-K MER (molar element ratio) diagram from Stanley and Madeisky (1996). Right: Alkali-alumina molar ratio plot (Davies & Whitehead, 2006). These two diagrams were combined to give Fig. 5.29.

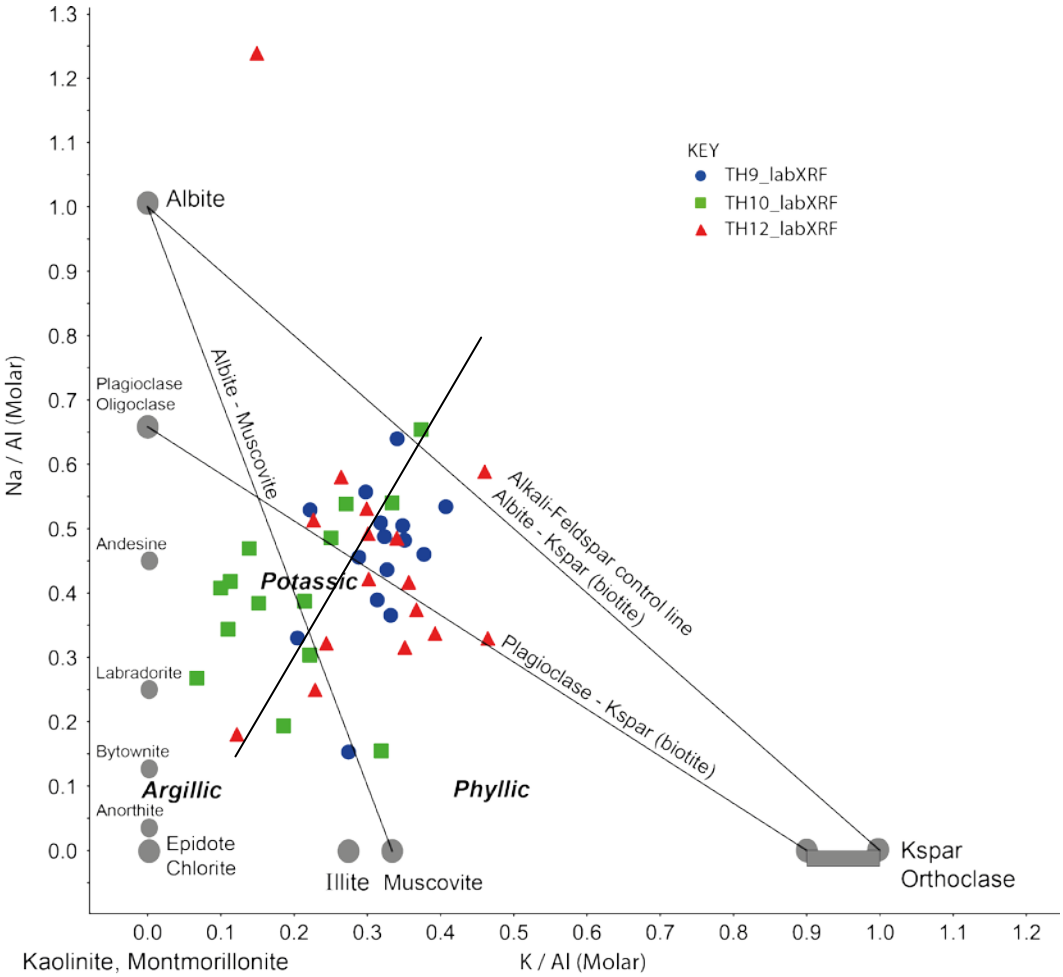

Fig. 5.29. Left: Amalgamation of Stanley and Madeisky's (1996) Feldspar Na-K MER (molar element ratio) diagram and Davies and Whitehead (2006) alkali-alumina molar ratio plot. Tauhara labXRF samples from each well showing the compositions of alteration minerals; plagioclase series, K-feldspar, muscovite, clay minerals and alumina-bearing ferromagnesian minerals.

The stoichiometries of various silicate minerals relating to Figure 5.29 are outlined below (Davies & Whitehead, 2006; 2011). According to Figure 5.29 the equations b) to e) highlighted in bold demonstrate the reactions occurring in the samples.

a) *K-feldspar to muscovite: H^+ is added, K^+ is lost*

$$3KAlSi_3O_8 + 12H_2O + 2H^+ = KAl_3Si_3O_{10}(OH)_2 + 2K^+ + 6H_4SiO_4$$

b) *Plagioclase to clinozoisite, albite, and muscovite: K^+ and H^+ added, Na^+ lost*

$$\mathbf{2Na_4CaAl_6Si_{14}O_{40} + K^+ + H^+ + 9H_2O =}$$
$$\mathbf{Ca_2Al_3Si_3O_{12}(OH) + 6NaAlSi_3O_8 + KAl_3Si_3O_{10}(OH)_2 + 2Na+ + 4H_4SiO_4}$$

c) *Albite to muscovite: K+ and H+ are added, Na+ is lost*

$$\mathbf{3NaAlSi_3O_8 + K^+ + 2H^+ + 12H_2O = KAl_3Si_3O_{10}(OH)_2 + 3Na^+ + 6H_4SiO_4}$$

d) *K-feldspar to albite*

$$\mathbf{KAlSi_3O_8 + Na^+ = NaAlSi_3O_8 + K^+}$$

e) *K-feldspar to sericite*

$$\mathbf{1.5KAlSi_3O_8 + H^+ \rightarrow 0.5KAl_3Si_3O_{10}(OH)_2 + K^+}$$

f) *Sericite to kaolinite*

$$2KAlSi_3O_{10}(OH)_2 + 2H^+ + 3H_2O \rightarrow 3Al_2Si_2O_5(OH)_4 + 2K^+$$

g) *Albite (in Na-plagioclase) to K-feldspar*

$$NaAlSi_3O_8 + K^+ \rightarrow KAlSi_3O_8 + Na^+$$

h) *Albite to Na-montmorillonite*

$$3NaAlSi_3O_8 + K^+ + 2H^+ \rightarrow KAl_3Si_3O_{10}(OH)_2 + 3Na^+ + 6SiO_2$$

As with the Alteration Index, the K/Al vs Na/Al MER plot is most beneficial for feldspar-destructive systems. Halley (2014) describes a fully sericitised rock where the mineralogy is muscovite-quartz-carbonate-pyrite and the muscovite mineral contains all of the K and Al ($KAl_3Si_3O_{10}(OH)_2$) to give a 1:3 ratio of K:Al. Likewise a fully K-feldspar ($KAlSi_3O_8$) altered rock is a 1:1 ratio of K:Al and a fully albitized ($NaAlSi_3O_8$) rock is also 1:1 of Na:Al. Thus the extent of alteration or mineralogical change can be evaluated. Additionally, when compared to fresh unaltered host rock, albitisation will cause the Na/Al ratio to increase whilst chlorite, sericite and K-feldspar alteration will cause the Na/Al ratio to decrease. K/Al ratios also aid in distinguishing between other alteration types for example a high K/Al ratio indicates K-feldspar alteration, moderate K/Al ratios are sericitic alteration and a low K/Al ratio denotes chlorite alteration (Van Der Wielen et al., 2013).

The formations in the Tauhara geothermal field are chiefly rhyolitic with some dacitic and andesitic samples. Feldspars and micas are the most common alumina-bearing minerals in rhyolites. However there are clay minerals and other non-alkali aluminous minerals such as epidote and chlorite which plot at the 0,0 origin and are produced as a result of sericite and chlorite alteration (Fig. 5.28, Davies & Whitehead, 2006). Where acidic hydrothermal fluids interact with rocks containing orthoclase feldspar, alunite is produced and plots in the same position as muscovite.

Figure 5.29 is an amalgamated K/Al vs Na/Al MER plot from the aforementioned diagrams, constructed with the 45 samples analysed by laboratory XRF across all three wells. According to Figure 5.29 there has been enrichment in the rocks (0.15-0.47 K/Al ratio) that arises during potassic alteration or K-metasomatism where exchange reactions take place in feldspars; Na ions are lost to the fluid and K ions are gained in the rock to produce potassic alteration. By contrast if K ions are lost and Na ions gained sodium alteration is produced (Kühn, 2004). Figure 5.29 clearly exhibits this potassic alteration trend. In the major upflow zone (Fig. 3.4) as ascending solutions begin to cool, K-metasomatism and silicification occur

forming K-feldspar, K-mica (pure illite end member), K-rich clays (illite and interlayered illite-smectite) and biotite (Warren et al., 2007).

Conversely as meteoric waters descend and are heated in areas like the periphery of the system (recharge zone, Fig. 3.4), propylitic alteration or Na-Mg-Ca metasomatism occurs and destroys K-feldspars such as K-feldspar microcline ($KAlSi_3O_8$) (Kühn, 2004; Warren et al., 2007). K+ is lost to the fluid and Na, Ca and Mg is added to rock resulting in an epidote ($CaFeAl_2Si_3O_{12}(OH)$), - chlorite ($(((Mg,Fe,Al)_6(Al,Si)_4O_{10}(OH)_8)$ - albite ($NaAlSi_3O_8$) alteration association (Kühn, 2004,Warren et al. 2007).

Additionally Figure 5.29 seems to show a trend towards argillic alteration where illite and maybe illite-smectite are starting to appear. This trend is corroborated by SWIR and XRD analyses that identify illite, illite-smectite and argillic alteration mineralogy. Na-depleted samples probably have illite, illite-smectite or smectite minerals present. In a hydrothermal system strong acids (HCl, H_2SO_4, HF) absorbed from the deep degassing magma body cause Na_2O or K_2O depletion or H+ metasomatism (acid leaching) to occur either primarily within the main neutralisation zone or next to the main upflow zone (Kühn, 2004, Warren et al., 2007). Pirajno (2009) maintains that towards the innermost zones of epithermal systems Na is depleted whilst outer zones may be enriched in K so that over distances of hundreds of metres, a progressive increase in K/Na ratios is observed towards the mineralised areas.

The relationship between muscovite (sericite) and chlorite is displayed by the MgO/Al_2O_3 vs. K_2O/Al_2O_3 molar ratio plot (Davies & Whitehead, 2006). Chlorite is a common phase in highly altered rhyolites. In Figure 5.30 a negative correlation is apparent between MgO and K_2O as muscovite (sericite) is converted to chlorite in the samples. TH10 has the strongest muscovite to chlorite conversion. Most of the samples are near the muscovite point $KAl_2(Si_3Al)O_{10}(OH,F)_2$, with some samples decreased in K pointing to a K-deficient variant of muscovite called illite. The conversion is explained by equation 1. The conversion of biotite to chlorite is demonstrated by equation 2:

1) *Muscovite to chlorite: Mg^{2+}, Fe^{2+}, OH-, H_4SiO_4 is added, K+ lost*

$$2KAl_3Si_3O_{10}(OH)_2 + 15(Mg,Fe)OH^+ + 3H_4SiO_4 + 3H_2O =$$
$$3(Mg,Fe)_5Al_2Si_3O_{10}(OH)_8 + 2K^+ + 13H^+$$

2) *Biotite to chlorite: H^+ is added, $(Mg,Fe)^{2+}$ and K^+ are lost*

$$2K(Mg,Fe)_3AlSi_3O_{10}(OH)_2 + 4H^+ + 6H_2O =$$
$$(Mg,Fe)_5Al_2Si_3O_{10}(OH)_8 + (Mg,Fe)^{2+} + 2K^+ + 3H_4SiO_4$$

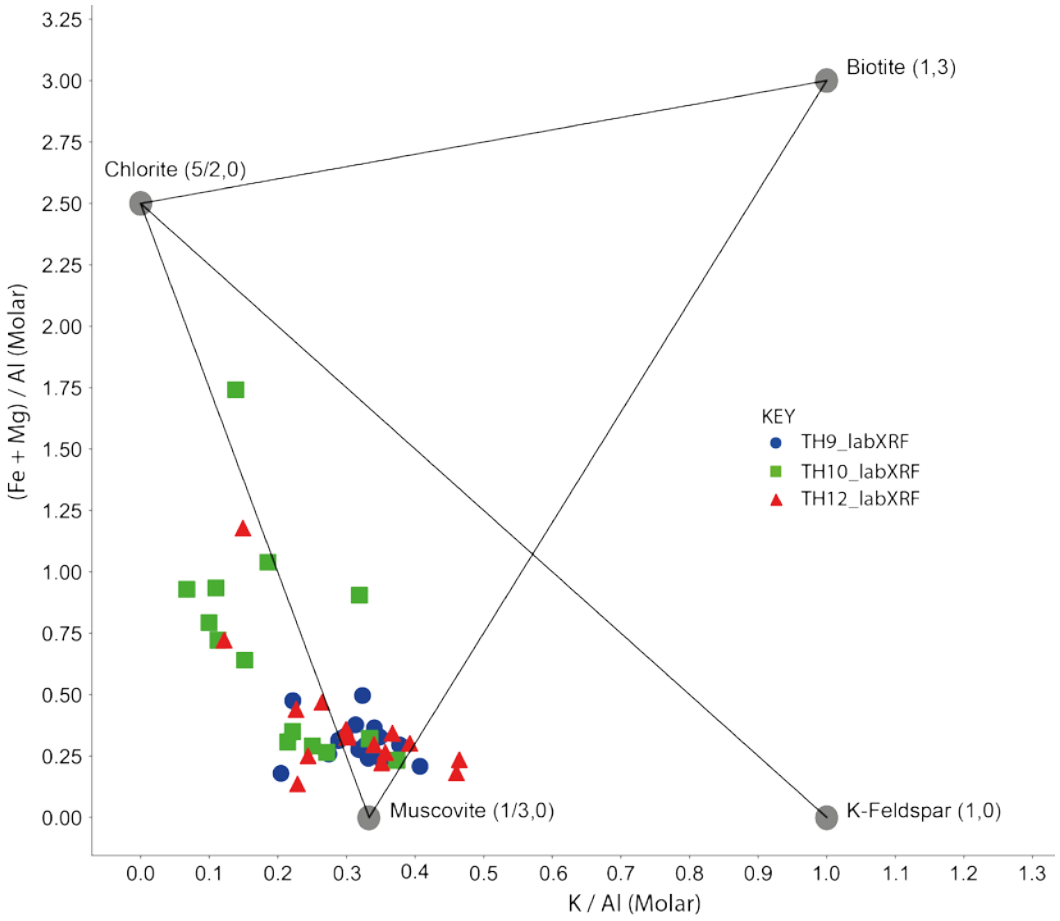

Fig. 5.30. MgO/Al_2O_3 vs. K_2O/Al_2O_3 plot showing the muscovite-chlorite relationship. Diagram based on Davies and Whitehead (2006).

5.5.5 Mineralogy and chemistry

The variability of Si, Fe, Rb and Ba at deeper levels (> 900 m, zig zag pattern) in TH9 may explain the variable replacement of primary plagioclase by hydrothermal albite (Simmons & Browne, 2000). The same occurs in TH12 where Ca increases in concentration from ~900-1050 mRF and is more abundant

in well logs, but becomes depleted form 1050 onwards suggesting destruction of plagioclase which is in agreement with the Sr distribution in this area as well.

In TH10 Rb has a similar pattern to K particularly in the lithic cyrstal breccia and andesite lava formations. Both Rb and K show increases in concentration at ~1800 mRF, near a feed zone and associated permeability. In TH12, increases in K and Rb is also seen in permeable areas from ~1050-1350 mRF. When primary plagioclase is replaced by adularia, Rb may substitute for K in adularia (Simpson & Mauk, 2000). Hence in both cases (TH10 and TH12), primary plagioclase is replaced by hydrothermal adularia allowing K and Rb to increase and Na and Sr to decrease accounting for the fluctuation in the elements (although Na is not analysed by pXRF). Strontium substitutes for Na in primary plagioclase that is preserved in moderately altered rocks (Simpson & Mauk, 2000). Therefore once it is replaced by adularia, Sr is lost. In TH12, Fe depletion from ~900-1050 may be because mafic minerals are being replaced by quartz and pyrite instead of chlorite.

5.6 SUMMARY

In order to assess the efficacy of pXRF and how well it compared to laboratory based XRF the Spearman correlation method was chosen because it removed the influence of outliers and is suitable for non-parametric data. The comparison between traditional lab-based XRF (fused and press powder discs) and portable XRF on cuttings showed generally excellent correlation ($\mathbf{r}_s$ >0.8) between the two methods for the elements As, Ba, Ca, K, Nb, Rb, Sr, Y, Zr. However, the elements Al, Cu, Mn, Mo, Pb, S, Si, Th, Cr, Sb, Sn, Ta, Zn were not as well correlated between the two methods ($\mathbf{r}_s$ <0.7).

The lab XRF samples were classified using diagrams devised by Winchester and Floyd (1977) and Pearce (1996) which utilise ratios of high field strength elements Zr/Ti and Nb/Y as the basis for rock classification. Both diagrams plotted samples very similarly into two categories, either rhyolite/dacite or andesite/andesite-basaltic which is consistent with stratigraphy.

Three samples plotted in the upper andesite/andesite-basaltic section closely bordering the rhyolite/dacite in Pearce's diagram rather than squarely in the rhyodacite/dacite area like in Winchester and Floyd's diagram. Construction of boundaries in the diagram is the likely reason for the distortion. One sample (TH10 1240 m, red, Waiora Ignimbrite) was categorised as andesite/andesite-basaltic, corroborated by geochemical trends downhole, indicating that the sample instead belongs in the lithic crystal breccia unit and that the stratigraphic formation boundary needs to be shifted. The chemical data is also consistent with the known tectonic setting of volcanic arc to back arc and the magma series as calc-alkaline.

Downhole pXRF element plots proved to be useful to distinguish variations in concentrations of immobile and mobile elements, which display geochemical variations that help with the evaluation of fluid flow zones, hydrothermal alteration and lithology. The immobile elements (Zr, Y, Nb) identified lithology packages, refined formation boundaries and distinguished subunits or slight changes in lithology otherwise difficult to determine by visual logging. Conversely elevations (or depletion) in mobile element concentrations (Ba, K, Ca, As, Rb and Pb) indicated feed zones or fluid movement in permeable zones.

The alteration index and chlorite-carbonate-pyrite index, two indices that are used to describe the intensity of alteration in a system and the constituents gained and lost was modified to accommodate the absence of Na and Mg in pXRF analysis. Both the alteration index downhole and the alteration box plot uncovered sericite, chlorite, and calcite/carbonate alteration in the well samples. In well TH10 and TH9 albite alteration was detected, and K-feldspar alteration was shown in TH12 by the box plot. More importantly the alteration index downhole in TH9 gave its highest values in the vicinity of the dike at ~ 1400 mRF indicating that there is an alteration halo around the dike.

As a result of the trends recognised, intermediate argillic (K, Ca, Mg, Na metasomatism), argillic (H-metasomatism) and propylitic (Na, Mg, Ca metasomatism) alteration associations were identified, assemblages commonly

found in epithermal and porphyry deposits. Propylitic alteration occurs where meteoric waters descend and are heated in the recharge zone. Compared to laboratory based XRF, pXRF performs well in calculating the alteration index (**r** = 0.9), but less so for the CCPI (**r** = 0.67).

The molar element ratio diagrams were extended to epithermal environments like the Tauhara geothermal field. The amalgamated K/Al vs Na/Al MER plot described enrichment in the rocks (0.15-0.47 K/Al ratio) and indicated potassic alteration or K-metasomatism typically found in the major upflow zone from cooling ascending solutions. Argillic alteration is also slightly expressed and normally occurs adjacent to the main upflow zone. The MgO/Al_2O_3 vs. K_2O/Al_2O_3 molar ratio plot displayed a clear trend where muscovite (sericite) is converted to chlorite, some samples decreased in K pointing to a K-deficient variant of muscovite called illite. Potassic alteration (K-metasomatism) and the sericite to chlorite conversion trend is strongest in TH10. Potassic alteration indicates that TH10 is closest to the main upflow zone.

Chapter 6
Summary

6.1 INTRODUCTION

The TVZ is set in a volcanic continental arc and back arc basin setting resulting from subduction processes at the Hikurangi margin. It is a segmented magmatic rift system with numerous NE-SW trending strike slip faults caused by continued extension. Most of the high temperature hydrothermal systems are located in a central zone of rhyolitic volcanism and caldera formation where extension allows magma to penetrate the crust, and the NE-SW faults permit hot fluids to ascend and convect as individual hydrothermal systems. The Tauhara Geothermal Field is one such system, connected hydrologically at shallower levels to the neighbouring Wairakei system, even though both have separate upflow zones.

In the Tauhara Geothermal Field, geological formations play a hydrological role to keep the hydrothermal system functioning. A hydrothermal system requires a heat source, convecting fluid, a host rock to store the fluid and a cap rock to the entire system. The Huka Falls Formation is the cap rock or aquitard to hot fluid circulating in the Waiora Formation and shallow groundwater. The Waiora Formation is the host rock or geothermal producing reservoir in the system because of its high permeability. The Jurassic greywacke basement hosts the deep fluid and heat source critical to geothermal systems.

This research was conducted to provide a detailed analysis of the hydrothermal alteration mineralogy and whole rock geochemistry of the Tauhara Geothermal Field. X-ray diffraction (XRD), short wave infrared (SWIR), x-ray fluorescence (XRF) and portable x-ray fluorescence (pXRF) were used to analyse 304 drill cutting samples and six drill core samples. Information on fluid flow pathways (feed zones), alteration types, alteration zones and hydrothermal conditions were identified and interpreted. Mineral inferred temperatures were interpreted and compared to modern measured well temperatures.

6.2 KEY FINDINGS

Hydrothermal alteration minerals identified from each analysis petrography, x-ray diffraction (XRD) and short wave infrared (SWIR) are generally consistent with previous alteration studies at Tauhara. The hydrothermal alteration minerals are summarised into three main alteration transition zones downhole at the Tauhara Geothermal Field.

Beige zone: a shallow zone of argillic to intermediate argillic alteration consisting of smectite, kaolinite, quartz, illite-smectite, calcite, pyrite and perhaps cristobalite and zeolite. The Oruanui and Huka Falls Formation are affected by argillic alteration. This zone acts as an aquitard to the whole hydrothermal system, but also as a shallow groundwater aquifer for residential boreholes. The unusual deeper occurrence of kaolinite (400-500 mRF) in the Tauhara geothermal field is likely from acid waters produced at the surface percolating downwards through fractures, to produce low-temperature acid alteration.

Orange zone: with increasing depth, the mineral associations change to illite, chlorite, illite-smectite, quartz, albite and calcite with minor epidote and pyrite. This is a transition zone where alteration intensity and rank increases and propylitic alteration begins to dominate. Chlorite-bicarbonate waters are in this zone.

Red zone: at the deepest level where the highest mineral inferred temperatures are over 250 °C is a more intense propylitic alteration zone with an assemblage of illite, chlorite, epidote, quartz, albite, adularia, wairakite and pyrite. Adularia indicates potassic alteration including K metasomatism. This zone hosts the chloride geothermal reservoir (Waiora Formation) and measured well temperatures over 280 °C.

SWIR and XRD mineral identification enabled mineral inferred temperatures to be established. Where discrepancies arose between the two techniques on mineral identification, the clay separated XRD result was favoured. Compared to measured well temperatures, the mineral inferred temperatures are generally cooler in all wells

except in TH10 where mineral inferred temperatures typically agree with measured well temperatures.

Molar element ratio (MER) plots were constructed using laboratory XRF geochemical data (i.e. not pXRF). The MER plots indicated potassic alteration or K-metasomatism (from cooling ascending fluid in the upflow zone), argillic alteration (adjacent to the upflow zone) and conversion of sericite to chlorite. Strong potassic alteration in TH10 indicates this well is closest to the major upflow zone. Hence the evidence for hotter fluids and proximity to the major upflow zone in TH10 make south Tauhara a prospective area for geothermal production.

In TH12 mineral inferred temperatures are inconsistent with measured well temperatures implying a recent increase of fluid temperature. However petrographic evidence suggests a cooler fluid at the bottom of well TH12. TH12 is perhaps more marginal to the upflow zone and the change in temperature regime may be related to blind faults at depth providing fluid conduits. Feed zones towards the bottom of TH12 may also be related to emplacement of a rhyolite lava body.

The efficacy of pXRF applied to geothermal drill cuttings was tested and Spearman correlation between lab-based XRF and pXRF showed generally excellent correlation ($\mathbf{r}_s$ >0.8) for the elements As, Ba, Ca, K, Nb, Rb, Sr, Y, Zr but poorer correlation ($\mathbf{r}_s$ <0.7) for elements Al, Cu, Mn, Mo, Pb, S, Si, Th, Cr, Sb, Sn, Ta and Zn.

Rock classification diagrams of Zr/Ti and Nb/Y relied on 45 samples analysed by XRF as samples analysed by pXRF had concentrations of Ti below the pXRF detection limit. Samples were classified as rhyolite/dacite or andesite/andesite-basaltic which is consistent with the described stratigraphy from GNS well reports. Samples also belong to the calc-alkaline magma series and represent a volcanic arc to back arc setting that is the TVZ.

One sample (TH10 1240 m, Waiora Ignimbrite) was classified on Zr/Ti and Nb/Y diagrams as andesite/andesite-basaltic rather than ignimbrite. Elemental data derived

from pXRF analyses enabled geochemical trends downhole to be recognised. The geochemical trends also corroborate this classification as they show that this sample belongs in the andesitic lithic crystal breccia unit. Hence stratigraphic boundaries are able to be refined geochemically.

Downhole pXRF geochemical trends of immobile elements (Zr, Y, Nb) were able to refine formation boundaries, separate lithology packets and distinguish subunits or internal stratigraphic variations. Conversely mobile elements (Ba, K, Ca, As, Rb and Pb) indicated feed zones or permeable zones of fluid movement by depletions or elevations in element concentrations. The results of the SWIR analysis enabled the aluminium hydroxyl and water ratio that represents white mica crystallinity to be plotted against depth downhole. Trends in the aluminium hydroxyl and water ratio (AlOH / H_2O) appear to coincide with some of the locations of feed zones (fluid pathways) in TH9 and TH12.

The Ishikawa alteration index (Ishikawa, 1976; Large et al., 2001) was developed to represent alteration intensity and components gained and lost during alteration. The alteration index plotted against well depth (depth downhole) was able to identify the sections of lithology where specific alteration types dominated and reflect the type of hydrothermal alteration. An alteration halo was identified in the vicinity of the dike in TH9 at ~1400 mRF by high AI values, which is useful because illite and chlorite detected by SWIR did not show any appreciable halo.

The alteration box plot devised by Large et al. (2001) utilises modified formulate for the alteration and chlorite-carbonate-pyrite indices, based on XRF and pXRF data and was applied to geothermal drill cuttings. The alteration box plot revealed alteration trends of sericite (illite), chlorite and calcite alteration in the well samples as well as detection of albite and K-feldspar in certain wells. Mineral species and alteration trends identified in the alteration box plot indicate intermediate argillic (K, Ca, Mg, Na metasomatism), argillic (H-metasomatism) and propylitic (Na, Mg, Ca metasomatism) alteration styles consistent with types identified by petrography, SWIR and XRD.

6.2 CONCLUDING REMARKS

The immobile elements (Zr, Y, Nb) show significantly more variation then would be expected if the formations were all the same lithology. The implication is that these slight variations in lithology are not easily recognised by visual logging alone. Therefore pXRF elemental concentration plots are useful in evaluating lithology changes, in the form of subtle internal lithological variations (such as multiple flow units, or subunits) or major formation boundaries. Mobile element concentrations downhole also act as vectors towards fluid flow and guide geothermal energy companies to permeable producing reservoirs. Hence this study finds that pXRF is rapid and reliable and could be used to provide "real time" information on lithology during drilling, such as logging geology faster to help in decision making.

Another cost effective and rapid data acquisition technique is SWIR. Identification of clay minerals can be performed during drilling (like pXRF) and mineral formation temperatures can be inferred which will provide insights on the geohydrology of the reservoir. Samples that produce reliable results are ideally those with minimal or no intercrystalline water as these distort the spectral profile and minimal to no volcanic glass as these produce a spectral profile similar to smectite. A limitation of the SWIR technique is that the spectral signature of a mineral present in smaller amounts will be obscured by minerals present in relative large amounts with strong spectral responses, for example in TH10 from 1200 – 2332 mRF strong calcite and chlorite spectral responses drown out the presence of illite.

6.3 FURTHER WORK

- The SWIR technique is also limited by a dominant water feature in the samples analysed that is likely additional water, probably from intercrystalline water such as fluid inclusions. The additional water results in a SWIR mis-identification and a poor spectral response. Recognising spectral characteristics that could be used to distinguish excess water will resolve this issue and future users of the technique will be more aware if the source of the excess water in the SWIR profiles could be verified.

- Application of quantitative alteration indices to active geothermal fields is uncommon (Bogie & Lawless, 2000) but was trialled on the samples obtained in this thesis. Further work may also involve extending the application of alteration indices to other geothermal fields.

- The Waiora Ignimbrite shows a "zig zag" trend in downhole pXRF element plots that is thought to be individual flow packages or zones that have undergone variable alteration. Consequently this finding is worth further investigation to ascertain the eruptive and magmatic history of this unit as it has not been previously studied.

- This study is the first of its kind to apply pXRF to geothermal drill cuttings. The results are promising as it is able to identify lithology boundaries, lithology variations and fluid flow pathways. Consequently if rapid geochemistry was applied on existing and future wells across the geothermal fields in the TVZ, detailed geology models could be generated and correlation between wells and across fields possible. This application is not limited to just the TVZ but any fields outside of that (e.g. Ngawha) and geothermal fields globally.

References

Adams, C. J., Mortimer, N., Campbell, H. J. & Griffin W. J. (2009). Age and isotopic characterisation of metasedimentary rocks from the Torlesse Supergroup and Waipapa Group in the central North Island, New Zealand. *New Zealand Journal of Geology and Geophysics*, *52*(2), 149-170.

Allaby, M. (2008). *Oxford dictionary of earth sciences* (3rd ed.). Oxford, England: Oxford University Press.

Allen, R. L. (1988). False pyroclastic textures in altered silicic lavas, with implications for volcanic-associated mineralization. *Economic Geology*, *1*, 1424-1446.

AusSpec. (2010). *AusSpec manual*. AusSpec International Ltd, Australia.

Bailey, S. W. (1988). Chlorites: Structures and crystal chemistry. *Reviews in Mineralogy, 19*, 347-398.

Bailleul, J., Chanier, F., Ferrière, J., Robin, C., Nicol, A., Mahieux, G., Gorini, C. & Caron, V. (2013). Neogene evolution of lower trench-slope basins and wedge development in the central Hikurangi subduction margin, New Zealand. *Tectonophysics 591*, 152–174.

Barker, A. J. (2014). *A key for identification of rock-forming minerals in thin section*. University of South Hampton, UK: Taylor & Francis Group.

Barrett, T. J. & MacLean, W. H. (1991). Chemical, mass, and oxygen-isotopic changes during extreme hydrothermal alteration of an Archean rhyolite, Noranda. *Economic Geology, 86*, 406-414.

Beck, A. C. & Robertson, E. I. (1955). Geology and geophysics. In, *Geothermal steam for power in New Zealand*. New Zealand Department of Scientific and Industrial Research Bulletin, 117, 15-19.

Bertani, R. (2010). Geothermal power generation in the world - 2005–2010 update report. *Proceedings, World Geothermal Congress, April 25-29, 2010.* Bali, Indonesia.

Bibby, H. M., Caldwell, T. G., Davey, F. J. & Webb, T. H. (1995). Geophysical evidence on the structure of the Taupo Volcanic Zone and its hydrothermal circulation. *Journal of Volcanology and Geothermal Research, 68,* 29 - 58.

Bignall, G. (2009). *Ngatamariki geothermal field: Geoscience overview* (Client Report 2009/94). Institute of Geological and Nuclear Sciences.

Bignall, G., Milicich, S., Ramirez, E., Rosenberg, M., Kilgour, G., & Rae, A. (2010). Geology of the Wairakei-Tauhara geothermal system, New Zealand. *Proceedings, World Geothermal Congress, 25-29 April 2010,* Bali, Indonesia.

Bish, D.L. & Howard, S.A. (1988). Quantitative phase analysis using the Rietveld Method. *Journal of Applied Crystallography, 21*. 86-91.

Bixley, P. F., Clotworthy, A. W. & Mannington, W. I. (2009). 13 Evolution of the Wairakei geothermal reservoir during 50 years of production. *Geothermics, 38,* 145-154.

Bland, K. J., Kamp, P. J. J. & Nelson, C. S. (2008). Late Miocene – Early Pleistocene paleogeography of the onshore central Hawke's Bay sector of the forearc basin, eastern North Island, New Zealand, and some implications for hydrocarbon prospectivity. *Proceedings, 2008 New Zealand Petroleum Conference*, Auckland, New Zealand.

Bogie, I. & Lawless, J. (2000). Application of mineral deposit concepts of geothermal exploration. *Proceedings, 2000 World Geothermal Congress*, Kyushu – Tohoku, Japan.

Bowen, N. L. (1928). *The evolution of the igneous rocks.* Princeton, NJ: Princeton University Press.

Bragg, W. H. & Bragg, W. L. (1913a). The reflection of x-rays by crystals. *Proceedings of the Royal Society of London: Series A, Containing Papers of a mathematical and physical character, A88,* 428-438.

Brand, N. W. & Brand, C. J. (2014). Performance comparison of portable XRF instruments. *Geochemistry: Exploration, Environment, Analysis, 14*(2), 125-138.

Brindley, (1968). Identification of clay minerals by x-ray diffraction analysis. *Clays and clay technology, Bulletin 169,* 119-129.

Broekmans, M. A. T. M. (2004). Structural properties of quartz and their potential role for ASR. *Materials Characterization, 53,* 129 – 140.

Bromley, C. J., Currie, S., Manville, V. R. & Rosenberg, M. D. (2009). Recent ground subsidence at Crown Road, Tauhara and its probable causes. *Geothermics, 38,* 181-191.

Bromley, C., Currie, S., Ramsay, G., Rosenberg, M., Pender, M., O'Sullivan, M. & Garvey, J. (2010). *Tauhara Stage II Geothermal Project: Subsidence Report*. GNS Science Consultancy Report (Vol. 2010/151, pp. 154). Institute of Geological and Nuclear Sciences.

Brown, G. & Brindley, G. W. (1980). *Crystal Structures of Clay Minerals and their X-Ray Identification.* London, UK: Mineralogical Society.

Browne, P. R. L. (1970). Hydrothermal alteration as an aid in investigating geothermal fields. *Geothermics, 2*(1), 564-570.

Browne, P. R. L. (1978). Hydrothermal alteration in active geothermal fields. *Annual Review of Earth Planet Science, 6*, 229-250.

Browne, P. R. L., & Ellis, A. J. (1970). The Ohaaki-Broadlands hydrothermal area, New Zealand. Mineralogy and related geochemistry. *American Journal of Science, 296*, 97-131.

Browne, P. R. L., & Lawless, J. V. (2001). Characteristics of hydrothermal eruptions, with examples from New Zealand and elsewhere. *Earth Science Reviews, 52*, 299 - 331.

Browne, P. R. L, & Lloyd, E. F. (1987). Water dominated geothermal systems and associated mineralisation. In I.A. Nairn & C.P. Wood (Eds.), *Active volcanoes and geothermal systems, Taupo Volcanic Zone*. New Zealand Geological Survey record 22, 85-152. International Volcanological Congress 1987.

Burnham, C. W. (1962). Facies and types of alteration. *Economic Geology, 57*, 768-784.

Cabanis, B., Lecolle, M. (1989). The La/10-Y/15-Nb/8 diagram; a tool for distinguishing volcanic series and discovering crustal mixing and/or contamination. *Comptes Rendus de l'Academie des Sciences, 309*, 2023-2029 (in French with an English abstract).

Camuti, K. (2008). *Clay minerals, alteration and Terry's pH temperature table.* Lantana Exploration Ltd.

Cappetti, G., Romagnoli, P. & Sabatelli, F. (2010). Geothermal power generation in Italy 2005–2009 update report. *Proceedings, World Geothermal Congress, April 25-30*, Bali, Indonesia.

Castendyk. D., Mauk. J.L., Brodie. K., & Simpson, M. (2003). A method to quantify wall rock mineralogy in an active open pit mine, and its application toward pit late prediction, Waihi, New Zealand. *Proceedings AusIMM 2003 Annual Conference, pp 501-512*. The Australasian Institute of Mining and Metallurgy.

Cattell. H., Cole, J., Bignall, G. Sepúlveda. F. (2015). Geological Depositional Processes and Environments on Geothermal Strata from Wairakei-Tauhara Geothermal Field, New Zealand. *Proceedings, World Geothermal Congress 2015 19-25 April,* Melbourne, Australia.

Caussiux, M., Proust, D., Siitari-Kauppi, M., Sardini, P. & Leutsch, Y. (2006). Clay minerals formed during propylitic alteration of granite and their influence on primary porosity: A multi-scale approach. *Clays and Clay minerals, 54*, 541-554.

Chambefort, I., Lewis, B., Wilson, C. J. N., Rae, A. J., Coutts, C., Bignall, G. & Ireland, T. R. (2014) Stratigraphy and structure of the Ngatamariki geothermal system from new zircon U-Pb geochronology: implications for Taupo Volcanic Zone evolution. *Journal of Volcanology and Geothermal Research, 274,* 51-70.

Charlier, B.L.A., Wilson, C.J.N., Lowenstern, J.B., Blake, S., van Calsteren, P.W. & Davidson, J.P. (2005). Magma generation at a large, hyperactive silicic volcano (Taupo, New Zealand) revealed by U-Th and U-Pb systematics in zircons. *Journal of Petrology, 46*, 3-32.

Christie, A. B., Rabone, S. D. C., Barker, R. G. & Merchant, R. J. (2006). Exploration of the Wharekirauponga epithermal Au-Ag deposit, Hauraki Goldfield. In A.B. Christie & R.L. Braithwaite (Eds.), *Geology and exploration of New Zealand Mineral Deposits* (pp137-144). Australasian Institute of Mining and Metallurgy.

Clarke, I. (2010). Statistics or geostatistics? Sampling error or nugget effect?. *The Journal of Southern African Institute of Mining and Metallurgy, 110*, 306-312.

Cocker, H. A. & Mauk, J. L. (2008). *Mineralogical and geochemical aspects of the Broken Hills gold-silver deposit, Hauraki Goldfield*. Paper presented at the AusIMM New Zealand Branch Conference 2008.

Cole, J. W. (1978). Andesites of the Tongariro Volcanic Centre, North Island, New Zealand. *Journal of Volcanology and Geothermal Research, 3*, 121-153.

Cole, J. W. (1979). Structure, petrology, and genesis of Cenozoic volcanism, Taupo Volcanic Zone, New Zealand - A review. *New Zealand Journal of Geology and Geophysics, 22*(6), 631 - 657.

Cole, J. W. (1990). Structural control and origin of volcanism in the Taupo Volcanic Zone, New Zealand. *Bulletin of Volcanology, 52,* 445-459.

Cole, J. W., Darby, D. J. & Stern, T. A. (1995). Taupo Volcanic Zone and Central Volcanic Region backarc structures of North Island, New Zealand. In B. Taylor (Ed), *Backarc Basins: Tectonics and Magmatism*. New York: Plenum Press.

Cole. J., Thordarson. T., & Burt., R.M. (2000). Magma origin and evolution of White Island (Whakaari) volcano, Bay of Plenty, New Zealand. *Journal of Petrology, 41,* 867-895.

Corbett, G. & Leach, T. (1997). *Southwest Pacific rim gold-copper systems: Structure, alteration and mineralisation*. Short course manual.

Cox, M. E. & Browne, P. R. L. (1998). Hydrothermal alteration mineralogy as an indicator of hydrology at the Ngawha Geothermal field, New Zealand. *Geothermics, 27(3),* 259-270.

Date. J., Watanabe, Y. & Saeki, Y. (1983). Zonal alteration around the Fukasawa Kuroko deposits, Akita prefecture, northern Japan: *Economic Geology, monograph 5*, 365-386.

Davies, J. F. & Whitehead, R. E. (2006). Alkali-Alumina and MgO-Alumina molar ratios of altered and unaltered rhyolites. *Exploration and Mining Geology, 15,* 75-88.

Davies, J. F. & Whitehead, R. E. (2011). Alkali/Alumina molar ratio trends in altered granitoid rocks hosting porphyry and related deposits. *Exploration and Mining Geology, 19*(1 & 2), 13-22.

Demange, M. (2012). *Mineralogy for petrologists: optics, chemistry, and occurrences of rock-forming minerals*. UK: CRC Press.

Dickson, M. H. & Fanelli, M. (2004). *What is Geothermal Energy?* Retrieved from www.geothermal-energy.org/what_is_geothermal_energy.html.

Dolejš. D. & Wagner. T. (2008). Thermodynamic modeling of non-ideal mineral-fluid equilibria in the system Si-Al-Fe-Mg-Ca-Na-K-H-O-Cl at elevated temperatures and pressures: Implications for hydrothermal mass transfer in granitic rocks. *Geochimica et Cosmochimica Acta, 72,* 526-553.

Ellis, A. J. & Mahon, W. A. J. (1977). *Chemistry and geothermal systems.* New York: Academic Press.

Fagan, C. J., Wilson, C. J. N., Spinks, K. D., Browne, P. R. L., & Simmons, S. F. (2006). Stratigraphy, hydrothermal alteration and evolution of the Mangakino geothermal system, New Zealand. *Proceedings, 28th NZ Geothermal Workshop 2006*.

Fenner. C. N. (1931). The residual liquids of crystallizing magmas. *Mineralogical Magazine, 22,* 539-560.

Floyd. P. A. & Winchester, J. A. (1975). Magma type and tectonic setting discrimination using immobile elements. *Earth and Planetary Science Letters, 27,* 211-218.

Floyd, P. A. & Winchester, J. A. (1978). Identification and discrimination of altered and metamorphosed volcanic rocks using immobile elements; *Chemical Geology, 21*, 291–306

Fournier, R. O. & Rowe, J. J. (1966). Estimation of underground temperatures from the silica content of water from hot springs and wet-steam wells. *American Journal of Science, 264,* 685-697.

Friedrich, W., Knipping, P. & Laue, M. (1912). Interferenz-Erscheinungen bei Röntgenstrahlen. *Sitzungsberichte der Kgl. Bayer. Akad. der Wiss*. 303–322

Furlong, K. P. & Kamp, P. J. J. (2009). The lithospheric geodynamics of plate boundary transpression in New Zealand: Initiating and emplacing subduction along the Hikurangi margin, and the tectonic evolution of the Alpine Fault System. *Tectonophysics, 474,* 449-462.

Gazley, M.F. & Fisher. (2014). A review of the reliability and validity of portable X-ray fluorescence spectrometry (pXRF) data. In *Mineral Resource and Ore Reserve Estimation – The AusIMM Guide to Good Practice* (2nd ed). The Australasian Institute of Mining and Metallurgy.

Gifkins, C., Herrmann, W. & Large, R. (2005). *Altered volcanic rocks: A guide to description and interpretation.* Centre for Ore Deposit Research. University of Tasmania, Australia.

Giggenbach, W. F. (1995). Variations in the chemical and isotopic composition of fluids discharged from the Taupo Volcanic Zone, New Zealand. *Journal of Volcanology and Geothermal Research, 68,* 89 - 116.

Giggenbach, W. F. (1997). The origin and evolution of fluids in magmatic-hydrothermal systems. In H.L. Barnes (Ed.), *Geochemistry of Hydrothermal Ore Deposits* (3rd ed.). New York: Wiley. p737-796.

Goodale, N., Bailey, D. G., Jones, G. T., Prescott, C., Scholz, E., Stagliano, N. & Lewis, C. (2012). pXRF: A study of inter-instrument performance. *Journal of Archaeological Science 39*(4), 875–883.

Graham, I. J. & Worthington, T. J. (1988). Petrogenesis of Tauhara dacite (Taupo Volcanic Zone, New Zealand): evidence for magma mixing between high-alumina andesite and rhyolite. *Journal of Volcanology and Geothermal Research, 35*(4), 279-294.

Grange, L. I. (1937). The geology of the Rotorua-Taupo Subdivision. *New Zealand Geological Society Bulletin, 37*.

Grange, L.I. (1955). *Geothermal steam for power in New Zealand*. New Zealand Department of Scientific and Industrial Research, Wellington, New Zealand, Bulletin 117, 15–19.

Gravley, D. M., Wilson, C. J. N., Rosenberg, M. D. & Leonard, G. S. (2006). The nature and age of Ohakuri Formation and Ohakuri Group rocks in surface exposures and geothermal drillhole sequences in the central Taupo Volcanic Zone, New Zealand. *New Zealand Journal of Geology & Geophysics, 49,* 305-308.

Gresens, R.L. (1967). Composition-volume relationships of metasomatism. *Chemical Geology 2*, 47–65.

Grindley, G. W. (1965). The geology, structure and exploitation of the Wairakei geothermal field, Taupo, New Zealand. *New Zealand Geological Society Bulletin, 75*.

Grindley, G. W. (1974). *Tauhara Geothermal Field* (Report NZGS 38, Part D Geothermal Resources). New Zealand Geological Survey.

Halley, S. (2014). Calculated mineralogy and its applications. In: *Mineral Resource and Ore Estimation – The AusIMM Guide to Good Practice* (2nd ed). The Australasian Institute of Mining and Metallurgy.

Harvey, C. & Browne, P. R. L (1991). Mixed-layer clay geothermometry in the Wairakei Geothermal Field, New Zealand. *Clays and Clay Minerals, 39,* 614-621.

Hastie, A. R., Kerr, A. C., Pearce, J. A. & Mitchell, S. F. (2007). Classification of altered volcanic island arc rocks using immobile trace elements: Development of the Th-Co discrimination diagram. *Journal of Petrology, 48*, 2341-2357.

Hauke, J. & Kossowski, T. (2011). Comparison of values of Pearson's And Spearman's correlation coefficients on the same sets of data. *Quaestiones Geographicae 30*(2).

Healy. J. (1964). Volcanic mechanisms in the Taupo Volcanic Zone, New Zealand, *New Zealand Journal of Geology and Geophysics, 7*(1), 6-23.

Healy. J. (1974). *Ngatamariki geothermal field* (Report NZGS 38, Part D). NZGS Minerals of NZ. New Zealand Geological Survey.

Healy, J. (1984). *Wairakei Geothermal Field in review*. New Zealand Geological Survey, unpublished Geothermal Circular JH/10, New Zealand, 34 pp.

Heasler, H.P., Jaworowski, C. & Foley, D. (2009). Geothermal systems and monitoring hydrothermal features. In R. Young & L. Norby (Eds.) *Geological Monitoring: Boulder, Colorado*. Geological Society of America, 105–140.

Hedenquist, J. W. (1990). The thermal and geochemical structure of the Broadlands-Ohaaki geothermal system, New Zealand. *Geothermics, 19*(2), 151-185.

Hedenquist, J. W. (1991). Boiling and dilution in the shallow portion of the Waiotopu geothermal system, New Zealand. *Geochimica et Cosmochimica Acta, 55*, 2753- 2765.

Hedenquist, J. W. & Browne, P. R. L. (1989). The evolution of the Waiotapu geothermal system, New Zealand, based on the chemical and isotopic composition of its fluids, minerals and rocks. *Geochemica et Cosmochimica Acta, 53*, 2235-2257.

Hedenquist, J. W. & Lowenstern, J. B. (1994). The role of magmas in the formation of hydrothermal ore deposits. *Nature, 370*, 519-526.

Heiken, G. (1982). Geology of geothermal systems. In L.M. Edwards., G.V. Chilingar, H.H. Rieke, III., W.H. Fertl, (Eds.). *Handbook of Geothermal Energy*, Houston: Gulf Publishing Company. p177-217.

Henley, R. W. & Ellis, A. J. (1983). Geothermal systems ancient and modern: a geochemical review. *Earth Science Reviews, 19*, 1 - 50.

Henneberger, R. C. & Browne, P. R. L. (1988). Hydrothermal alteration and evolution of the Ohakuri hydrothermal system, Taupo Volcanic Zone, New Zealand. *Journal of Volcanology and Geothermal Research, 34,* 211-231.

Hikuroa, D. C. H., Morgan, T. K. K. B., Henare, M. & Gravley D. M. (2010). Integrating indigenous values into geothermal development. *Geothermal Resources Council Transactions, 34*, 51-54.

Hobden, B.J. (1997). *Modelling magmatic trends in time and space: eruptive and magmatic history of Tongariro volcanic complex, New Zealand*. (Unpublished PhD thesis). University of Canterbury, Christchurch.

Hodder, A.P.W. (2008). *Geothermal waters: a source of energy and metals*. XIII-Water-AGeothermal-1. Department of Earth Sciences, University of Waikato. Retrieved from http://nzic.org.nz/ChemProcesses/water/13A.pdf

Hole, J. K., Bromley, C. J., Stevens, N. F. & Wadge, G. (2007). Subsidence in the geothermal fields of the Taupo Volcanic Zone, New Zealand from 1996 to 2005 measured by InSAR. *Journal of Volcanology and Geothermal Research, 166,* 125-146.

Houghton, B. F., Wilson, C. J. N., McWilliams, M. O., Lanphere, M. A., Weaver, S. D., Briggs, R. M. & Pringle, M. S. (1995). Chronology and dynamics of a large scale silicic magmatic system, New, Zealand. *Geology, 23*, 13-16.

Hulen, J. B. & Sibbett, B. S. (1982). Sampling and interpretation of drill cuttings from geothermal wells. In, *Geothermal log interpretation handbook* (pp1-54). Tulsa: Society of Professional Well Log Analysts.

Hunt, T. M., Bromley, C. J., Risk, G. F., Sherburn, S. & Soengkono, S. (2009). Geophysical investigations of the Wairakei Field. *Geothermics, 38,* 85-97.

Hunt, T. M. & Graham, D. J. (2009). Gravity changes in the Tauhara sector of the Wairakei–Tauhara geothermal field, New Zealand. *Geothermics, 38*, 108-116.

Hutchinson, R. W. (1983). Hydrothermal concepts: the old and the new. *Economic Geology, 78*, 1734-1741.

InnovX-XRF manual (2005). *Innov-X User Manual Version 2.1*. Retrieved from http://www.equipcoservices.com/pdf/manuals/innov-x_alpha_series.pdf

Irvine, T. N. & Baragar, W. R. A. (1971). A guide to the chemical classification of the common volcanic rocks. *Canadian Journal of Earth Sciences, 8,* 523-548.

Ishikawa, Y., Sawaguchi, T., Iwaya, S. & Horiuchi, M. (1976). Delineation of prospecting targets for Kuroko deposits based on modes of volcanism of underlying dacite and alteration halos. *Mining Geology 26*, 105-117.

Jackson, J.A. (1997). *Glossary of Geology* (4th ed). American Geological Institute.

Jenner, G.A. (1996). Trace element geochemistry of igneous rocks: Geochemical nomenclature and analytical geochemistry. In D.A. Wyman (Ed.), *Trace element geochemistry of volcanic rocks: application massive sulphide exploration.* Geological Association of Canada, Short Course Notes 12, p51–77.

Jones. M.C., Williams-Thorpe. O., Potts. P.J., Webb, P.C. (2005). Using field-portable XRF to assess geochemical variations within and between dolerite outcrops of Preseli, south Wales. *Geostandards and Geoanalytical Research, 29*(3), 251–269.

Kamp. P. J. J. (1984). Neogene and Quaternary extent and geometry of the subducted Pacific Plate beneath North Island, New Zealand: Implications for Kaikoura tectonics. *Tectonophysics, 108*, 241-266.

Kamp. P. J. J. & Furlong, K. P. (2006). Neogene plate tectonic reconstructions and geodynamics of the North Islands sedimentary basins: Implications for the petroleum systems. *Proceedings, 2006 New Zealand Petroleum Conference, 6-10 March*.

Kilgour, G. N., Rae, A. J. & Milicich, S. D. (2006). *Geology of Exploration Well TH12, Tauhara Geothermal Field*. GNS Science Consultancy Report (Vol. 2006/219, pp. 34). Taupo, New Zealand: Institute of Geological and Nuclear Sciences.

Kissling, W. M. & Weir, G. J. (2005). The spatial distribution of the geothermal fields in the Taupo Volcanic Zone, New Zealand. *Journal of Volcanology and Geothermal Research, 145*, 136 - 150.

Kiyosaki. J., Tanaka. K., Taguchi., Chiba. H., Motomura. Y., Takeuchi. K., Fujino. T. & Nagahama. N. (2003). Subsurface high temperature hypogene acid alteration at the Hatchobaru geothermal field, Kyushu, Japan. *Proceedings 25th NZ Geothermal Workshop.*

Kühn, M. (2004). *Reactive Flow Modeling of Hydrothermal Systems*. Lecture notes in Earth Sciences, 103. Springer.

Lagat, J. (2009). *Hydrothermal alteration mineralogy in geothermal fields with case examples from Olkaria Domes Geothermal Field, Kenya*. Short Course IV on Exploration for Geothermal Resources, organized by UNU-GTP, KenGen and GDC, at Lake Naivasha, Kenya, November 1 - 22, 2009.

Large, R.R., Gemmell., B & Paulick, H. (2001). The alteration box plot : a simple approach to understanding the relationship between alteration mineralogy and lithogeochemistry assoicated with volcanic-hosted massive sufide deposits. *Economic Geology, 96*(5). 957-971.

Le Maitre, R. W., Bateman, P., Dudek, A., Keller, J., Lameyre Le Bas, M. J., Sabine, P. A., Schmid, R., Sorensen, H., Streckeisen, A., Wolley, A. R. & Zanettin, B. (1989). *A classification of igneous rocks and glossary of terms.* Blackwell, Oxford.

Le Vaillant, M., Barnes, S. J., Fisher, L., Fiorentini, M. L. & Caruso. S. (2014). Use and calibration of portable X-Ray fluorescence analysers: application to lithogeochemical exploration for komatiite-hosted nickel sulphide deposits. *Geochemistry: Exploration, Environment, Analysis, 14(3)*. 199-209.

Lindgren, W. (1933). *Mineral Deposits* (4th ed.). McGraw Hill.

Lund, J. W., *Freeston, D. H. & Boyd, T.* L. (2010). Direct utilization of geothermal energy 2010 world overview. *Proceedings, World Geothermal Congress 25-29 April 2010*. Bali, Indonesia.

Macintosh, I.W, Simmons, S.F., Browne P.R.L. (2000). Hydrothermal feldspars in the Broadlands-Ohaaki geothermal system, New Zealand. *New Zealand Geothermal Workshop.*

Manville, V. 2002. Sedimentary and geomorphic responses to ignimbrite emplacement: Readjustment of the Waikato River after the A.D. 181 Taupo eruption, New Zealand. *Journal of Geology, 110.* 519-541.

McPhie, J., Doyle, M. & Allen, R. (1993). *Volcanic textures: a guide to the interpretation of textures in volcanic rocks.* Centre for Ore Deposit and Exploration Studies, Hobart: University of Tasmania.

Milicich, S.D., Chambefort. I., Bignall. G., & Clark. J. (2014b). Overprinting hydrothermal systems in the Taupo Volcanic Zone. *GRC Transactions, 38*. 511-516.

Milicich, S. D., Bardsley, C., Bignall, G. & Wilson, C. J. N. (2014). 3-D interpretative modelling applied to the geology of the Kawerau geothermal system, Taupo Volcanic Zone, New Zealand. *Geothermics, 51*, 344-350.

Milicich, S. D., Bignall, G., Rae, A. J. & Rosenberg, M.D. (2008) Lithological and structural controls on fluid flow and hydrothermal alteration in the western Ohaaki Geothermal Field (New Zealand): insights from recent deep drilling. *Transactions Geothermal Resources Council, 32*, 303-307.

Milicich, S. D., Rosenberg, M. D., Ramirez, L. E. & Kilgour, G. N. (2008a). *Geology of Exploration Well TH9 Tauhara Geothermal Field* (Consultancy Report 2008/56). Institute of Geological and Nuclear Sciences.

Milicich, S. D., Rosenberg, M. D., Ramirez, L. E. & Kilgour, G. N. (2008b). *Geology of Exploration Well TH10 Tauhara Geothermal Field* (Consultancy Report 2008/80). Institute of Geological and Nuclear Sciences.

Milicich, S. D., Wilson, C. J. N., Bignall, G., Pezaro, B. & Bardsley, C. (2013). Reconstructing the geological and structural history of an active geothermal field: A case study from New Zealand. *Journal of Volcanology and Geothermal Research, 262*, 7-24.

Milloy, S.M. & Wei Lim, Y. (2012). Wairakei-Tauhara pressure regime update. *Proceedings 34th New Zealand Geothermal Workshop 2012*, New Zealand.

Ministry of Business, Innovation and Employment. (2014). *Renewable energy in New Zealand*. Retrieved from http://www.med.govt.nz/sectors-industries/energy/energy-modelling/data/renewables.

Morad, S., El-Ghali, M. A. K., Caja, M. A., Sirat, M., Al-Ramadan, K. & Mansurbeg, H. (2009). Hydrothermal alteration of plagioclase in granitic rocks from Proterozoic basement of SE Sweden. *Geological Journal, 45,* 105-116.

Morgan, T.K.K.B. (2006). An indigenous perspective on water recycling, *Desalination, 187,* 127-136.

Morris, P.A. (2009). *Field-portable X-ray fluorescence analysis and its application in GSWA*. Geological Survey of Western Australia, Record.

Moore, D. M. & Reynolds Jnr, R. C. (1997). *X-ray diffraction and the identification and analysis of clay minerals*, (2nd ed.). New York: Oxford University Press.

Nicholson, K. (1993). *Geothermal fluids: Chemistry and exploration techniques.* Berlin, Germany: Springer-Verlag.

Nicol, A., Mazengarb, C., Chanier, F., Rait, G., Uruski, C. & Wallace, L. (2007). Tectonic evolution of the active Hikurangi subduction margin, New Zealand, since the Oligocene. *Tectonics 26*(4).

Parry, W. T. (1998). Fault-fluid composition from fluid-inclusion observations and solubilities of fracture-sealing minerals. *Tectonophysics, 290,* 1-26.

Pearce, T. H. (1968). A contribution to the theory of variation diagrams. Mineralogical Association of Canada Annual Meeting, *Program with Contributions to Mineralogy and Petrology, 19*, 142-157.

Pearce, J. A. (1996). A user's guide to basalt discrimination diagrams. In D.A. Wyman (Ed.), *Trace element geochemistry of volcanic rocks: Applications for massive sulphide exploration.* Geological Association of Canada, Short Course Notes 12, 79-113.

Pearce, J. A. & Cann, J. R. (1971). Ophiolite origin investigated by discriminant analysis using Ti, Zr and Y. *Earth and Planetary Science Letters 12(3),* 339–349.

Pearce, J. A. & Cann, J. R. (1973). Tectonic setting of basic volcanic rocks determined using trace element analyses. *Earth and Planetary Science Letters, 19,* 290-300.

Peccerillo, A. & Taylor, S. R. (1976). Geochemistry of Eocene calc-alkaline volcanic rocks from the Kastamonu area, Northern Turkey. *Contributions to Mineralogy and Petrology, 58,* 63-81.

Piercey, S. J. & Devine, M. C. (2013). Analysis of powdered reference materials and known samples with a benchtop, field portable x-ray fluorescence (pXRF) spectrometer: evaluation of performance and potential applications for exploration lithogeochemistry. *Geochemistry: Exploration, Environment, Analysis* (in press).

Pirajno, F. (2009). *Hydrothermal processes and mineral systems:* Springer Science.

Pirajno, F. (1992). *Hydrothermal mineral deposits, principles and fundamental concepts for the exploration geologist*. Springer Verlag.

Potts, P.J., Bowles, J. F. W., Reed, S. J. B. & Cave, M.R. (1995). *Microprobe Techniques in Earth Sciences.* London: Chapman and Hall.

Potts, P. J., Bernardini, F., Jones, M. C., Williams-Thorpe, O. & Webb, P.C. (2006). Effects of weathering on in situ portable x-ray fluorescence analyses of geological outcrops: Dolerite and rhyolite outcrops from the Preseli Mountains, South Wales. *X-Ray Spectrometry, 35,* 8–18.

Rae, A. J., Rosenberg, M. D., Bignall, G., Kilgour, G. N. & Milicich, S. D. (2007). Geological results of production well drilling in the western steamfield, Ohaaki geothermal system: 2005–2007. *Proceedings, 29th New Zealand Geothermal Workshop*. Auckland, New Zealand.

Ramirez, L. E., McCoy-West, A. J., Alcaraz, S. A., Rosenberg, M.D. & Rae, A. J. (2009). *Geology of Exploration Well TH18 Tauhara Geothermal Field* (Consultancy Report 2009/277). Institute of Geological and Nuclear Sciences.

Raudsepp, M., & Pani, E. (2003). Application of Rietveld analysis to environmental mineralogy. In J. L. Jambor, D. W. Blowes & A. I. M. Ritchie (Eds.), *Mineralogical Association of Canada, Short Course Series, 31*, 165-180.

Reyes, A. G. (1990). Petrology of Philippine geothermal systems and the application of alteration mineralogy to their assessment: *Journal of Volcanology and Geothermal Research, 43*, 279-309.

Rickwood, P. C. (1989). Boundary lines within petrologic diagrams which use oxides of major and minor elements. *Lithos, 22*, 247-263.

Rogan, M. (1982). A geophysical study of the Taupo Volcanic Zone, New Zealand. *Journal of Geophysical Research: Solid Earth, 87*, 4073-4088.

Rollinson, H. R, (1993). *Using geochemical data: Evaluation, presentation, interpretation.* New York, USA: Longman, Essex, 352p.

Rosenberg, M. D., Bignall, G. & Rae, A. J. (2009). The geological framework of the Wairakei–Tauhara Geothermal System, New Zealand. *Geothermics, 38*, 72-84.

Rosenberg, M., Wallin, E., Bannister, S., Bourguignon, S., Sherburn, S., Jolly, G. & Links, F. (2010). *Tauhara Stage II Geothermal Project: Geoscience Report.* GNS Science Consultancy Report (Vol. 2010/138, pp. 318). Institute of Geological and Nuclear Sciences.

Rowland, J., Bardsley, C., Downs, D., Sepúlveda, F., Simmons, S., and Scholz, C. (2012). Tectonic controls on hydrothermal fluid flow in a rifting and migrating arc, Taupo Volcanic Zone, New Zealand. *Proceedings, New Zealand Geothermal Workshop, 19 – 21 November.* Auckland, New Zealand.

Rowland, J. V. & Sibson, R. H. (2001). Extensional fault kinematics within the Taupo Volcanic Zone, New Zealand: soft-linked segmentation of a continental rift system. *New Zealand Journal of Geology and Geophysics*, *44*, 271-84.

Rowland, J. V. & Sibson, R. H. (2004). Structural controls on hydrothermal flow in a segmented rift system, Taupo Volcanic Zone, New Zealand. *Geofluids, 4*, 259-283.

Rowland, J. F. & Simmons, S. F. (2012). Hydrologic, magmatic, and tectonic controls on hydrothermal flow, Taupo Volcanic Zone, New Zealand: Implications for the formation of epithermal vein deposits. *Economic Geology, 107*, 427 - 457.

Sack, P. J. & Lewis, L. L. (2013). Field-portable x-ray fluorescence spectrometer use in volcanogenic massive sulphide exploration with examples from the Touleary occurrence (MINFILE Occurrence 115O 176) in west-central Yukon. In K.E. MacFarlane, M.G. Nordling, and P.J. Sack (Eds.), *Yukon Exploration and Geology 2012*. Yukon Geological Survey, p115-131.

Schwartz, G. M. (1959). Hydrothermal alteration. *Economic Geology*, *54*(2), 161-183.

Shindo, D. & Oikawa, T. (2002). *Analytical electron microscopy for materials science*. Tokyo: Springer-Verlag.

Simmons, S.F. & Browne, P. R. L. (2000). Hydrothermal minerals and precious metals in the Broadlands-Ohaaki geothermal system: Implications for understanding low-sulfidation epithermal environments. *Economic Geology, 95*, 971-999.

Simmons, S. F. & Brown, K. L. (2007). The flux of gold and related metals through a volcanic arc, Taupo Volcanic Zone, New Zealand. *Geology*, *35*(12), 1099–1102.

Simmons, S. F. & Christenson, B. W. (1994). Origins of calcite in a boiling geothermal system. *American Journal of Science, 294*(3), 361-400.

Simmons, S. F., White, N. C. & John, D. A. (2005). Geological characteristics of epithermal precious and base metal deposits. *Economic Geology, 100,* 485-522.

Simpson, M. P. & Mauk, J. L. (2000). Geochemistry of wall rock alteration at the Golden Cross deposit, New Zealand. *Proceedings, New Zealand Minerals & Mining Conference, 29-31 October 2000*.

Simpson, M. P., Mauk, J. L. & Kendrick, R. G. (2004). Telescoped porphyry-style and epithermal veins and alteration at the central Maratoto valley prospect, Hauraki Goldfield, New Zealand. *Journal of Geology and Geophysics, 47*(1), 39-56.

Simpson, M. P., Mauk, J. L., Bowyer, D. & Worland, R. J. (2006). Alteration mineral studies of an epithermal prospect and a geothermal field using the Terraspec. *Proceedings, 39th Annual Conference of the New Zealand Branch of the AusIMM.*

Simpson, M. P. & Mauk, J. L. (2011). Hydrothermal alteration and veins at the epithermal Au-Ag deposits and prospects of the Waitekauri Area, Hauraki Goldfield, New Zealand. *Economic Geology, 106,* 945-973.

Simpson, M. P., Rae, A. J., Ganefianto, N. & Sepulveda, F. (2013). Short wavelength infrared (SWIR) spectral characterisation of smectite, illite-smectite and illite for geothermal fields of the Taupo Volcanic Zone, New Zealand. *Proceedings, 35th New Zealand Geothermal Workshop 17-20 November 2013,* Rotorua, New Zealand.

Soengkono, S. (2011). Deep interpretation of gravity and magnetic data of the central Taupo Volcanic Zone. *Proceedings New Zealand Geothermal Workshop,* Auckland.

Soengkono, S., Hochstein, M. P., Smith, I. E. & Itaya, T. (1992). Geophysical evidence for widespread reversely magnetised pyroclastics in the western Taupo Volcanic Zone, New Zealand. *New Zealand Journal of Geology and Geophysics, 35,* 47-55.

Spearman, C. E. (1904). The proof and measurement of association between two things. *American Journal of Psychology, 15,* 72–101.

Spinks, K. D., Acocella V., Cole, J. W. & Bassett, K. N. (2005). Structural control of volcanism and caldera development in the transtensional Taupo Volcanic Zone, New Zealand. *Journal of Volcanology and Geothermal Research, 144,* 7-22.

Stagpoole, V. M. & Bibby, H. M. (1999). Residual gravity anomaly map of the Taupo Volcanic Zone, New Zealand, 1:250:000. Geophysical map 13. Institute of Geological and Nuclear Sciences.

Stanley, C. (2011). *Pearce and general element ratio diagrams; molar scatterplots allowing rigorous investigation of material transfer in geochemical systems*. Paper presented at the 25th International Applied Geochemistry Symposium (IAGS), Rovaniemi, Finland.

Stanley, C. R. & Madeisky, H. E. (1996). *Lithogeochemical exploration for metasomatic zones associated with hydrothermal mineral deposits using Pearce Element Ratio Analysis*. Short Course Notes on PER analysis. University of British Columbia.

Stanley, C. R. & Madeisky, H. E. (1994). Lithogeochemical exploration for hydrothermal ore deposits using Pearce element ratio analysis. In D. R. Lentz (Ed.), *Alteration and alteration processes associated with ore-forming systems* (Vol. 11, pp. 193-211). Canada: Geological Association of Canada, Short Course Notes.

Steiner, A. (1970). Genesis of hydrothermal K-feldspar (adularia) in an active geothermal environment at Wairakei, New Zealand. *Mineralogical magazine, 37* (292). 916-922.

Steiner, A. (1977). The Wairakei Geothermal Area, North Island, New Zealand: its subsurface geology and hydrothermal rock alteration. *New Zealand Geological Survey Bulletin, 90,* 134.

Steiner, A. & Rafter, T.A. (1966). Sulfur isotopes in pyrite, pyrrhotite, alunite and anhydrite from steam wells in the Taupo Volcanic Zone, New Zealand. *Economic Geology,* 15p.

Stern, R. J. (1982). Strontium isotopes from circum-Pacific intra-oceanic island arcs and marginal basins: Regional variations and implications for magmagenesis. *Geological Society of America Bulletin, 93*(6), 477–486.

Stokes, E. (2000). *The legacy of Ngatoroirangi: Maori customary use of geothermal resources*. Department of Geography, The University of Waikato.

Sutton, A., Blake, S. & Wilson, C. J. N. (1995). An outline geochemistry of rhyolite eruptives from Taupo volcanic centre, New Zealand. *Journal of Volcanology and Geothermal Research, 68,* 153-175.

Thompson, A.J.B. & Thompson, J.F.H. (1996). *Atlas of alteration: a field guide to hydrothermal alteration minerals*. Canada: Mineral Deposits Division, Geological Association of Canada.

Van Der Wielen, S., Fabris, A., Keeling, J., Mauger, A., Gordon, G., Keeping, Tim., Heath, P., Reed, G., Katona, L., Fairclough, M., Giles, D. & Halley, S. (2013). Integrated 3D mineral systems maps for iron oxide copper gold (IOCG) deposits, Eastern Gawler Craton, South Australia. *Proceedings, mineral deposit research for a high-tech world ? 12th SGA Biennial, Meeting 2013, 1,* 108-111.

Warren, I., Simmons, S. F. & Mauk, J. L. (2007). Whole-rock geochemical techniques for evaluating hydrothermal alteration, mass changes, and compositional gradients associated with epithermal Au-Ag mineralisation. *Economic Geology, 102,* 923-948.

White, B., Morris, G. & Lumb, T. (1995). New Zealand geothermal resource ownership: cultural and historical perspective. *Proceedings, World Geothermal Congress 1st, 1995*, Florence, Italy.

White, D. E., Muffler, L. J. P. & Truesdell, A. H. (1971). Vapour-dominated hydrothermal systems compared with hot-water systems. *Economic Geology, 66*, 75-97.

White, N. C. & Hedenquist, J. W. (1995). Epithermal gold deposits: Styles, characteristics and exploration. *SEG Newsletter, 23*, 9-13.

Wilson, C. J. N. (1993). Stratigraphy, chronology, styles and dynamics of late Quaternary eruptions from Taupo volcano. *Philosophical Transactions of the Royal Society, London A343*, 205-306.

Wilson, C. J. N. (2001). The 26.5 ka Oruanui eruption, New Zealand: An introduction and overview. *Journal of Volcanology and Geothermal Research, 112*, 133-174.

Wilson, C. J. N., Gravley, D. M., Leonard, G. S. & Rowland, J. V. (2009). Volcanism in the central Taupo Volcanic Zone, New Zealand: tempo, styles and controls. In T. Thordarson., S. Self., G. Larsen., S.K. Rowland & A. Hoskuldsson (Eds.), *Studies in Volcanology: The Legacy of George Walker, Special Publications of IAVCEI, 2*, 225-247. London: The Geological Society.

Wilson, C. J. N., Houghton, B. F., McWilliams, M. O., Lanphere, M. A., Weaver, S. D. & Briggs, R. M. (1995). Volcanic and structural evolution of Taupo Volcanic Zone, New Zealand: A review. *Journal of Volcanology and Geothermal Research, 68*, 1-28.

Wilson, C. J. N. & Rowland, J. V. (2011). Volcanological and tectonic insights into geothermal system in the central Taupo Volcanic Zone, New Zealand. *Proceedings, New Zealand Geothermal Workshop 21-23 November 2011*, Auckland, New Zealand.

Winchester, J. A. & Floyd, P. A. (1976). Geochemical magma type discrimination: application to altered and metamorphosed basic igneous rocks. *Earth and Planetary Science Letters, 28*, 459-469.

Winchester, J. A. & Floyd, P. A. (1977). Geochemical discrimination of different magma series and their differentiation products using immobile elements. *Chemical Geology, 20*, 325-343.

Wohletz, K. & Heiken, G. (1992). *Volcanology and Geothermal Energy*. USA: University of California Press.

Wood, C. P. (1994). Aspects of the geology of Waimangu, Waiotapu, Waikite and Reporoa geothermal systems, Taupo Volcanic Zone, New Zealand. *Geothermics, 23*(5/6), 401-421.

Yang, K., Browne, P. R. L., Huntington, J. F. & Walshe, J. L. (2001). Characterising the hydrothermal alteration of the Broadlands Ohaaki geothermal system, New Zealand, using short-wave infrared spectroscopy. *Journal of Volcanology and Geothermal Research, 106*, 53 - 65.

Appendices

Due to their size, all raw appendices are in digital format on a CD (see pocket at back thesis). The following appendices categorised into folders outlined below:

Appendix A: Sample collection data

Appendix B: Short wave infrared (SWIR) data
Includes raw spectral profiles and interpreted mineral data

Appendix C: X-ray diffraction data (XRD)
Includes both raw and interpreted XRD graphs

Appendix D: X-ray fluorescence data (XRF)
All raw element concentrations and loss on ignition values

Appendix E: Portable x-ray fluorescence data (pXRF)
All raw element concentrations

Appendix F: Petrography
All petrographic photos

Appendix G: Deering et al. (2011)
Geochemical data used for other units of the TVZ and TgVC in rock classification diagrams